MELT TRANSPORT AND MAGMA ACCUMULATION IN A MIGMATITE-CORED GNEISS DOME, FOSDICK MOUNTAINS, WEST ANTARCTICA

A DISSERTATION
SUBMITTED TO THE FACULTY OF THE GRADUATE SCHOOL
OF THE UNIVERSITY OF MINNESOTA
BY

RORY MCFADDEN

IN PARTIAL FULFILLMENT OF THE REQUIREMENTS
FOR THE DEGREE OF
DOCTOR OF PHILOSOPHY

CHRISTIAN TEYSSIER, DONNA L. WHITNEY, ADVISORS

July 2009

Acknowledgments

I have many people that I would like to thank and there are probably more people that feel they deserve my thanks. To those that I do not acknowledge directly, I thank you for your time, effort, and friendship.

First, I want to thank the established scientists who have mentored me and shown me what it means to be a scientist. My advisors, Christian Teyssier and Donna Whitney, deserve many thanks. They were excellent at steering me towards interesting questions and ideas. Their approach to adivising gave me the freedom to explore ideas and let my project evolve, allowing me to learn how research works. The amount they revel in their work has helped me realize how much I enjoy Geology. Finally, I thank them for their guidance and interest in my future as a scientist. I also want to thank Christine Siddoway (Colorado College). She has been an additional advisor for me. Her support and effort in this project has been immeasurable. Christine, thank you for introducing me to Antarctica! Memories from Antarctica are some of my most vivid. I want to thank additional members of my examining committee, David Kohlstedt and Annia Fayon, for discussions and taking the time to read through my work. The analytical work in this thesis benefited from collaborations with Mark Fanning (ANU-PRISE) and Mike Cosca (USGS-Denver). Mark showed my around Canberra and gave me a bike to commute to the SHRIMP lab. I found that very cool. When in

Switzerland, working with Christian and Mike Cosca, I ate many lunches with Mike. I liked one of his dinner suggestions so much I ate there four times in two weeks.

Next, I want to thank my fellow students in the department and especially in the S.T.A.M.P. group. It has been enjoyable to work and grow with all of you. The camaraderie (facilitated by fondue and Thursdays at the Dinktyowner) has made working and living in Minnesota a pleasure. Beer sessions with many of you (e.g. Seth Kruckenberg, Eric Goergen, and Peter Davis) helped relieve stress (at least for some of us) and ease (lack of) work progress frustrations.

Finally, I want to thank my family and friends. Mom, dad, Melany, Brady, and Caroline, your support has made my life fun and easygoing, just how I like it. You all mean the world to me. Dad, thanks for hiking with me and occasionally hauling rocks for me. Mom, thanks for being ever inquisitive and finding Geology "cool". Brady and Melany, thanks for being wonderful siblings, and Melany thanks for suggesting I take a Geology course. Caroline, thank you for being supportive of my work and interested in it. Thanks for being my best friend and always reminding me I am not quite as witty as I think I am. Lucy, thanks for knowing just when I needed a face lick or a run in the park.

I want to acknowledge my funding sources. Thanks to the University of Minnesota Department of Geology and Geophysics and to the Geological Society of America for the Bruce L. "Biff" Reed scholarship. Yes, "Biff" is really part of the award title. Sorry Donna, I still have not come up with my own one syllable moniker.

Abstract

Expansive cliff-face exposures in the Fosdick Mountains (Antarctica) migmatite-cored gneiss dome enabled the documentation of suprasolidus deformation and melt migration structures in middle to lower crustal rocks at a scale significant for continental differentiation and crustal flow. Using field relations, U-Pb geochronology, and argon thermochronology, work in the Fosdick dome has examined the role of oblique deformation in the flow of partially molten crust, the internal segregation and emplacement of granite, and the relation between oblique detachment systems and exhumation of migmatite terrains.

The Fosdick dome developed in the mid-Cretaceous during oblique plate convergence along the East Gondwana margin of Marie Byrd Land–New Zealand. Structures and fabrics in the dome record the middle to lower crustal response to intracontinental crustal extension and a transition from wrench to transtension associated with development of the West Antarctic Rift System. In the mid-Cretaceous, the dome was constructed and exhumed within a dilation zone that developed along an inferred, crustal-scale, dextral strike-slip fault owing to contrasting competency of granodiorite and metasedimentary gneiss. The pressure gradients created by the opening of the dilation zone induced melt migration into the low-pressure region, forming migmatites and leucogranite sheets. The opening of the dilation zone, influx of melt, and the accumulation of leucogranite sheets initiated movement on the dextral normal oblique South Fosdick Detachment zone, which led to cooling and exhumation of the dome.

Mid-crustal migmatites and granites comprise the Fosdick dome. Residual metatexitic paragneiss, metatexitic orthogneiss units, and diatexite migmatites form an ~5 km thick section that partially preserves the lithologic heterogeneities developed in the Paleozoic. An ~2 km thick subhorizontal leucogranite sheeted complex was emplaced above the migmatites. The leucogranite sheets grade into, and syntectonically intrude, a km thick metatexitic migmatite unit that preserves solid-state fabrics related to the South Fosdick Detachment zone. Interconnected leucosome and leucogranite networks are the remnant pathways of a polyphase permeability network that allowed the transport of melt through, and the accumulation of magma in, the crustal layer of the Fosdick dome.

In the Fosdick dome, lineations and fold axes record a stretching axis oriented 235 ± 5. Steep foliation domains that host granite and leucosome strike NE-SW. These foliations are crosscut and folded by subhorizontal foliation domains that strike ENE-WSW and also host granite and leucosome. The stretching axis of 055–235 is oblique to the strike of the bounding strike-slip fault, oriented 100–280, and the long axis of the dome, oriented 080–260. Solid-state structures in the detachment zone that trend NE-SW and record top-to-the-SW motion are overprinted by brittle structures that record N-S stretching, consistent with N-S stretching brittle structures in the hanging wall rocks. These fabrics and structures record a transition from wrench deformation to extension-dominated transtension within the Fosdick dome related to oblique plate convergence along the East Gondwana margin and development of the West Antarctic Rift System.

U-Pb SHRIMP zircon ages of leucosome and granite indicate a 15 myr period of suprasolidus deformation between ca. 117–102 Ma. Steep foliation domains host an older group of leucosome and granite with ages between ca. 117–115 Ma, whereas subhorizontal foliation domains and the detachment zone host younger leucosome and granite with ages between ca. 109–102 Ma. These ages suggest the transition from wrench to extension-dominated transtension and detachment development occurred within 6 myr. Steep domains preserve steep former melt pathways that are relatively minor in abundance, and this may indicate melt transport through the crustal level of the Fosdick dome during wrench. Subhorizontal domains host thick and laterally extensive leucogranitic sheets, possibly suggesting magma accumulation during extension-dominated transtension.

U-Pb SHRIMP zircon and titanite ages on discordant felsic and mafic dikes and $^{40}Ar/^{39}Ar$ biotite and amphibole cooling ages record cooling between ca. 101–97 Ma, suggesting rapid cooling of the Fosdick migmatites and granites. Rotation of the strain field that created a pressure gradient for the accumulation of magma and initiation of detachment-related exhumation is inferred to have caused rapid cooling of the rocks in the Fosdick dome.

Table of Contents

List of Figures

List of Tables

Chapter 1: Introduction to the thesis

Introduction

The transport of melt and the accumulation of magma are fundamental mechanisms by which the crust differentiates and heat and mass are redistributed in orogens (Sawyer, 1996, 2001; Brown, 1994; Brown and Solar, 1998b; Vanderhaeghe, 2001; Teyssier and Whitney, 2002; Marchildon and Brown, 2003; Olsen et al., 2004; Teyssier, et al., 2005; Brown, 2007). Exhumed orogens commonly expose migmatite-cored gneiss domes that represent former partially molten crust (Whitney et al., 2004). The exhumed domes provide access to middle and lower crust where the flow and deformation of partially molten crust can be documented (e.g. Sawyer, 2001; Solar and Brown, 2001; Weinberg and Mark, 2008).

Orogenic systems commonly undergo oblique deformation, ranging from wrench to only slightly oblique divergence or convergence (e.g. Solar and Brown, 2001; Andronicos et al., 2003; Dewey and Strachan, 2003; Whitney et al., 2007). Oblique deformation along orogen-parallel strike-slip faults, particularly when the faults are near obliquely convergent margins, can accommodate large lateral and vertical displacement. Vertical displacement can rapidly bring hot rocks (partially molten crust) from depth to shallow levels, profoundly affecting the thermal structure of the orogenic crust (e.g. Teyssier and Whitney, 2002). Obliquely divergent (transtensional) systems with an extensional component are a common setting for the

exhumation of middle to lower crust. Recent investigations of exhumed partially molten crust in oblique tectonic settings show that migmatite-cored gneiss domes and metamorphic core complexes develop in dilation zones of large-scale wrench systems (e.g. Oldow, 2003; Foster et al., 2007; Whitney et al., 2007). The dilation zone creates space for ascent and emplacement of magma and partially molten crust (= migmatite) in low-pressure regions (e.g. Hutton, 1990; D'Lemos et al., 1992; Tikoff and Teyssier, 1992; Talbot et al., 2005; Weinberg et al., 2009). Field studies in these orogens indicate that dilation zones play an integral role in the localization and exhumation of partially molten crust by enhancing melt transport, magma accumulation, and formation of detachments (e.g. Brown and Solar, 1998; Teyssier et al., 2005; Weinberg and Mark, 2008; Weinberg et al., 2009).

Orogenic crust differentiates through partial melting, melt segregation and extraction, melt transport, and emplacement of melt as granite into upper crustal levels (Brown, 1994; Petford et al., 2000; Brown, 2007). The record of transfer of melt from segregation to emplacement is commonly preserved in migmatite terrains and migmatite-cored gneiss domes as a remnant permeability network, represented by interconnected leucosomes and granite dikes and veins (Brown, 2008; Sawyer, 2008; Weinberg and Mark, 2008). The flow of melt along the permeability pathways and the geometries of the permeability network are controlled by pressure gradients created by local anisotropies, magma buoyancy, and tectonic deformation (e.g. Collins and Sawyer, 1996; Brown and Rushmer, 1997; Brown and Solar, 1998; Sawyer, 2001; Leitch and Weinberg, 2002).

The movement of melt occurs over a range of scales, from the grain-scale to orogen-scale (Brown et al., 1995; Brown, 2007). Grain-scale (mm- to cm-scale) to outcrop-scale (cm- to m-scale) studies of partially molten crust commonly consider processes related to segregation of melt from the solid framework and the collection of melt along grain boundaries and in dilatant sites (Sawyer, 1999; Sawyer, 2001; Guernia and Sawyer, 2003; Marchildon and Brown, 2001, 2003; Rosenberg and Handy, 2005; Hasalová et al., 2008). These studies are essential for understanding the development of migmatites and the role of partial melting in crustal differentiation.

However, studies of exhumed partially molten crust need to address the role of tectonics in the kinematics and timing of melt flow and melt distribution (e.g. Vanderhaeghe et al., 1999; Vanderhaeghe and Teyssier, 2001; Williams and Jiang, 2005). Square kilometer to several tens of square kilometers scale observations in migmatite terrains show the relationship between the distribution of melt in a migmatite terrain and large tectonic structures (e.g. Brown and Solar, 1998; Solar and Brown, 2001; Weinberg et al., 2009). Observations from these studies are used to infer aspects of crustal flow and crustal differentiation.

This thesis concentrates on the Fosdick Mountains migmatite-cored gneiss dome in Marie Byrd Land, Antarctica. A layered plutonic association intruded metasedimentary rocks in the Devonian-Carboniferous, leading to partial melting of regions of the metasedimentary rocks. A second partial melting event occurred during mid-Cretaceous intracontinental crustal extension associated with the West Antarctic Rift System (WARS) (Siddoway et al., 2004; McFadden et al., 2007; Siddoway,

2008). The benefit of this area is the exposure of glacially carved cliffs with pristine, three-dimensional faces that are crucial for documenting the spatial and temporal associations of migmatites, granites, and structures at the square kilometer to several square kilometers scales. Field-based structural analysis assesses the role of deformation through description of structures that developed in the presence of melt, the geometries of the remnant permeability network, and the distribution of melt-rich and melt-poor rocks. U-Pb geochronology and argon thermochronology determine the duration of suprasolidus deformation and the timing of granite crystallization, detachment initiation, cooling, and exhumation. The field relations and geothermochronology that document the construction and exhumation of a migmatite-cored gneiss dome are employed to explore the influence of oblique tectonic deformation on the transport of melt through the crust, the accumulation of magma in the crust, and the initiation of detachment systems.

Following this introduction, the chapters each are individual manuscripts that were prepared for scientific publication. Each chapter addresses a different, integrated aspect of this research, explained in the background and rationale for each chapter.

Chapter 2 of this thesis, *Cretaceous oblique detachment tectonics in the Fosdick Mountains, Marie Byrd Land, Antarctica*, published in the Online Proceedings of the International Symposium of Antarctic Earth Sciences by the US Geological Survey, discusses the field relations in the Fosdick Mountains migmatite-cored gneiss dome, focusing on the newly discovered dextral normal oblique fault zone, the South Fosdick Detachment zone (McFadden et al., 2007). The chapter

documents high temperature fabrics, solid-state fabrics, and brittle structures that are used to understand the interface between the ductile, melt-rich footwall rocks of the Fosdick dome and the brittle hanging wall rocks of neighboring ranges. The study presents U-Pb SHRIMP (Sensitive High Resolution Ion Microprobe) zircon ages from a leucosome and a crosscutting granitic dike within the South Fosdick Detachment zone that bracket the timing of solid-state deformation. The detachment zone was in part responsible for exhumation of the migmatite-cored gneiss dome and is evidence for intracontinental extension along the Cretaceous East Gondwana margin of Marie Byrd Land – New Zealand.

Chapter 3, *Cretaceous intracontinental extension in the Fosdick Mountains migmatite-cored gneiss dome, West Antarctica*, submitted to Tectonics, focuses on the km-scale architecture, the duration of suprasolidus deformation, and the timing of granite crystallization in the Fosdick Mountains (McFadden et al., *in review*). This study documents suprasolidus deformation in the Fosdick dome and shows the influence of strain heterogeneities in anisotropic crust and crustal-scale structures on structural fabrics and lithologic relationships. U-Pb SHRIMP geochronology on zircon and titanite are employed to determine the timing and duration of suprasolidus deformation in the Fosdick dome. In addition, the study examines the role of the middle crust during the transition from convergence to intracontinental extension and transtension along the East Gondwana margin.

Chapter 4 of this thesis, *Oblique dilation, melt transfer, and gneiss dome emplacement*, submitted to Geology, discusses the effects of oblique tectonics and

three-dimensional strain on melt transport and fabric development (McFadden et al., *submitted*). Migmatite and granite structures from the Fosdick dome are utilized to explore the implications of progressive rotation of oblique motion and the opening of a dilation zone in the crust. Field relations and U-Pb SHRIMP zircon ages show that steep fabrics that host "older" granite are overprinted by subhorizontal fabrics that host "younger" granite, indicating a transition from wrench deformation to oblique divergence (transtension). Thus, this chapter shows that the angle of oblique divergence affects the flow of partially molten crust, the internal segregation and emplacement of granite, and the relationship between oblique detachment systems and exhumation of migmatite terrains.

Chapter 5, *Melt transport and magma accumulation during oblique tectonics in the Fosdick Mountains migmatite-cored gneiss dome, Marie Byrd Land, Antarctica*, focuses on observations of the remnant permeability network in the Fosdick Mountains. The permeability network, represented by leucosome and granite dikes and veins, is used to document fabrics that develop during wrench deformation and fabrics that develop during oblique divergence (transtension). Field relations and U-Pb zircon ages indicate that during the wrench stage, fabrics and the permeability network suggest transport of melt through the Fosdick dome to higher crustal levels, whereas during transtension magma accumulated in the Fosdick dome. The switch from wrench to oblique divergence created a dilation zone where magma accumulated, leading to movement on the South Fosdick Detachment zone. Based on $^{40}Ar/^{39}Ar$ cooling ages, once the detachment initiated, the migmatites and granites cooled very

rapidly. Therefore, the Fosdick dome was constructed and stabilized during the transition from wrench to transtension, and exhumed once the detachment initiated, highlighting the self-creative nature of the Fosdick dome.

References Cited

Andronicos, C.L., Chardon, D.H., Hollister, L.S., Gehrels, G.E., and Woodsworth, G.L., 2003, Strain partitioning in an obliquely convergent orogen, plutonism, and synorogenic collapse: Coast Mountains Batholith, Canada, Tectonics, v. 22, doi: 10.1029/2001TC001312.

Brown, M., 1994, The generation, segregation, ascent and emplacement of granite magma: the migmatite-to-crustally-derived granite connection in thickened orogens, Earth-Science Reviews, v. 36, p. 83–130

Brown, M., 2007, Crustal melting and melt extraction, ascent and emplacement in orogens: mechanisms and consequences, Journal of the Geological Society of London, v. 164, p. 709–730.

Brown, M., 2008, Granites, migmatites and residual granulites: relationships and processes, Mineralogical Association of Canada Short Course 38, Quebec City, Quebec, p. 97–144.

Brown, M., Averkin, Y.A., McLellan, E.L., and Sawyer, E.W., 1995, Melt segregation in migmatites, Journal of Geophysical Research, v. 100, p. 15,655–15,679.

Brown, M, and Rushmer, T., 1997, The role of deformation in the movement of granite melt: views from the laboratory and the field, *Deformation-enhanced*

Fluid Transport in the Earth's Crust and Mantle, edited by M. Holness, Mineral. Soc. Series: 8, London: Chapman and Hall, p. 111–144.

Brown, M., and Solar, G.S., 1998, Granite ascent and emplacement during contractional deformation in convergent orogens, Journal of Structural Geology, v. 20, p. 1365–1393.

Collins and Sawyer, 1996, Pervasive granitoid magma transfer through the lower-middle crust during non-coaxial compressional deformation, Journal of Metamorphic Geology, v. 14, p. 565–579.

D'Lemos, R.S., Brown, M., and Strachan, R.A., 1992, Granite magma generation, ascent and emplacement within a transpressional orogen: Journal Geological Society of London, v. 149, p. 487–490.

Dewey, J.F., and Strachan, R.A., 2003, Changing Silurian-Devonian relative plate motion in the Caledonides: Sinistral transpression to sinistral transtension, Journal of the Geological Society, London, v. 160, p. 219–229.

Foster, D.A., Dought, P.T., Kalakay, T.J., Fanning, C.M., Coyner, S., Grice, W.C., and Vogl, J., 2007, Kinematics and timing of exhumation of metamorphic core complexes along the Lewis and Clark fault zone, northern Rocky Mountains, USA, *in* Till, A.B., Roeske, S.M., Sample, J.C., and Foster, D.A., eds., Exhumation Associated with Continental Strike-slip Fault Systems: Geological Society of America Special paper 434, p. 207–232, doi: 10.1130/2007.2434(10).

Guernia, S, and Sawyer, E.W., 2003, Large-scale melt-depletion in granulite terrains: An example from the Archean Ashuanipi Subprovince of Quebec, Journal of Metamorphic Geology, v. 21, p. 181–201.

Hasalová, P., Schulmann, K., Lexa, O., Stipska, P., Hrouda, F., Ulrich, S., Haloda, J., and Tycova, 2008, Origin of migmatites by deformation-enhanced melt infiltration of orthogneiss: a new model based on quantitative microstructural analysis, Journal of Metamorphic Geology, v. 26, p. 29–53.

Hutton, D.H.W., 1990, A new mechanism of granite emplacement: Intrusion in active extensional shear zones: Nature, v. 343, p. 452–455.

Leitch, A.M., and Weinberg, R.F., 2002, Modeling granite migration be mesoscale pervasive flow, Earth and Planetary Science Letters, v. 200, p. 131–146.

Marchildon, N., and Brown, M., 2001, Melt segregation in late syn-tectonic anatectic migmatites: an example from the Onawa Contact aureole, Maine, USA, Physics and Chemistry of Earth (A), v. 26, p. 225–229.

Marchildon, N., and Brown, M., 2003, Spatial distribution of melt-bearing structures in anatectic rocks from southern Brittany: implications for melt-transfer at grain-to orogen-scale, Tectonophysics, v. 364, p. 215–235.

McFadden, R., Siddoway, C.S., Teyssier, C., Fanning, C.M., and Kruckenberg, S.C., 2007, Cretaceous oblique detachment tectonics in the Fosdick Mountains, Marie Byrd Land, Antarctica, *in* Cooper, A.K., Raymond, C.R., and ISAES Editorial Team, eds., Antarctica: A Keystone in a Changing World - Online

Proceedings of the 10th ISAES, USGS Open-File Report 2007-1047, Short Research Paper 047, 5 p.; doi: 10.3133/of2007-1047.srp047.

McFadden, R., Siddoway, C.S., Teyssier, C., and Fanning, C.M., *in review*, Cretaceous intracontinental extension in the Fosdick Mountains migmatite-cored gneiss dome, West Antarctica: Tectonics.

Oldow, J.S., 2003, Active transtensional boundary zone between the western Great Basin and Sierra Nevada block, western U.S. Cordillera: Geology, v. 31, p. 1033–1036, doi: 10.1038/333349a0.

Olsen, S.N., Marsh, B.D., and Baumgartner, L.P., 2004, Modelling mid-crustal migmatite terrains as feeder zones for granite plutons: the competing dynamics of melt transfer by bulk versus porous flow, Transactions of the Royal Society Edinburgh: Earth Sciences, v. 95, p.49–58.

Petford, N., Cruden, A.R., McCaffrey, K.J.W., and Vigneresse, J.L., 2000, Granite magma formation, transport and emplacement in the Earth's crust, Nature, v. 408, p. 669–673.

Rosenberg, C.L., and Handy, M.R., 2005, Experimental deformation of partially melted granite revisited: implication for the continental crust, Journal of Metamorphic Geology, v. 23, p. 19–28.

Sawyer, E.W., 1996, Melt segregation and magma flow in migmatites: Implications for the generation of granite magmas: Transactions of the Royal Society Edinburgh: Earth Sciences, v. 87, p. 85–94.

Sawyer, E.W., 1999, Criteria for the recognition of partial melting, Physics and Chemistry of the Earth (A), v. 24, p. 269–279.

Sawyer, E.W., 2001, Melt segregation in the continental crust: distribution and movement of melt in anatectic rocks, Journal of Metamorphic Geology, v. 19, p. 291–309.

Sawyer, E.W., 2008, Working with migmatites: nomenclature for the constituent parts, Mineralogical Association of Canada Short Course 38, Quebec City, Quebec, 1–28.

Siddoway, C.S., Richard, S.M., Fanning, C.M., and Luyendyk, B.P., 2004, Origin and emplacement of a middle Cretaceous gneiss dome, Fosdick Mountains, West Antarctica, *in* Whitney, D.L., Teyssier, C., and Siddoway, C.S., eds., Gneiss domes in Orogeny, Geological Society America Special Paper 380, p. 267–294.

Solar, G.S., and Brown, M., 2001, Deformation partitioning during transpression in response to Early Devonian oblique convergence, northern Appalachian orogen, USA, Journal of Structural Geology, v. 23, p. 1043–1065.

Talbot, J-Y, Faure, M., Chen, Y., and Martelet, G., 2005, Pull-apart emplacement of the Margeride granitic complex (French Massif Central). Implications for the late evolution of the Variscan orogen, Journal of Structural Geology, v. 27, p. 1610–1629.

Teyssier, C., and Whitney, D.L., 2002, Gneiss domes and orogeny, Geology, v. 30, p. 1139–1142.

Teyssier, C., Ferre, E.C., Whitney, D.L., Norlander, B., Vanderhaeghe, O., and Parkinson, D., 2005, Flow of partially molten crust and origin of detachments during collapse of the Cordilleran orogen, *in* Bruhn, D., and Burlini, L., eds, High-strain zones: Structure and Physical Properties: Geological Society, London, Special Publications, 245, p. 39–64.

Tikoff, B., and Teyssier, C., 1992, Crustal-scale, en echelon "P-shear" tensional bridges: A possible solution to the batholithic room problem, Geology, v. 20, p. 927–930.

Vanderhaeghe, O., 1999, Pervasive melt migration from migmatites to leucogranite in the Shuswap metamorphic core complex, Canada: control of regional deformation, Tectonophysics, v. 312, p. 35–55.

Vanderhaeghe, O., and Teyssier, C., 2001, Partial melting and flow of orogens, Tectonophysics, v. 342, p. 451–472.

Weinberg, R.F., and Mark, G., 2008, Magma migration, folding, and disaggregation of migmatites in the Karakoram shear zone, Ladakh, NW India, Geological Society of America Bulletin, v. 120, p. 994–1009, doi: 10.1130/B26227.1.

Weinberg, R.F, Mark, G., and Reichardt, H., 2009, Magma ponding in the Karakoram shear zone, Ladakh NW India, Geological Society of America Bulletin, v. 121, p. 278–285, doi: 10.1130/B26358.1.

Whitney, D.L., Teyssier, C., and Vanderhaeghe, O., 2004, Gneiss domes and crustal flow, *in* Whitney, D.L., Teyssier, C., and Siddoway, C.S., eds., Gneiss domes in orogeny: Geological Society of America Special Paper 380, p. 15–33.

Whitney, D.L., Teyssier, C., and Heizler, M.T., 2007, Gneiss domes, metamorphic core complexes, and wrench zones: Thermal and structural evolution of the Nigde Massif, central Anatolia: Tectonics, v. 26, doi: 10.1029/2006TC002040.

Williams, P.F., and Jiang, D, 2005, An investigation of lower crustal deformation: evidence for channel flow and its implications for tectonic and structural studies, Journal of Structural Geology, v. 27, p. 1486–1505.

Chapter 2: Cretaceous oblique detachment tectonics in the Fosdick Mountains, Marie Byrd Land, Antarctica

Rory McFadden[a], Christine S. Siddoway[b], Christian Teyssier[a], C. Mark Fanning[c], and Seth C. Kruckenberg[a]

[a]*Department of Geology & Geophysics, University of Minnesota-Twin Cities, Minneapolis, MN, 55455, USA*

[b]*Department of Geology, Colorado College, Colorado Springs, CO 80903, USA*

[c]*Research School of Earth Sciences, Australian National University, Canberra, ACT 0200, Australia*

Published in USGS OF-2007-1047, Short Research Paper 046; Doi:10.3133/of/2007-1047.srp046

Synthesis

The Fosdick Mountains form an E-W trending migmatite dome in the northern Ford Ranges of Marie Byrd Land, Antarctica. Pervasively folded migmatites derived from lower Paleozoic greywacke and middle Paleozoic plutonic rocks constitute the dome. New field research documents a transition from melt-present to solid-state deformation across the south flank of the dome, and a mylonitic shear zone mapped for 30 km between Mt. Iphigene and Mt Richardson. Kinematic shear sense is dextral normal oblique, with top-to-the-SW and -WSW transport. A U-Pb age of 107 Ma, from a leucosome-filled extensional shear band, provides a melt-present deformation

age, and a U-Pb age of 96 Ma, from a crosscutting granitic dike, gives a lower age limit for deformation. The shear zone, here named the South Fosdick detachment zone, forms the south flank of the migmatite dome and was in part responsible for the exhumation of mid-crustal rocks.

Keywords: Fosdick Mountains, Antarctica, migmatite dome, U-Pb SHRIMP, detachment zone

1. Introduction

The final event in breakup of the Gondwana supercontinent was rifting across the Mesozoic active margin in the Pacific sector. Onset of extension at *circa* 100 Ma is recorded in the once contiguous parts of the margin Marie Byrd Land – New Zealand – Campbell Plateau by alkalic plutonism (Storey et al., 1998; Pankhurst et al., 1998; Siddoway et al., 2005), core complex formation (Tulloch and Kimbrough, 1989; Gibson, 1988), and exhumation and rapid cooling of migmatite terrains (Richard et al., 1994; White, 1995; Siddoway et al. 2004a; Flowers et al., 2005). The Ross Sea extension has been attributed to detachment systems (Fitzgerald and Baldwin, 1997), and the presence of crustal-scale exhumation structures has been inferred for the most extensive exposure of high-grade rocks in West Antarctica, the Fosdick Mountains (Luyendyk et al., 1996). Whereas the shear zones responsible for Cretaceous exhumation of mid-crustal rocks in South Island, New Zealand are well-exposed (Tulloch and Kimbrough, 1989; Gibson et al., 1988; White, 1995; Scott and Cooper, 2006; Kula et al., 2007), the exhumation structures in West Antarctica have been elusive, with only cryptic information coming from drill hole (Fitzgerald and Baldwin, 1997), dredge (Siddoway et al., 2004b) and airborne geophysical data (Luyendyk et al., 2003).

New investigations on the south flank of the Fosdick Mountains identify a regionally extensive shear zone that accommodated dextral normal oblique sense of transport. This shear zone forms the carapace of the Fosdick Mountains migmatite dome (Siddoway et al., 2004) and corresponds spatially and temporally to a transition

in the conditions of deformation from melt-present (leucosome-filled shear bands) to solid-state (mylonites and brittle fractures).

2. Fosdick Mountains

The Fosdick Mountains (Fig. 2.1) form an elongate migmatite dome (Wilbanks, 1972; Siddoway et al., 2004a), emplaced and cooled rapidly between 101–94 Ma (Richard et al., 1994). The footwall of the dome includes migmatitic gneisses and metaplutonic rocks that underwent plastic deformation at upper amphibolite grade and that preserve high temperature fabrics (Siddoway et al., 2005). The hanging wall consists of non-metamorphosed Ford Granodiorite and the detachment zone consists of mylonitic gneisses that record transitional fabrics from melt-present to solid-state deformation.

2.1 Footwall rocks – Fosdick migmatite dome

The footwall of the Fosdick migmatite dome consists of numerous generations of leucogranitic sheets, dikes, and diatexite bodies that intruded km-scale folds of pervasively folded paragneisses and granodioritic to leucogranitic intrusions (Fig. 2.2). The structurally deepest rocks define the diatexite core, exposed at the Ochs Glacier area (Fig. 2.1), which consists of felsic rocks with nebulitic and agmatitic migmatite structures (e.g. Mehnert, 1968), affected by km-scale recumbent folds. Structurally above the diatexite is a pervasively folded metatexite. The metatexite displays 100 m to km-scale folds of residual paragneisses interlayered with metaplutonic rocks. The paragneiss layers are internally deformed with dm- to m-scale asymmetric folds. The

metaplutonic rocks are inferred (Siddoway et al., 2006) to be phases of the regionally extensive Ford Granodiorite (Pankhurst et al. 1998; Weaver et al., 1991) in Marie Byrd Land. Anatectic leucosome is ubiquitous in structural sites (e.g. Brown et al., 1994; Sawyer, 1994, 1999; Siddoway et al., 2004b). Leucosome occupies layers concordant to metamorphic foliation, is entrained in folds, and accumulated in fold limbs, shear bands, and inter-boudin regions. Commonly, lower limbs of km-scale folds are strongly sheared and syntectonic leucogranite is localized in the sheared limbs. Above the metatexite is a leucogranitic sheeted complex that consists of narrow bands of paragneissic rocks intruded by sheeted leucogranitic rocks that have moderate to weak foliation, or lack visible fabrics.

Throughout the dome, the migmatitic foliation generally strikes NE-SW and dips to the SE. The predominant preferred mineral alignment, which is commonly a biotite mineral stretching lineation, has a shallowly plunging SW trend. Foliation, mineral lineation, and fold axes orientations, associated with both "melt-present" and solid state fabrics, record normal oblique slip motion (Fig. 2.2a-e). Foliations in the diatexitic rocks are variable in attitude, but generally strike ENE, with shallow SSE dips (Fig. 2.2c). Poles to foliation define a fold axis that is oriented (11, 210) (plunge, trend). In the metatexite of the north flank, the predominant foliation is steeply SE dipping and the poles to foliation produce a NE fold axis with an orientation of (10, 065) (Fig. 2.2b). The biotite stretching lineation orientation is (10, 240), which is sub-parallel to the fold axis. The foliations in the metatexite on the south flank are predominantly ENE striking with a SSE dip. The biotite stretching lineations define a

group at (20, 240), additionally, there is a suite of biotite lineations that display a preferred mineral alignment caused by crenulation cleavage, these lineation trends range from 140–250 (Fig. 2.2d). Structural features in the leucogranitic sheeted complex include rootless isoclinal folds, oblate boudin shapes, outcrop-scale leucosome-filled shear bands, and variably deformed mafic dikes. The foliations are sub-horizontal with ENE-WSW strike and the predominant mineral stretching lineation is NE-SW at (10, 245) (Fig. 2.2a).

2.2 Hanging wall rocks

Non-metamorphosed rocks exist 24 km to the south of the Fosdick Mountains, in the Chester Mountains. The Chester Mountain range trends east-west and comprises Ford Granodiorite of Devono-Carboniferous age (Weaver et al., 1991), cut by few m-scale dikes of diorite and S-type granite that have Cretaceous cooling ages ($^{40}Ar/^{39}Ar$ ages 146 to 96 Ma; Richard et al., 1994; Siddoway et al., 2005). The hornblende-biotite granodiorite has a medium-grained, inequigranular hypidiomorphic texture, and lacks visible fabrics. However, consistently oriented minor faults marked by chloritic or oxidized surfaces are pervasive (Fig. 2.3a). Meters in length and spaced 1 to10 m apart, the dominant shear planes are oriented NE-SW, with oblique-slip striae that trend SSW-NNE (Fig. 2.3a).

A fault analysis in the Chester Mountains defines a principal extension (T) direction of (19, 003), and a shortening (P) direction of (60, 232) (Fig. 2.4a). Shear sense is normal dextral oblique, from offset markers and from fault-surface textures

(Angelier, 1994) such as riedel fracture arrays, crystal fiber steps, and smooth-rough texture.

3. South Fosdick Detachment Zone

The South Fosdick detachment (SFD) is a transitional zone of melt-present to solid-state deformation that is mapped at Mt. Richardson, the un-named ridge East of Mt. Getz, Mt. Getz, and at southern Mt. Iphigene (Fig. 2.1). The shear zone generally dips 20–45° to the SE, deforms granodiorite and paragneiss units, and exposes a progression of structures from extensional shear bands containing anatectic granite, mylonitic fabrics, and penetrative brittle structures.

3.1 Extensional detachment structures in the presence of melt

The southern Mt. Richardson segment of the SFD has a penetrative metamorphic foliation that has a NE-SW strike and a steep SE dip. The shear zone is intruded by syntectonic granite incorporated in extensional structures that exhibit presence of melt, such as extensional shear bands and inter-boudin regions that are leucosome-filled (Fig. 2.3b). The shear bands define two broad groups that are either oblique (at an angle of ~20°) or at a high angle (~70°) to the metamorphic foliation. Synthetic top-to-the-SW shear bands predominate; with antithetic top-to-the-NE shear bands occurring rarely. The shear bands range in length from 10s of centimeters to 10s of meters, and they are commonly 1 to 10 cm in width. These shear bands define an extension direction (T) of (13, 028), and a shortening direction (P) of (61, 273) (Fig. 2.4b). Melt-enhanced deformation is also manifest as sigmoidal boudins of biotite

granodiorite host rock surrounded by leucogranite within shears, with the boudins asymmetry recording top-to-the-SSW simple shear deformation. At Mt. Richardson and Mt. Getz, offset on shear bands, S-C fabrics, and asymmetric sigma porphyroclasts indicate top-to-the-SW to -WSW kinematic sense.

3.2 Mylonitic detachment

The mylonitic portion of the SFD is well exposed at central Mt. Richardson and Mt. Getz. The SFD is an L>S tectonite. The mylonitic gneisses have a pervasive foliation, a lineation defined by stretched quartz and biotite grains, S-C fabrics, and asymmetric sigma porphyroclasts of feldspar (Fig. 2.3c). In thin section, quartz grains are crystal-plastically deformed displaying dynamic recrystallization and development of a strong crystallographic preferred orientation. Feldspar porphyroclasts commonly display internal micro-fracturing and recrystallization of feldspar, forming core and mantle structures. The mylonitic fabrics deform leucogranitic rocks as young as 102.4 ± 0.7 Ma (U-Pb zircon; Siddoway et al. 2006).

The southern Mt. Richardson segment that is intruded by leucogranite has a steep mylonitic foliation, whereas the mylonitic foliation in the central Mt. Richardson and Mt. Getz segments dips shallowly. The Mt. Richardson mylonitic fabrics have an orientation of (070, 25) (strike, dip) with a quartz and biotite stretching lineation of (15, 235). The Mt. Getz mylonitic fabrics have an orientation of (040, 35) and a biotite stretching lineation of (12, 080) (Fig. 2.2e). Lineations are oblique to strike of the solid-state fabrics and to the detachment zone, and reflect normal oblique dip slip.

3.3 Brittle structures associated with detachment zone

Mylonitic and migmatitic gneisses at Mt Richardson are cut by a conjugate array of moderately dipping mesoscopic shear fractures that strike NE-SW and contain normal dip-slip to normal oblique-slip striae. Stretched quartz and chloritic streaks define the lineation. Shear fractures analysis indicates (T) and (P) axes oriented (11, 202) and (72, 331), respectively (Fig. 2.4c).

4. Timing of Detachment Tectonics

We present U-Pb SHRIMP data (Fig. 2.5) for two Fosdick migmatite dome samples from the SFD (Fig. 2.1): (1) an equigranular biotite granite from a top-to-the-SW oblique synthetic shear band (sample M5-R136B; S 76° 32.877, W 144° 41.248) from Mt. Richardson and (2) a medium-grained biotite granite dike (sample M5-G174; S 76° 33.237, W 145° 12.055) that crosscuts the mylonitic fabric of Mt. Getz and has a weak magmatic foliation.

The U-Th-Pb isotopic analyses were made using the SHRIMP II at the Research School of Earth Sciences, The Australian National University, Canberra, Australia, following procedures given in Williams (1998). Each analysis consisted of 6 scans through the mass range, with a U-Pb reference grain, Temora, analyzed for every three unknown analyses. The data have been reduced using the SQUID Excel Macro of Ludwig (2001). The U/Pb ratios have been normalized relative to a value of 0.0668 for the Temora reference zircon, equivalent to an age of 417 Ma (Black et al., 2003).

Zircon grains of the biotite leucogranite from the top-to-the-SW oblique synthetic shear band are predominantly euhedral prismatic grains with bipyramidal terminations. Cathodoluminescence images of the grains reveal oscillatory-zoned cores and high U rim overgrowths. Analyses of rim and core domains (N=15) display no discernible distinction and give Cretaceous ages between ca. 118–104 Ma. Eleven Cretaceous rim and core domain analyses (2σ limit) yield a weighted mean $^{206}Pb/^{238}U$ age of 107.3 ± 0.9 Ma (MSWD=0.60).

The granitic dike contains euhedral to subhedral zircon grains that are predominantly prismatic with bipyramidal terminations. Under cathodoluminescence, the cores are oscillatory-zoned and strongly luminescent, whereas the rim overgrowths are weakly luminescent (Fig. 2.5B). Analyses of core and rim (N=25) domains have a wide scatter of Paleozoic ages, but eleven analyses yielded Cretaceous ages that define a group of ages at ca. 107–95 Ma with no systematic difference between core and rim analyses. Six of these analyses were discarded because they fall more than three sigma from the mean, thus the sample (N=5) yields a mean $^{206}Pb/^{238}U$ age of 96.1 ± 1.4 Ma (MSWD=0.53; 2σ limit).

5. Significance of Geochronologic Data

A U-Pb age of 107.3 ± 0.9 Ma was obtained for igneous zircon within granite emplaced in an extensional shear band within the detachment shear zone. The sample indicates that anatexis and melt-present deformation was underway at that time. A younger age limit on shear zone deformation is provided by the U-Pb age of 96.1 ± 1.4 Ma for igneous zircon from the granite dike that crosscuts mylonitic gneisses at Mt.

Getz. These zircon data establish the syn- to post-deformational history for the SFD, and corroborate prior U-Pb monazite ages from syn- to post-tectonic granites in the Fosdick Mountains (106 ± 1 Ma and 99.8 ± 1 Ma; Richard et al., 1994). The new U-Pb zircon data establish the timing of partial melting and onset of tectonic exhumation of the Fosdick Mountains migmatite dome in a wrench setting during intracontinental extension along the actively extending Gondwana margin in Marie Byrd Land – New Zealand – Campbell Plateau (Tulloch and Kimbrough, 1989; Bradshaw, 1990; Weaver et al., 1991, 1992; Richard et al., 1994; Muir et al., 1997; Spell et al., 2000; Scott and Cooper, 2005). These data correspond with the youngest arc magmatism (~106 Ma) recorded in New Zealand (Tulloch and Kimbrough, 2003) and volcanic tuffs (~102 Ma) associated with the change from convergence to extension in New Zealand (Crampton et al., 2004).

6. Discussion

The high-grade migmatitic rocks of the Fosdick Mountains dome display cm- to km-scale folds, high-temperature (sillimanite, biotite) stretching lineations, and leucogranite-filled extensional shear bands and inter-boudin regions. The hanging wall in the Chester Mountains comprises unfoliated plutonic rocks penetrated by brittle faults. The detachment zone exposes leucosome-filled extensional structures (shear bands, inter-boudin regions), mylonitic stretching lineations, and brittle faults. We interpret the presence of these fabrics and structures to indicate a transition from melt-present to solid-state deformation in the detachment zone that likely occurred during movement on the shear zone and translation of dome rocks toward shallow

crustal levels. The geometrical and kinematic consistency of fabrics and structures in the footwall, hanging wall, and detachment zone indicate a shared deformational history that involved exhumation of the high-grade core by oblique detachment tectonics. The Chester Mountains block was translated down and to the west with respect to dome rocks. The dextral sense of translation is consistent with previous interpretations of dextral transtension in the broader region of the Ford Ranges (Siddoway et al., 2005; Luyendyk et al., 2003).

The NE-SW fold axes and mineral stretching lineations in the high temperature footwall are sub-parallel to NE-SW to ENE-WSW mylonitic stretching lineations in the SFD (Fig. 2.2b-d), whereas the stretching axis from extensional shear bands is oriented more NNE-SSW (Fig. 2.4b). The infinitesimal extensional strain axes determined from brittle shear fractures, which overprint mylonitic fabrics at Mt. Richardson, and from brittle shear fractures cutting non-metamorphosed plutonic rocks of the Chester Mountains, also trend SSW (Fig. 2.4c). The SSW orientation is parallel to fold axes of concentric folds overprinting the mylonitic shear zone and to the stretching direction from late tensile structures throughout the dome (shear bands and dike arrays: Richard, 1992; Siddoway et al. 2005). The change in orientation of stretching axes from ENE-WSW during migmatization and melt-present deformation to NNE-SSW after the transition to solid-state deformation may be a consequence of upward translation of the dome during tectonic exhumation. This hypothesis is being investigated presently.

7. Summary

The South Fosdick detachment zone bounds the southern flank of the Fosdick Mountains migmatite dome and accommodated unroofing of the dome by dextral-normal shearing (top-to-the-SW oblique motion on the south flank of the dome). The dextral component of motion determined for the detachment system is consistent with interpretations of dextral transtension in the broader Ford Ranges (Siddoway et al., 2005; Luyendyk et al., 2003). The first well-documented detachment zone in West Antarctica, the SFD separates foliated and pervasively folded phases of middle Paleozoic Ford Granodiorite in the footwall from unfoliated Ford Granodiorite in the Chester Mountains hanging wall. The detachment records the translation of rocks that underwent melt-present deformation into the realm of solid-state deformation, through right-oblique motion. High temperature fabrics in the footwall, extensional structures in the presence of melt, mylonitic fabrics in the SFD, and brittle structures in the hanging wall are interpreted to indicate that the footwall, detachment zone, and hanging wall share a deformational history that involved exhumation of the high-grade core by oblique detachment tectonics. U-Pb SHRIMP investigations provide evidence for crystallization of melt in extensional structures related to the detachment zone at 107 Ma and a lower age limit of 96 Ma for ductile deformation on the South Fosdick detachment zone.

Acknowledgments

Work supported by National Science Foundation-Office of Polar Programs grants NSF-OPP 0338279 to Siddoway and NSF-OPP 0337488 to Teyssier. This

manuscript has been improved greatly by recommendations by Andy Tulloch and an anonymous reviewer. Thanks to mountain guides Mike Roberts, Allen O'Bannon, and Forrest McCarthy. Thanks to employees of Raytheon Polar Services (Berg Field Center and USAP Cargo in particular); ANG 109th; Kenn Borek Air crews; and Chuck Magee and Barbara Armstrong (PRISE-ANU).

References Cited

Allmendinger, R. W. (2006), FaultKin Version 4.3.5, computer program and user's manual, 28 p.

Allmendinger, R. W. (2002), Stereonet Version 6.3.3, computer program and user's manual, 42p.

Angelier, J. (1994), Fault slip analysis and paleostress reconstruction, in Continental Deformation, edited by P. L. Hancock, pp. 53–100, Tarrytown, New York: Pergamon Press.

Black, L. P., S. L. Kamo, C. M. Allen, J. N. Aleinikoff, D. W. Davis, R. J. Korsch, and C. Foudoulis, (2003), TEMORA 1: a new zircon standard for Phanerozoic U-Pb geochronology, Chemical Geology, 20, 155–170.

Bradshaw, J. D. (1990), Geology of crystalline rocks of northern Fiordland: details of the granulite facies Western Fiordland Orthogneiss and associated rock units, New Zealand Journal of Geology and Geophysics, 33, 465–484.

Brown, M. (1994). The generation, segregation, ascent and emplacement of granite magma: the migmatite-to-crustally-derived granite connection in thickened orogens, Earth-Science Reviews, 36, 83–130.

Crampton, J. S., A. J. Tulloch, G. J. Wilson, J. Ramezani, and I. G. Speden, (2004), Definition, age, and correlation of the Clarence Series stages in New Zealand (late Early to early Late Cretaceous), New Zealand Journal of Geology and Geophysics, 47, 1–19.

Fitzgerald, P. G., and S. L. Baldwin (1997), Detachment fault model for the evolution of the Ross Embayment, in Ricci, C.A., ed., The Antarctic Region: Geological Evolution and Processes, Terra Antarctica Publication, Siena, 555–564.

Flowers, R. M., S. A. Bowring, A. J. Tulloch, and K. A. Klepeis, (2005), Tempo of burial and exhumation within the deep roots of a magmatic arc, Fiordland, New Zealand, Geology, 33, 17–20.

Gibson, G. M., I. McDougall, and T. R. Ireland (1988), Age constraints on metamorphism and the development of a metamorphic core complex in Fiordland, southern New Zealand, Geology, 16, 405–408.

Kula, J., A. Tulloch, T. L. Spell, and M. L. Wells, (2007), Two-stage rifting of Zealandian-Australia-Antarctica: Evidence from $^{40}Ar/^{39}Ar$ thermochronometry of the Sisters shear zone, Stewart Island, New Zealand, Geology, 35, 411–414.

Ludwig, K. R., (2001) SQUID 1.02, A User's Manual, Berkely Geochronology Center Special Publication. Berkeley, CA.

Ludwig, K. R., (2003), User's manual for Isoplot.Ex, Version 3.0, A geochronological toolkit for Microsoft Excel, Berkeley Geochronology Center Special Publication. Berkeley, CA.

Luyendyk B., S. Cisowski, C. Smith, S. Richard, and D. K. Kimbrough (1996), Paleomagnetic study of the northern Ford Ranges, western Marie Byrd Land, West Antarctica: Motion between West and East Antarctica, Tectonics, 15, 122–141.

Luyendyk, B. P., C. C. Sorlien, D. S. Wilson, L. R. Bartek, G. Ely, C. S. Siddoway, and K. Zellmer (2001), Structural and tectonic evolution of the Ross Sea rift in the Cape Colbeck region, Eastern Ross Sea, Tectonics, 20, 933–958.

Luyendyk, B. P., D. S. Wilson, and C. S. Siddoway (2003), Eastern margin of the Ross Sea Rift in western Marie Byrd Land, Antarctica: Crustal structure and tectonic development, Geochemistry, Geophysics, Geosystems, 4, 1090, doi:10.1029/2002GC000462.

Mehnert, K. R., (1968), Migmatites and the Origin of Granitic Rocks, Amsterdam: Elsevier

Muir, R. J., T. R. Ireland, S. D. Weaver, J. D. Bradshaw, T. E. Waight, R. Jongens, and G. N. Eby (1997), SHRIMP U-Pb geochronology of Cretaceous magmatism in northwest Nelson-Westland, South Island, New Zealand, New Zealand Journal of Geology and Geophysics, 40, 453–463.

Pankhurst, R. J., S. D. Weaver, J. D. Bradshaw, B. C. Storey, and T. R. Ireland (1998), Geochronology and geochemistry of pre-Jurassic superterranes in Marie Byrd Land, Antarctica, Journal of Geophysical Research, 103, 2529-2547.

Richard, S.M. (1992), Structure and Cooling History of the Fosdick Metamorphic Complex, Marie Byrd Land, West Antarctica, in Recent Progress in Antarctic Earth Science, edited by Y. Yoshida et al., Terra Scientific Publishing, Tokyo, p. 289-294.

Richard, S. M., C. H. Smith, D. K. Kimbrough, P. G. Fitzgerald, B. P. Luyendyk, and M. O. McWilliams (1994), Cooling history of the northern Ford Ranges, Marie Byrd Land, West Antarctica, Tectonics, 13, 837–857.

Sambridge, M. S., and W. Compston, (1994), Mixture modeling of multicomponent data sets with application to ion-probe zircon ages: Earth and Planetary Science Letters, 128. 373–390.

Sawyer, E. W., (1994), Melt segregation in the continental crust, Geology, 22, 1019–1022.

Sawyer, E. W. (1996), Melt-segregation and magma flow in migmatites: implications for the generation of granite magmas, Transactions of the Royal Society of Edinburgh: Earth Science*s* 87, 85–94.

Siddoway, C. S., S. M. Richard, C. M. Fanning, and B. P. Luyendyk (2004a), Origin and emplacement of a middle Cretaceous gneiss dome, Fosdick Mountains, West Antarctica, in Gneiss Domes in orogeny, edited by D. L. Whitney, C. Teyssier, and C. S. Siddoway, Boulder, Colorado, GSA Special Paper 380, 267–294.

Siddoway, C. S., S. L. Baldwin, P. G. Fitzgerald, C. M. Fanning, and B. P. Luyendyk (2004b), Ross Sea mylonites and the timing of intracontinental extension within the West Antarctic rift system, Geology, 32, 57–60.

Siddoway, C. S., L. C. III Sass, and R. P. Esser (2005), Kinematic history of the Marie Byrd Land terrane, West Antarctica: Direct evidence from Cretaceous mafic dykes, in Terrane Processes at the Margin of Gondwana, edited A. Vaughan, P. Leat, and R. J. Pankhurst, Geological Society of London, Special Publication 246, 417–438.

Siddoway, C. S., C. M. Fanning, S. C. Kruckenberg, and S. C. Fadrhonc (2006), U-Pb SHRIMP investigation of the timing and duration of melt production and migration in a Pacific margin gneiss dome, Fosdick Mountains, Antarctica, Eos Trans. AGU, 87 (52), Fall Meet. Suppl., abstract V23D-0661.

Scott, J. M., and A. F. Cooper (2006), Early Cretaceous extensional exhumation of the lower crust of a magmatic arc: Evidence from the Mount Irene Shear Zone, Fiordland, New Zealand, Tectonics, 25, TC3018, doi: 1029/2005TC001890.

Spell, T. L., I. McDougall, and A. J Tulloch (2000), Thermochronological constraints on the breakup of the Pacific Gondwana margin: The Paparoa metamorphic core complex, South Island, New Zealand, Tectonics, 19, 433–451.

Storey, B. C., P. T. Leat, S. D. Weaver, J. D. Pankhurst, and S. Kelley (1999), Mantle plumes and Antarctic-New Zealand rifting: Evidence from mid-Cretaceous mafic dykes, Journal of the Geological Society, 156, 659–671.

Sutherland, R., (1999), Basement geology and tectonic development of the greater New Zealand region: an interpretation from regional magnetic data, Tectonophysics, 308, 341–362.

Tera, F., and G. Wasserburg, (1972), U-Th-Pb systematics in three Apollo 14 basalts and the problem of initial Pb in lunar rocks, Earth and Planetary Science Letters, 14, 281–304.

Tulloch, A. J., and D. L. Kimbrough (1989), The Paparoa metamorphic core complex, New Zealand: Cretaceous extension associated with fragmentation of the Pacific margin of Gondwana, Tectonics, 8, 1217–1234.

Tulloch, A. J., and D. L., Kimbrough, (2003), Paired plutonic belts in convergent margins and the development of high Na, Al, Sr, low Y magmatism: the Peninsular Ranges Batholith of California and the Median Batholith of New Zealand, in Tectonic evolution of the northwestern Mexico and the southwestern USA, edited by S. E. Johnson, S. R. Paterson, J. Fletcher, G. H. Girty, D. L. Kimbrough, A. Martin-Barajas, Boulder, Colorado, GSA Special Paper 374, 275–295.

Weaver, S. D., J. D. Bradshaw, and C. J. Adams (1991), Granitoids of the Ford Ranges, Marie Byrd Land, Antarctica, in Geological evolution of Antarctica, edited by M. R. A. Thomson, J. A. Crame, and J. W. Thomson, Cambridge, Cambridge University Press, 345–351.

Weaver, S. D., C. J. Adams, R. J. Pankhurst, and I. L. Gibson (1992), Granites of Edward VII Peninsula, Marie Byrd Land: anorogenic magmatism related to Antarctic-New Zealand rifting, Transactions of the Royal Society of Edinburgh, 83, 281–290.

White, P. J. (1995), Thermobarometry of the Charleston Metamorphic Group and implications for the evolution of the Paparoa Metamorphic Core Complex, New Zealand, New Zealand Journal of Geology and Geophysics, 37, 201–209.

Wilbanks, J. R. (1972), Geology of the Fosdick Mountains, Marie Byrd Land, in Antarctic Geology and Geophysics, edited by R. J. Adie, Oslo, Universitetsforlaget, 277–284.

Williams, I. S., (1998), U-Th-Pb Geochronology by Ion Microprobe, in Applications of microanalytical techniques to understanding mineralizing processes, edited by M. A. McKibben, W. C. Shanks III, W. I. Ridley, Reviews in Economic Geology, 7, 1–35.

Figure Captions

Figure 2.1. (A) Geologic map of the Fosdick Mountains in Marie Byrd Land, Antarctica. AA' is the line of the cross section in Figure 2. Sample numbers and ages in boxes are locations of U-Pb SHRIMP zircon ages. Dashed lines mark the upper and lower boundaries of the South Fosdick detachment zone. The group of inferred and observed faults in the Chester Mountains dip moderately to the south, save for the structures bounding the north side of that range, which corresponds to a strong topographic and geophysical lineament (Luyendyk et al., 2003).

Figure 2.2. North-south cross section of the Fosdick Mountains migmatite dome with no vertical exaggeration. The subsurface geology is constrained from cliff exposures west of the cross section line, where deeper rocks have been exhumed.

Equal area stereographic diagrams display poles to foliation and mineral lineations from the footwall of the Fosdick Mountains migmatite dome. Stereographic diagrams were prepared using Stereonet v. 6.3.3X, academic version, by R.W. Allmendinger. The filled circles are the mineral lineations and the filled triangles are the poles to metamorphic foliation. To differentiate shear zone data of the South Fosdick detachment (E) from Mt. Getz and Mt. Richardson, Mt. Getz mineral lineations are open circles and poles to metamorphic foliation are open triangles. The dashed lines are pi-circle girdles and the open rectangles are the pi-axis, or fold axis.

Figure 2.3. (A) Photograph of a brittle shear from the Chester Mountains hanging wall block. The orientation of the plane is (257, 48) with dip slip striae. Secondary PT structures (Petit, 1987) corresponding to the smooth-rough texture indicate normal shear sense. (B) Photograph of extensional leucosome-filled synthetic top-to-the-SW shear bands in the SFD shear zone from Mt. Richardson (structures also exposed on southwest Mt. Iphigene. (C) Photograph of S-C fabrics and asymmetric sigmoidal feldspar porphyroclasts that define sense of shear for mylonitic fabrics in the SFD.

Figure 2.4. (A) Brittle shears of the Chester Mountains. (B) Extensional shear band data from the SFD (C) Brittle shears of Mt. Richardson. Kinematic solutions were calculated with the FaultKin 4.3.5 application, by R.W. Allmendinger.

Figure 2.5. (A, B) Uncertainties given for individual analyses (ratios and ages) are at the one sigma level. Tera-Wasserburg (1972) concordia plots and weighted mean

$^{206}Pb/^{238}U$ age calculations were carried out using ISOPLOT/EX (Ludwig, 2003). The "Mixture Modelling" algorithm of Sambridge and Compston (1994), via ISOPLOT/EX, was used to un-mix statistical age populations or groupings; from these groups weighted mean $^{206}Pb/^{238}U$ ages were calculated and the uncertainties are reported as 95% confidence limits. Insets are frequency distribution plots and cathodoluminescence images with labeled, calibrated but uncorrected for common Pb, analysis spots for representative grains and rims. (A) Biotite granite from extensional shear band (M5-R136B). (B) Biotite granite dike of Mt. Getz (M5-G174).

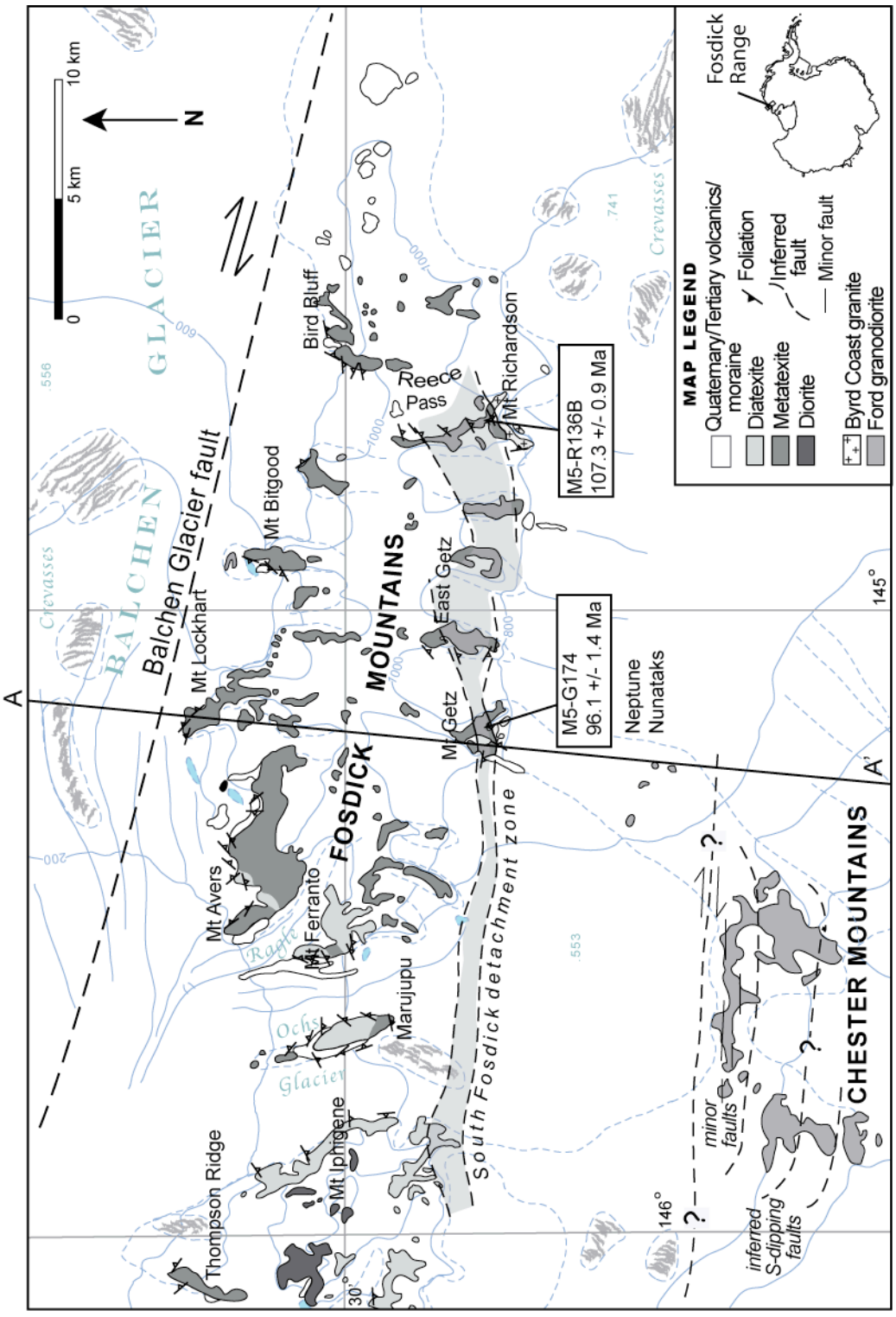

Figure 2.1 Geologic map of the Fosdick Mountains.

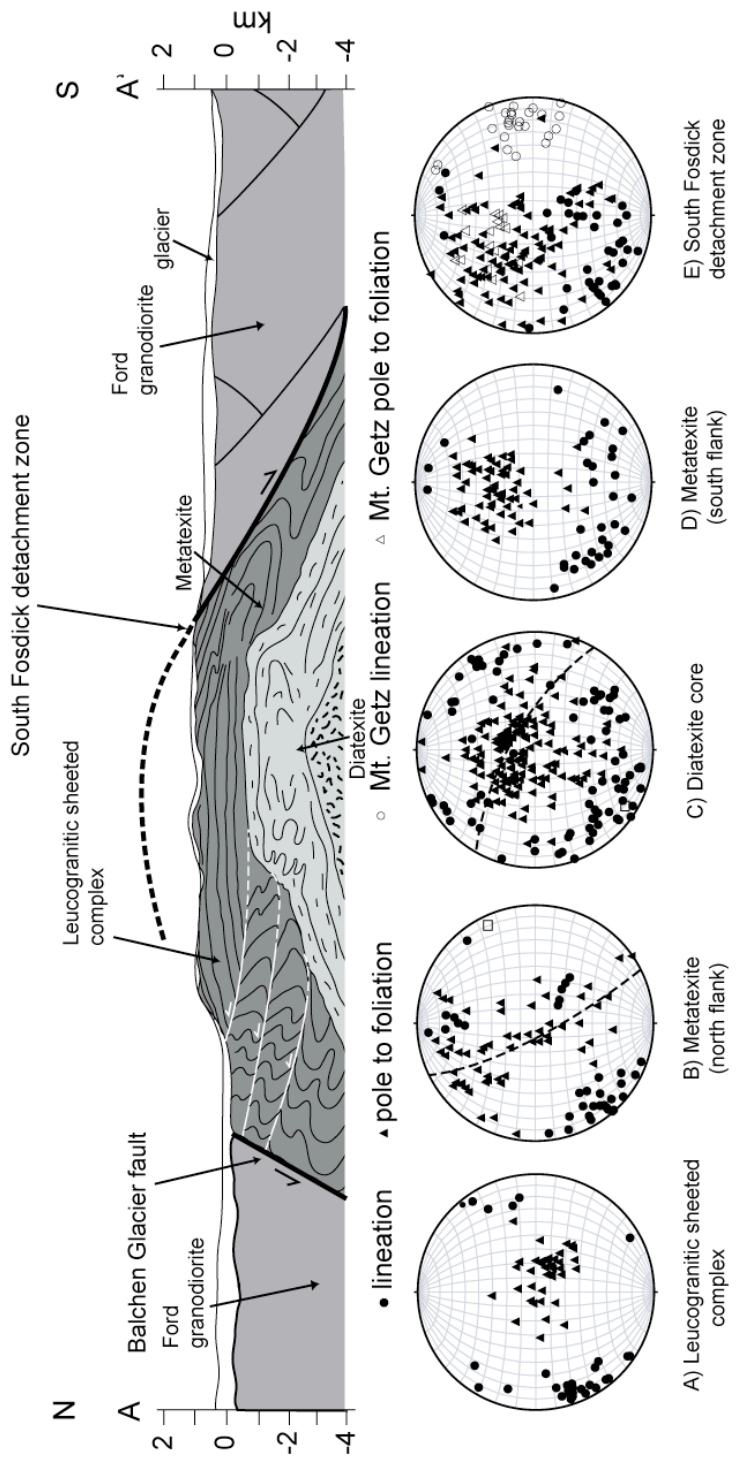

Figure 2.2 Geologic cross-section and structural data from the Fosdick dome.

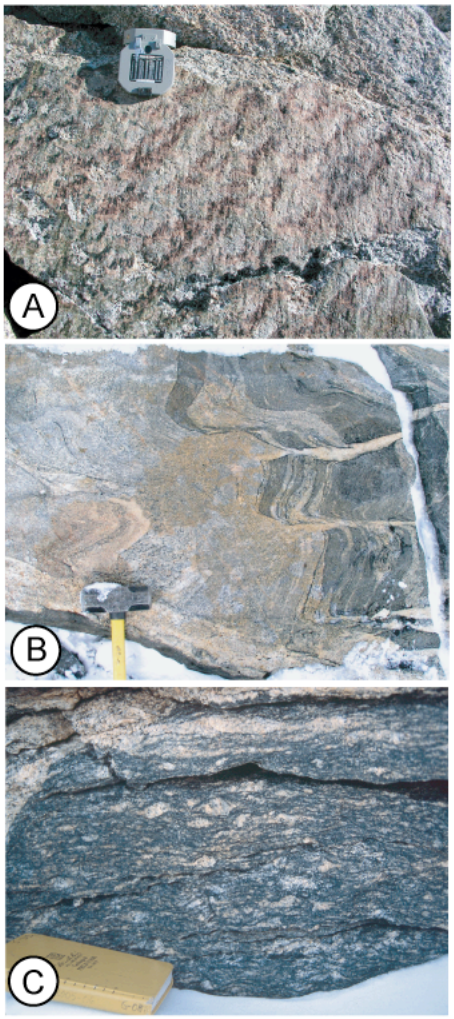

Figure 2.3 Photos of structures from the South Fosdick Detachment zone.

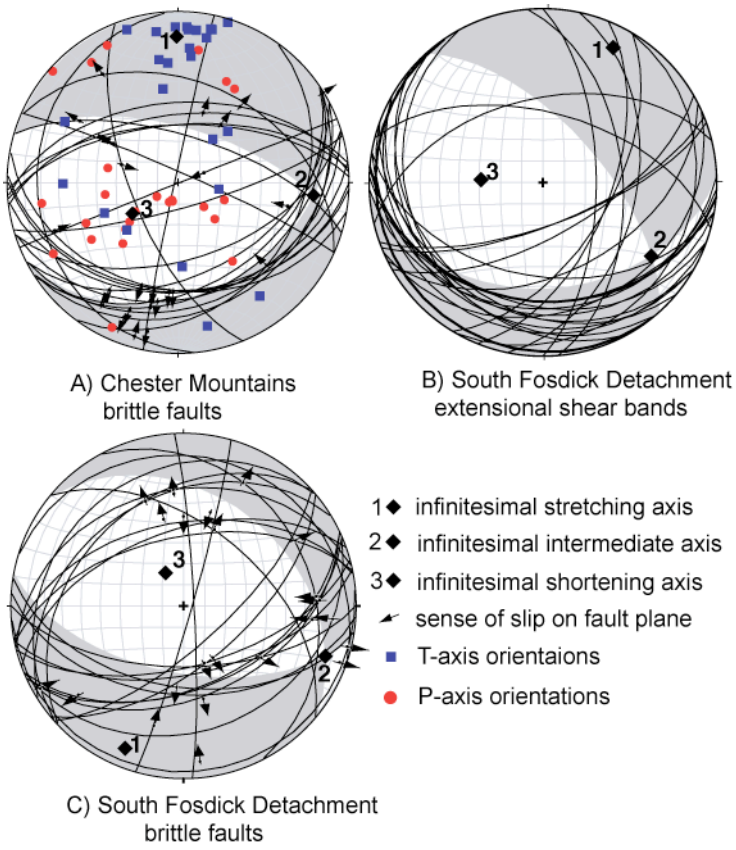

Figure 2.4 Kinematic data plots of brittle structures and shear bands.

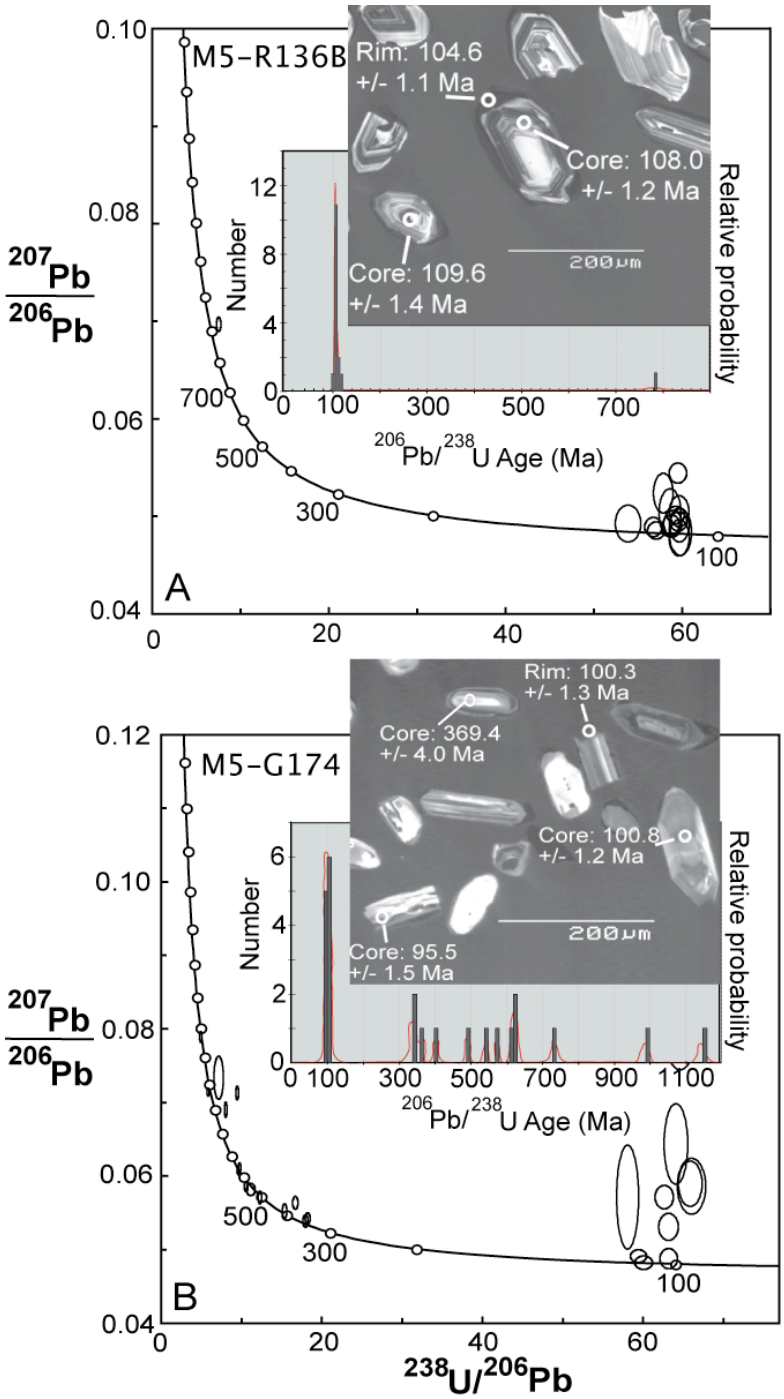

Figure 2.5 U-Pb zircon data plots from granites in the South Fosdick Detachment zone.

Chapter 3: Cretaceous intracontinental extension in the Fosdick Mountains migmatite-cored gneiss dome, West Antarctica

Rory R. McFadden[a], Christine S. Siddoway[b], Christian Teyssier[a], C. Mark Fanning[c]

[a]*Department of Geology & Geophysics, University of Minnesota-Twin Cities, Minneapolis, MN, 55455, USA*

[b]*Department of Geology, Colorado College, Colorado Springs, CO 80903, USA*

[c]*Research School of Earth Sciences, Australian National University, Canberra, ACT 0200, Australia*

Synthesis

The Fosdick Mountains, West Antarctica, expose a 15 x 80 km migmatite-core gneiss dome consisting of residual metasedimentary migmatites, migmatitic intermediate plutonic rocks, and leucogranite. Granite and leucosome are pervasive in dilatant sites over length scales ranging from cm to km, demonstrated to represent a former interconnected melt network. Migmatitic structures, solid-state fabrics, and U-Pb analyses from well-characterized structural sites indicate the dome formed during oblique plate convergence along the East Gondwana margin and subsequent back-arc extension and transtension associated with the West Antarctic Rift System. A normal-oblique structure bounds the gneiss dome on the south side. Leucogranite sheets that are syntectonic with respect to the detachment suggest emplacement of the

leucogranite sheets initiated the detachment. Younging of crystallization ages and thickening of leucogranite sheets eastward and upward in the crustal section reflect propagation of the melt front related to top to the SW unroofing through transtension. Sites occupied by former melt now correspond to granite-filled sills and dilatant structures, leucosomes, and discordant granitic dikes. These were sampled for U-Pb SHRIMP geochronology to determine the timing and duration of melt-present deformation. U-Pb ages of zircon in granitic rocks and of titanite in dioritic dikes are used to establish age brackets and determine when solid-state deformation commenced. Two suites record a 7–10 myr period for melt-present deformation of the Fosdick migmatite-cored gneiss dome. The structural observations and SHRIMP U-Pb ages bear on the transition from convergence to intracontinental extension and transtension of the Cretaceous East Gondwana margin.

Key words: West Antarctica, East Gondwana, U-Pb SHRIMP, migmatites

1. Introduction

Structural and petrological investigations of migmatite terrains have refined our view of the fundamental role crustal melting plays in advection of heat and mass and the mechanical evolution of orogens (Vernon et al., 1990; Sawyer, 1996, 2001; Brown, 1994; Brown and Solar, 1998b; Kriegsman, 2001; Milord et al., 2001; Vanderhaeghe, 2001; Teyssier and Whitney, 2002; Marchildon and Brown, 2003; Olsen et al., 2004; Teyssier, et al., 2005; Bellot, 2007; Brown, 2007; Hasalová et al., 2008). Field evidence suggests that melt transport in the orogenic crust may occur by pervasive flow of a rock/melt volume, controlled by pressure gradients created by local anisotropies, magma buoyancy, and tectonic deformation (e.g. Collins and Sawyer, 1996; Brown and Rushmer, 1997; Brown and Solar, 1998b; Weinberg and Searle, 1998; Vanderhaeghe, 1999, Leitch and Weinberg, 2002). Major tectonic structures may have a role in that they create dilational space for ascent and emplacement of magma and partially molten crust (e.g. Hutton, 1990; Glazner, 1991; D'Lemos et al., 1992; Tikoff and Teyssier, 1992; Grocott et al., 1994), or may halt magma ascent (e.g. Clemens and Mawer, 1992; Hogan and Gilbert, 1995; Roman-Berdiel et al., 1995; Pavlis, 1996). These studies raise important questions about melt distribution in orogenic crust and the time-scale of melting during orogenesis: What controls do deformation, anisotropies arising from preexisting geologic elements (e.g. heterogeneous crust), and tectonic structures (e.g. detachment zones, strike-slip faults) have on the distribution of melt or of magma? What was the duration of deformation that occurred in the presence of melt, and is it continuous or episodic?

Exhumed migmatite terrains represent "fossil" melt domains that may be used to determine the mechanisms and length-scale of melt generation, the interplay between deformation and melt migration, and the comparative importance of pervasive flow versus bulk viscous flow. They are sites where the duration of melt-present deformation can be determined, and the question of continuous or discontinuous behavior of melt crystallization can be resolved. Furthermore, they offer direct access to the km-scale structural architecture of melt dominated middle and lower crust where deformation processes that are critical to our understanding of orogenic crust in contemporary orogens can be studied.

The Fosdick Mountains migmatite-cored gneiss dome in Marie Byrd Land (MBL), West Antarctica, offers 3-D exposures over a 15 x 80 km area. The distribution and continuity of migmatite units have been established through structural mapping; major, trace, and isotope geochemistry; and aerial photograph interpretation (Siddoway et al., 2004b; Korhonen et al., *in review*). Structural relief reaches or exceeds 8 km, through layered plutonic associations, nappe-scale recumbent folds of paragneisses, and tabular granite intrusions. Spatial analysis of granite veins and networks in outcrops determines that the granite component is as high as 40–50% and as low as 5–10%. Thin section study of granites and host gneisses reveals microstructures indicative of the former presence of melt and of solid framework grains (Siddoway et al., 2004b; Siddoway, 2008). In keeping with contemporary migmatites research (e.g. Brown, 2008; Sawyer, 2008), the granites are viewed as a remnant melt flow network through which an unknown volume of melt passed.

Associated deformation produced dilatant structures that aided and influenced melt and magma flow. The km-scale exposures in the Fosdick range allow us to relate meso- and micro-scale observations to megascopic structures such as nappe-scale folds and sheeted leucogranite at a scale that is consequential for our understanding of the role of a melt/fluid layer beneath orogenic plateaus (Nelson et al., 1996; Schilling and Partszch, 2001) and strain within crust that deforms in the presence of melt (McKenzie et al., 2000; Beaumont et al., 2001; Soula et al., 2001; Babeyko et al., 2002; Teyssier et al., 2005).

Metamorphism, crystallization, and deformation in the Fosdick Mountains occurred during a transition from convergence to intracontinental extension and transtension along the East Gondwana margin of West Antarctica (WANT) – New Zealand (NZ) and during development of the West Antarctic Rift System (WARS) (Siddoway, 2008). To understand the tectonic history of West Antarctica and the role of melt-present deformation in middle to lower crust, we present structural observations of fabrics and lithologic relationships to develop the km-scale architecture of the Fosdick migmatite-cored gneiss dome. To determine the time scales and duration of melt-influenced deformation and granite crystallization, we report U-Pb SHRIMP zircon ages from leucosome (light-colored, quartzofeldspathic portion derived from segregated partial melt) and granite in inter-boudin regions, shear bands, and dikes. For a younger limit on timing of melt-present deformation, we present U-Pb SHRIMP titanite crystallization ages from diorite dikes that crosscut the predominant metamorphic foliation.

2. Tectonic Context for Cretaceous High Temperature Metamorphism

The Fosdick Mountains are situated in the Ford Ranges on the eastern margin of the Ross Sea, bordering the Southern Ocean (Fig. 3.1a). Formation of the vast West Antarctic rift system (WARS) in Cretaceous time (Storey et al. 1999; Siddoway et al, 2004a, 2005; Siddoway, 2008) thinned the Marie Byrd Land crust where the Ford Ranges are exposed. Airborne and marine geophysics data indicate crustal thicknesses of 23 km (Luyendyk et al 2003; Ferraccioli et al., 2002), diminishing to 17-19 km for stretched continental crust within the Ross Sea basins (Cooper et al., 1991; Davey and Brancolini, 1995; Luyendyk et al., 2001). The Cretaceous extension affected the wide accretionary zone developed in Paleozoic-Mesozoic time along the East Gondwana margin, which corresponds to present-day West Antarctica and Zealandia (New Zealand + submarine plateaux; Luyendyk, 1995; Mortimer et al., 2006) (Fig. 3.1b).

Significant extension occurred inboard of the Median Batholith (Mortimer et al., 1999), the Mesozoic magmatic arc that was constructed upon then-contiguous WANT-Zealandia (Bradshaw et al., 1997). The core complexes of South Island, NZ (Tulloch and Kimbrough, 1989; Forster and Lister, 2003), and deep level shear zones in Fiordland (Gibson et al., 1988; Scott and Cooper, 2006) formed at this time, together with detachment structures in the Fosdick Mountains (McFadden et al., 2007), and off-shore (Fitzgerald and Baldwin, 1997; Siddoway et al., 2004a) (Fig. 3.1). Contemporaneous NW-SE striking brittle structures found in the Ford Ranges include a regional array of mafic dikes (Storey et al., 1999; Siddoway et al., 2005), brittle faults (Luyendyk et al., 2003), and crustal-scale faults inferred from airborne

geophysics (Ferraccioli et al., 2002; Luyendyk et al., 2003). Backarc plutonism that accompanied the regional deformation (Adams, 1987; Weaver et al., 1992, 1994; Muir et al., 1994; Storey et al., 1999; Mukasa and Dalziel, 2000) is a further expression of extension to transtension across the region from ca. 142–95 Ma, broadly speaking, but intensifying at 105–98 Ma (Siddoway et al., 2004a)

Studies in New Zealand (Cook et al., 1999; Tulloch et al., 2006) and West Antarctica (Davey and Brancolini, 1995; Siddoway, 2008) document the episode of divergent tectonism that caused large intracontinental extension, and determine, in broad terms, the timing of crustal thinning and concomitant crustal heating of the Gondwana margin. U-Pb ages on accessory minerals within gneisses affected by high temperature (HT) metamorphism and anatexis in Fiordland, NZ, are ca. 126–110 Ma (Hollis et al., 2004; Ireland and Gibson, 1998; Scott and Cooper, 2006) and in the Paparoa metamorphic core complex are ca. 119–109 Ma (Kimbrough and Tulloch, 1989; Ireland and Gibson, 1998). Migmatites from the Fosdick Mountains yield *in situ* U-Pb-Th monazite metamorphic ages as old as ~140 Ma (Korhonen et al., 2007), and U-Pb ages for igneous zircon within leucosome date back to 116 Ma and older (Siddoway, 2008). Based on these data, it is clear regional heating coincided with the subduction-related calc-alkaline magmatism recorded by the Median Batholith of ca. 145–120 Ma age (Muir et al., 1997, 1998; Mortimer et al., 1999; Tulloch and Kimbrough, 2003). Metamorphic conditions of 830–865 °C and 6.2–7.4 kbar that are sufficient to induce melting were attained in sillimanite + cordierite + garnet + biotite paragneisses of the Fosdick Mountains (Korhonen et al., *in revision*).

The Paleozoic rock associations of the Ford Ranges consist of lower greenschist facies turbiditic sedimentary rocks (greywacke) of the Swanson Formation (Wade et al., 1978; Bradshaw et al. 1983; Adams, 1986) and the calc-alkaline Ford Granodiorite (Pankhurst et al., 1998). The association of Ford Granodiorite and Swanson Formation characterize the Ross Province of West Antarctica, which correlates closely with the Western Province of New Zealand (Greenland Group / Karamea Batholith; Muir et al., 1996) and more broadly with the Lachlan Orogen of Australia (Foster et al., 2005; Glen, 2005). The greywacke turbidite provinces were once contiguous along the convergent margin of East Gondwana (e.g. Cooper and Tulloch, 1992; Gibson and Ireland, 1996; Pankhurst et al., 1998; Wandres and Bradshaw, 2005; Foster et al., 2005; Squire and Wilson, 2005; Vincenzo et al., 2007). They were derived from the Ross-Delamerian and Lachlan Orogens, as evidenced by characteristic detrital zircon populations of ca. 500 to 450 Ma (Ireland et al., 1998). Ford Granodiorite is a calc-alkaline suite linked to Devono-Carboniferous convergent margin plutonism at the border of East Gondwana. It intruded the Swanson Formation at 375 Ma and 338 Ma, determined from Sr isotopes and zircon crystallization ages (Adams, 1986, 1987; Weaver et al., 1992; Pankhurst et al., 1998).

Paragneisses and granodioritic orthogneisses in the Fosdick dome are the high temperature metamorphosed products of the Swanson Formation and the Ford Granodiorite. Paragneisses in the Fosdick Mountains consist of migmatitic sillimanite + cordierite + garnet + biotite gneiss and biotite + quartz gneiss, and contain detrital zircons derived from the Swanson Formation (Siddoway et al., 2004b). The

granodioritic gneisses within the Fosdick range form a layered complex produced from laterally continuous layers of biotite granodiorite to monzogranite with Ford Granodiorite affinity. The orthogneisses contain acicular prismatic igneous zircons with pronounced oscillatory zoning that yield U-Pb SHRIMP zircon ages of 375 Ma (Siddoway et al., 2004b, 2006; Korhonen et al., *in review*). The ages correspond to the age of Ford Granodiorite in the region, a clear indication that the granodioritic gneisses in the Fosdick dome are metamorphosed Ford Granodiorite.

3. Fosdick Migmatite-Cored Gneiss Dome Architecture

The Fosdick Mountains consist of granite sheets and metatexite to diatexite migmatite with a foliation that defines an asymmetrical, east-southeast plunging elongate antiform, or migmatite dome (Figs. 3.2, 3.3, and 3.6). The dome is bounded to the south by the South Fosdick detachment zone (SFD), a S-dipping, dextral oblique structure (McFadden et al., 2007), and to the north by the Balchen Glacier fault, an inferred steep dextral strike-slip fault (Siddoway et al., 2004b, 2005). The dome consists of intermediate orthogneisses and folded paragneisses within a ~5 km thick layered sequence. The units correspond to Ford Granodiorite and Swanson Formation in the Ford Ranges outside the Fosdick migmatite-core gneiss dome (Siddoway et al., 2004b**)**. The gneisses host multiple generations of granite in sheets, discordant bodies, dikes, and veins; and they contain pervasively distributed leucosome (Fig. 3.4). The orthogneiss-paragneiss association is folded into kms-scale nappes that are refolded about the arch of the dome. The fold nappes pass upward into a ~2 km thick section of voluminous sheeted leucogranites with interlayered

metatexite to diatexite migmatite. Above the leucogranite complex is a km thick section of leucosome-poor metatexite migmatite exhibiting solid-state fabrics associated with the SFD (McFadden et al. 2007).

3.1 Rock Units and Structures

3.1.1 Residual Paragneiss

Domains of refractory, residual paragneisses are exposed at Mt. Avers and the western Fosdick Range (western Mt. Iphigene, Swarm, and Maigetter Peaks) (Figs. 3.2, 3.3). The rocks are dark to red-brown stromatic metatexite with cm- to dm-scale compositional layering alternating with m-thick layers of concordant garnet + K-feldspar leucogranite (Fig. 3.5a) ('massive gneiss' of Siddoway et al., 2004). The peak metamorphic assemblage in this unit is sillimanite + garnet + red-brown (titaniferous) biotite + ilmenite ± melt, determined from mineral equilibria modeling to have formed at Ts of 830–865 °C (Korhonen et al., *in revision*). The garnet-K-feldspar-bearing leucogranite is not internally foliated. The stromatic metatexites record polyphase fabrics (Siddoway et al., 2004b), steep foliation, upright dm-scale folds (Figs. 3.5a, 3.6a, b), and, together with the granite, are folded at the km-scale into megascopic fold nappes.

3.1.2 Ford Orthogneiss Metaplutonic Complex

Foliated, medium-grained 65–100 m thick sheets of biotite granodiorite and monzogranite, with minor, m- to 10 m thick paragneiss layers comprise ridges and summits to the east (Mt. Lockhart (Fig. 3.5b) and East Mt. Avers) and west (Marujupu

and central to northern Mt. Iphigene (Fig. 3.4)) (Figs. 3.2, 3.3). The orthogneisses are metatexitic, but lack well developed dynamic fabric and commonly preserve magmatic fabrics. Narrow, concordant leucosome layers and oblique, crosscutting granite networks transect the orthogneisses (Fig. 3.5b). Folded, boudinaged, and disrupted amphibolite and diorite dikes and sills intrude the metaplutonic complex. In numerous locations, the disrupted and dismembered dikes form m-wide coherent blocks and microgranitoid enclaves (Fig. 3.4). The gneissic foliation dips gently to the SSE, folds are rare, and the mineral lineation is weak (Fig. 3.6c). However, there are asymmetric fabrics and composite (C-S) fabrics, but asymmetric fabrics do not give a consistent shear sense.

3.1.3 Leucogranite Sheeted Complex

Granite sheets and diatexite overlie the residual paragneiss and metaplutonic complex. In the southern and eastern Fosdick Mountains, leucogranite sheets and diatexite layers up to 100 m thick alternate with <1 to 10 m thick layers of paragneiss and orthogneiss, constituting a composite 2 km thick leucogranite sheeted complex ("planar gneisses" of Siddoway et al., 2004b) (Figs. 3.5c and d). The leucogranite sheeted complex is exposed in cliff faces for over 40 km along the length of the range. Intervening orthogneiss and paragneiss layers are metatexitic in the central Fosdick Mountains, becoming diatexitic at upper structural levels.

Structural characteristics of paragneisses and orthogneisses that are interlayered with granite sheets differ considerably from those of gneisses in the residual paragneiss and the metaplutonic complex. The paragneiss and orthogneiss

within dm- to m-scale sheets exhibit subhorizontal to shallowly SE-dipping foliation (Fig. 3.2c) and symmetrical, tight to isoclinal folds with subhorizontal fold axes. Foliation defined by crystallographic preferred orientation of anisotropic mineral phases such as biotite and sillimanite (Siddoway et al., 2004b) is parallel to compositional layering defined by alternation of leucogranite sheets and intervening gneisses. Centimeter to m-scale folds and strain shadows bordering mineral porphyroblasts are symmetrical. Rootless, intrafolial folds are found. Boudinaged mafic dikes and fragmented paragneiss enclaves form ellipsoidal shapes with symmetrical interboudin partitions evidence for a significant region affected by coaxial deformation. Mineral lineations are less common, but occurrences record subhorizontal plunge and stretching oriented 070-250 (Fig. 3.6d). Diatexite and schollen-rich granite are exposed at central Mt. Iphigene and Mt. Ferranto (Fig. 3.4). The diatexites display a subdued color distinction and indistinct boundaries between leucosome and residuum, indicating a high degree of chemical interaction of leucogranite melt with host gneisses (Sawyer, 1998). Boudins and enclaves of mafic dikes and paragneiss are randomly oriented with non-uniform shapes.

3.1.4 Granite and Leucosome

Granite and leucosome exist in diverse structural settings (Fig. 3.5). At the 100 m- to km-scale, individual granite sheets, up to 100 m thick occur at lithologic contacts within residual paragneiss (Fig. 3.5a), between units, and along sheared fold limbs. Granite, at the dm- to 10 m-scale, is found in thin to thick concordant sills, dilational sites such as inter-boudin regions, fold hinges, and shear zones, and

discordant structures including dikes, veins, and shear bands (Fig. 3.5b). Leucosomes, the segregated portions of melt (accumulated grains + crystallized melt), are observed between foliated layers and within layers, recording in situ and in-source leucosome (e.g. Sawyer, 2008) (Figs. 3.5e and f).

In the Fosdick dome, interstitial, optically uniform quartz form grain boundary films along subhedral, interlocking feldspar grains with cuspate or lobate interstices (Figs. 3.5e and f). Monomineralic, optically continuous quartz is the final crystallization product upon solidification of granite melt in cuspate interstices (Holness, 2008). Microstructures in the Fosdick dome also display tiling of feldspar grains, indicative of alignment by magmatic flow (Blumenfeld and Bouchez, 1988; Mulchrone et al., 2005). Magmatic rim overgrowths on sub-solidus cores are also preserved, interpreted as a changed composition of the interstitial melt portion (e.g. Marchildon and Brown, 2001, 2002; Sawyer, 2001) (Figs. 3.5e and f). Interlocking feldspar grains display mechanical kinking at grain-to-grain contacts in coarse-grained phases, indicating the phases acted as a solid framework with interstitial permeability that allowed migration of a melt portion (Philpotts et al., 1998; Bachmann and Bergantz, 2004; Weinberg, 2006). The microstructures preserved in the Fosdick dome provide clear evidence of the former presence of (likely voluminous) melt.

3.1.5 South Fosdick Detachment Zone

The SFD preserves a km-thick zone of solid-state deformation for approximately 30 km along the south flank of the range (McFadden et al., 2007). Influence of the SFD is displayed as penetrative deformation 100s to 1000 m beneath

the SFD, as expressed by solid-state deformation structures from Mt. Lockhart to Bird Bluff and on the South side of the range (Mt. Richardson, Mt. Getz, S. Iphigene). Transects across the dome in the eastern Fosdick Mountains (Bird Bluff-Mt Richardson transect, Fig. 3.2) and along the Ochs glacier show that the leucogranite sheeted complex passes upward into metatexitic orthogneiss with interlayered paragneiss at highest structural levels on the southern flank of the range (Fig. 3.3). The metatexites display concordant, cm-scale leucosome with poorly developed sills and interconnected networks of granite. The prevalent metatexite unit is Mt. Richardson orthogneiss, a coarse- to medium-grained, dark gray, homogeneous biotite granodiorite determined from mapping and zircon geochronology (see below) to be a phase of Ford Granodiorite (Figs. 3.5e, f, and g). In low abundance is dark brown paragneiss interpreted to be metamorphosed Swanson Formation (Fig. 3.5h). The paragneiss has the assemblage biotite + plagioclase + K-feldspar ± sillimanite, overprinted by cordierite + melt microstructures (Siddoway et al., 2004b). Cliff-face observations at Mt. Getz reveal a folded contact between the orthogneiss and paragneiss metatexite based on cm- to m-scale folds. Both rock types contain microstructures indicative of the former presence of melt (Fig. 3.5e and f), together with C-S fabrics and asymmetric porphyroclasts with tails that overprint migmatitic foliation. Kinematic criteria indicate dextral normal oblique shear sense. Top-to-the-SW transport was along the mean azimuth 240 (Fig. 3.6f) (McFadden et al., 2007). An overprinting crenulation lineation has a trend of 080 (Fig. 3.6f). The foliation in the SFD is not mylonitic (i.e., no evidence for grain size reduction), but rather it is

gneissic. Foliations commonly dip from 20° in the west to 35° in the east, with dips as steep as 70° at Mt. Richardson. Open, upright, low amplitude folds (corrugations) deform the SFD foliation with fold axes parallel to the trend of lineation and kinematic transport (Fig. 3.6e)

3.1.5 Late Structures

Late- to post-tectonic structures that crosscut the detachment zone and all rock units include, in older to younger sequence based on crosscutting relationships: 1) normal-sense, moderately south- and north dipping anatectic granite-filled shear bands cutting across metamorphic foliation and folds (Siddoway et al., 2004b), 2) subvertical, discordant leucocratic veins and mafic dikes (Siddoway et al., 2005), 3) muscovite-coated brittle fractures (Richard, 1992), and 4) brittle normal-sense shears (McFadden et al., 2007). The structures strike ~E-W and record ~N–S stretching. Shear bands record top-down-to-north or south kinematic sense and veins and dikes record a N–S extension direction.

3.1.6 Synthesis

The prevalence of granite and leucosome in structural sites indicates deformation took place in the presence of melt (e.g. Brown and Solar, 1998a). To address the timing of melt-present deformation, folded, boudinaged, and crosscutting granite tied to specific structural characteristics of the Fosdick migmatite-cored gneiss dome were sampled (Fig. 3.6).

The duration of zircon crystallization related to partial melting in the middle to lower crust may significantly influence orogenic evolution. To address the duration of crystallization in the Fosdick dome we focused on the youngest crystallization events by predominantly analyzing rims on igneous zircons. From these studies we present new data that brackets the timing and duration of crystallization during deformation in the tectonic evolution of the Fosdick dome and our interpretations have bearing on the influence of middle to lower crustal melting on orogenic evolution.

4. U-Pb Samples

To focus on the timing of deformation and the duration of zircon crystallization in the Fosdick migmatite-cored gneiss dome, sampling for U-Pb geochronology concentrated on granite and migmatitic leucosome (zircon) from specific structural settings in all rock units, plus syn- to post-tectonic diorite dikes (titanite) (Figs. 3.2, 3.3, and 3.7). The timeframe of migmatization, melting, and coalescence of granite into discrete bodies was considered with a suite of samples along the Ochs glacier. To address the time magma migrated into structural sites, crystallized, and was subsequently deformed, granite samples that occupy foliation planes, shear bands, and interboudin necks were selected from the SFD. We present U-Pb zircon data for seven samples and U-Pb titanite data for two samples.

4.1 Ochs Glacier Suite

The Ochs glacier preserves a transect from the leucogranite sheeted complex to the underlying Ford orthogneiss metaplutonic complex and the residual paragneiss. A biotite

granite sheet from the leucogranite sheeted complex on southern Mt. Iphigene was sampled (C5-Is54) (Fig. 3.7a). The granite sheet is structurally below the SFD. It is medium-grained, hypidiomorphic granular biotite granite commingled in a sheath of granite aplite with a dioritic dike. A concordant granite sill from residual paragneiss of Mt. Ferranto was sampled (M5-F57B). The sill is below the leucogranite sheeted complex. It is 20 cm thick, coarse-grained, and parallel to the migmatitic fabric.

4.2 South Fosdick Detachment Zone Suite

Orthogneiss and granite from dilatant structures in the SFD on Mt. Richardson were sampled (Figs. 3.7c, d, and e). The samples present a relative chronology based on crosscutting relationships. Granodioritic orthogneiss is boudinaged and migmatized displaying foliation-parallel granite sills and crosscutting granite-filled shear bands and dikes. The four samples are: a boudinaged, medium-grained granodioritic orthogneiss (M5-R136A); a 10 cm wide granite layer concordant to the shear zone foliation (M5-R136C); an equigranular biotite granite from a discordant dextral normal shear band (M5-R136B); and a 100 m wide tabular, concordant leucogranite sheet that intruded the migmatized granodioritic orthogneiss.

4.3 Late to Post-tectonic Discordant Dikes

Late to post-tectonic dikes were chosen to assess the youngest age limit for the development of migmatite structures and solid-state deformation. A post-tectonic, equigranular medium-grained biotite granite dike crosscuts the SFD solid-state fabric on Mt.

Getz was sampled (M5-G174) (Fig. 3.7f). The dike is part of an array of felsic dikes that postdate the metamorphic fabric developed in the Fosdick dome. A post-tectonic, undeformed two-mica granite from this suite of granites has a $^{207}Pb/^{235}U$ monazite age of 99.8 ± 0.4 Ma.

Diorite dikes that crosscut migmatite structures were sampled for U-Pb titanite analyses. A ~10 m wide diorite dike that intrudes the granite sill (C5-Is54) on southern Mt. Iphigene was sampled (C5-I3) (Fig. 3.7a). The diorite is medium-grained with 'pockets' of appinite. Subhedral to euhedral titanite grains 1–2 mm in dimension are evenly distributed throughout the diorite. Distribution is not uniform in appinite and grain size is 5 mm or greater. The ~10 m thick dike is folded about a subhorizontal axis, together with surrounding leucogranite and granodiorite orthogneiss. The diorite-leucogranite contact is interdigitated along foliation. Cm-wide aplitic veins crosscut the diorite. We sampled a post-tectonic, tabular dike that crosscuts the Ford orthogneiss metaplutonic complex on Marujupu Peak (C5-Mj70A) (Fig. 3.7b). It is an ~2 m thick medium-grained diorite dike that dips moderately to the SW, with planar discordant contacts and lacking internal foliation. Visible igneous titanites of 0.3 to 1 mm in length are evenly distributed throughout the diorite.

5. U-Pb Geochronology

5.1 Analytical Procedure

Zircon mineral separates were prepared from bulk rock samples by crushing, gravity and magnetic separation, heavy liquids, and hand picking at the Australian National University Research School of Earth Sciences. Zircons were mounted in epoxy, ground to approximately half-thickness, and polished with 3 μm and 1 μm

diamond paste. Due to the coarse grain size of titanite in diorite samples, titanite mineral separates were prepared by crushing and hand picking at Colorado College. All grains were imaged in transmitted and reflected light on a petrographic microscope. Zircons were imaged using cathodoluminescence (CL) on a scanning electron microscope (SEM) and titanites were imaged using back-scattered secondary electrons (BSE) on the SEM. Zircon grains were analyzed using SHRIMP II and titanite grains were analyzed using SHRIMP RG at the Research School of Earth Sciences, Australian National University. Procedures are as given in Williams [1998]. Data were reduced using the SQUID Excel Macro of Ludwig [2001]. The zircon U/Pb ratios have been normalized relative to a value of 0.0668 for the Temora reference zircon, equivalent to an age of 417 Ma (Black et al., 2003). The U/Pb ratios for titanite have been normalized relative to a value of 0.17636 for the BLR-1 titanite standard, from a Namibian pegmatite (1047 Ma, Aleinikoff et al., 2007).

Uncertainties given for individual analyses (ratios and ages) are at the one-sigma level. Tera-Wasserburg [1972] concordia plots, probability density plots with stacked histograms, and weighted mean $^{206}Pb/^{238}U$ age calculations were carried out using ISOPLOT/EX (Ludwig, 2003). The "Mixture Modeling" algorithm of Sambridge and Compston [1994], via ISOPLOT/EX, was used to un-mix statistical age populations or groupings. These groupings were used to calculate weighted mean $^{206}Pb/^{238}U$ ages and the uncertainties are reported as 95% confidence limits.

Analyses of rare earth element (REE) and trace element concentrations for zircons of known age were conducted to acquire geochemical information on zircon formation processes

and source materials (e.g. Ireland and Wlotzka, 1992; Maas et al., 1992). REE data were acquired using SHRIMP RG at ANU-RES for selected spots that had been analyzed for U-Pb geochronology. The energy filtering method was used to reduce interferences (Ireland and Wlotzka, 1992; Guo et al., 1996) and in most instances two isotopes were measured (Table 2) so that the isotopic ratios could be used to check for isobaric interferences. Operating conditions and data reduction methods are as in Hoskins [1998]. REE detection limits are in the vicinity of 0.01 ppm for the analysis spots that are 30 mm across and a few micrometers deep.

5.2 Zircon and Titanite Morphology and Geochronology

The goals of our U-Pb geochronology studies presented here are to document the duration of Cretaceous melt-present deformation in a characteristic migmatite-cored gneiss dome. We analyzed both rims and cores of zircon grains, but made the majority of analyses of rims because we wanted to acquire data with bearing on the youngest crystallization and metamorphic events. Additionally, we conducted reconnaissance analyses of cores for identification of the host rock and for provenance associations. We present zircon data sets that record Cretaceous rim ages between ca. 121 to 96 Ma and titanite data sets that display ages between ca. 102 to 94 Ma (Fig. 3.8).

5.2.1 Ochs Glacier Suite

Zircon populations from the biotite granite sheet, C5-Is54, of the leucogranite sheeted complex are 1) euhedral to subhedral, acicular to more equant proportioned

bipyramidal grains and 2) round grains with low U cores, bright in CL (Fig. 3.9a). Euhedral grains form the majority of the C5-Is54 separate. The grains display weak oscillatory zoning with low U cores and wide, high U (dark in CL) rims or tips. Crystals are typically 100-250 μm in length with an axial ratio of 2:1. The prismatic grains have preserved tips infrequently, due to fracturing. Euhedral grain rims have high U, low Th concentrations, and low Th/U ratios. Round grains are less abundant. They display round or oval shapes suggesting that they originated as inherited grains; with slightly irregular margins, and occasionally wide, high U rims. The grains have cores with low U, low Th concentrations, and moderate Th/U ratios and rims with high U, low Th concentrations, and very low Th/U ratios.

Rim and core analyses of the igneous zircon grains give Cretaceous ages (N=17) between ca. 121 to 107 Ma, with a few grains that give Devonian or Proterozoic ages. The inherited grains give either Cretaceous ages or Paleozoic to Proterozoic ages. Eleven analyses from the Cretaceous population yield a weighted mean $^{206}Pb/^{238}U$ age of 114.8 ± 1.1 Ma (Fig. 3.10a; Table 3.1).

Zircon populations from the granite sill, M5-F57B, of the residual paragneiss are predominantly prismatic bipyramidal grains, 100–300 μm in size, with oscillatory-zoning, moderate U overgrowths surrounding high U, corroded cores (Fig. 3.9b). Numerous grains are fractured. Rims have high U, low Th concentrations, and very low Th/U ratios. Rim ages are between ca. 111 to 102 Ma, with a prevalence of younger grains that yielded a mean $^{206}Pb/^{238}U$ age of 104.5 ± 0.8 Ma (Fig. 3.10b;

Table 3.1). One core age was collected, on a grain that was not metamict, and it gave an age of 117 Ma.

5.2.2 South Fosdick Detachment Zone

Zircon populations for the boudinaged granodioritic orthogneiss, M5-R136A, are 1) prismatic and acicular grains with bipyramidal terminations, and 2) round grains. The euhedral grains are 100–400 μm in length with a 2:1 to 3:1 axial ratio (Fig. 3.9c). Under CL, the grains display oscillatory-zoned core domains, embayments, and corroded textures, with wide, high U rims. Rims have high U, low Th concentrations, and low Th/U ratios, whereas cores have moderate U, low Th concentrations, and moderate Th/U ratios. The round grains are ~100 μm with high U cores and moderate U rims. Cores have moderate Th/U ratios and rims have low Th/U ratios

Core analyses fall in two distinct age groups, Devono-Carboniferous ages (N=5) in the range ca. 368 to 357 Ma, and Cretaceous ages (N=3) in the range ca. 111 to 105 Ma. The rims give Cretaceous ages (N=18) in the range ca. 110 to 102 Ma (Fig. 3.11a; Table 3.1). The zircon rim analyses show a broad bimodal age distribution with a tail at the young side. The older sub-maxima yielded a mean $^{206}Pb/^{238}U$ age of 109.1 ± 0.8 Ma (11 analyses) and the younger sub-maxima yielded a mean $^{206}Pb/^{238}U$ age of 105.4 ± 1.0 Ma (8 analyses).

The concordant biotite granite (M5-R136C) contains zircon grains quite similar to R136A in morphology and luminescence (Fig. 3.9d). The grains are a mixed population of euhedral to subhedral grains that are acicular or prismatic with

bipyramidal terminations. Under CL, grains have oscillatory-zoned core domains, embayments, and high U rims. Rims are commonly homogeneous and are interpreted to be metamorphic. Rims predominantly have high U, low Th concentrations, and low Th/U ratios, whereas cores commonly have moderate U, moderate Th concentrations, and moderate to high Th/U ratios. Cores and rims were analyzed on 19 zircon grains. Analyses reveal two major age groups, a Devono-Carboniferous group (N=8) at ca. 379 to 358 Ma, and a Cretaceous cluster (N=16) at ca. 110 to 102 Ma. Thirteen analyses from rim and cores yielded a mean $^{206}Pb/^{238}U$ age of 107.4 ± 0.8 Ma (Fig. 3.11b; Table 3.1).

Zircon grains from the discordant granite-filled shear band (M5-R136B) are predominantly pristine, prismatic grains with bipyramidal terminations (Fig. 3.9e), oscillatory-zoned cores, and high U rims. Rims have high U, low Th concentrations with very low Th/U ratios. The cores of the prismatic grains have moderate to low U, moderate to high Th concentrations, and high Th/U ratios. Analyses of rim (N=4) and cores (N=11) give Cretaceous ages in the range ca. 118 to 104 Ma. No zircons analyzed yielded Devono-Carboniferous ages, however one grain recorded a Proterozoic age. Eleven analyses from Cretaceous rims and cores yielded a mean $^{206}Pb/^{238}U$ age of 107.3 ± 0.9 Ma (Figs. 3.11c; Table 3.1).

Zircon populations from the concordant granite sheet, C5-R60B, include: 1) blocky, bipyramidal, oscillatory-zoned grains that are 100–400 μm in length; 2) round grains with cores of uniform brightness in CL; and 3) irregularly shaped grains with complex margins (Type 3) (Fig. 3.9f). Predominant blocky zircons display a wide, low

U rim succeeded by a narrow high U rim overgrowth upon low U, euhedral cores or moderate U, round cores. Blocky zircon rims have moderate Th/U ratios and cores have high Th/U ratios. Round zircons are small with uniform moderate to low U cores. Round grain rims have low Th/U ratios and cores have high Th/U ratios. Irregular-shaped grains are a third minor population with embayed margins and complex or domainal internal CL textures.

Rims and cores (N=21) yield Cretaceous ages in the range ca. 106 to 95 Ma and two older results that are 348 and 344 Ma. A mean $^{206}Pb/^{238}U$ age of 102.4 ± 0.7 Ma was determined from fourteen analyses (Fig. 3.11d; Table 3.1).

REE for sample M5-R136A

Rare earth element data for two igneous zircons in sample M5-R136A are reported in Table 3.2 and normalized to chondrite in Figure 3.11e. The patterns for both core and rim analyses are similar. Both show steeply rising slopes from light REE to heavy REE with positive Ce and negative Eu anomalies. However, the rim analysis of grain 17 (17.2) has a significantly higher concentration of La and Ce, creating a shallower slope from light REE to heavy REE. Grain 1 is from the dominant zircon population of prismatic grains and is part of the older age distribution. Grain 17 is a less common, round grain from the younger age distribution. From the data available, it appears that REE systematics were stable and unaffected by changes in melt composition during zircon growth of the type that might arise due to feldspar fractionation effects on zircon or replenishment of melt through a permeability

network of framework grains. Further study will be required to evaluate zircon compositional zoning and multiple melting events.

5.2.3 Late to Post-tectonic Discordant Dikes

Late to post-tectonic dikes offer information about the lower age limit of melt-present deformation and solid-state deformation. One post-tectonic granitic dike that cuts the SFD was dated using zircon U-Pb geochronology and two late to post-tectonic diorite dikes that cut the migmatitic fabric were dated using titanite U-Pb geochronology.

A post-tectonic dike that crosscuts the solid-state fabric in the SFD offers constraints on the lower age limit of deformation. Zircon populations from the granite dike (M5-G174) that crosscuts the SFD fabric include: 1) blocky and acicular, doubly terminated grains, 100–250 μm in length and 2) small, round grains 50–150 μm in length (Fig. 3.9g). Euhedral grains have oscillatory-zoned low U cores with high U rims. Round grains have oscillatory-zoned, inherited cores that range from low to high U, overgrown by oscillatory-zoned rims that embay the inherited cores.

Analyses were of the rims and cores of euhedral grains and round grains to examine zircon inheritance. Older age groups have a wide scatter of Neoproterozoic and Paleozoic ages (Table 3.1). Eleven analyses fall in the range 107 to 95 Ma, with no systematic difference between core and rim results. There are three groupings of ages at 110–106 Ma, 102–100 Ma, and 96 Ma. Five analyses yielded a mean $^{206}Pb/^{238}U$ age of 96.1 ± 1.4 Ma (Fig. 3.12a) (McFadden et al., 2007).

Two diorite dikes that display late to post-tectonic crosscutting relationships were studied. Titanite grains are red-brown, clear, and sub- to euhedral, with only few inclusions or cracks. In BSE images (Fig. 3.9h), they display oscillatory growth zoning and less common sector zoning. Some grains display high U (bright) embayments. The analyzed mineral separates are grain fragments that were broken during hand crushing and picking. Titanite crystals are 2 to 6 mm in size in sample C5-I3, the folded and interdigitated diorite dike on southern Mt. Iphigene, and 0.3 to 1 mm in C5-Mj70A, the tabular, discordant diorite dike on Marujupu Peak. C5-I3 analyses have higher U and lower Th concentrations than C5-Mj70A, with C5-Mj70A having higher Th/U ratio.

For the folded dike from Mt. Iphigene (C5-I3), analyzed areas gave Cretaceous $^{206}Pb/^{238}U$ ages in the range ca. 102–94 Ma for center and edge analyses (Fig. 3.12b; Table 3.3). The analyses define a simple distribution with a weighted mean age for 21 analyses of 99.7 ± 0.9 Ma. One analysis is younger than the age range and is considered to have lost radiogenic Pb. The 3-D linear fit shows evidence of significant common Pb, giving an age of 101.2 ± 1.2 Ma. The $^{206}Pb/^{238}U$ ages for the tabular, discordant dike from Marujupu Peak are in the range ca. 101–94 Ma. The weighted mean age for 20 analyses is 96.7 ± 1.0 Ma (Fig. 3.12c; Table 3.3). The grains are enriched in common Pb and cluster so the linear 3-D fit is not an effective way of treating the data set.

6. Discussion

6.1 Interpretation of Geochronological Data

U-Pb SHRIMP age determinations are used together with zircon morphologies

and CL characteristics to assess the timing and duration of deformation in the presence of granite melt in the Fosdick Mountains. Situated within dilatant structural sites and variably overprinted by deformation that followed emplacement, the migmatites and granite record a 13 myr period of melt-present deformation within an 8 km section of crust.

In order to address our questions regarding Cretaceous deformation and crustal melting, we selected rim and tip overgrowths identified in CL images that, on textural grounds such as truncation of growth zones, former melt-presence textures, and zircon morphologies, we judged to have formed during the youngest episode of zircon growth. The U-Pb SHRIMP zircon ages obtained when applying this criterion are predominantly Cretaceous. Single analyses range from ca. 121 to 95 Ma and the calculated mean $^{206}Pb/^{238}U$ ages for 7 samples range from ca. 115 to 96 Ma (Fig. 3.8).

Older cores that were analyzed to obtain baseline data on inheritance yield $^{206}Pb/^{238}U$ ages that are Neoproterozoic to early Paleozoic (ca. 701 to 542 Ma) and Devono-Carboniferous (ca. 379 to 344 Ma) (Table 3.1). The Neoproterozoic to early Paleozoic ages closely resemble U-Pb SHRIMP results for detrital zircons from Swanson Formation metagraywacke (Pankhurst et al., 1998), Fosdick Mountain paragneiss (Siddoway et al., 2004b), and the characteristic age distribution for lower Paleozoic Gondwana margin sediments (Ireland et al., 1998). The Devono-Carboniferous core ages are similar to crystallization ages for Ford Granodiorite (Pankhurst et al., 1998). The geochronologic data indicate that zircons inherited from Paleozoic Swanson Formation and Devono-Carboniferous Ford Granodiorite are present in the Cretaceous granites we analyzed, consistent with

petrogenetic interpretations of the granites based upon a Sr-Nd isotope results (Korhonen et al., *in review*).

Cretaceous SHRIMP zircon ages for Cretaceous granites sampled in the Fosdick dome provide evidence that anatexis of crustal sources, mobilization, and coalescence of granite into discrete bodies were underway by ca. 115 Ma. In the Ochs Glacier suite, a body of folded granite yields an age for igneous zircon that is 10 myr older than zircon rim growths in a late tectonic sill. The granite sheet [C5-Is54] records zircon ages for core and rim analyses from ca. 121 to 107 Ma with a mean $^{206}Pb/^{238}U$ age of 114.8 ± 1.0 Ma, whereas the granite sill [M5-F57B] records zircon rim ages from ca. 111 to 102 Ma with a mean $^{206}Pb/^{238}U$ age of 104.5 ± 0.7 Ma. The single core analysis of a 117 Ma for the granite sill suggests the presence of earlier-formed xenocrystic zircon into late dikes, with subsequent rim growth in dikes due to interaction with infiltrating melt. These observations and analyses indicate a 10 myr period of zircon growth for the Ochs Glacier suite.

In the SFD, granites moved into structural sites of foliation planes, shear bands, and low strain areas, such as interboudin necks, and crystallized from ca. 109–102 Ma. The geometries of the structures suggest that melt migration was induced by detachment faulting, with movement of granite into the SFD along a pressure gradient that existed for a 7 myr period. We associate the ages with the duration of deformation on the SFD and use them to place a younger limit on the timing of deformation recorded from Mt. Lockhart to Bird Bluff and on the South side of the range (Mt. Richardson, Mt. Getz, S. Iphigene).

The presence of Carboniferous euhedral zircon within the Mt. Richardson granodiorite that forms the sigmoidal boudin (M5-R136A) and petrological characteristics indicate that the sample is a member of the Ford Granodiorite suite. Inherited Carboniferous zircons are found in the concordant granite sill (M5-R136C), but analyzed zircons of Ford age are rare to absent in the granite-filled shear band (M5-R136B) and the syntectonic leucogranite sheet (C5-R60B). These observations suggest the possibility of a different external source for the shear band and leucogranite sheet, resorption of zircon grains during migration into the shear band, or a sampling bias towards Cretaceous zircons.

Geochronology and structural data from the Mt. Richardson segment indicate that the ca. 109 to 102 Ma granites were affected by deformation in the SFD. Growth rims on primary igneous zircon within the sigmoidal granodiorite boudin (M5-R136A) fall into two subgroups, one $^{206}Pb/^{238}U$ age of 109.1 ± 0.8 Ma and the other $^{206}Pb/^{238}U$ age of 105.4 ± 1.0 Ma. The zircon grains that yield the two rim ages have no evident difference in morphology, U ppm, Th ppm, or Th/U ratio (Table 1), or REE and trace element concentrations (Fig. 3.11e; Table 3.2). The concordant granite sill (M5-R136C) yields Cretaceous igneous grains and rims that overlap in age at ca. 110–102 Ma, which combine for a mean $^{206}Pb/^{238}U$ age of 107.4 ± 0.8 Ma. The mean $^{206}Pb/^{238}U$ age determined from igneous grains and rim overgrowths from the granite-filled discordant shear band (M5-R136B) is 107.3 ± 0.9 Ma. The tabular syntectonic granite sheet (C5-R60B) with no internal foliation that intrudes parallel to compositional layering has a mean $^{206}Pb/^{238}U$ age of 102.4 ± 0.7 Ma. The association of this sample

set with mesoscale dilatant structures that record dextral oblique, top to the SW, motion upon the SFD shows that the M5-R136B, C granites are syntectonic with respect to movement of the SFD. The younger age limit of movement on the SFD is provided by zircon from the granite of the tabular sheet (M5-R60B) that intrudes the detachment zone.

Late and post-tectonic discordant dikes were emplaced (e.g. C5-Mj70A, C5-I3, M5-G174) between ca. 102–96 Ma. These dikes cut migmatite structures and solid-state fabrics of the SFD, thus providing a lower age limit on deformation at ca. 97–96 Ma.

The discordant granitic dike, M5-G174, crosscuts the SFD solid-state fabric and lacks foliation. There is considerable spread in the zircon ages, from ca. 107 to 95 Ma, with a mean $^{206}Pb/^{238}U$ age is 96.1 ± 1.4 Ma. The ages cluster into 3 groups (Fig. 3.12a), suggesting that the zircons in M5-G174 are xenocrystic or that the material coalesced from multiple Cretaceous sources, the youngest of which is ca. 96 Ma. Thus, we interpret that this granitic dike postdated melt-present deformation and is post-tectonic with respect to the SFD. It provides a minimum age bracket on solid-state deformation within the SFD of ca. 97 Ma. A similar U Pb age was obtained from monazite from a post-tectonic granite stock (Kimbrough and Richard, 1992; Richard et al., 1994).

U-Pb titanite ages for diorite dikes that crosscut the migmatitic foliation range from ca. 102 to 94 Ma. One dike is discordant but deformed, and the other is strongly discordant and undeformed, so it is possible that the dikes intruded during the

culminating stages of movement of the SFD. Judging from the pristine character of the prismatic, clear, oscillatory-zoned titanite grains, the $^{206}Pb/^{238}U$ ages correspond to crystallization of titanite and the diorite host. The differences in U ppm, Th ppm, and Th/U ratio between samples C5-I3 and C5-Mj70A indicate that the two dikes are different generations or are extracted from different sources (Table 3). Dike emplacement coincided with or only narrowly preceded the crystallization and cooling of the entire dome that is documented by $^{40}Ar/^{39}Ar$ cooling ages between ca. 101 to 94 Ma for hornblende, muscovite, biotite, and K-feldspar across the range (Richard et al., 1994). The U-Pb titanite crystallization data (closure temperature of titanite: 670–580 °C; e.g. Cherniak, 1993) confirm that high temperatures were sustained in the Fosdick Mountains migmatite-cored gneiss dome until the verge of the exhumation event. Zircon data show that elevated temperatures were achieved by 115 Ma and sustained until 109–102 Ma when exhumation occurred on the SFD.

6.2 Structural Organization of the Relict Melt Flow Network

In orogenic systems it has been shown that major tectonic structures may create dilational space for ascent and emplacement of magma (e.g. Hutton, 1990; Glazner, 1991; D'Lemos et al., 1992; Tikoff and Teyssier, 1992; Grocott et al., 1994) and may control localization of gneiss domes (e.g. Whittington and Treloar, 2002). These studies suggest that the proclivity of magma to flow towards dilational sites, or lower stress regions, controls magma ascent and emplacement. Recent studies of the Fosdick Mountains proposed that the crustal-scale Balchen Glacier dextral fault (Fig. 3.2) controlled the site of exhumation of the gneiss dome (Siddoway et al., 2004b) and

the SFD acted as the unroofing structure (McFadden et al., 2007). The spatial association of granites with the SFD, in the leucogranite sheeted complex, in small tabular plutons (e.g. C5-R60B), and in mesoscale dilatant structural sites suggests that the influx and accumulation of melt initiated the detachment (Fig. 3.13). Mesoscopic structures indicative of high strain (Figs. 3.2 and 3.6) and the intensification of strain upward, through the leucogranite sheeted complex and approaching the SFD, support this interpretation. Axial planes of folds in paragneiss indicate a component of vertical shortening and flow that overprinted preexisting steep Carboniferous fabrics (Fig. 3.6a and e) across a 5 to 8 km thickness of crust.

In the deformation environment beneath the SFD, strain heterogeneities developed where anisotropies existed at contacts between rocks of contrasting competency. We have documented the contrasting deformation behavior of refractory paragneiss, moderately competent orthogneisses derived from Ford suite, and granites that contained melt and solid phases. At the cm- to m-scale, leucosome, leucogranite, and granite form concordant layers (Fig. 3.5a and b), occupy extensional shear bands (Fig. 3.7c and d), and develop obliquely crosscutting, interconnected networks (Fig. 3.5b). Microstructures in the leucogranites contain evidence of former melt (Fig. 3.5e and f) indicating that the leucogranite networks and concordant to discordant leucogranite layers entered dilational structures as magmatic phases (e.g. Brown, 2007, 2008); thus, pervasive flow and coalescence of granite melt occurred (cf. Collins and Sawyer, 1996; Brown and Rushmer, 1997; Brown and Solar, 1998b; Weinberg and Searle, 1998; Vanderhaeghe, 1999; Leitch and Weinberg, 2002).

The role of asperities in focusing the melt can be documented in the Fosdick Mountains. The paragneisses at Mt. Avers and the Western Fosdick range preserve Carboniferous structures that were largely unaffected by Cretaceous deformation. The lack of Cretaceous deformation is attributable to the refractory, residual character of the paragneisses (Korhonen et al., *in revision*) that rendered them mechanically strong and resistant to deformation. Residual paragneisses experienced prior HT metamorphism and anatexis during the Carboniferous events when Ford Granodiorite was emplaced (Siddoway et al., 2004b; Korhonen et al., *in revision*; Siddoway and Fanning, 2009). They contain polyphase fabrics (Siddoway et al., 2004b), steep foliation, and megascopic fold nappes (Fig. 3.5a) within paragneiss. These coherent, melt-depleted units that are more competent created a large-scale strain perturbation, causing the residual paragneiss unit at Mt. Avers and a second paragneiss domain at Mt. Iphigene to act as 'mega-boudins', or refractory blocks (Fig. 3.13), inducing migration of melt into the extensive low strain regions to the ENE and WSW (*in the stretching direction)* of the blocks. The single-stage fabric within Ford Granodiorite, that is geometrically consistent with that in the leucogranite sheeted complex suggests it underwent metamorphism and melting for the first time in the Cretaceous.

At Mt. Getz and Mt. Richardson, within the SFD, presence of granite within discrete shear zones and dikes that have microstructures (Fig. 3.5e and f) indicative of magmatic flow and pervasive flow is evidence that granite melt was mobile and migrated into the detachment zone. Limited migmatitic differentiation within paragneiss produced concordant, cm-scale leucosome, with discontinuous sills and

interconnected networks. Syntectonic granite sheets intruded the Mt. Richardson segment of the shear zone and these sheets have younger zircon ages than granites in networks (C5-R60B vs. M5-R136) (Fig. 3.11), suggesting that melt migrated upward and laterally into the detachment zone through discrete dilatant sites such as dikes and shear bands.

The comparison between the Ford orthogneiss and minor paragneiss units in the central Fosdicks, with low but important granite proportion, versus the leucogranite sheeted complex, with a high proportion of granite and diatexite (and lesser component of Ford orthogneiss and paragneiss), is consistent with the interpretation that the Fosdick Mountains are a melt transfer zone. We infer that mesoscale granites in structural sites constituted a melt flow network that transported melt from source regions, whether outside or from within the Fosdick Mountains, into the leucogranite sheeted complex and into the SFD (Fig. 3.13). The granites, with entrained boudins and layers of gneisses, experienced subvertical shortening and bulk viscous flow to form subhorizontal sheets that led to initiation of movement on the SFD.

6.3 Duration of Melt-Present Deformation

The Ochs Glacier and SFD suites record two successions of zircon crystallization ages, respectively. The ‘older’, Ochs Glacier succession in the west, documents crystallization from ca. 115–105 Ma, whereas the ‘younger’, SFD succession in the east, records crystallization from ca. 109–102 Ma (Fig. 3.8). There is overlap in ages between the two

suites, and considerable overlap in single zircon analyses (Table 1), but the crystallization ages in the SFD suite, which is eastward and higher in the structural section, documents a younger age range. The age ranges indicate propagation of the melt front upward and to the east, related to top to the SW unroofing through transtension. This interpretation is consistent with the increase in thickness of granite in the leucogranite sheeted complex towards the east, which we suggest is controlled by the SFD. Alternatively, the younger ages in the SFD suite may represent late pulses of granite magma that was focused along dikes and shear zones.

The age successions in the Ochs Glacier and SFD suites verify the duration of melt-present deformation. In each suite, the duration of melt-present deformation recorded by granites was 7 to 10 myr (Fig. 3.8). The Ochs Glacier suite records a 10 myr period of deformation, from the inception of granite crystallization at 115 Ma to the emplacement of granite sills with rim overgrowths of 105 Ma. The SFD suite documents a 7 myr period from granite localizing in dilatant structures at ca. 109–105 Ma to emplacement of a syn- to late - tectonic granitic sheet at 102 Ma. Late- to post-tectonic dikes and $^{40}Ar/^{39}Ar$ cooling ages (Richard et al., 1994) indicate that rapid cooling immediately followed the time period of melt-present deformation. Lack of deformation of post-tectonic felsic dikes suggest that they were emplaced after movement on the detachment ceased.

The duration of melt-present deformation and the time to cool the structural system has implications for the Cretaceous evolution of West Antarctica and the development of the WARS. The 7–10 myr period for crystallization and cooling of the granites indicates a rapid event possibly related to advection of buoyant melt-rich volume of material near transcurrent faults.

6.4 Cretaceous Tectonic Evolution of West Antarctica and Zealandia

High temperature metamorphism and growth of new igneous zircon within anatectic granites, in progress by ca. 115 Ma, we attribute to convergent tectonism along the East Gondwana active margin (Tulloch et al., 1991; Mortimer et al., 1999; Sutherland and Hollis, 2001; Tulloch et al., 2006; Siddoway, 2008). Oblique plate convergence and subduction of young oceanic lithosphere, including oceanic plateaus (Bradshaw, 1989; Luyendyk, 1995) occurred along the Mesozoic convergent margin (Fig. 3.14). Crustal thickness is not constrained from the Fosdick Mountains data, but we have found no evidence of high pressure metamorphism that is expected if crustal thickness was great. Maximum Ps of 7.4 kbar are determined from mineral equilibria modeling (Korhonen et al., *in revision*) suggesting elevated and compressed isotherms. Granulite metamorphism in Fiordland at ~108 Ma (Gibson and Ireland, 1995) is an indication that the extensive part of the convergent margin was affected. The Lachlan belt, representative of the Gondwana margin, of which the Ross Province is a part, does not have evidence for thick, high crust (cf. O'Halloran and Rey, 1999). Tulloch et al. (2006) suggest there was a 'Cordillera Zealandia' albeit not a plateau.

HT metamorphism of deep crustal rocks exhumed upon detachment structures are recognized over a wide region along the East Gondwana margin in WANT and NZ reflecting regionally significant middle to lower crustal flow (Fig. 3.1). In Marie Byrd Land (MBL), elevated heat flow is attributed to subduction of hot oceanic lithosphere at the Phoenix-Pacific ridge (Bradshaw, 1989; Luyendyk, 1995) with back-arc

magmatism (Fig. 3.14) (Weaver et al., 1991, 1994; Mukasa and Dalziel, 2000) driven by slab rollback (cf. Crawford, 2003). At ca. 100 Ma, in the Fosdick Mountains, there was a change to transtension, with oblique opening across pre-existing high angle faults. Age and timing of transtension on the SFD and cooling of Ar chronometers (Richard et al., 1994) in the Fosdick Mountains from ca. 109–97 Ma occurred at a comparable time and required a similar, comparably short, time with other sites in WANT (Siddoway et al., 2004a), and in New Zealand (Gibson et al., 1988; Tulloch and Kimbrough, 1989; Forster and Lister, 2003; Scott and Cooper, 2006; Kula et al., 2007). $^{40}Ar/^{39}Ar$ cooling ages from the Fosdick Mountains further confirm the sequence of rapidly decreasing temperature over time.

Evidence from the Fosdick migmatite-cored gneiss dome and other sites rapidly exhumed in the footwall of detachments, suggest that when melt is present, exhumation and cooling of a flow zone of middle crust can be achieved in a dramatically rapid event that takes <10 myr. Suites across the Fosdick dome that record a 7 to 10 myr period for the duration of melt-present deformation and cooling of the structural system indicate elevated isotherms and the enhancement of tectonic exhumation and cooling next to transcurrent faults.

7. Summary

Structural mapping and SHRIMP U-Pb geochronology document the time-scale for migmatization, generation of melts, and deformation-induced melt migration in the Fosdick migmatite-cored gneiss dome, with coalescence of granite beneath a

regional detachment, the SFD. The results from the present study allow the following conclusions to be made.

Two suites of granitoid rocks in structural sites record zircon crystallization ages over a 7 to 10 myr span. The western Ochs Glacier suite records crystallization ages from ca. 115–105 and the eastern SFD suite documents crystallization ages from ca. 109–102 Ma. A granite sheet crystallization age of 115 Ma indicates melting and crystallization occurred in the Fosdick region during Gondwana margin convergent tectonics. Crystallization ages from ca. 109 to 102 Ma bracket the timing of granite localizing in structures and experiencing deformation within the SFD.

The lower age limit for melt-present and solid-state deformation is bracketed by late to post-tectonic discordant diorite and granite dikes, as well as Ar cooling ages. The late to post-tectonic discordant diorite dikes that crosscut migmatite structures give a lower age limit for melt-present deformation at ca. 102 Ma, consistent with Ar thermochronology across the range (Richard et al., 1994). A late discordant granite dike that crosscuts the solid-state fabrics provides a lower age limit for solid-state deformation on the SFD at ca. 97 Ma consistent with the U Pb monazite result for a post-tectonic granite stock at deeper levels (Richard et al., 1994).

Subhorizontal compositional layering, axial planes of folds, and ellipsoidal boudin shapes in the leucogranite sheeted complex, underlying the SFD, reflect high strain. High strain regions documented below the SFD indicates the SFD equates with the ‘top’ of a granite-charged region of migmatitic crust. Kinematics, eastward and upward increase in leucogranite sheet thickness, and younger crystallization ages in

the east record top to the southwest unroofing through transtension in the Fosdick dome. These observations are evidence for the eastward and upward propagation of the melt front.

The Fosdick crystallization ages that we can tie to structural fabrics and use to constrain movement on the SFD are contemporaneous with crystallization ages and detachment structures in Zealandia and WANT. These results refine the timing for Fosdick migmatization revealing that migmatization began during convergent tectonism and continued in a back-arc setting, possibly influencing intra-arc extension and transtension during slab rollback.

Acknowledgments

Work supported by National Science Foundation-Office of Polar Programs grants NSF-OPP 0338279 to Siddoway and NSF-OPP 0337488 to Teyssier. We thank Seth Kruckenberg, Fawna Korhonen, and Jenny Haywood for field work collaboration, Mike Roberts, Allen O'Bannon, and Forrest McCarthy for field safety, and employees of Raytheon Polar Services (Berg Field Center and USAP Cargo in particular); ANG 109th; Kenn Borek Air crews; and Chuck Magee and Brenda Armstrong (PRISE-ANU).

References Cited

Adams, C. J. (1986), Geochronological studies of the Swanson Formation of Marie Byrd Land, West Antarctica, and correlation with northern Victoria Land, East

Antarctica and the South Island, New Zealand, *New Zealand J. Geol. Geophys., 29,* 345–358.

Adams, C. J. (1987), Geochronology of granite terranes in the Ford Ranges, Marie Byrd Land, West Antarctica, *New Zealand J. Geol. Geophys., 30,* 51–72.

Aleinikoff, J. N., R. P. Wintsch, R. P. Tollo, D. M. Unruh, C. M. Fanning, and M. D. Schmitz (2007), Ages and origins of rocks of the Killingworth dome, south-central Connecticut: Implications for the tectonic evolution of southern New England, *Am J Science, 307*, 63–118.

Babeyko, A. Y., S. V. Sobolev, R. B. Trumbull, P. Oncken, and L. L. Lavier (2002), Numerical models of crustal scale convection and partial melting beneath the Altiplano-Puna plateau, *Earth Planet. Sci. Let. 199*, 373–388.

Bachmann, O., and G. W. Bergantz (2004), On the origin of crystal-poor rhyolites: Extracted from batholithic crystal mushes, *J. Petrol., 45,* 1565–1582.

Beaumont, C., R. A. Jamieson, M. H. Nguyen, and B. Lee (2001), Himalayan tectonics explained by extrusion of a low-viscosity crustal channel coupled to focus surface denudation, *Nature 414*, 738–742.

Bellot, J.P. (2007), Pre- to syn-extensional melt-assisted nucleation and growth of extensional gneiss domes: The western French Massif Central (Variscan belt), *J. Struct. Geol.*, *29*, 863–880.

Black, L. P., S. L. Kamo, C. M. Allen, J. N., Aleinikoff, D. W. Davis, R. J. Korsch, and C. Foudulis (2003), TEMORA 1: a new zircon standard for Phanerozoic U-Pb geochronology, *Chem. Geol.*, 200, 155–170.

Blumenfeld, P., and J. -L. Bouchez (1988), Shear criteria in granite and migmatite deformed in the magmatic and solid states, *J. Struct. Geol. 10,* 361–372.

Bradshaw, J. D., B. Andrew, and B. D. Field (1983), Swanson Formation and related rocks of Marie Byrd Land and a comparison with the Robertson Bay Group of northern Victoria Land, in *Antarctic Earth Science*, edited by R. L. Oliver et al., 274–279, Australian Academy of Science, Canberra.

Bradshaw, J. D. (1989), Cretaceous geotectonic patterns in the New Zealand region, *Tectonics, 8,* 803–820.

Bradshaw, J. D., R. J. Pankhurst, S. D. Weaver, B. C. Storey, R. J. Muir and T. R. Ireland (1997), New Zealand superterranes recognized in Marie Byrd Land and Thurston Island, in *The Antarctic Region, Geological Evolution and Processes*, edited by C. A. Ricci, pp. 429–436, *Terra Antartica* Publication, Siena, Italy.

Brown, M. (1994). The generation, segregation, ascent and emplacement of granite magma: the migmatite-to-crustally-derived granite connection in thickened orogens, *Earth-Science Reviews*, *36*, 83–130.

Brown, M. (2007), Crustal melting and melt extraction, ascent and emplacement in orogens: mechanisms and consequences, *J. Geol. Soc. London, 164*, 709–730.

Brown, M. (2008), Granites, migmatites and residual granulites: relationships and processes, *Min. Assc. Canada Short Course 38*, Quebec City, Quebec, 97–144.

Brown, M., and G. S. Solar (1998a), Shear zone systems and melts: feedback relations and self-organisation in orogenic belts. *J. Struct. Geol., 20*, 211–227.

Brown, M., and G. S. Solar (1998b), Granite ascent and emplacement during contractional deformation in convergent orogens, *J. Struct. Geol.*, 20, 1365–1393.

Brown, M., and T. Rushmer, (1997), The role of deformation in the movement of granite melt: views from the laboratory and the field, *Deformation-enhanced Fluid Transport in the Earth's Crust and Mantle,* edited by M. Holness, Mineral. Soc. Series: 8, London: Chapman and Hall, pp. 111–144.

Collins, W. J., and E. W. Sawyer (1996), Pervasive granitoid magma transfer through the lower-middle crust during non-coaxial compressional deformation, *J. Metamorph. Geol., 14*, 565–579.

Cooper, A. K., F. J. Davey, and K. Hinz (1991), Crustal extension and origin of sedimentary basins beneath the Ross Sea and Ross Ice Shelf, Antarctica, *Geologic Evolution of Antarctica*, edited by M. R. A. Thomson et al., Cambridge: Cambridge University Press, p. 285–291.

Cooper, R. A., and A. Tulloch (1992), Early Paleozoic terranes in New Zealand and their relationship to the Lachlan Fold Belt, *Tectonophysics, 214,* 129–144.

Davey F. J., and G. Brancolini (1995), The Late Mesozoic and Cenozoic structural setting of the Ross Sea region, in *Geology and Seismic Stratigraphy of the Antarctic Margin*, edited by A. K. Cooper, P. F. Barker, and G. Brancolini, *Antarct. Res. Ser. AGU 68*, 167–182.

D'Lemos, R. S., M. Brown, and R. A. Strachan (1992), Granite magma generation, ascent and emplacement within a transpressional orogen, *J. Geol. Soc. London, 149*, 487–490.

Ferraccioli, F., E. Bozzo and D. Damaske, (2002), Aeromagnetic signatures over western Marie Byrd Land provide insight into magmatic arc basement, mafic magmatism and structure of the eastern Ross Sea rift flank, *Tectonophysics, 347,* 139–65.

Fitzgerald, P. G., and S. L. Baldwin (1997), Detachment fault model for the Evolution of the Ross Embayment, in *The Antarctic Region: Geological Evolution and Processes*, edited by C. A. Ricci, pp. 555–564, *Terra Antarctica* Publication, Siena, Italy.

Forster, M.A., and G.S. Lister (2003), Cretaceous metamorphic core complexes in the Otago Schist, New Zealand, *Austr. J. Earth Sci., 50,* 181–198.

Foster, D. A., D. R. Gray, and C. Spaggiari (2005), Timing of subduction and exhumation along the Cambrian East Gondwana margin and the formation of Paleozoic back-arc basins, *GSA Bulle*tin, *117*, 105–116.

Gibson, G. M., I. McDougall, and T. R. Ireland (1988), Age constraints on metamorphism and the development of a metamorphic core complex in Fiordland, southern New Zealand, *Geology*, *16*, 405–408.

Gibson, G. M., and T.R. Ireland (1996), Extension of Delamerian (Ross) Orogen into western New Zealand; evidence from zircon ages and implications for crustal growth along the Pacific margin of Gondwana, *Geology, 24,* 1087–1090.

Glazner, A. F. (1991), Plutonism, oblique subduction and continental growth: An example from the Mesozoic of California, *Geology, 19*, 784–786.

Glen, R. A. (2005), The Tasmanides of eastern Australia, *Terrane Processes at the Margin of Gondwana*, edited by A. Vaughan et al., Geol. Soc. London Spec. Pub. 246, pp. 23–96, Geol. Soc., London.

Grocott, J., M. Brown, R. D. Dallmeyer, G. K. Taylor, and P. J. Trelor (1994), Mechanisms of continental growth: An example from the Andean plate-boundary zone, *Geology*, *22*, 391–394.

Guo, J., S. Y. O'Reilly, and W. L. Griffin (1996), Zircon inclusions in corundum megacrysts: I. Trace element geochemistry and clues to the origin of corundum megacrysts in alkali basalts, *Geochim. Cosmochim. Acta, 60*, 2347–2363.

Hasalová, P., K. Schulmann, O. Lexa, P. Stipska, F. Hrouda, S. Ulrich, J. Haloda, and P. Tycova (2008), Origin of migmatites by deformation-enhanced melt infiltration of orthogneiss: a new model based on quantitative microstructural analysis, *J. Metamorph. Geol.*, *26*, 29–53.

Hollis, J. A., G. L. Clarke, K. A. Klepeis, N. R. Daczko, and T. R. Ireland (2004), The regional significance of Cretaceous magmatism and metamorphism in Fiordland, New Zealand, from U-Pb zircon geochronology, *J. Metamorph. Geol., 22,* 607–627.

Holness, M. B. (2008), Decoding migmatite microstructures, *Mineralogical Association of Canada Short Course 38*, Quebec City, Quebec, 57–76.

Hoskin, P. W. O. (1998), Minor and trace element analysis of natural zircon (ZrSiO4) by SIMS and laser ablation ICPMS: a consideration and comparison of two broadly competitive techniques, *J. Trace Microprobe Tech., 16*, 301–326.

Ireland, T. R., and F. Wlotzka (1992), The oldest zircons in the solar system, *Earth Plan. Sci. Let., 109*, 1–10.

Ireland, T. R., T. Flottmann, C. M. Fanning, G. M. Gibson, and W. V. Preiss (1998), Development of the early Paleozoic Pacific margin of Gondwana from detrital-zircon ages across the Delamerian orogen, *Geology, 26,* 243–246.

Ireland, T. R., and G. M. Gibson (1998), SHRIMP monazite and zircon geochronology of high-grade metamorphism in New Zealand, *J. Metamorph. Geol., 16,* 149–167.

Kimbrough, D. L., and A. J. Tulloch (1989), Early Cretaceous age of orthogneiss from the Charleston Metamorphic Group, New Zealand, *Earth Planet. Sci. Lett., 95,* 130–140.

Korhonen, F. J., M. Brown, and Siddoway, C. S. (2007), Unraveling polyphase high-grade metamorphism and anatexis in the Fosdick migmatite dome, West Antarctica, using mineral equilibria modeling and in situ monazite geochronology: Eos Trans. AGU Fall Meet. Suppl., 88, abstract V04-4536.

Korhonen, F. J., S. Saito, M. Brown, and C. S. Siddoway (*in revision*), Modeling multiple melt loss events in the evolution of an active continental margin, *Lithos*.

Korhonen, F., S. Saito, M. Brown, C. S. Siddoway, and J. Day (*in review*), Multiple generations of granite in the Fosdick Mountains, Marie Byrd Land, West Antarctica: Implications for polyphase intracrustal differentiation in a continental margin setting, *Journal of Petrology*.

Kula, J., A. J. Tulloch, T. L. Spell, and M. L. Wells (2007), Two-stage rifting of Zealandia-Australia-Antarctica: Evidence from 40Ar/39Ar thermochronometry of

the Sisters shear zone, Stewart Island, New Zealand, *Geology, 35,* 411-414, doi: 10.1130/G23432A.1.

Leitch, A. M., and R. F. Weinberg, (2002), Modeling granite migration be mesoscale pervasive flow, *Earth Planet. Sci. Lett.*, *200*, 131–146.

Ludwig, K. R. (2001), SQUID 1.02, A User's Manual; Berkeley Geochronology Center Special Publication. No. 2, 2455 Ridge Road, Berkeley, CA 94709, USA.

Ludwig, K. R. (2003), User's Manual for Isoplot/Ex, Version 3.0, A geochronological toolkit for Microsoft Excel; Berkeley Geochronology Center Special Publication. No. 4, 2455 Ridge Road, Berkeley, CA 94709, USA.

Luyendyk, B. (1995), Hypothesis for Cretaceous Rifting of East Gondwana Caused by Subducted Slab Capture: Geology, 23, 373-376.

Luyendyk, B. P., C. C. Sorlien, D. S. Wilson, L. R. Bartek and C. S. Siddoway (2001), Structural and tectonic evolution of the Ross Sea Rift in the Cape Colbeck region, eastern Ross Sea, Antarctica, *Tectonics, 20,* 933–958.

Luyendyk, B. P., D. S. Wilson, and C. S. Siddoway (2003), The eastern margin of the Ross Sea Rift in western Marie Byrd Land: Crustal structure and tectonic development, *Geochem. Geophys. Geosys.,* doi:10.1029/2002GC000462.

Marchildon, N., and M. Brown (2001), Melt segregation in late syn-tectonic anatectic migmatites: an example from the Onawa Contact Aureole, Maine, U.S.A., *Phys. Chem. Earth (A)*, *26*, 225–229.

Marchildon, N., and M. Brown (2002), Grain-scale melt distribution in two contact aureole rocks: implication for controls on melt localization and deformation, *J. Metamorph. Geol.*, *20*, 381–396.

Marchildon, N., and M. Brown (2003), Spatial distribution of melt-bearing structures in anatectic rocks from southern Brittany: implications for melt-transfer at grain-to orogen-scale, *Tectonophysics*, *364*, 215–235.

Maas, R., P. D. Kinny, I. S. Williams, D. O. Froude, and W. Compston (1992), The Earth's oldest known crust: a geochronological and geochemical study of 3900–4200 Ma old detrital zircons from Narryer and Jack Hills, Western Australia, *Geochem. Cosmochim. Acta 56*, 1281–1300.

McFadden, R., C. S. Siddoway, C. Teyssier, C. M. Fanning, and S. C. Kruckenberg (2007), Cretaceous oblique detachment tectonics in the Fosdick Mountains, Marie Byrd Land, Antarctica, in *Antarctica: A Keystone in a Changing World - Online Proceedings of the 10th ISAES*, edited by A. K. Cooper, C. R. Raymond and ISAES Editorial Team, USGS Open-File Report 2007-1047, Short Research Paper 059, 4 pp.; doi: 10.3133/of2007-1047.srp047.

McKenzie, D., F. Nimmo, J. Jackson, P. B. Gans, and E. L. Miller (2000), Characteristics and consequences of flow in the crust, *J. Geophys. Res, 105*, 11029–11046.

Milord, I., E. W. Sawyer, and M. Brown (2001), Formation of diatexite migmatite and granite magma during anatexis of semi-pelitic metasedimentary rocks: an example from St. Malo, France, *J. Petrol*., *42,* 487–505.

Mortimer, N., A. J. Tulloch, R. N. Spark, N. W. Walker, E. Ladley, A. Allibone, and D. L. Kimbrough (1999), Overview of the Median Batholith, New Zealand: a new interpretation of the geology of the Median Tectonic Zone and adjacent rocks, *J. African Earth Sci.*, *29*, 257–268.

Mortimer, N., K. Hoernle, F. Hauff, J.M. Palin, W. J. Dunlap, R. Werner, and K. Faure (2006), New constraints on the age and evolution of the Wishbone Ridge, southwest Pacific Cretaceous microplates, and Zealandia-West Antarctica breakup, *Geology*, *3*, 185–188.

Muir, R., T. R. Ireland, S. D. Weaver, and J. D. Bradshaw (1994), Ion microprobe U-Pb zircon geochronology of granitic magmatism in the Western Province of the South Island, New Zealand: *Chem. Geol.*, *113*, 171–189.

Muir, R. J., T. R. Ireland, S. D. Weaver and J. D. Bradshaw (1996), Ion microprobe dating of Paleozoic granitoids: Devonian magmatism in New Zealand and correlations with Australia and Antarctica: *Chem. Geol.*, 127, 191–210.

Muir, R. J., T. R. Ireland, S. D. Weaver, J. D. Bradshaw, T. E. Waight, R. Jongens, and G. N. Eby (1997), SHRIMP U-Pb geochronology of Cretaceous magmatism in northwest Nelson-Westland, South Island, New Zealand, *New Zealand J. Geol. Geophys., 40,* 453–463.

Muir, R., T. R. Ireland, S. D. Weaver, J. D. Bradshaw, J. D., J. A. Evans, G. N. Eby, and D. Shelley (1998), Geochronology and geochemistry of a Mesozoic magmatic arc system, Fiordland, New Zealand, *J. Geol. Soc. London, 155,* 1037–1053.

Mukasa, S. B., and I. W. D. Dalziel (2000), Marie Byrd Land, West Antarctica: Evolution of Gondwana's Pacific margin constrained by zircon U-Pb geochronology and feldspar common-Pb isotopic compositions: *Bull. Geol. Soc. Am*., *112*, 611–627.

Mulchrone, K. F., S. Grogan, and P. De (2005), The relationship between magmatic tiling, fluid flow and crystal fraction, *J. Struct. Geol., 27*, 179–197.

Nelson, K.D., W. Zhao, L. D. Brown, J. Kuo, J. Che, X. Liu, S. L. Klemperer, Y. Makovsky, R. Meissner, J. Mechie, R. Kind, F. Wenzel, J. Ni, J. Nabelek, C. Leshou, H. Tan, W. Wei, A. G. Jones, J. Booker, M. Unsworth, W. S. F. Kidd, M. Hauck, D. Alsdorf, A. Ross, M. Cogan, C. Wu, E. Sandoval, and M. Edwards (1996), Partially molten middle crust beneath southern Tibet: Synthesis of Project INDEPTH results, *Science*, 274, 1684–1688.

O'Halloran, G. J., and P. F. Rey (1999), Isostatic constraints on the Central Victorian lower crust: Implications for the tectonic evolution of the Lachlan Fold Belt, *Aus. J. Earth Sci., 46*, 633–639.

Olsen, S. N., B. D. Marsh, and L. P. Baumgartner (2004), Modelling mid-crustal migmatite terrains as feeder zones for granite plutons: the competing dynamics of melt transfer by bulk versus porous flow, *Trans. Royal Soc. Edinburgh: Earth Sciences, 95,* 49–58.

Pankhurst, R. J., S. D. Weaver, J. D. Bradshaw, B. C. Storey, and T. R. Ireland (1998), Geochronology and geochemistry of pre-Jurassic superterranes in Marie Byrd Land, Antarctica, *J. Geophys. Res*., *103*, 2529–2547.

Pavlis, T. L. (1996), Fabric development in syn-tectonic intrusive sheets as a consequence of melt-dominated flow and thermal softening of the crust, *Tectonophys.*, *253*, 1–31.

Philpotts, A. R., J. Shi, and C. Brustman (1998), Role of plagioclase crystal chains in the differentiation of partly crystallized basaltic magma, *Nature, 395*, 343–346.

Richard, S. M. (1992), Structure and Cooling History of the Fosdick Metamorphic Complex, Marie Byrd Land, West Antarctica, in *Recent Progress in Antarctic Earth Science*, edited by Y. Yoshida et al., pp. 289–294, *Terra* Publications, Tokyo, Japan.

Richard, S. M., C. H. Smith, Kimbrough, D. K., Fitzgerald, G., B. P. Luyendyk, and M. O. McWilliams (1994), Cooling history of the northern Ford Ranges, Marie Byrd Land, West Antarctica, *Tectonics*, *13*, 837–857.

Sambridge, M. S., and W. Compston (1994), Mixture modeling of multicomponent data sets with application to ion-probe zircon ages, *Earth Planet. Sci. Lett., 128*, 373–390.

Sawyer, E. W. (1996), Melt segregation and magma flow in migmatites: Implications for the generation of granite magmas, *Trans. Royal Soc. Edinburgh: Earth Sciences, 87*, 85–94.

Sawyer, E. W. (1998), Formation and evolution of granite magma during crustal reworking: The significance of diatexites, *J. Petrol., 39*, 1147–1167.

Sawyer, E. W. (2001), Melt segregation in the continental crust: distribution and movement of melt in anatectic rocks, *J. Metamorph. Geol*., *19*, 291–309.

Sawyer, E. W. (2008), Working with migmatites: nomenclature for the constituent parts, *Min. Assc. Canada Short Course 38*, Quebec City, Quebec, 1–28.

Scott, J. M., and A. F. Cooper (2006), Early Cretaceous extensional exhumation of the lower crust of a magmatic arc: Evidence from the Mount Irene Shear Zone, Fiordland, New Zealand, *Tectonics*, *25,* doi.10.1029/2005TC001890.

Schilling, F. R., and G. M. Partzsch (2001), Quantifying partial melt fraction in the crust beneath the central Andes and the Tibetan Plateau, *Phys. Chem. Earth, 26*, 239–246.

Siddoway, C. S., S. L. Baldwin, P. G. Fitzgerald, C. M. Fanning, and B. P. Luyendyk (2004a), Ross Sea mylonites and the timing of intracontinental extension within the West Antarctic rift system, *Geology*, *32,* 57–60.

Siddoway, C. S., S. M. Richard, C. M. Fanning, and B. P. Luyendyk (2004b), Origin and emplacement of a middle Cretaceous gneiss dome, Fosdick Mountains, West Antarctica, *Gneiss Domes in Orogeny*, edited by D. L. Whitney et al., Geol. Soc. Am. Spec. Paper 380, 267–294, Boulder, Colorado, USA.

Siddoway, C. S., L. C. Sass III, and R. Esser (2005), Kinematic history of Marie Byrd Land terrane, West Antarctica: Direct evidence from Cretaceous mafic dykes, *Terrane Processes at the Margin of Gondwana*, edited by A. Vaughan et al., Geol. Soc. London Spec. Pub. 246, 417-438, Geological Society, London.

Siddoway, C. S., C. M. Fanning, S. C. Kruckenberg, and S. C. Fadrhonc (2006), U-Pb SHRIMP investigation of the timing and duration of melt production and

migration in a Pacific margin gneiss dome, Fosdick Mountains, Antarctica: *Eos Trans. AGU* Fall Meet. Suppl., *87*, Abstract V23D-0661.

Siddoway, C. S. (2008), Tectonics of the West Antarctic rift system: New light on the history and dynamics of distributed intracontinental extension, edited by A. K. Cooper et al., *Antarctica: A Keystone in a Changing World*, National Academy of Sciences.

Siddoway, C. S., and C. M. Fanning, (2009), SHRIMP U-Pb zircon geochronology of a migmatite-granite complex in West Antarctica, with bearing on the character and extent of Paleozoic tectonism on the East Gondwana margin, *Tectonophyiscs,* doi: 10.1016/j.tecto.2009.04.021.

Soula, J. P. Debat, S. Brusset, G. Bessiere, F. Christophoul, and J. Deramond (2001), Thrust-related, diapiric, and extensional doming in a frontal orogenic wedge: Example of the Montagne Noire, Southern French Hercynian Belt, *J. Struct. Geol., 23*, 1677–1699. doi: 10.1016/S0191-8141(01)00021-9.

Squire, R. J., and C. J. Wilson (2005), Interaction between collisional orogenesis and convergent-margin processes: evolution of the Cambrian proto-pacific margin of East Gondwana, *J. Geol. Soc. London, 162*, 749–761.

Storey, B., T. Leat, S. D. Weaver, R. J. Pankhurst, J. D. Bradshaw, and S. Kelley (1999), Mantle plumes and Antarctica-New Zealand rifting: evidence from mid-Cretaceous mafic dykes, *J. Geol. Soc. London, 156*, 659–671.

Sutherland, R., and C. Hollis (2001), Cretaceous demise of the Moa plate and strike-slip motion at the Gondwana margin, *Geology, 29,* 279–282.

Tera, F., and G. Wasserberg (1972), U-Th-Pb systematics in three Apollo 14 basalts and the problem of initial Pb in lunar rocks, *Earth Planet. Sci. Lett., 14*, 281–304.

Teyssier, C., and D. L. Whitney (2002), Gneiss domes and orogeny, *Geology, 30*, 1139–1142.

Teyssier. C., E. C. Ferre, D. L. Whitney, B. Norlander, O. Vanderhaeghe, and D. Parkinson (2005), Flow of partially molten crust and origin of detachments during collapse of the Cordilleran Orogen, *in High-strain zones; structures and physical properties, Geol. Soc. Sp. Pub., 245*, 39–64.

Tikoff, B. and C. Teyssier (1992), Crustal-scale, en echelon "P-shear" tensional bridges: A possible solution to the batholithic room problem, *Geology, 20*, 927–930.

Tulloch A. J., and D. L. Kimbrough (1989), The Paparoa metamorphic core complex, New Zealand: Cretaceous extension associated with fragmentation of the Pacific margin of Gondwana, *Tectonics, 8,* 1217–1234.

Tulloch A. J., and D. L. Kimbrough (2003), Paired plutonic belts in convergent margins and the development of high Na, Al, Sr, low Y magmatism: the Peninsular Ranges Batholith of California and the Median Batholith of New Zealand, *Geol. Soc. Am. Spec. Publ. 374,* 275–295.

Tulloch, A. J., D. L. Kimbrough, and R. A. Wood (1991), Carboniferous granite basement dredged from a site on the southwest margin of the Challenger Plateau, Tasman Sea, *New Zealand J. Geol. Geophys. 34*, 121–126.

Tulloch, A. J., Beggs, M., Kula, J., Spell, T. and Mortimer, N. (2006), Cordillera Zealandia, the Sisters Shear Zone and their influence on the early development of the Great South Basin, Field Developments and Production/Keynote paper.

Vanderhaeghe, O. (1999), Pervasive melt migration from migmatites to leucogranite in the Shuswap metamorphic core complex, Canada: control of regional deformation, *Tectonophys., 312,* 35–55.

Vanderhaeghe, O. (2001), Melt segregation, pervasive melt migration and magma mobility in the continental crust: the structural record from pores to orogens: *Phys. Chem. Earth, (A), 26*, 213–223.

Vernon, R. H., G. L. Clarke, and W. J. Collins (1990), Local, mid-crustal granulite facies metamorphism and melting: and example in the Mount Stafford area, central Australia, *High Temperature Metamorphism and Crustal Anatexis*, edited by J. R. Ashworth, and M. Brown, Unwin-Hyman, London, 272–319.

Vincenzo, G. D., R. Carosi, R. Palmer, and M. Tiepolo (2007), A comparative U-Th-Pb (zircon-monazite) and ^{40}Ar-^{39}Ar (muscovite-biotite) study of shear zones in northern Victoria Land (Antarctica): implications for geochronology and localized reworking of the Ross Orogen, *J. Metamorph. Geol. 25*, 605–630, doi: 10.1111/j.1525-1314.2007.00717.x.

Wade, F. A., C. A. Cathey, and J. B. Oldham (1978), Reconnaissance geologic map of the Gutenko Nunataks quadrangle, Marie Byrd Land, Antarctica: USARP Antarctic Geological Map A-11: Reston, Virginia, U. S. Geological Survey, scale 1:250,000.

Wandres, A. M. and J. D. Bradshaw (2005), New Zealand tectonostratigraphy and implications from conglomeratic rocks for the configuration of the SW Pacific margin of Gondwana, in *Terrane Processes at the Margin of Gondwana*, edited by A. Vaughan et al., Geol. Soc. London, Spec. Publ. 246, 179–216.

Weaver, S. D., J. D. Bradshaw, and C. J. Adams (1991), Granitoids of the Ford Ranges, Marie Byrd Land, Antarctica, in *Geological Evolution of Antarctica*, edited by M. R. A. Thomson et al., pp. 345–351, Cambridge Univ. Press, Cambridge, U.K.

Weaver, S. D., C. J. Adams, R. J. Pankhurst, and I. L. Gibson (1992), Granites of Edward VII Peninsula, Marie Byrd Land: anorogenic magmatism related to Antarctic-New Zealand rifting, in *Proceedings of the Second Hutton Symposium on the Origin of Granites and Related Rocks,* edited by E. Brown and B. W. Chappell, Trans. Royal Soc. Edinburgh - Earth Sciences, pp. 281-290, The Geological Society, London.

Weaver, S. D., B. C. Storey, R. J. Pankhurst, S. B. Mukasa, V. Divenere, and J. D. Bradshaw (1994), Antarctic-New Zealand rifting and Marie Byrd Land lithospheric magmatism linked to ridge subduction and mantle plume activity, *Geology, 22,* 811–814.

Weinberg, R. F. (2006), Melt segregation structures in granitic plutons, *Geology, 34,* 305–308.

Weinberg, R. F., and M. P. Searle (1998), The Pangong Injection Complex Indian Karakoram: a case of pervasive granite flow through hot viscous crust, *J. Geol. Soc. London*, 1*55*, 883–891.

Whittington, A. G., and P. J. Treloar (2002), Crustal anatexis and its relation to the exhumation of collisional orogenic belts, with particular reference to the Himalaya, *Mineral. Mag., 66*, 53–91.

Williams, I. S. (1998), U-Th-Pb Geochronology by Ion Microprobe, edited by M. A. McKibben, W. C. Shanks, and W. I. Ridley, *Applications of microanalytical techniques to understanding mineralizing processes: Reviews in Economic Geology, 7*, 1–35.

Figure Captions

Figure 3.1. (a) Geographical map of West Antarctica (after Pankhurst et al., 1998). (b) Tectonic plate reconstruction of the East Gondwana margin at 95 Ma, modified from Tulloch et al. (2006). The locations of detachment structures are shown as dark gray ovals. The long axes of the ovals are parallel to the stretching direction in the detachments. Cape Colbeck (Siddoway et al., 2004a); DSDP 270 (Deep sea drill core: Fitzgerald and Baldwin, 1997); Paparoa complex (Tulloch and Kimbrough, 1989); Fiordland (Gibson et al., 1988; Scott and Cooper, 2006); and Sisters Shear zone (Tulloch et al., 2006; Kula et al., 2007).

Figure 3.2. Geologic map of the Fosdick Mountains migmatite-cored gneiss dome and the Chester Mountains (after Siddoway et al., 2004b). The geographic location of the

Fosdick Mountains in West Antarctica is shown in the map legend. South Fosdick Detachment zone is shown in grey, with arrows to represent the lineation trend for the zone. Dashed red lines represent mapped foliation trajectories. U-Pb SHRIMP ages are given for sample localities described in the text. A-A', B-B', and C-C' are the locations of the cross-sections in Fig. 3. Stereographic projections with kamb contours at a contour interval (c.i.) of 2 sigma are displayed. The projections summarize poles to foliation data from three regions of the Fosdick Mountains. (a) Ochs glacier in the west; (b) Mt. Avers in the central part; and (c) Bitgood to Bird Bluff in the east. Equal area stereographic diagrams were made with Stereonet v.6.3.3, by Richard Allmendinger.

Figure 3.3. Geologic cross-sections of the Fosdick Mountains migmatite-cored gneiss dome. Scale: 1 cm = 5 km, with no vertical exaggeration. The residual paragneiss (dark gray) is the deepest unit, and forms thin layers and coherent blocks. The Ford orthogneiss (blue) intruded the paragneisses and forms subhorizontal layers. The leucogranite sheeted complex (pink) overlies the paragneisses and orthogneisses, coalesced below the SFD, and is thicker to the East. The Mt. Richardson orthogneiss (grey) in the SFD is folded and has a strong foliation. Ford Granodiorite (light blue) is a massive unit that forms the hanging wall of the Fosdick dome. Byrd Coast Granite (red) plutons intrude the hanging wall and the SFD. A diorite (green) pluton intrudes the orthogneisses and paragneisses on Mt. Iphigene. (a) Cross-section from A-A'. (b) Cross-section from B-B'. (c) Cross-section from C-C'.

Figure 3.4. (a) Cliff-face sketch of the east face of Mt. Iphigene showing the shallow layering and folded layering of the residual paragneiss, the orthogneiss metaplutonic complex, and the leucogranitic sheeted complex. The residual paragneiss and orthogneiss units are intruded by an integrated network of granite in dilatant sites, as well as folded, boudinaged, and disrupted diorite and amphibolite dikes and sills. (b) Cliff-face photographic stitch of the east face of Mt. Iphigene. Photos by S. Kruckenberg.

Figure 3.5. Photos that record evidence of former melt-presence from the km-scale to the mm-scale. (a) Photo of residual paragneiss (dark brown) with interlayered leucogranite (light grey) that forms a concentric upright fold. Limbs of the concentric fold display small-scale folding. (b) Photo of Ford orthogneiss of Mt. Lockhart. Migmatitic Ford Granodiorite (grey) with thin, laterally continuous paragneiss layers (dark brown) and boudinaged mafic dikes (medium and dark grey). Cretaceous leucogranite (light grey) form concordant layers with granite in the inter-boudin regions and shear bands. Photo by C. S. Siddoway. (c) Concordant to discordant leucogranite (light grey) within migmatized Ford Granodiorite (gray), and residual paragneiss (dark brown) of Mt. Bitgood. The granitic body that crosscuts the foliation is a dike. The cliff is ~350 m in height. Photo by C. S. Siddoway. (d) Photo of leucogranite sheeted complex (light yellow) and paragneiss (dark brown), with minor orthogneiss layers (gray). Crosscutting the compositional layering are outcrop-scale low angle normal sense shear bands that commonly contain granite. Dikes within leucogranite layers are boudinaged and buckled. Enclaves are generally elongate and parallel to the foliation.

Geologists are circled for scale. Photo by F. McCarthy. (e, f) Photomicrographs of granite with euhedral feldspars from a discordant shear band within the SFD at Mt. Richardson. (e) Optically continuous quartz fills interstices and forms grain boundary films (arrows), two indications of former presence of melt (Holness, 2008). (f) Image shows optically uniform quartz in interstices between lamellar twinned plagioclase grains. Plagioclase contacts are irregular suggesting impingement at grain to grain contacts; possible evidence that rigid grains held open a porosity network that allowed migration of anatectic melt.

Figure 3.6. Schematic block diagram of the SFD and footwall rock associations during the Cretaceous. Diagram shows the distribution of structures and regions of granite accumulation. Stereographic projections from the Fosdick dome display data points and kamb contours with a 2 sigma contour interval. Symbols represent plotted field data as shown on figure. a) Fold hinges and determined fold axes from Mt. Avers have a preferred NE-SW orientation with a dominant orientation of 15, 244. b) Lineations from Mt. Avers have a similar preferred orientation and a dominant orientation of 10, 235. c) Lineations from the Ochs glacier region have considerable scatter, however, the predominant orientation is 10, 245. d) Lineations from the Mt. Bitgood-Bird Bluff region are less common, consistently shallowly plunging, and have a NE-SW preferred orientation. The dominant orientation is 07, 250. e) Sparse fold hinges from the SFD record an ENE-WSW trend with a dominant orientation of 15, 080. f) Lineations from the SFD record two major groups. The overall mineral stretching lineation is 15, 225, and a secondary orientation is 17, 080, which represents a

lineation related to crenulation. Equal area stereographic projections were made with Stereonet v.6.3.3., by Richard Allmendinger.

Figure 3.7. Field photographs of granite in structural sites and late to post-tectonic diorite dikes sampled for U-Pb SHRIMP geochronology. (a) Diorite dike that cuts across compositional layering and foliation, but is folded and interdigitated with neighboring granite. Zircon sample C5-Is54 comes from the granite and titanite sample C5-I3 is from the diorite dike. Photo by C. S. Siddoway. (b) Diorite dike that cuts the Ford suite metaplutonic complex of Marujupu Peak. Titanite sample C5-Mj70A was collected from the dike. Photo by C. S. Siddoway. (c, d) Photo and interpretation of the sample site for 3 U-Pb zircon samples, M5-R136 suite, at Mt. Richardson. Biotite granodiorite of the Ford suite is migmatized and now forms sigmoidal boudins that indicate top to the SW normal oblique shear sense. Leucogranite forms concordant layers and exists in inter-boudin necks and shear bands. Photo by R. McFadden. (e) Photo of a tabular, syntectonic granite body within the SFD; the granite lacks visible foliation but passive markers in the granite are deformed. Sample C5-R60B comes from this site, approximately 60 m from the M5-R136 sites. Photo by R. McFadden. (f) Crosscutting dike at Mt. Getz with margins that cut the solid-state fabric. There is a weak magmatic fabric in the dike that parallels its margins. Photo by R. McFadden.

Figure 3.8. Summary diagram for all U-Pb samples that show the duration of zircon and titanite crystallization: Probability density plots with stacked histograms calculated using ISOPLOT (Ludwig, 1999). Weighted mean $^{206}Pb/^{238}U$ age and uncertainty is given at 95% confidence and includes the uncertainty in the U/Pb ratio calibration of

the reference zircon or titanite. (a-d) Data show a 10 myr duration of melt-present deformation and titanite crystallization ages of late to post-tectonic dikes in the Ochs Glacier suite. (e-i) Results from the SFD suite displays 7 myr duration of melt-present deformation, and a zircon crystallization age of post-tectonic dike.

Figure 3.9. CL and BSE images of selected grain types and areas analyzed for SHRIMP U-Pb geochronology. Small numbers refer to grain number designations in Table 1. Large numbers are $^{206}Pb/^{238}U$ ages in Ma for individual area analyses (see Table 1 for corresponding error on area analyses).

Figure 3.10. Tera-Wasserburg concordia diagrams of SHRIMP U-Pb isotopic data. Insets are probability density plots with stacked histograms calculated using ISOPLOT (Ludwig, 1999). Weighted mean $^{206}Pb/^{238}U$ age and uncertainty is given at 95% confidence and includes the uncertainty in the U/Pb ratio calibration of the reference zircon. (a) Granite sheet C5-Is54 and (b) granite sill M5-F57B.

Figure 3.11. Tera-Wasserburg concordia diagrams of SHRIMP U-Pb isotopic data. Insets are probability density plots with stacked histograms calculated using ISOPLOT (Ludwig, 1999). Weighted mean $^{206}Pb/^{238}U$ age and uncertainty is given at 95% confidence and includes the uncertainty in the U/Pb ratio calibration of the reference zircon. (a) biotite granodiorite sigmoidal boudin M5-R136A, (b) granite sill M5-R136C, (c) granite-filled shear band M5-R136B, and (d) syntectonic tabular granite C5-R60B. e) Rare earth element (REE) data from the core and rim of two igneous grains from two zircon populations in sample M5-R136A from the Mt. Richardson granodiorite suite. Data are provided in Table 2. Plot is normalized to chondrite. Grain

1 is from the dominant zircon population of prismatic grains and grain 2 is from the less common population of round grains. Both core and rim analyses record Cretaceous ages. Core and rim analyses for both grains have steeply rising slopes from light REE to heavy REE, with positive Ce and negative Eu anomalies. However, the rim analysis from grain 17 (17.2) has a significantly higher concentration of La and Ce, creating a shallower slope from light REE to heavy REE.

Figure 3.12. (a) Tera-Wasserburg concordia diagrams of SHRIMP U-Pb isotopic data for crosscutting granite dike M5-G174. Insets are probability density plots with stacked histograms calculated using ISOPLOT (Ludwig, 1999). Weighted mean $^{206}Pb/^{238}U$ age and uncertainty is given at 95% confidence and includes the uncertainty in the U/Pb ratio calibration of the reference zircon. (b and c) Tera-Wasserburg concordia diagram of isotopic data from SHRIMP-RG for diorite dikes C5-I3 and C5-Mj70A. Analyses plotted as one-sigma error ellipses. The 3-D linear regression line is shown from the measured $^{204}Pb/^{206}Pb$ ratio for each analysis along with total $^{207}Pb/^{206}Pb$ and $^{238}U/^{206}Pb$ ratios to define a lower concordia intercept.

Figure 3.13. Geologic map pattern interpretation that shows the distribution of structures, regions of granite accumulation, and corresponding SHRIMP U-Pb ages during the Cretaceous. Map shows regions of residual paragneiss that acted as “mega-boudins”, the accumulation of melt in low strain regions, and the coalescence of leucogranite below the SFD.

Figure 3.14. Three-dimensional schematic cross-section of the Cretaceous East Gondwana margin at ca. 100 Ma. Diagram depicts the subduction of hot oceanic lithosphere at the

Phoenix-Pacific ridge (Bradshaw, 1989; Luyendyk, 1995) and back-arc extension (Weaver et al., 1991, 1994; Mukasa and Dalziel, 2000), possibly driven by slab rollback. Cross-section shows the position of continental crust of WANT and Zealandia, and the edge of the East Antarctica, where the Transantarctic Mountains will form. The Fosdick migmatite-cored gneiss dome in WANT and migmatites in NZ suggest there was an extensive melt horizon that caused regionally significant middle to lower crustal flow. Lateral flow of weak partially molten crust is accompanied by brittle deformation in the shallow upper crust. Strain perturbations along the faults allowed localized gravity-driven vertical flow of lower density migmatite and formation of gneiss domes. Asthenospheric upwelling and slab rollback are depicted for plutonism in the magmatic arc, and crustal melting, plutonism, and extension in the backarc.

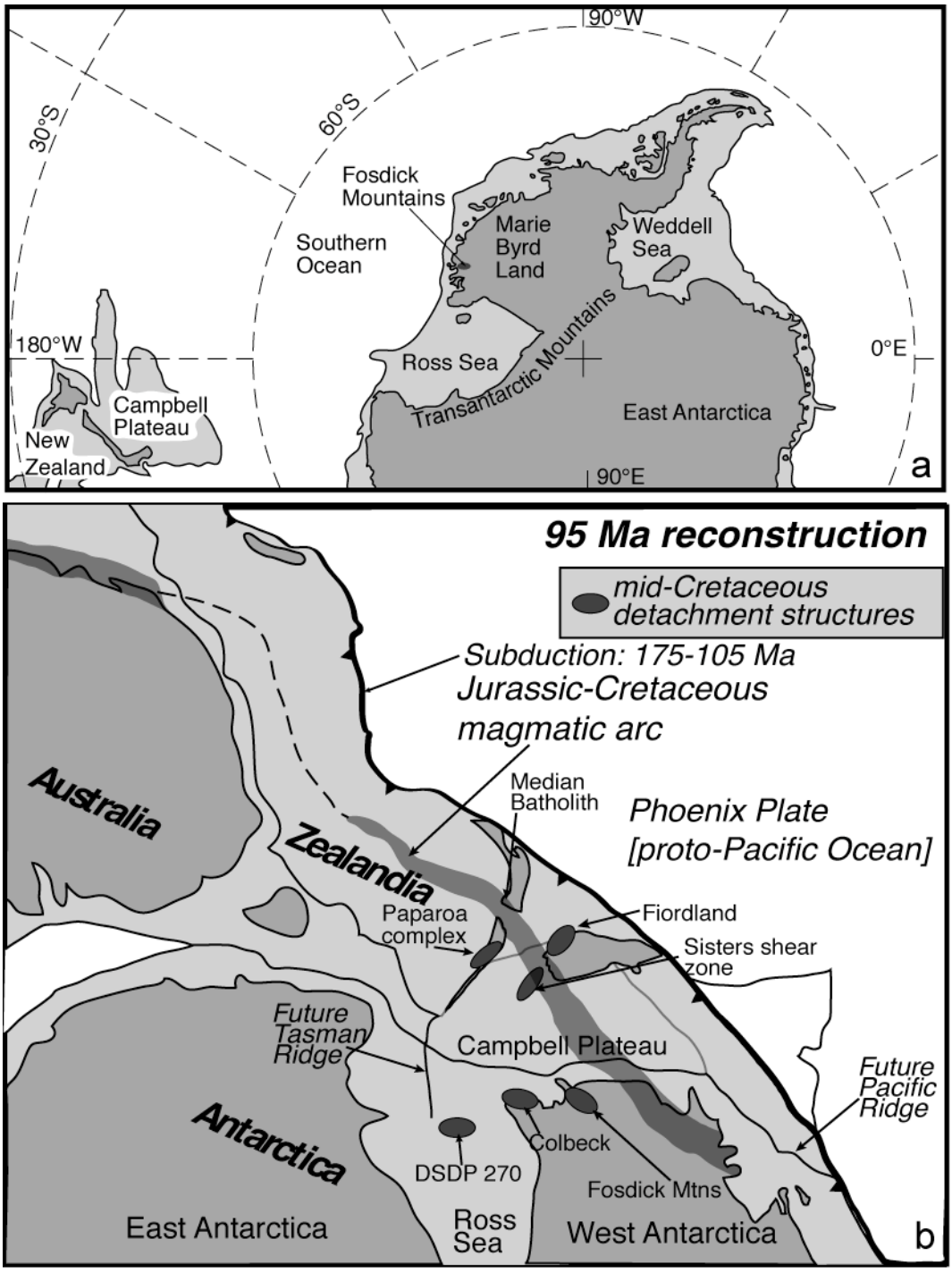

Figure 3.1 Geographic map of West Antarctica and tectonic reconstruction of East Gondwana margin.

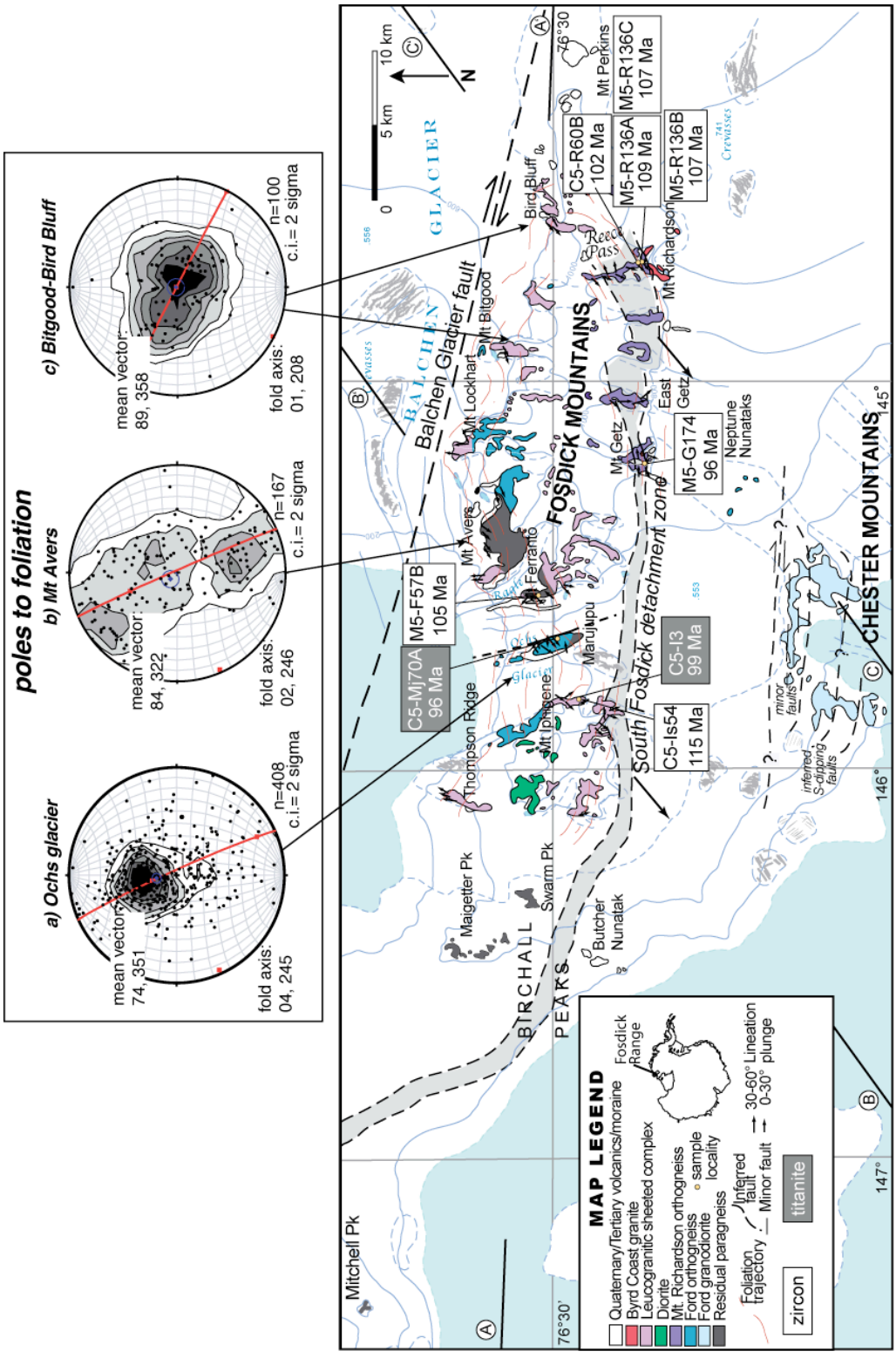

Figure 3.2 Geologic map of the Fosdick Mountains.

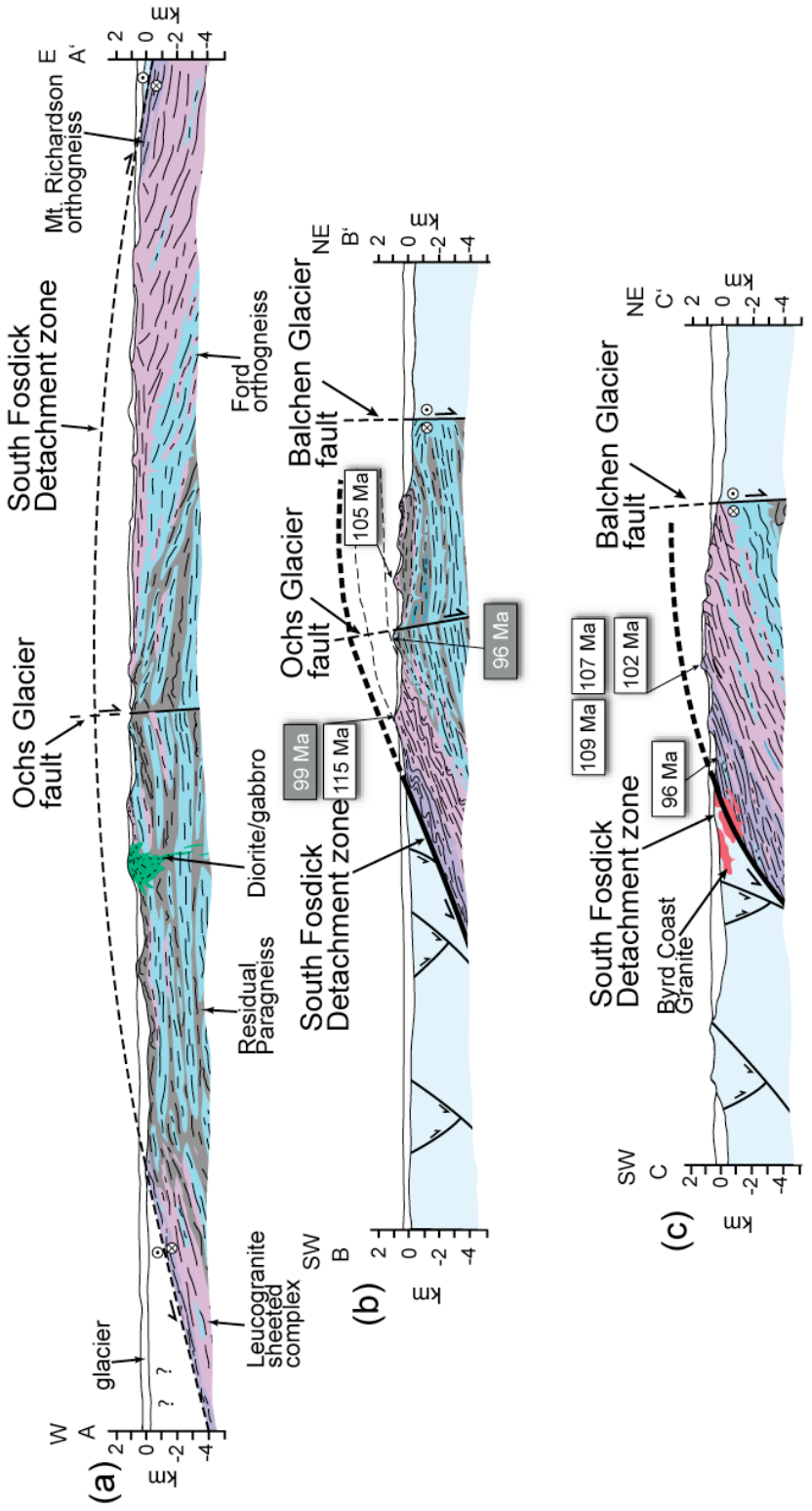

Figure 3.3 Geologic cross-sections of the Fosdick Mountains.

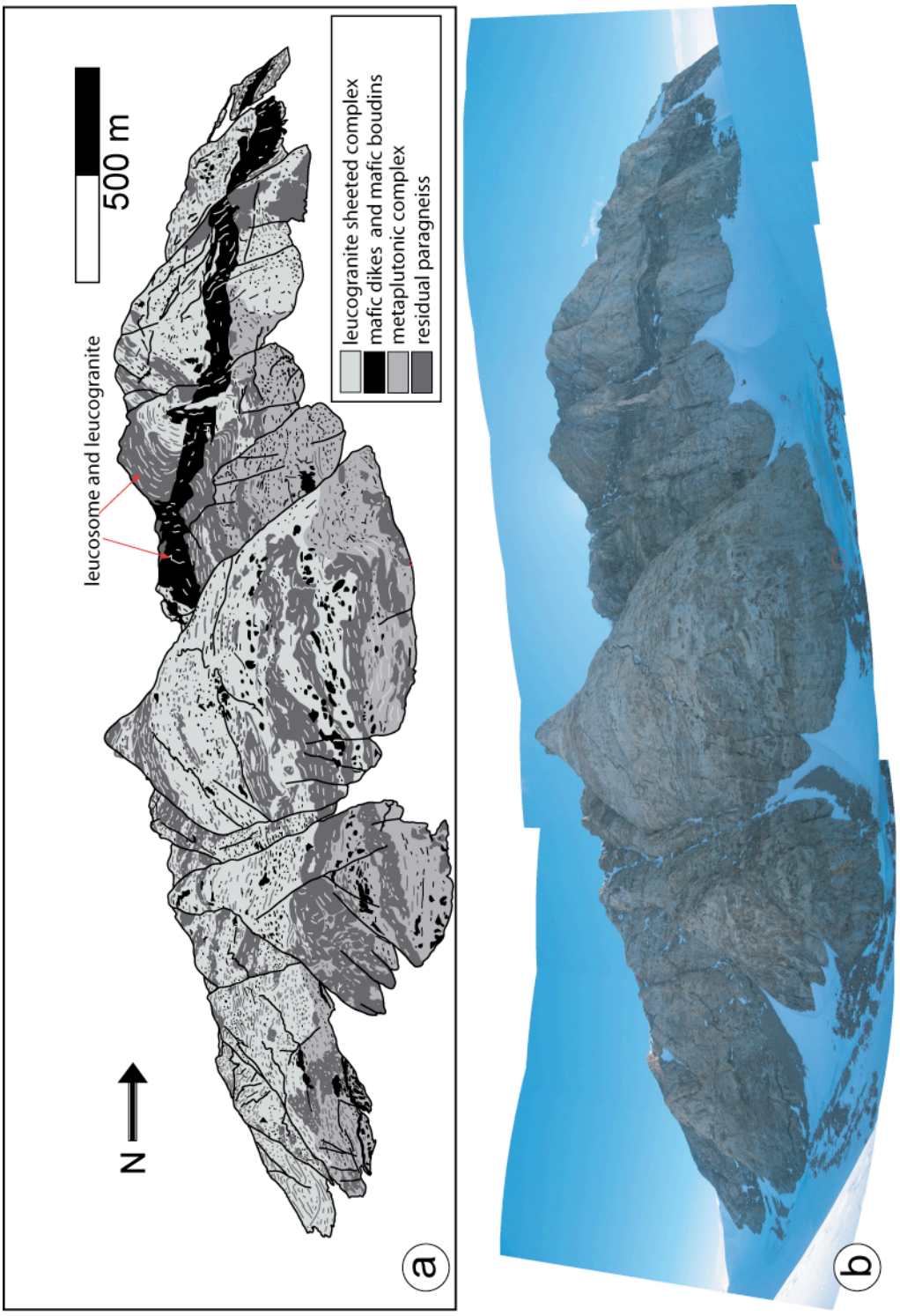

Figure 3.4 Cliff-face sketch and photo of Mt. Iphigene.

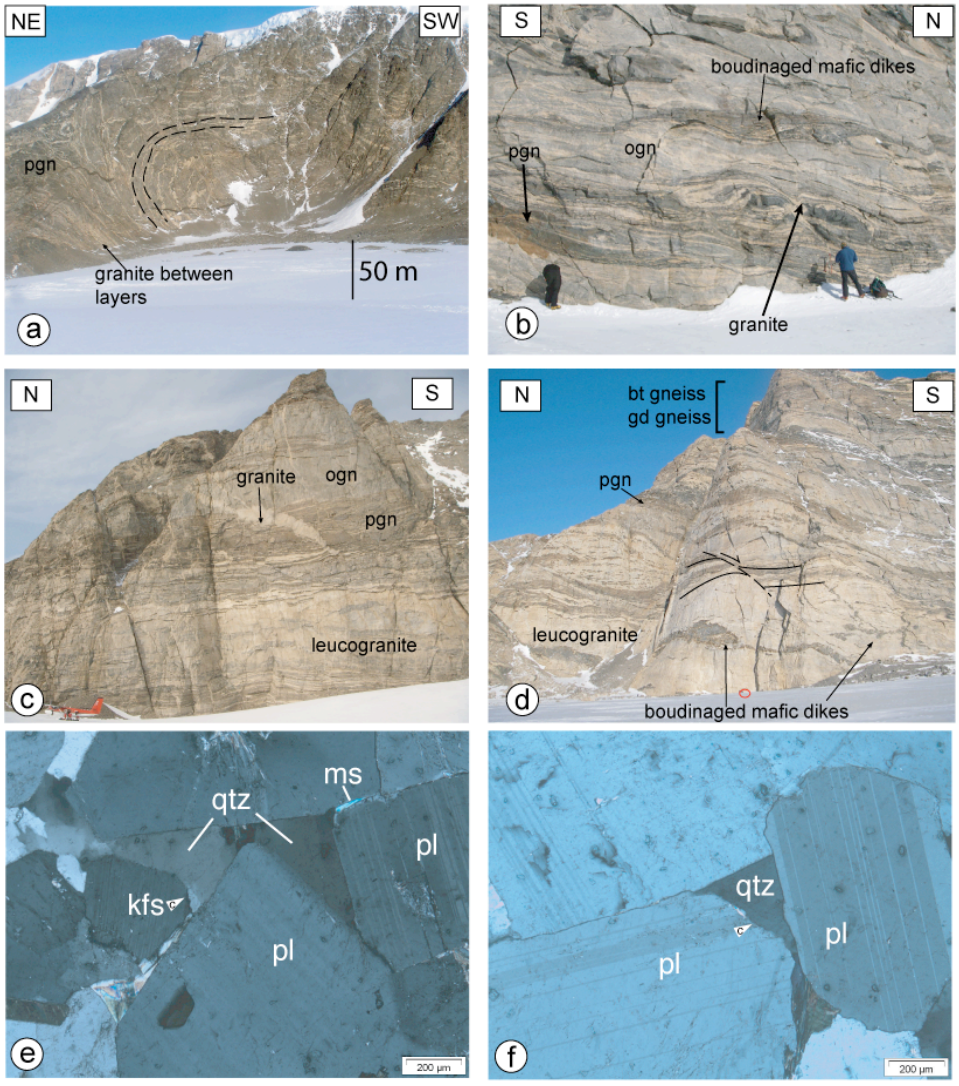

Figure 3.5 Photos of melt-present deformation.

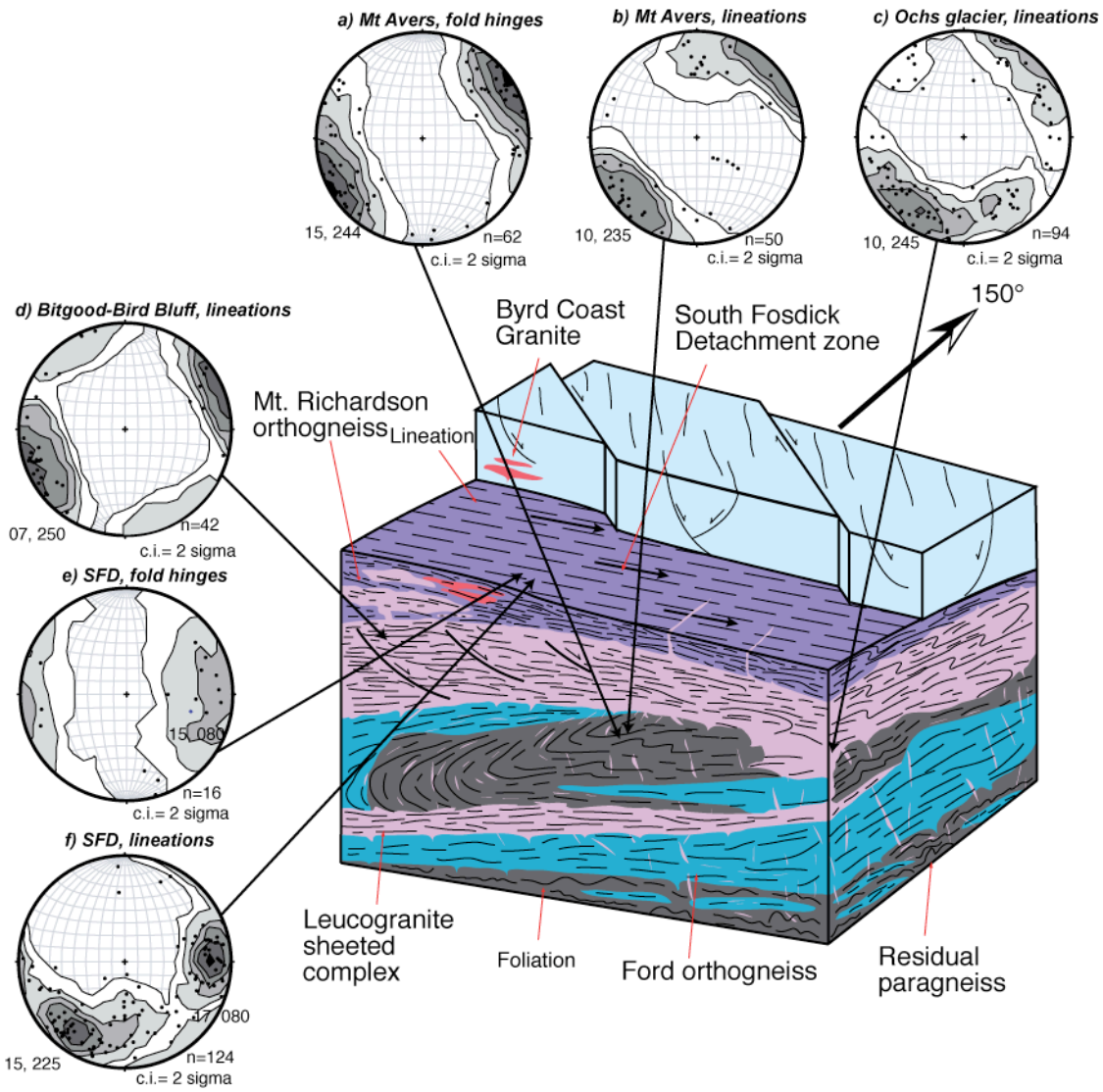

Figure 3.6 Block diagram of the Fosdick dome and stereonets of structural data.

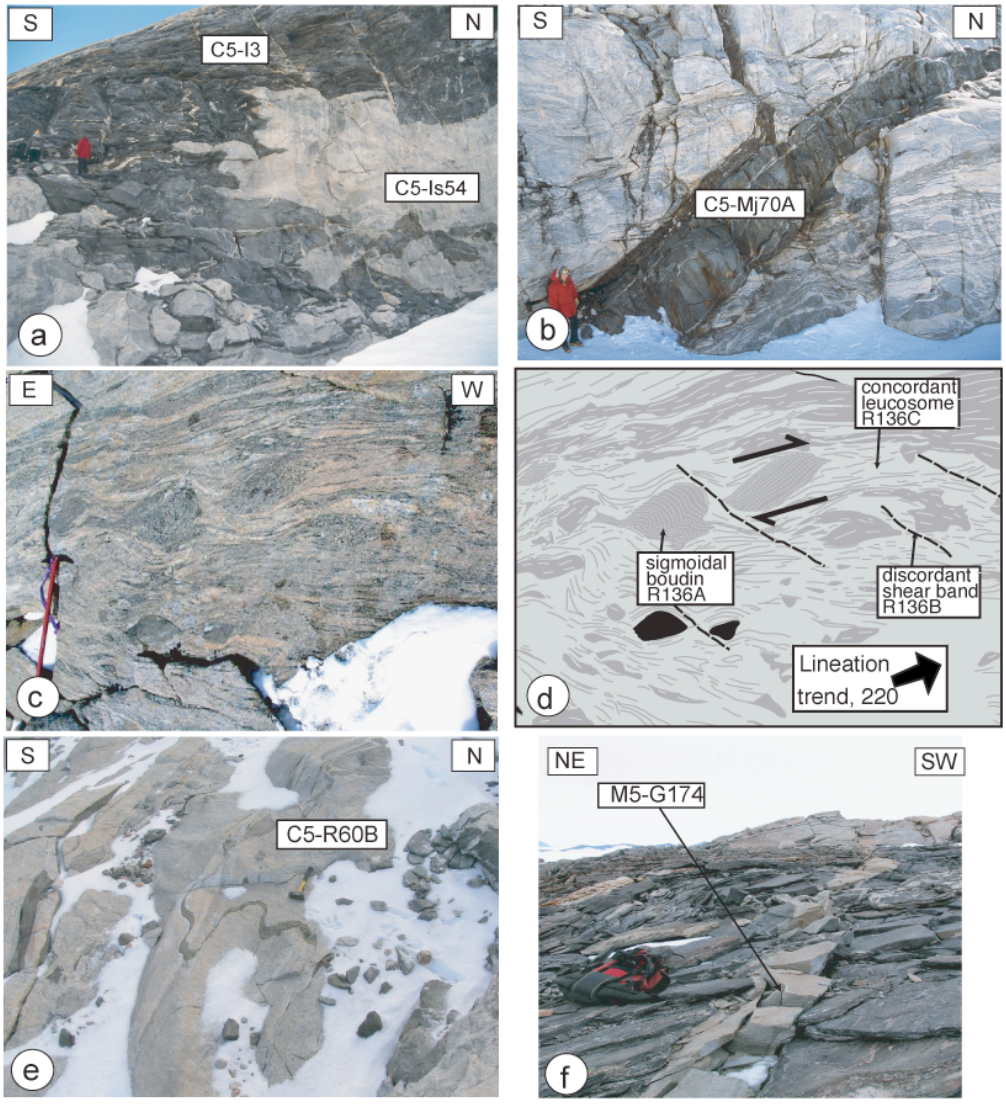

Figure 3.7 Photos of granite in structural sites and mafic dikes that were sampled for U-Pb geochronology.

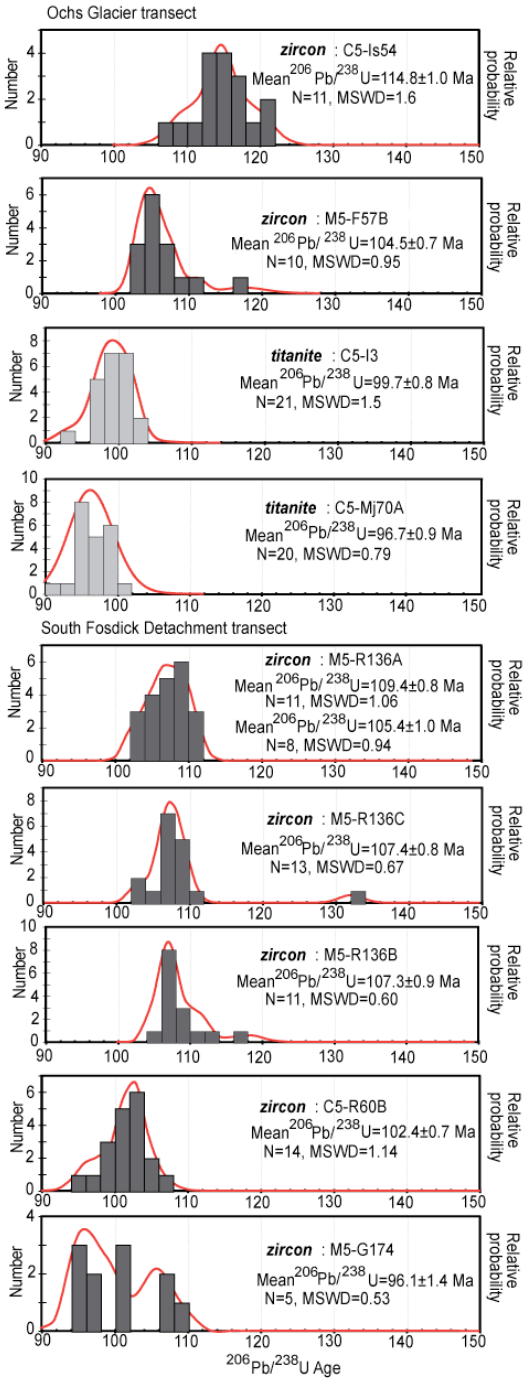

Figure 3.8 U-Pb data histograms and probability density plots.

Figure 3.9 Cathodoluminescence images of zircon and titanite.

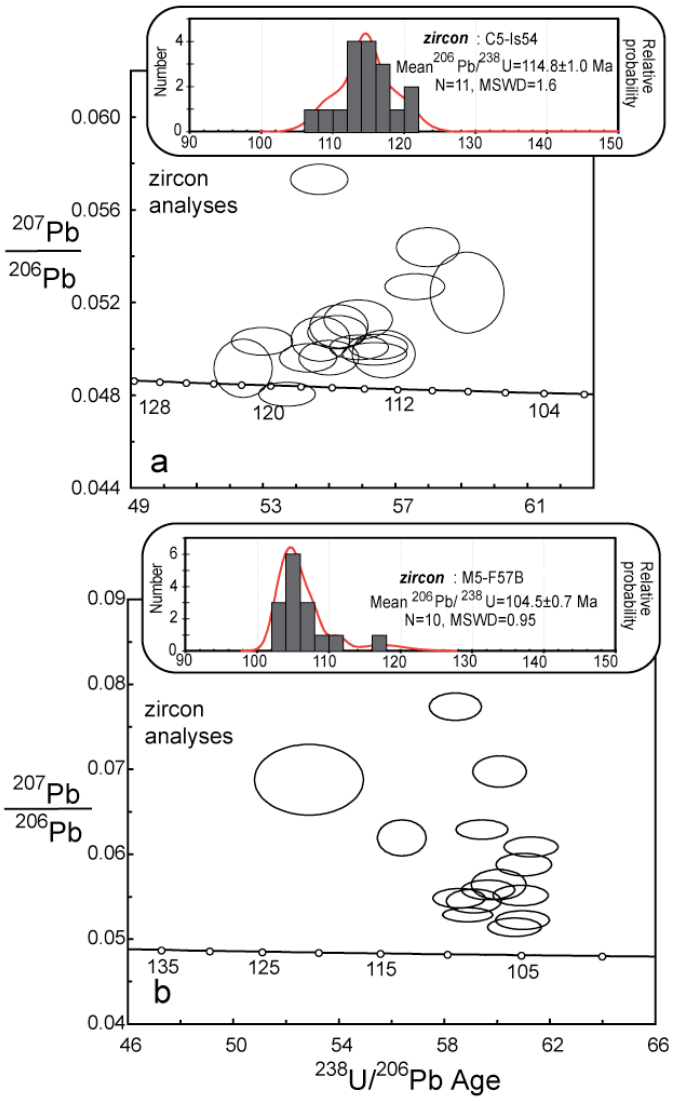

Figure 3.10 U-Pb data plots from the Ochs Glacier suite.

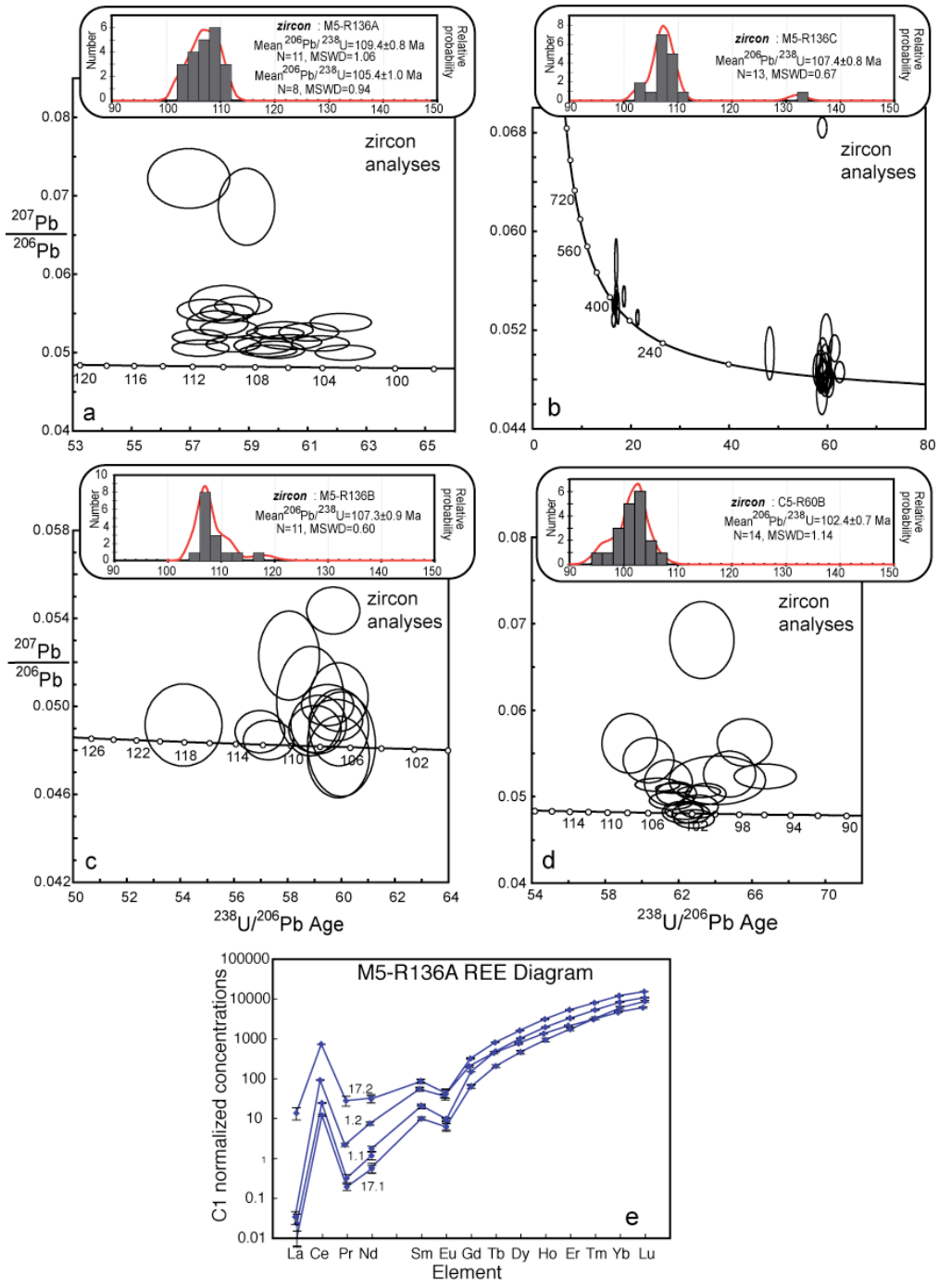

Figure 3.11 U-Pb data plots from the South Fosdick Detachment zone suite.

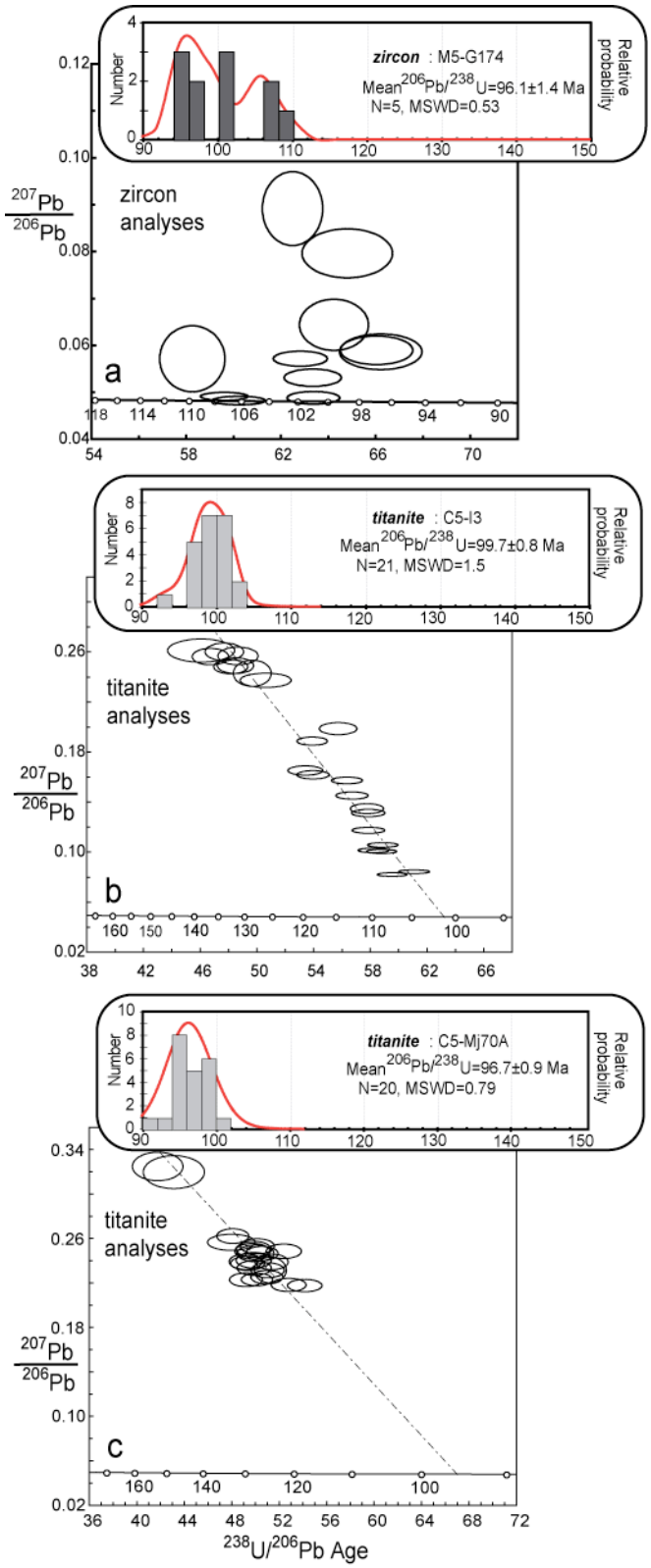

Figure 3.12 U-Pb data plots of titanite from discordant dikes.

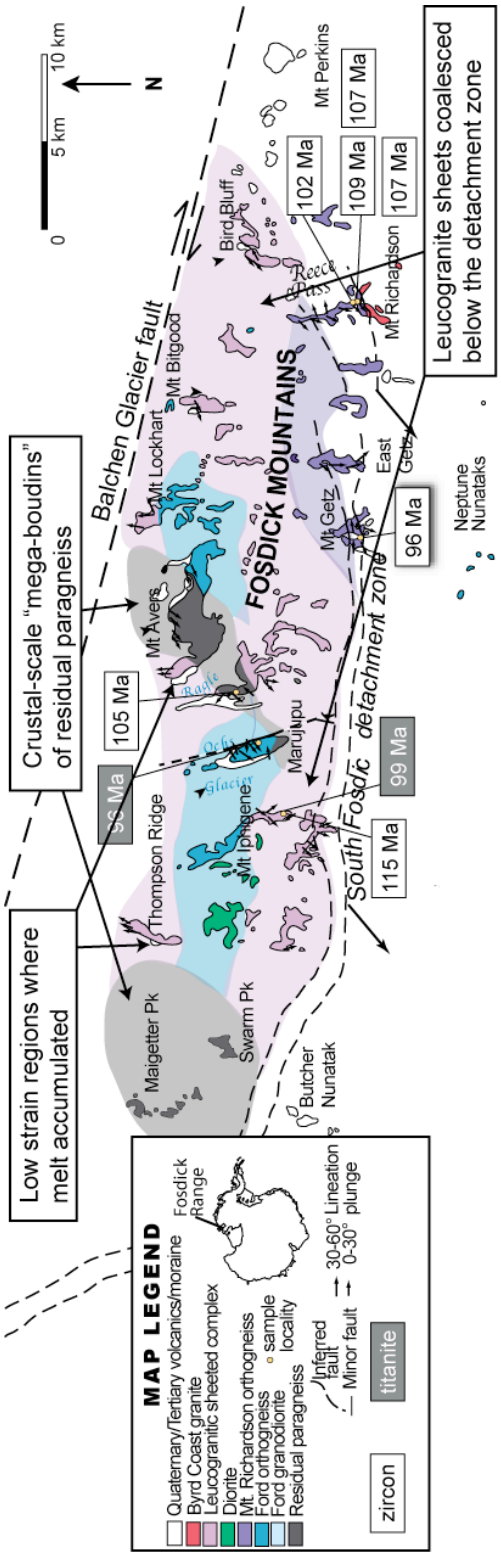

Figure 3.13 Geologic map pattern interpretation of the Fosdick dome.

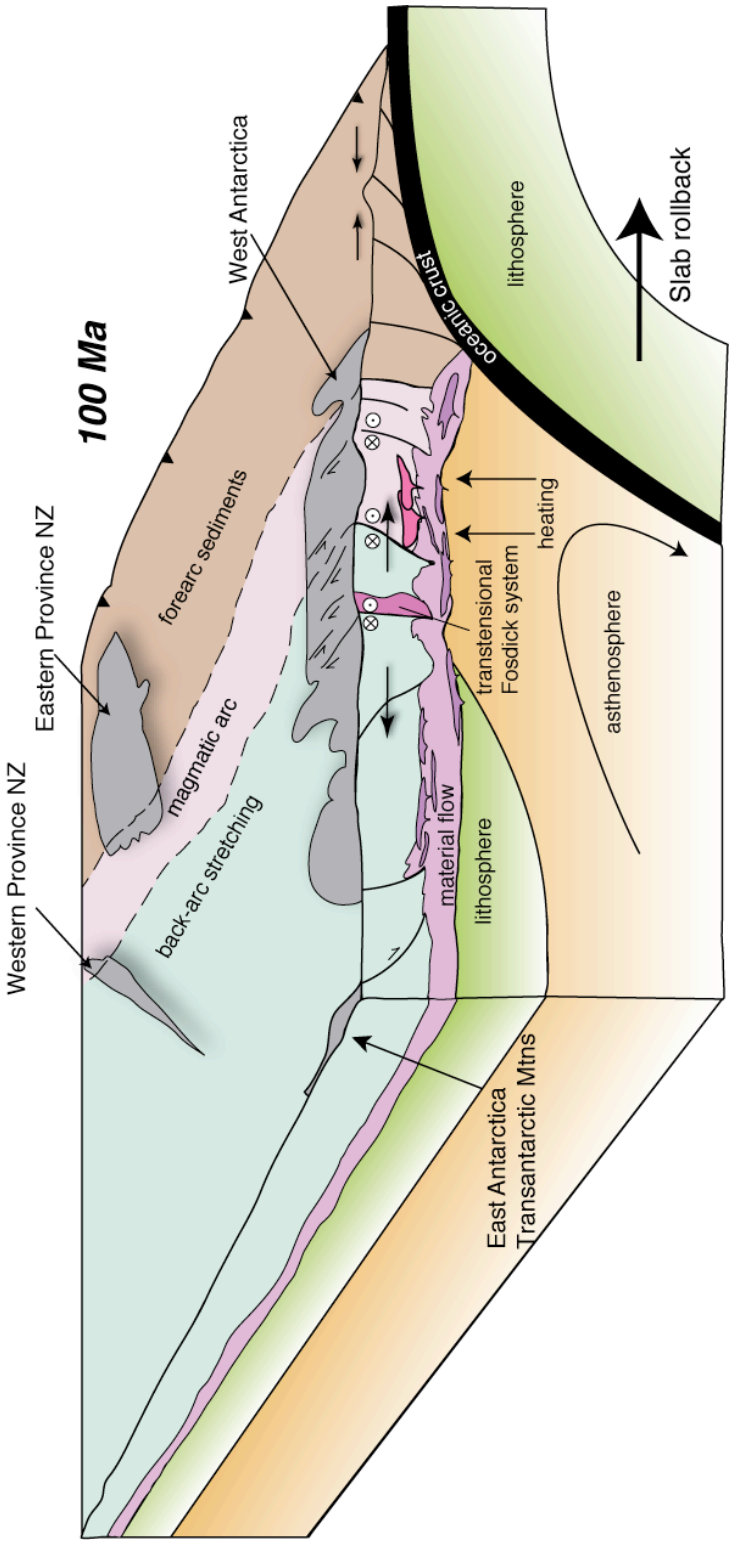

Figure 3.14 Three-dimensional schematic of the Cretaceous East Gondwana margin.

TABLE 3.1 Summary of SHRIMP U-Pb zircon results for migmatitic leucosome and granite in the Fosdick Mountains

							Total				Radiogenic ratios		Age (Ma)	
Grain spot	U (ppm)	Th (ppm)	Th/U	$^{206}Pb^*$ (ppm)	$^{204}Pb/^{206}Pb$	f_{206} %	$^{238}U/^{206}Pb$	±	$^{207}Pb/^{206}Pb$	±	$^{206}Pb/^{238}U$	±	$^{206}Pb/^{238}U$	±
***Sample C5-ls54** - granite sheet from Mt. Iphigene (Location: S 76° 32.318, W 145° 51.061)														
Rims														
1.1	2626	592	0.23	40.4	0.000044	0.22	55.891	0.586	0.0501	0.0004	0.0179	0.0002	114.1	1.2
2.1	1887	73	0.04	275.2	0.000000	0.36	5.892	0.068	0.0757	0.0002	0.1691	0.0020	1007.3	11.2
3.1	1001	206	0.21	14.8	0.000239	0.78	57.981	0.630	0.0544	0.0006	0.0171	0.0002	109.4	1.2
4.1	2039	281	0.14	169.3	0.000018	5.46	10.349	0.163	0.1034	0.0005	0.0913	0.0015	563.5	8.7
5.1	1225	227	0.19	19.1	0.000072	0.30	55.230	0.593	0.0507	0.0005	0.0181	0.0002	115.3	1.2
8.1	2542	472	0.19	38.7	0.000013	0.23	56.465	0.588	0.0501	0.0004	0.0177	0.0002	112.9	1.2
9.1	954	8	0.01	14.7	0.000068	0.37	55.865	0.685	0.0513	0.0006	0.0178	0.0002	113.9	1.4
10.1	1375	130	0.09	66.7	0.000028	0.29	17.714	0.217	0.0559	0.0005	0.0563	0.0007	353.0	4.2
11.1	1864	482	0.26	29.0	0.000040	0.33	55.270	0.587	0.0510	0.0006	0.0180	0.0002	115.2	1.2
12.1	1769	8	0.00	28.0	0.000037	0.15	54.346	0.573	0.0496	0.0004	0.0184	0.0002	117.4	1.2
14.1	2448	183	0.07	36.5	0.000181	0.56	57.572	0.601	0.0527	0.0004	0.0173	0.0002	110.4	1.1
15.1	1504	297	0.20	23.5	0.000265	0.16	54.975	0.589	0.0496	0.0005	0.0182	0.0002	116.0	1.2
16.1	2859	540	0.19	45.7	0.000049	<0.01	53.701	0.562	0.0480	0.0003	0.0186	0.0002	119.0	1.2
17.1	772	101	0.13	11.7	0.000193	0.19	56.642	0.630	0.0498	0.0007	0.0176	0.0002	112.6	1.2
18.1	957	368	0.39	15.7	0.000011	0.09	52.368	0.584	0.0491	0.0008	0.0191	0.0002	121.8	1.4
19.1	300	268	0.89	4.4	-	0.54	59.163	0.732	0.0524	0.0012	0.0168	0.0002	107.5	1.3
20.1	2426	237	0.10	38.1	0.000603	1.14	54.685	0.578	0.0574	0.0004	0.0181	0.0002	115.5	1.2
21.1	376	22	0.06	37.9	0.000040	2.00	8.520	0.247	0.0793	0.0053	0.1150	0.0035	701.8	20.3
Cores														
6.1	2732	279	0.10	41.6	0.000033	0.19	56.370	0.643	0.0498	0.0003	0.0177	0.0002	113.1	1.3
7.1	932	212	0.23	14.6	0.000049	0.26	54.718	0.590	0.0504	0.0006	0.0182	0.0002	116.4	1.3
9.2	129	26	0.20	9.7	0.000235	0.48	11.476	0.174	0.0621	0.0008	0.0867	0.0013	536.1	8.0
13.1	1962	347	0.18	31.8	0.000020	0.24	52.954	0.605	0.0503	0.0004	0.0188	0.0002	120.3	1.4
14.2	275	112	0.41	23.1	0.000135	0.06	10.225	0.120	0.0604	0.0006	0.0977	0.0012	601.2	6.9
20.2	1845	331	0.18	164.8	-	<0.01	9.617	0.114	0.0599	0.0005	0.1041	0.0013	638.5	7.4

Grain spot	U (ppm)	Th (ppm)	Th/U	$^{206}Pb^*$ (ppm)	$^{204}Pb/^{206}Pb$	f_{206} %	Total $^{238}U/^{206}Pb$	±	$^{207}Pb/^{206}Pb$	±	Radiogenic ratios $^{206}Pb/^{238}U$	±	Age (Ma) $^{206}Pb/^{238}U$	±
****Sample M5-F57B** - concordant granitic sill in residual paragneiss from Mt. Ferranto (Location:S 76° 29.734, W 145° 32.153)														
Rims														
2.1	2291	67	0.029	33.4	0.000424	0.64	58.901	0.625	0.0532	0.0005	0.0169	0.0002	107.8	1.1
3.1	1178	23	0.020	16.8	0.001507	2.75	60.112	0.669	0.0699	0.0012	0.0162	0.0002	103.5	1.2
4.1	1570	37	0.023	22.7	0.001265	1.89	59.438	0.646	0.0632	0.0007	0.0165	0.0002	105.5	1.1
5.1	1572	16	0.010	23.9	0.000910	1.75	56.421	0.612	0.0622	0.0014	0.0174	0.0002	111.3	1.2
6.1	1094	17	0.016	15.4	0.000713	1.38	61.018	0.686	0.0591	0.0009	0.0162	0.0002	103.4	1.2
7.1	1564	38	0.024	21.9	0.001028	1.65	61.294	0.669	0.0612	0.0007	0.0160	0.0002	102.6	1.1
8.1	1258	19	0.015	17.7	0.000350	0.93	60.910	0.689	0.0555	0.0008	0.0163	0.0002	104.0	1.2
9.1	1419	35	0.025	20.1	0.000362	0.46	60.667	0.666	0.0518	0.0007	0.0164	0.0002	104.9	1.1
10.1	1401	29	0.020	20.2	0.000696	1.01	59.680	0.657	0.0561	0.0007	0.0166	0.0002	106.1	1.2
11.1	1457	8	0.005	21.4	0.000432	0.88	58.580	0.642	0.0551	0.0007	0.0169	0.0002	108.2	1.2
12.1	1215	18	0.015	17.9	0.002257	3.70	58.436	0.652	0.0775	0.0011	0.0165	0.0002	105.4	1.2
13.1	1109	9	0.008	16.1	0.000579	0.84	59.137	0.680	0.0548	0.0009	0.0168	0.0002	107.2	1.2
14.1	1629	43	0.027	23.0	0.000409	0.57	60.967	0.667	0.0526	0.0007	0.0163	0.0002	104.3	1.1
15.1	1277	26	0.020	18.3	0.000569	1.08	60.064	0.680	0.0567	0.0012	0.0165	0.0002	105.3	1.2
Cores														
1.1	1280	8	0.006	20.8	0.001104	2.59	52.921	1.362	0.0690	0.0027	0.0184	0.0005	117.6	3.0

Grain spot	U (ppm)	Th (ppm)	Th/U	$^{206}Pb^*$ (ppm)	$^{204}Pb/^{206}Pb$	f_{206} %	Total $^{238}U/^{206}Pb$	±	$^{207}Pb/^{206}Pb$	±	Radiogenic ratios $^{206}Pb/^{238}U$	±	Age (Ma) $^{206}Pb/^{238}U$	±
****Sample M5-R136A** - granodioritic sigmoidal boudin from the SFD at Mt. Richadson (Location: S 76° 32.877, W 144° 41.248)														
Rims														
1.1	3143	218	0.069	46.2	0.000167	0.36	58.495	0.605	0.0510	0.0006	0.0170	0.0002	108.9	1.1
2.1	3082	94	0.031	45.4	0.000360	0.88	58.279	0.597	0.0552	0.0007	0.0170	0.0002	108.7	1.1
3.1	692	344	0.496	10.3	0.000648	0.90	57.545	0.641	0.0554	0.0009	0.0172	0.0002	110.1	1.2
5.1	1500	50	0.033	75.4	0.000047	0.19	17.105	0.193	0.0554	0.0004	0.0584	0.0007	365.6	4.1
6.1	1307	31	0.023	19.2	0.000408	0.61	58.350	0.642	0.0530	0.0007	0.0170	0.0002	108.9	1.2
7.1	1646	17	0.011	22.7	0.000075	0.24	62.314	0.677	0.0500	0.0007	0.0160	0.0002	102.4	1.1
9.1	163	59	0.364	2.5	0.000998	3.04	56.981	0.920	0.0723	0.0025	0.0170	0.0003	108.8	1.8
10.1	658	30	0.045	9.7	0.001136	0.69	57.958	0.688	0.0537	0.0010	0.0171	0.0002	109.5	1.3
11.1	2484	14	0.006	34.7	0.000191	0.38	61.456	0.652	0.0511	0.0007	0.0162	0.0002	103.7	1.1
12.1	1407	417	0.296	20.3	0.000143	0.35	59.519	0.654	0.0509	0.0007	0.0167	0.0002	107.0	1.2
13.1	1341	50	0.037	18.9	0.000343	0.57	61.079	0.675	0.0526	0.0007	0.0163	0.0002	104.1	1.1
15.1	1380	19	0.014	19.1	0.000405	0.73	62.163	0.687	0.0539	0.0008	0.0160	0.0002	102.1	1.1
16.1	3099	47	0.015	46.4	0.000183	0.29	57.378	0.643	0.0506	0.0007	0.0174	0.0002	111.1	1.2
17.1	2219	38	0.017	31.5	0.000177	0.40	60.445	0.702	0.0513	0.0006	0.0165	0.0002	105.4	1.2
18.1	2813	443	0.158	40.3	0.000173	0.55	59.930	0.638	0.0525	0.0005	0.0166	0.0002	106.1	1.1
19.1	1517	23	0.015	21.6	0.000137	0.60	60.214	0.658	0.0529	0.0007	0.0165	0.0002	105.5	1.2
20.1	2624	599	0.228	37.8	0.000123	0.26	59.688	0.637	0.0502	0.0005	0.0167	0.0002	106.8	1.1
21.1	1372	20	0.014	19.7	0.000166	0.27	59.935	0.658	0.0503	0.0007	0.0166	0.0002	106.4	1.2
22.1	1732	28	0.016	25.3	0.000391	0.98	58.841	0.638	0.0560	0.0008	0.0168	0.0002	107.6	1.2
Cores														
1.2	895	174	0.194	13.4	0.000262	0.47	57.355	0.613	0.0520	0.0006	0.0174	0.0002	110.9	1.2
2.2	384	95	0.247	17.3	0.000234	0.30	19.100	0.222	0.0554	0.0006	0.0522	0.0006	328.0	3.8
4.1	446	137	0.307	22.7	0.000276	0.62	16.879	0.183	0.0590	0.0006	0.0589	0.0006	368.8	3.9

Grain spot	U (ppm)	Th (ppm)	Th/U	$^{206}Pb^*$ (ppm)	$^{204}Pb/^{206}Pb$	f_{206} %	Total $^{238}U/^{206}Pb$	±	$^{207}Pb/^{206}Pb$	±	Radiogenic ratios $^{206}Pb/^{238}U$	±	Age (Ma) $^{206}Pb/^{238}U$	±
4.2	122	1	0.010	9.9	0.000752	1.54	10.631	0.141	0.0717	0.0011	0.0926	0.0013	571.0	7.4
7.2	414	173	0.419	6.1	0.001588	1.00	58.175	0.791	0.0562	0.0016	0.0170	0.0002	108.8	1.5
8.1	470	43	0.092	17.3	0.000179	0.66	23.304	0.267	0.0569	0.0008	0.0426	0.0005	269.1	3.1
14.1	271	97	0.360	13.4	0.000395	1.12	17.355	0.210	0.0627	0.0010	0.0570	0.0007	357.2	4.3
17.2	2418	1753	0.725	35.2	0.001532	2.59	58.952	0.632	0.0687	0.0032	0.0165	0.0002	105.7	1.2
23.1	1304	706	0.542	43.5	0.061008	35.30	25.784	2.056	0.3307	0.1507				
24.1	393	43	0.110	12.9	0.000700	0.80	26.105	0.322	0.0574	0.0015	0.0380	0.0005	240.4	3.0
25.1	198	180	0.910	9.9	0.000434	0.92	17.166	0.232	0.0612	0.0013	0.0577	0.0008	361.7	4.8
26.1	990	731	0.739	50.0	0.000056	0.09	17.016	0.185	0.0546	0.0007	0.0587	0.0006	367.8	3.9

Grain spot	U (ppm)	Th (ppm)	Th/U	$^{206}Pb^*$ (ppm)	$^{204}Pb/^{206}Pb$	f_{206} %	Total $^{238}U/^{206}Pb$	±	$^{207}Pb/^{206}Pb$	±	Radiogenic ratios $^{206}Pb/^{238}U$	±	Age (Ma) $^{206}Pb/^{238}U$	±
****Sample M5-R136C** - concordant granite from the SFD at Mt. Richardson (Location: S 76° 32.877, W 144° 41.248)														
Rims														
1.1	889	45	0.051	44.4	0.000007	0.17	17.187	0.201	0.0552	0.0005	0.0581	0.0007	364.0	4.2
3.1	2376	21	0.009	32.7	-	0.09	62.365	0.667	0.0488	0.0006	0.0160	0.0002	102.5	1.1
4.1	536	195	0.363	7.7	0.000249	0.05	59.453	0.740	0.0486	0.0012	0.0168	0.0002	107.5	1.3
5.1	2748	71	0.026	39.8	-	0.09	59.329	0.625	0.0489	0.0005	0.0168	0.0002	107.7	1.1
6.1	3372	49	0.014	49.3	0.001594	2.55	58.811	0.615	0.0684	0.0005	0.0166	0.0002	105.9	1.1
7.1	1342	24	0.018	18.8	0.000164	0.33	61.343	0.674	0.0507	0.0007	0.0162	0.0002	103.9	1.1
8.2	2066	53	0.026	107.4	-	<0.01	16.535	0.172	0.0541	0.0003	0.0605	0.0006	378.6	3.9
9.1	1001	23	0.023	14.3	0.000179	<0.01	60.172	0.679	0.0480	0.0008	0.0166	0.0002	106.3	1.2
10.1	2804	11	0.004	40.3	-	<0.01	59.764	0.635	0.0481	0.0005	0.0167	0.0002	107.0	1.1
11.1	2254	17	0.008	32.3	-	0.01	59.995	0.645	0.0482	0.0005	0.0167	0.0002	106.6	1.1
12.1	1524	492	0.323	61.1	-	0.12	21.427	0.225	0.0532	0.0004	0.0466	0.0005	293.7	3.0
Cores														
1.2	785	230	0.293	36.0	0.000046	0.21	18.713	0.202	0.0549	0.0005	0.0533	0.0006	334.9	3.6
2.1	1305	34	0.026	67.4	-	<0.01	16.624	0.274	0.0530	0.0004	0.0602	0.0010	377.1	6.1
3.2	628	327	0.520	9.0	0.000350	0.42	59.652	0.759	0.0515	0.0013	0.0167	0.0002	106.7	1.4
6.2	953	587	0.616	48.4	0.000031	0.03	16.901	0.184	0.0543	0.0005	0.0591	0.0007	370.5	4.0
8.1	188	75	0.402	9.4	-	0.47	17.150	0.228	0.0576	0.0012	0.0580	0.0008	363.7	4.8
9.2	611	340	0.556	9.0	0.000321	0.08	58.604	0.724	0.0488	0.0011	0.0171	0.0002	109.0	1.3
10.2	395	197	0.499	5.8	-	0.17	58.949	0.761	0.0496	0.0013	0.0169	0.0002	108.3	1.4
13.1	568	90	0.159	10.1	0.000022	0.20	48.170	0.599	0.0503	0.0014	0.0207	0.0003	132.2	1.6
14.1	450	144	0.321	22.1	0.000259	0.03	17.498	0.205	0.0539	0.0008	0.0571	0.0007	358.2	4.1
15.1	1331	418	0.314	19.7	0.000171	0.09	58.000	0.659	0.0490	0.0009	0.0172	0.0002	110.1	1.2
16.1	750	342	0.457	11.0	-	<0.01	58.784	0.717	0.0471	0.0011	0.0170	0.0002	108.9	1.3

							Total				Radiogenic ratios		Age (Ma)	
Grain spot	U (ppm)	Th (ppm)	Th/U	$^{206}Pb^*$ (ppm)	$^{204}Pb/^{206}Pb$	f_{206} %	$^{238}U/^{206}Pb$	±	$^{207}Pb/^{206}Pb$	±	$^{206}Pb/^{238}U$	±	$^{206}Pb/^{238}U$	±
17.1	607	251	0.414	8.8	0.000202	0.12	59.472	0.754	0.0491	0.0012	0.0168	0.0002	107.4	1.4
18.1	1300	693	0.533	19.0	-	0.03	58.875	0.670	0.0484	0.0008	0.0170	0.0002	108.5	1.2
19.1	1059	652	0.615	53.3	0.000069	0.08	17.059	0.184	0.0546	0.0005	0.0586	0.0006	366.9	3.9

Grain spot	U (ppm)	Th (ppm)	Th/U	$^{206}Pb^*$ (ppm)	$^{204}Pb/^{206}Pb$	f_{206} %	Total $^{238}U/^{206}Pb$	±	$^{207}Pb/^{206}Pb$	±	Radiogenic ratios $^{206}Pb/^{238}U$	±	Age (Ma) $^{206}Pb/^{238}U$	±
****Sample M5-R136B** - granite in discordant shear band from the SFD at Mt. Richardson (Location: S 76° 32.877, W 144° 41.248)														
Rims														
1.1	3773	201	0.053	56.1	0.003071	5.44	57.796	0.602	0.0913	0.0022	0.0164	0.0002	104.6	1.1
2.1	1958	23	0.012	29.4	-	0.03	57.275	0.616	0.0485	0.0006	0.0175	0.0002	111.5	1.2
3.1	1743	44	0.025	25.2	0.000250	0.24	59.479	0.641	0.0501	0.0006	0.0168	0.0002	107.2	1.2
4.1	1676	45	0.027	24.1	-	0.15	59.793	0.659	0.0494	0.0006	0.0167	0.0002	106.8	1.2
Cores														
1.2	1043	474	0.455	15.2	-	0.13	59.139	0.677	0.0492	0.0009	0.0169	0.0002	108.0	1.2
4.2	1739	1068	0.614	25.0	0.000305	0.79	59.688	0.651	0.0544	0.0007	0.0166	0.0002	106.3	1.2
5.1	1730	1129	0.652	25.2	-	0.10	59.008	0.649	0.0490	0.0007	0.0169	0.0002	108.2	1.2
6.1	355	299	0.843	5.1	-	0.02	59.995	0.837	0.0483	0.0016	0.0167	0.0002	106.5	1.5
7.1	645	206	0.320	71.9	0.000024	0.55	7.708	0.150	0.0698	0.0005	0.1290	0.0026	782	15
8.1	553	196	0.355	8.8	-	0.10	54.102	0.946	0.0492	0.0012	0.0185	0.0003	118.0	2.1
9.1	2072	1490	0.719	31.3	0.000072	0.07	56.942	0.617	0.0489	0.0006	0.0175	0.0002	112.1	1.2
10.1	345	165	0.478	5.0	-	0.26	58.847	0.833	0.0503	0.0017	0.0169	0.0002	108.3	1.5
11.1	588	364	0.619	8.4	0.000301	<0.01	59.873	0.758	0.0477	0.0012	0.0167	0.0002	106.8	1.4
12.1	854	511	0.598	12.3	0.000219	0.29	59.898	0.713	0.0504	0.0010	0.0166	0.0002	106.4	1.3
13.1	726	309	0.425	10.4	0.000370	0.11	59.896	0.738	0.0490	0.0011	0.0167	0.0002	106.6	1.3
14.1	551	331	0.602	8.2	-	0.52	58.039	0.747	0.0523	0.0013	0.0171	0.0002	109.6	1.4

Grain spot	U (ppm)	Th (ppm)	Th/U	$^{206}Pb^*$ (ppm)	$^{204}Pb/^{206}Pb$	f_{206} %	Total $^{238}U/^{206}Pb$	±	$^{207}Pb/^{206}Pb$	±	Radiogenic ratios $^{206}Pb/^{238}U$	±	Age (Ma) $^{206}Pb/^{238}U$	±
***Sample C5-R60B** - syntectonic granite sheet from the SFD at Mt. Richardson (Location: S 76° 32.877, W 144° 41.248)														
Rims														
3.1	137	64	0.47	1.8	-	1.06	65.652	0.985	0.0564	0.0018	0.0151	0.0002	96.4	1.5
4.1	124	74	0.60	1.6	0.000351	0.60	64.837	0.938	0.0527	0.0017	0.0153	0.0002	98.1	1.4
7.1	2615	515	0.20	123.3	0.000014	0.24	18.212	0.189	0.0553	0.0003	0.0548	0.0006	343.8	3.5
9.1	449	41	0.09	5.8	0.000336	0.57	66.763	1.114	0.0525	0.0009	0.0149	0.0002	95.3	1.6
10.1	143	124	0.87	2.0	0.000310	0.78	60.418	0.914	0.0543	0.0017	0.0164	0.0003	105.0	1.6
11.1	766	345	0.45	10.4	0.000440	0.31	63.533	0.725	0.0505	0.0008	0.0157	0.0002	100.4	1.1
12.1	1379	682	0.49	18.9	0.000112	0.02	62.738	0.680	0.0482	0.0007	0.0159	0.0002	101.9	1.1
13.1	909	413	0.45	12.7	0.000133	0.20	61.662	0.805	0.0497	0.0007	0.0162	0.0002	103.5	1.3
14.1	933	23	0.03	12.7	0.000146	0.12	63.129	0.708	0.0490	0.0009	0.0158	0.0002	101.2	1.1
18.1	463	109	0.23	39.0	-	0.06	10.201	0.114	0.0605	0.0005	0.0980	0.0011	602.5	6.5
19.1	736	354	0.48	10.2	0.000189	0.03	62.256	0.737	0.0483	0.0008	0.0161	0.0002	102.7	1.2
21.1	1185	26	0.02	16.3	0.000116	0.05	62.380	0.690	0.0485	0.0006	0.0160	0.0002	102.5	1.1
Cores														
1.1	118	77	0.65	1.6	-	0.51	64.159	1.735	0.0520	0.0018	0.0155	0.0004	99.2	2.7
2.1	1710	1085	0.63	23.2	0.000051	0.34	63.175	0.765	0.0507	0.0004	0.0158	0.0002	100.9	1.2
5.1	1353	1094	0.81	19.1	-	0.43	60.912	0.797	0.0515	0.0005	0.0163	0.0002	104.5	1.4
6.1	58	39	0.68	0.8	0.003232	2.54	63.322	1.155	0.0681	0.0029	0.0154	0.0003	98.5	1.8
8.1	2720	3311	1.22	37.8	0.000017	0.38	61.793	0.646	0.0511	0.0004	0.0161	0.0002	103.1	1.1
15.1	605	430	0.71	8.4	0.000024	0.31	61.924	0.725	0.0505	0.0009	0.0161	0.0002	103.0	1.2
16.1	208	222	1.07	2.9	0.000296	0.46	61.495	0.858	0.0517	0.0017	0.0162	0.0002	103.5	1.5
17.1	569	421	0.74	27.2	0.000031	0.17	17.965	0.197	0.0548	0.0005	0.0556	0.0006	348.6	3.8
20.1	114	78	0.69	1.6	0.002421	1.02	59.392	0.992	0.0563	0.0023	0.0167	0.0003	106.5	1.8
22.1	939	542	0.58	12.8	0.000006	<0.01	62.908	0.724	0.0476	0.0007	0.0159	0.0002	101.7	1.2

Grain spot	U (ppm)	Th (ppm)	Th/U	$^{206}Pb^*$ (ppm)	$^{204}Pb/^{206}Pb$	f_{206} %	Total $^{238}U/^{206}Pb$	±	$^{207}Pb/^{206}Pb$	±	Radiogenic ratios $^{206}Pb/^{238}U$	±	Age (Ma) $^{206}Pb/^{238}U$	±
***Sample M5-G174** - granitic dike from the SFD at Mt. Getz (Location: S 76° 33.237, W 145° 12.055)														
Rims														
1.1	125	39	0.31	14.6	0.000013	0.86	7.338	0.390	0.0734	0.0019	0.1351	0.0074	816.9	42.1
3.1	331	93	0.28	26.4	0.000075	<0.01	10.760	0.137	0.0585	0.0004	0.0930	0.0012	573.3	7.1
4.1	936	55	0.06	51.6	0.000039	0.06	15.592	0.186	0.0552	0.0006	0.0641	0.0008	400.5	4.7
5.1	420	223	0.53	36.3	0.000080	0.09	9.946	0.107	0.0611	0.0004	0.1004	0.0011	617.0	6.5
8.1	387	328	0.85	19.7	0.000153	0.29	16.907	0.187	0.0563	0.0006	0.0590	0.0007	369.4	4.0
9.1	72	100	1.38	0.9	0.000680	1.34	66.255	1.148	0.0586	0.0026	0.0149	0.0003	95.3	1.7
12.1	577	256	0.44	26.9	0.000092	0.11	18.435	0.200	0.0542	0.0005	0.0542	0.0006	340.2	3.6
14.1	353	80	0.23	26.6	0.000059	<0.01	11.389	0.354	0.0581	0.0005	0.0878	0.0028	542.7	16.5
15.1	1334	253	0.19	19.2	0.000105	0.11	59.645	0.661	0.0490	0.0006	0.0167	0.0002	107.1	1.2
26.1	399	576	1.44	5.4	0.000036	0.63	63.395	0.796	0.0530	0.0012	0.0157	0.0002	100.3	1.3
Cores														
2.1	608	111	0.18	53.0	-	0.02	9.862	0.115	0.0607	0.0004	0.1014	0.0012	622.4	7.0
6.1	538	209	0.39	7.3	0.000239	0.08	63.425	0.731	0.0486	0.0009	0.0158	0.0002	100.8	1.2
7.1	1365	68	0.05	19.5	0.000074	<0.01	60.269	0.725	0.0481	0.0006	0.0166	0.0002	106.1	1.3
10.1	114	98	0.85	1.7	0.000199	1.11	58.299	0.912	0.0570	0.0047	0.0170	0.0003	108.4	1.8
11.1	477	396	0.83	49.6	0.000091	0.64	8.257	0.089	0.0690	0.0007	0.1203	0.0013	732.4	7.7
13.1	563	185	0.33	80.3	0.000033	<0.01	6.023	0.064	0.0714	0.0003	0.1662	0.0019	991.0	10.2
16.1	454	1226	2.70	6.2	0.000751	1.15	62.863	0.745	0.0571	0.0010	0.0157	0.0002	100.6	1.2
17.1	247	29	0.12	41.5	0.000045	0.10	5.111	0.057	0.0790	0.0005	0.1955	0.0023	1150.9	12.3
18.1	64	67	1.05	0.8	0.002715	4.01	64.857	1.261	0.0797	0.0035	0.0148	0.0003	94.7	1.9
19.1	301	117	0.39	26.9	0.000131	1.30	9.621	0.109	0.0714	0.0006	0.1026	0.0012	629.6	7.0
22.1	474	86	0.18	22.3	0.000160	0.05	18.220	0.208	0.0538	0.0006	0.0549	0.0006	344.3	3.9
23.1	346	195	0.56	23.9	0.000109	<0.01	12.450	0.141	0.0570	0.0006	0.0803	0.0009	498.1	5.5
24.1	265	465	1.75	3.6	0.002798	5.21	62.546	0.843	0.0893	0.0052	0.0152	0.0002	97.0	1.5

							Total				Radiogenic ratios		Age (Ma)	
Grain spot	U (ppm)	Th (ppm)	Th/U	$^{206}Pb^*$ (ppm)	$^{204}Pb/^{206}Pb$	f_{206} %	$^{238}U/^{206}Pb$	±	$^{207}Pb/^{206}Pb$	±	$^{206}Pb/^{238}U$	±	$^{206}Pb/^{238}U$	±
25.1	174	134	0.77	2.3	0.001514	1.38	66.099	1.011	0.0589	0.0020	0.0149	0.0002	95.5	1.5
27.1	181	244	1.35	2.4	0.002606	2.06	64.288	0.963	0.0644	0.0036	0.0152	0.0002	97.5	1.5

Uncertainties given at the 1σ level.

f_{206} % denotes the percentage of ^{206}Pb that is common Pb.

Correction for common Pb made using the measured $^{238}U/^{206}Pb$ and $^{207}Pb/^{206}Pb$ ratios following Tera and Wasserburg (1972) as outlined in Williams (1998).

*Error in Temora reference zircon calibration was 0.29% for the analytical session. (not included in above errors but required when comparing data from different mounts).

**Error in Temora reference zircon calibration was 0.39% for the analytical session. (not included in above errors but required when comparing data from different mounts).

Table 3.2 REE and trace element data for Two Cretaceous zircons (SHRIMP RG), sample M5-R136A

area	La	Ce	Pr	Nd	Sm	Eu	Gd	Tb	Dy	Ho	Er
1.1	0.005	14.60	0.029	0.53	2.92	0.54	28.71	16.90	244.4	104.0	520.9
1.1				0.78	3.02	0.50	28.81		246.4		511.2
1.2	0.008	52.69	0.190	3.22	7.54	1.95	37.53	15.03	175.6	68.3	318.3
1.2				3.20	7.56	1.95	38.07		178.4		308.2
17.1	0.002	6.60	0.016	0.22	1.33	0.31	11.54	6.70	101.3	46.2	252.7
17.1				0.24	1.33	0.32	11.16		104.2		247.7
17.2	3.346	456.45	2.674	15.16	12.94	2.51	65.60	30.14	403.6	174.2	875.0
17.2				14.49	13.30	2.32	64.96		406.6		865.2

area	Tm	Yb	Lu	Hf	Y
1.1	126.3	1302.4	259.3	19009	3579.4
1.1		1312.8		19067	
1.2	71.1	692.3	140.1	14111	2221.1
1.2		704.1		14207	
17.1	72.2	849.8	192.9	18125	1462.2
17.1		865.7		18174	
17.2	202.8	1975.5	384.0	16189	6552.8
17.2		1993.8		16336	

Weight %
Analysed agains standard glass NIST611
All REE and Y concentrations are in ppm

Zircon, isotope µml/g: 153.187
Zircon isotope ppm, 13940

TABLE 3.3 Summary of SHRIMP U-Pb titanite results for diorite dikes in the Fosdick Mountains

Grain spot	U (ppm)	Th (ppm)	Th/U	$^{206}Pb^*$ (ppm)	$^{204}Pb/^{206}Pb$	±	f_{206} %	Total $^{238}U/^{206}Pb$	±	$^{207}Pb/^{206}Pb$	±	Radiogenic ratios $^{206}Pb/^{238}U$	±	Age (Ma) $^{206}Pb/^{238}U$	±
Sample C5-I3 - diorite dike from southern Mt. Iphigene (Location:)															
fraction B															
1.1	92	232	2.53	1.7	0.010115	0.001480	26.92	46.160	1.546	0.2619	0.0061	0.0158	0.0006	101.3	3.6
1.2	63	160	2.55	1.1	0.015902	0.001605	26.32	46.800	0.840	0.2571	0.0043	0.0157	0.0003	100.7	2.1
1.3	56	125	2.24	1.0	0.012680	0.001896	26.39	48.738	0.924	0.2576	0.0046	0.0151	0.0003	96.6	2.1
2.1	311	397	1.28	4.6	0.003421	0.000399	7.04	58.255	0.710	0.1040	0.0012	0.0160	0.0002	102.1	1.3
3.1	73	186	2.55	1.2	0.012256	0.001282	23.96	50.668	1.178	0.2382	0.0038	0.0150	0.0004	96.0	2.4
4.1	446	546	1.22	6.4	0.002962	0.000280	4.63	59.558	0.689	0.0848	0.0009	0.0160	0.0002	102.4	1.2
5.1	104	119	1.14	1.6	0.010274	0.001086	19.19	55.751	0.871	0.2003	0.0031	0.0145	0.0002	92.8	1.6
6.1	65	88	1.35	1.1	0.012395	0.001435	24.66	49.731	0.879	0.2438	0.0068	0.0151	0.0003	96.9	2.1
fraction A															
1.1	122	131	1.08	2.0	0.007110	0.000847	15.00	53.469	0.796	0.1672	0.0025	0.0159	0.0003	101.7	1.6
1.2	415	311	0.75	5.8	0.002336	0.000275	4.94	61.100	0.711	0.0873	0.0010	0.0156	0.0002	99.5	1.2
2.1	151	790	5.23	2.4	0.006855	0.000732	14.55	54.005	0.751	0.1636	0.0022	0.0158	0.0002	101.2	1.5
2.2	55	229	4.15	1.0	0.013969	0.001574	26.79	47.764	0.890	0.2607	0.0045	0.0153	0.0003	98.1	2.1
3.1	206	209	1.02	3.1	0.005856	0.000562	9.06	57.890	0.753	0.1200	0.0016	0.0157	0.0002	100.5	1.3
4.1	66	243	3.65	1.2	0.010832	0.001246	25.44	48.564	0.845	0.2500	0.0040	0.0154	0.0003	98.2	1.9
5.1	196	202	1.03	3.0	0.006786	0.000613	12.52	56.726	0.742	0.1474	0.0018	0.0154	0.0002	98.7	1.3
6.1	332	401	1.21	4.8	0.003916	0.000380	7.57	58.890	0.704	0.1081	0.0012	0.0157	0.0002	100.4	1.2
6.2	331	342	1.03	4.8	0.003676	0.000372	6.95	58.804	0.703	0.1032	0.0012	0.0158	0.0002	101.2	1.2
7.1	78	310	4.00	1.4	0.013814	0.001301	25.30	48.219	0.787	0.2490	0.0037	0.0155	0.0003	99.1	1.8
8.1	178	193	1.08	2.6	0.005828	0.001109	10.76	57.887	0.773	0.1335	0.0018	0.0154	0.0002	98.6	1.4
9.1	188	235	1.25	3.0	0.008623	0.000702	17.92	53.944	0.708	0.1903	0.0021	0.0152	0.0002	97.3	1.4
10.1	226	250	1.10	3.4	0.007496	0.000606	13.99	56.389	0.716	0.1591	0.0018	0.0153	0.0002	97.6	1.3
11.1	187	233	1.25	2.8	0.006104	0.000624	11.21	57.796	0.763	0.1370	0.0025	0.0154	0.0002	98.3	1.4

Grain spot	U (ppm)	Th (ppm)	Th/U	$^{206}Pb^*$ (ppm)	$^{204}Pb/^{206}Pb$	±	f_{206} %	Total $^{238}U/^{206}Pb$	±	$^{207}Pb/^{206}Pb$	±	Radiogenic ratios $^{206}Pb/^{238}U$	±	Age (Ma) $^{206}Pb/^{238}U$	±
Sample C5-Mj70A - diorite dike from central Marujupu (Location:)															
1.1	60	522	8.67	1.0	0.014508	0.001804	25.34	52.483	0.969	0.2490	0.0045	0.0142	0.0003	91.1	1.9
2.1	72	283	3.93	1.1	0.012198	0.001377	21.46	54.242	0.937	0.2183	0.0038	0.0145	0.0003	92.7	1.8
3.1	65	458	7.10	1.1	0.011924	0.001372	22.40	51.064	0.900	0.2259	0.0039	0.0152	0.0003	97.2	1.9
4.1	21	35	1.64	0.4	0.023623	0.003149	34.34	43.163	1.704	0.3208	0.0098	0.0152	0.0007	97.3	4.3
5.1	53	331	6.27	0.9	0.015509	0.001730	25.32	49.803	0.984	0.2490	0.0048	0.0150	0.0003	95.9	2.1
6.1	54	340	6.31	0.9	0.012187	0.001540	24.34	49.914	0.975	0.2413	0.0046	0.0152	0.0003	97.0	2.1
7.1	66	307	4.64	1.2	0.010344	0.001362	22.07	49.304	0.906	0.2234	0.0042	0.0158	0.0003	101.1	2.0
8.1	58	316	5.41	1.0	0.012975	0.002037	23.43	49.983	0.962	0.2341	0.0044	0.0153	0.0003	98.0	2.1
8.2	58	336	5.80	1.2	0.020179	0.002912	34.99	41.864	1.413	0.3260	0.0086	0.0155	0.0006	99.3	3.9
9.1	53	332	6.27	0.9	0.015226	0.001742	26.38	48.042	1.327	0.2575	0.0048	0.0153	0.0005	98.0	2.9
10.1	49	262	5.30	0.8	0.013975	0.001823	25.12	50.089	1.013	0.2474	0.0049	0.0149	0.0003	95.7	2.2
10.2	59	402	6.81	1.1	0.015007	0.001634	27.06	48.181	0.888	0.2629	0.0045	0.0151	0.0003	96.9	2.0
11.1	52	313	6.06	0.9	0.015843	0.002194	25.59	49.929	0.981	0.2511	0.0048	0.0149	0.0003	95.4	2.1
12.1	63	348	5.50	1.1	0.012198	0.001377	24.12	51.448	0.929	0.2395	0.0047	0.0147	0.0003	94.4	1.9
13.1	66	527	7.94	1.1	0.010734	0.001262	23.19	51.135	0.921	0.2321	0.0045	0.0150	0.0003	96.1	1.9
14.1	62	499	8.09	1.0	0.011252	0.001349	21.54	52.897	0.969	0.2189	0.0040	0.0148	0.0003	94.9	1.9
15.1	72	556	7.74	1.2	0.011216	0.001265	22.12	50.240	0.857	0.2237	0.0037	0.0155	0.0003	99.2	1.9
15.2	57	431	7.53	1.0	0.014383	0.001548	25.13	50.640	0.920	0.2474	0.0043	0.0148	0.0003	94.6	1.9

Grain spot	U (ppm)	Th (ppm)	Th/U	$^{206}Pb^*$ (ppm)	$^{204}Pb/^{206}Pb$	±	f_{206} %	Total $^{238}U/^{206}Pb$	±	$^{207}Pb/^{206}Pb$	±	Radiogenic ratios $^{206}Pb/^{238}U$	±	Age (Ma) $^{206}Pb/^{238}U$	±
15.3	66	556	8.36	1.1	0.012536	0.001386	23.21	51.356	0.895	0.2323	0.0078	0.0150	0.0003	95.7	2.1
16.1	56	353	6.34	1.0	0.012957	0.001565	24.16	49.254	0.925	0.2399	0.0044	0.0154	0.0003	98.5	2.1
16.2	58	370	6.34	1.0	0.014447	0.001684	23.99	49.421	0.920	0.2385	0.0043	0.0154	0.0003	98.4	2.0
17.1	53	303	5.70	0.9	0.014188	0.001563	25.90	50.258	0.944	0.2536	0.0046	0.0147	0.0003	94.4	2.0

Uncertainties given at the 1σ level.

Error in BLR-1 reference titanite calibration was 0.43% for the analytical session.
(not included in above errors but required when comparing data from different mounts).

f_{206} % denotes the percentage of ^{206}Pb that is common Pb.

Correction for common Pb made using the measured $^{238}U/^{206}Pb$ and $^{207}Pb/^{206}Pb$ ratios
following Tera and Wasserburg (1972) as outlined in Williams (1998).

Chapter 4: Oblique dilation, melt transfer, and gneiss dome emplacement

McFadden, R.R.[1], Teyssier, C.[1], Siddoway, C.S.[2], Whitney, D.L.[1], and Fanning, C.M.[3]

[1]*Geology and Geophysics, University of Minnesota, Minneapolis, MN 55455, USA*

[2]*Department of Geology, Colorado College, Colorado Springs, CO 80903, USA*

[3]*Research School Earth Sciences, Australian National University, Canberra, ACT 0200, Australia*

Synthesis

The rapid transfer of partially molten crust and the formation of gneiss domes and metamorphic core complexes commonly take place by localization of normal or oblique extension in the upper crust. In Marie Byrd Land, Antarctica, a transition from wrench to oblique extension occurred during the development of the West Antarctic Rift System in mid-Cretaceous time. Migmatites in the Fosdick Mountains, Marie Byrd Land, Antarctica, record steep fabrics formed during wrenching, and associated granite networks that display crystallization ages of 117–115 Ma. These steep fabrics are overprinted by subhorizontal foliation and leucogranite sheets with crystallization ages of 109–102 Ma. Subhorizontal leucogranite sheets of that age occupy the edges of the elongate migmatite-cored gneiss dome, suggesting melt migration into dilational sites in transtension. Syntectonic granite sheets emplaced in the South Fosdick Detachment zone yield ages for the onset of detachment tectonics leading to rapid exhumation of the terrain; corroborated by argon ages of biotite and hornblende that

are 100-98 Ma. This study has implications for understanding melt transport, magma accumulation, and the formation of detachments in an oblique tectonic setting.

Keywords: transtension, wrench, migmatites, melt transport, U-Pb SHRIMP

1. Introduction

The transfer of partially molten crust to shallow crustal levels is a fundamental mechanism by which heat and mass are redistributed in orogens. In exhumed orogens, metamorphic core complexes cored by migmatite ± granite domes are a ubiquitous structure and indicate the crust was partially molten during dome emplacement (Whitney et al., 2004). Current models of gneiss domes and metamorphic core complexes are largely two-dimensional and emphasize extension of the upper crust by detachment tectonics, whereby the partially molten crust rises isostatically and fills the gap created by fault movements at shallow levels (Brun et al., 1994; Rey et al., 2009). However, the simple, plane strain geometry that is predicted by two-dimensional models does not explain the internal structure (orientations of foliation, lineation, fold axes) of migmatite complexes that commonly occur in zones of wrench or oblique tectonic settings (e.g. Brown and Solar, 1998; Whitney et al., 2007; Weinberg and Mark, 2008).

Recent investigations of thermally softened lithosphere in transcurrent systems suggest that metamorphic core complexes and/or gneiss domes may develop in dilational jogs of large-scale wrench systems (e.g. Oldow, 2003; Foster et al., 2007; Whitney et al., 2007). Dilation zones that arise at asperities along transcurrent faults are effective in creating space for ascent and emplacement of magma and partially molten crust in low-pressure regions (e.g. Hutton, 1990; D'Lemos et al., 1992; Tikoff and Teyssier, 1992; Talbot et al., 2005; Weinberg et al., 2009).

In this paper, we explore the implications of oblique divergence for the flow of partially molten crust, the internal segregation and emplacement of granite, and the association between oblique detachment systems and exhumation of migmatite terrains. Our study is based on field relations and crystallization ages in the Fosdick Mountains, Marie Byrd Land, Antarctica, a migmatite-cored gneiss dome that developed during mid-Cretaceous intracontinental crustal extension associated with the West Antarctic Rift System (WARS) (Siddoway, 2008). Three-dimensional exposures in the Fosdick Mountains allow us to examine the spatial and temporal associations of migmatites, leucogranite sheets, and structures. Geometric and kinematic analysis of migmatites and upper crustal brittle structures delineate an evolution of fabrics from wrenching to oblique extension accompanied by a systematic decrease in U-Pb SHRIMP zircon crystallization ages. The strain, melt transfer mechanism, granite emplacement, and exhumation of the migmatite dome were fundamentally affected when oblique divergence reached a critical angle.

2. Transtension and Three-Dimensional Strain

Transtension theory offers a rigorous deformation model for oblique divergence that involves a combination of wrench motion and extensional strain (thinning of crust). In transtension, the maximum finite strain axis and material lines and planes are all attracted toward the direction of oblique divergence. Therefore, the orientation of lineation, fold and boudin axes, and any elongate, anisotropic objects track both the obliquity and the orientation of divergence (Teyssier and Tikoff, 1999). To predict the foliation and lineation orientations and examine the complex

relationship between instantaneous and finite strain, transtensional deformation is commonly subdivided into wrench-dominated transtension ($0° < \alpha < 20°$) (α = divergence angle) and extension-dominated transtension ($20° < \alpha < 90°$) (Fossen and Tikoff, 1993; Tikoff and Teyssier, 1994). During pure wrench deformation ($\alpha = 0°$), vertical foliation and horizontal lineation prevail, but with increasing angle of divergence, constrictional fabrics develop and foliation switches to horizontal (Teyssier and Tikoff, 1999) (Fig. 4.1). If the angle of divergence is >20°, horizontal foliation develops.

3. Transcurrent Structures in Marie Byrd Land

Marie Byrd Land in West Antarctica formed upon the accretionary Paleozoic-Mesozoic active continental margin of East Gondwana (Siddoway, 2008). Paleozoic metagraywacke and granodiorite intruded by Cretaceous alkalic granitic rocks and mafic dikes were extended and thinned during formation of the WARS (Bradshaw et al., 1983; Weaver et al., 1992; Pankhurst et al., 1998; Storey et al., 1999; Siddoway et al., 2004, 2005; Siddoway, 2008). Concurrent with alkalic plutonism and WARS opening, Cretaceous high temperature metamorphism and voluminous crustal melting occurred in the Fosdick Mountains gneiss dome (Siddoway et al., 2004) (Fig. 4.2).

The kinematics of brittle and ductile structures in Marie Byrd Land indicate transcurrent deformation during the initial stages of intracontinental rifting (Siddoway et al., 2005). A mafic dike array and brittle faults in the Ford Ranges (Siddoway et al., 2005) and ductile structures in the Fosdick gneiss dome (Siddoway et al., 2004; McFadden et al., 2007) record ENE-WSW stretching due to dextral transtension over

a >1000 km^2 region. Aerogeophysical data (Ferraccioli et al., 2002; Luyendyk et al., 2003) and brittle fault studies identify a conjugate geometry of ~E-W-oriented dextral and NE-SW sinistral strike-slip faults formed in this strain environment (Siddoway et al., 2005). The timing of events is loosely bracketed by $^{40}Ar/^{39}Ar$ ages of 142 to 96 Ma for the regional dike array (Siddoway et al., 2005) and U-Pb zircon ages of ca. 117 to 102 Ma for migmatites and granites of the Fosdick Mountains that underwent suprasolidus deformation (McFadden et al., *in review*).

4. Structures in the Fosdick Gneiss Dome

The Fosdick Mountains migmatite-cored gneiss dome is an asymmetric dome consisting of mid-crustal migmatite and granite (Siddoway et al., 2004) (Fig. 4.2). The dome is bounded to the north by an inferred dextral strike-slip fault, the Balchen Glacier fault (Siddoway et al., 2004, 2005), and to the south by the dextral-normal South Fosdick detachment zone (McFadden et al., 2007). Migmatites are folded into kms-scale recumbent nappes and host multiple generations of leucosome and granite in sheets, discordant bodies, dikes, and veins. Diverse structures observed within the migmatites and granites include m-scale symmetric folds with subhorizontal axial planes; steep foliation with sparse lineation overprinted by subhorizontal fabrics with pronounced lineation; isoclinal folds; and transposed layering (Siddoway et al., 2004). Mafic dikes that intruded throughout dome evolution are boudinaged and buckled (Fig. 4.3), providing strain markers for progressive deformation (Smith, 1997). Steep fabric domains are prevalent near the Balchen Glacier fault that forms the northern boundary of the dome (Fig. 4.3).

The migmatites pass upward into voluminous subhorizontal leucogranites in a sheeted complex 2 km thick. Individual leucogranite bodies are up to 100 m thick. Within the leucogranite sheeted complex, early steep fabric is overprinted by a subhorizontal fabric defined by shallow foliations, oblate boudins, and recumbent isoclinal folds (Fig. 4.3). The leucogranite complex is bounded one km above by lower melt fraction migmatites that exhibit solid-state fabrics imparted by deformation within the South Fosdick Detachment zone (McFadden et al., 2007).

Kinematic data within the gneiss dome and from brittle upper crust in neighboring ranges show that the faults bounding the Fosdick dome accommodated dextral to dextral oblique motion (Siddoway et al., 2005; McFadden et al., 2007). In the migmatites, shallowly plunging linear structures within the subhorizontal foliation trend 235 ± 5 azimuth (McFadden et al., *in review*) (Fig. 4.2). This lineation, oriented 055–235 is interpreted as the maximum finite stretching axis. It is oblique to the Balchen Glacier fault, oriented 100–280, as well as to the long axis of the dome, oriented 080–260 (Fig. 4.2).

5. U-Pb Zircon Geochronology

To establish the timing of crystallization and emplacement of the leucogranite sheeted complex and the steep fabrics within the dome, we obtained U-Pb SHRIMP zircon rim and core analyses from a steeply dipping granite sill folded with the migmatite foliation and a subhorizontal leucogranite sheet (Fig. 4.3; Table 4.1). The steep, folded granite sill is from Mt. Lockhart and the subhorizontal leucogranite sheet is from the sheeted complex at Bird Bluff (Fig. 4.2).

5.1. Analytical Methods

Zircon mineral separates were prepared from bulk rock samples by crushing, gravity, and magnetic separation, heavy liquids, and hand picking under fiber optic illumination at the Australian National University Research School of Earth Sciences (ANU-RSES). Zircons were mounted in epoxy, ground to approximately half-thickness, and polished with 6 μm and 1 μm diamond suspension. Cathodoluminescence (CL) images for zircon characterization were collected using scanning electron microscope, together with transmitted and reflected light images using a petrographic microscope. Zircon U-Th-Pb isotopic analyses were collected using SHRIMP II at ANU-RSES and SHRIMP RG at Geoscience Australia, following procedures described in Williams (1998). Data were reduced using the SQUID Excel Macro of Ludwig (2001). The U-Pb ratios have been normalized relative to a value of 0.0668 for the Temora reference zircon, equivalent to an age of 417 Ma (Black et al., 2003) (Table 4.1). Ages are reported as weighted mean of $^{206}Pb/^{238}U$ ages for coherent zircon populations.

Uncertainties given for individual analyses (ratios and ages) are at the one-sigma level. Probability density plots with stacked histograms and weighted mean $^{206}Pb/^{238}U$ ages and Tera-Wasserburg (1972) concordia plots were calculated using ISOPLOT/EX (Ludwig, 2003). ISOPLOT/EX employs the "Mixture Modeling" algorithm of Sambridge and Compston (1994) to un-mix statistical age populations or groupings, which are in turn used to calculate weighted mean $^{206}Pb/^{238}U$ ages. Uncertainties are reported as 95% confidence limits.

5.2. Geochronologic Data

Zircons from the granite sill at Mt. Lockhart, sample M6-L188, are predominantly prismatic and less commonly acicular. The prismatic and acicular grains have low U (bright in CL), zoned cores, and high U rims or overgrowth that truncate internal zoning. The axial ratios of the grains range from 2:1 to 3:1 and the grains are generally 200–400 μm in length. Combined rim and core analyses (N=11) of the main Cretaceous population yield a weighted mean $^{206}Pb/^{238}U$ age of 116.3 ± 1.0 Ma (Fig. 4.4; Table 4.1).

Zircons from the horizontal leucogranite sheet at Bird Bluff, sample C6-BB112, are prismatic and rarely acicular. Both grain types have low U, zoned cores, and high U thinly zoned rims. Prismatic grains are 200–300 μm in length, with a 3:1 axial ratio. Cores of prismatic grains yield Proterozoic ages and cores of acicular grains yield Devono-Carboniferous ages, indicating that zircons are inherited from the host rock (e.g. Siddoway et al., 2004). Analyses (N=10) of rims on prismatic and acicular grains give Cretaceous ages between ca. 107–101 Ma with a weighted mean $^{206}Pb/^{238}U$ age of 103.6 ± 0.7 Ma (Fig. 4.4; Table 4.1).

6. Evolution of Oblique Motion

Domains of migmatite with steep foliation and poorly developed lineations host concordant leucosome and granite layers. The steep structures are commonly folded with subhorizontal fold axes and are generally aligned with the 080 trend of the dome (Smith, 1997). The long axis of the dome is oblique to the 055–235 stretching direction (Fig. 4.2). We attribute the steep structures and the orientation of the long

axis of the dome to the wrench phase of deformation. Domains of migmatite with subhorizontal foliation ENE-WSW strike and well-developed lineation that trends 055–235, along with shallowly plunging microfolds that trend 060–240 overprint the relict steep structures that strike NE-SW (Fig. 4.2). The subhorizontal migmatites host subhorizontal leucogranite sheets (Fig. 4.3). Mafic dikes are buckled about subhorizontal axes and boudinaged, in response to vertical shortening and horizontal stretching (Fig. 4.3). The overprinting of steep structures by subhorizontal structures, emplacement of subhorizontal granite sheets, and deformation of mafic dikes occurred during the extension-dominated transtension phase of deformation. These structures record a progressive change from wrench to transtension.

Spatial and temporal relationships for Cretaceous granites of the Fosdick dome show that the granites fall within two groups (cf. McFadden et al., *in review*; Siddoway and Fanning, 2009) (Fig. 4.2). The "older" granites are associated with steep structures of the central Fosdicks dome. These include: a) a folded granite sheet from Mt. Iphigene, U-Pb zircon age, 115 Ma (McFadden et al., *in review*) (Table 4.1); b) and a subvertical granite sill from Mt. Lockhart, age 117 Ma. The "younger" group comprises granites emplaced in the South Fosdick detachment, which have U-Pb zircon ages between 109–102 Ma (McFadden et al., *in review*) and the subhorizontal granite sheet of 104 Ma age from the leucogranite sheeted complex at Bird Bluff (Fig. 4.3). Thus, the large volume of younger granite that forms the sheeted complex is situated in a dilation zone that formed along the refractory migmatites and early granite that have steep fabric imparted during the wrench phase. The refractory

migmatites acted as a lithologic asperity that created a right step in a dextral fault zone.

The older granites emplaced in steep structures or prior to the change to transtension in the Fosdick dome record magma accumulation during wrench deformation. The younger granites are in subhorizontal layers in the dilation zone or were emplaced in the South Fosdick detachment after transtension commenced. The younger granites were emplaced during extension-dominated oblique divergence (divergence angle >20º). Thus, the granites reflect the rotation of the oblique divergence angle that led to dome emplacement. The youngest recorded granite emplaced into steep structures is 115 Ma and the oldest recorded granite emplaced into subhorizontal structures is 109 Ma. These ages indicate that the switch from wrench to extension-dominated transtension occurred within 6 myr. The ca. 109–102 Ma horizontal sheets are syntectonic with respect to the South Fosdick Detachment zone, a structure partly responsible for exhumation of the Fosdick dome (McFadden et al., 2007; *in review*). In addition, the migmatites cooled rapidly through biotite closure temperature by 98 Ma (Richard et al., 1994). Therefore, the emplacement of the subhorizontal leucogranite sheets and movement on the detachment led to rapid cooling in the Fosdick dome.

7. Deformation and Melt Pathways

Field relations and U-Pb ages of granites can be used in concert with predictions from three-dimensional deformation models to understand the strain field and pressure gradients that govern internal fabrics and sites of magma accumulation.

The pattern of decreasing granite age toward the margins of the gneiss dome indicate that magma migration and accumulation were controlled by pressure gradients produced by the change from wrench deformation to transtension induced by rotation of the divergence angle. The maximum finite strain axis rotated counterclockwise out of alignment with the dome axis. A dilation zone developed, creating space and a low-pressure region that opened (increased in size) in the maximum stretching direction. The interconnectivity of melt networks in migmatites implies flow toward magma traps in low-pressure regions (e.g. Sawyer, 1996; Weinberg et al., 2009). Thus, the pressure gradient aided migration of magma into traps at the edges of the dome, leading to emplacement of dominantly subhorizontal leucogranite sheets in low pressure sinks (Fig. 4.2).

Fabrics and granite crystallization ages in the Fosdicks suggest that melt transport and magma accumulation are linked with the development of detachments. Early wrench deformation created steep foliation, which functioned as migration paths for transport of melt and heat towards higher structural levels (e.g. Brown, 2008). The change to transtension created a pressure gradient that enhanced melt migration into an asperity along the Balchen Glacier fault zone, triggering emplacement of the subhorizontal leucogranite sheets and movement on the South Fosdick detachment. Initial motion on the detachment occurred in response to the increased divergence angle and added volume and heat of granite magma (e.g. Teyssier et al. 2005). As the South Fosdick detachment zone accommodated upper crustal displacement the dilation zone enlarged, facilitating further granite emplacement.

8. Gneiss Domes and Oblique Tectonics

In the Fosdick dome, steep migmatitic foliations with syn-kinematic steep granite sheets developed during wrench deformation. The steep fabrics were subsequently folded about subhorizontal axes and overprinted by subhorizontal migmatitic foliations with subhorizontal granite sheets during extension-dominated transtension. The dominant lineation records the stretching direction during extension-dominated transtension, whereas the long axis of the dome preserves the earlier wrench deformation. These structures preserve the switch from wrench to extension-dominated transtension. U-Pb crystallization ages from steep granite sheets and subhorizontal granite sheets show the maximum time for the switch from wrenching to oblique extension was 6 myr. Crystallization ages young towards the dome edges, with the youngest crystallization ages in the subhorizontal granite sheets. The age progression during evolving oblique motion was due to melt flowing towards low-pressure sites created by the opening of a dilation zone. The emplacement of subhorizontal granite sheets coincides with the development of a detachment and subsequent exhumation of the dome, which ultimately leads to rapid cooling of the gneiss dome and a switch to detachment tectonics. Work in the Fosdick Mountains shows that in oblique tectonic regions the divergence angle controls fabric development and the evolution of dilation zones enhance melt transport, magma accumulation, and detachment-related exhumation.

Acknowledgments

Work supported by National Science Foundation-Office of Polar Programs grants NSF-OPP 0337488 to Teyssier and NSF-OPP 0338279 to Siddoway, and partially supported by GSA Bruce L. "Biff" Reed Student Scholarship awarded to McFadden.

References Cited

Black, L. P., Kamo, S.L., Allen, C.M., Aleinikoff, J.N., Davis, D.W., Korsch, R.J., and Foudulis, C., 2003, TEMORA 1: a new zircon standard for Phanerozoic U-Pb geochronology, Chemical Geology, v. 200, p. 155–170.

Bradshaw, J.D., Andrew, B., and Field, B.D., 1983, Swanson Formation and related rocks of Marie Byrd Land and a comparison with the Robertson Bay Group of northern Victoria Land, *in* Oliver, R.L., James, P.R., and Jago, J.B., eds., Antarctic Earth Science, Australian Academy of Science, p. 274–279.

Brown, M., 2008, Granites, migmatites and residual granulites: relationships and processes, Mineralogical Association of Canada Short Course 38, Quebec City, Quebec, p. 97–144.

Brown, M., and Solar, G.S., 1998, Granite ascent and emplacement during contractional deformation in convergent orogens, Journal of Structural Geology, v. 20, p. 1365–1393.

Brun, J.P., Sokoutis, D., and Van Den Driessche, J., 1994, Analogue modeling of detachment fault systems and core complexes; Geology, v. 22, p. 319–322.

D'Lemos, R.S., Brown, M., and Strachan, R.A., 1992, Granite magma generation, ascent and emplacement within a transpressional orogen: Journal Geological Society of London, v. 149, p. 487–490.

Ferraccioli, F., Bozzo E., and Damaske, D., 2002, Aeromagnetic signatures over western Marie Byrd Land provide insight into magmatic arc basement, mafic magmatism and structure of the eastern Ross Sea rift flank: Tectonophysics, v. 347, p. 139–65.

Fossen, H., and Tikoff, B., 1993, The deformation matrix for simultaneous simple shearing, pure shearing and volume change, and its application to transpression-transtension tectonics, Journal of Structural Geology, v. 15, p. 413–422.

Foster, D.A., Dought, P.T., Kalakay, T.J., Fanning, C.M., Coyner, S., Grice, W.C., and Vogl, J., 2007, Kinematics and timing of exhumation of metamorphic core complexes along the Lewis and Clark fault zone, northern Rocky Mountains, USA, *in* Till, A.B., Roeske, S.M., Sample, J.C., and Foster, D.A., eds., Exhumation Associated with Continental Strike-slip Fault Systems: Geological Society of America Special paper 434, p. 207–232, doi: 10.1130/2007.2434(10).

Hutton, D.H.W., 1990, A new mechanism of granite emplacement: Intrusion in active extensional shear zones: Nature, v. 343, p. 452–455.

Ludwig, K.R., 2001, SQUID 1.02, A User's Manual; Berkeley Geochronology Center Special Publication, vol. 2, Berkeley Geochronology Center Special Publication, 2455 Ridge Road, Berkeley, CA 94709, USA.

Ludwig, K.R., 2003, User's Manual for Isoplot/Ex, Version 3.0, A geochronological toolkit for Microsoft Excel Berkeley Geochronology Center Special Publication, v. 4, Berkeley Geochronology Center, 2455 Ridge Road, Berkeley, CA 94709, USA.

Luyendyk, B. P., Wilson, D.S., and Siddoway C.S., 2003, The eastern margin of the Ross Sea Rift in western Marie Byrd Land: Crustal structure and tectonic development: Geochemistry, Geophysics, Geosystems, doi: 10.1029/2002GC000462.

McFadden, R., Siddoway, C.S., Teyssier, C., Fanning, C.M., and Kruckenberg, S.C., 2007, Cretaceous oblique detachment tectonics in the Fosdick Mountains, Marie Byrd Land, Antarctica, *in* Cooper, A.K., Raymond, C.R., and ISAES Editorial Team, eds., Antarctica: A Keystone in a Changing World - Online Proceedings of the 10th ISAES, USGS Open-File Report 2007-1047, Short Research Paper 047, 5 p.; doi: 10.3133/of2007-1047.srp047.

McFadden, R., Siddoway, C.S., Teyssier, C., and Fanning, C.M., *in review*, Cretaceous intracontinental extension in the Fosdick Mountains migmatite-granite complex, West Antarctica: Tectonics.

Oldow, J.S., 2003, Active transtensional boundary zone between the western Great Basin and Sierra Nevada block, western U.S. Cordillera: Geology, v. 31, p. 1033–1036, doi: 10.1038/333349a0.

Pankhurst, R.J., Weaver, S.D., Bradshaw, J.D., Storey, B.C., and Ireland, T.R., 1998, Geochronology and geochemistry of pre-Jurassic superterranes in Marie Byrd Land, Antarctica: Journal of Geophysical Research, v. 103, p. 2529–2547.

Sambridge, M. S. Compston, W., 1994, Mixture modeling of multi-component data sets with application to ion-probe zircon ages, Earth and Planetary Science Letters 128, v. 3–4, p.373–390.

Sawyer, E.W., 1996, Melt segregation and magma flow in migmatites: Implications for the generation of granite magmas: Transactions of the Royal Society Edinburgh: Earth Sciences, v. 87, p. 85–94.

Siddoway, C.S., Richard, S.M., Fanning, C.M., and Luyendyk, B.P., 2004, Origin and emplacement of a middle Cretaceous gneiss dome, Fosdick Mountains, West Antarctica, *in* Whitney, D.L., Teyssier, C., and Siddoway, C.S., eds., Gneiss domes in Orogeny, Geological Society America Special Paper 380, p. 267–294.

Siddoway, C.S., Sass III, L.C., and Esser, R., 2005, Kinematic history of Marie Byrd Land terrane, West Antarctica: Direct evidence from Cretaceous mafic dykes, *in* Vaughan et al., eds., Terrane Processes at the Margin of Gondwana, Geological Society, London, Special Publications, 246, p. 417-438.

Siddoway, C.S., 2008, Tectonics of the West Antarctic rift system: New light on the history and dynamics of distributed intracontinental extension, *in* Cooper, A.K., et al., eds. Antarctica: A Keystone in a Changing World, National Academy of Sciences.

Siddoway, C.S., and Fanning, C.M., 2009, SHRIMP U-Pb zircon geochronology of a migmatite-granite complex in West Antarctica, with bearing on the character and extent of Paleozoic tectonism on the East Gondwana margin: Tectonophysics, doi: 10.1016/j.tecto.2009.04.021

Smith, C.H., 1997, Mid-crustal processes during Cretaceous rifting, Fosdick Mountains, Marie Byrd Land, *in* Ricci, C.A., ed., The Antarctic Region: Processes and Evolution, Terra Antarctica Publications, p. 313–320.

Storey, B., Leat, T., Weaver, S.D., Pankhurst, R.J., Bradshaw, J.D., and Kelley, S., 1999, Mantle plumes and Antarctica-New Zealand rifting: Evidence from mid-Cretaceous mafic dykes, Journal of the Geological Society of London, v. 156, p. 659–671.

Talbot, J-Y, Faure, M., Chen, Y., and Martelet, G., 2005, Pull-apart emplacement of the Margeride granitic complex (French Massif Central). Implications for the late evolution of the Variscan orogen, Journal of Structural Geology, v. 27, p. 1610–1629.

Tera, F., and Wasserberg G., 1972, U-Th-Pb systematics in three Apollo 14 basalts and the problem of initial Pb in lunar rocks, Earth and Planetary Science Letters, v. 14, p. 281–304.

Teyssier, C., and Tikoff, B., 1999, Fabric stability in oblique convergence and divergence, Journal of Structural Geology, v. 21, p. 969–974.

Teyssier, C., Ferre, E.C., Whitney, D.L., Norlander, B., Vanderhaeghe, O., and Parkinson, D., 2005, Flow of partially molten crust and origin of detachments during collapse of the Cordilleran orogen, *in* Bruhn, D., and Burlini, L., eds, High-strain zones: Structure and Physical Properties: Geological Society, London, Special Publications, 245, p. 39–64.

Tikoff, B., and Teyssier, C., 1992, Crustal-scale, en echelon "P-shear" tensional bridges: A possible solution to the batholithic room problem, Geology, v. 20, p. 927–930.

Tikoff, B., and Teyssier, C., 1994, Strain modeling of displacement-field partitioning in transpressional orogens, Journal of Structural Geology, v. 16, p. 1575–1588.

Rey, P.F., Teyssier, C., and Whitney, D.L., 2009, Extension rates, crustal melting, and core complex dynamics: Geology, v. 37, p. 391–394, doi:10.1130G25460A.1

Weaver, S.D., Adams, C.J., Pankhurst, R.J., and Gibson, I.L., 1992, Granites of Edward VII Peninsula, Marie Byrd Land, Antarctica, *in* Brown, E., and Chappell, B.W., eds., Proceedings of the Second Hutton Symposium on the Origin of Granites and Related Rocks, Transactions of the Royal Society of Edinburgh, Earth Sciences, v. 83, p. 281–290.

Weinberg, R.F., and Mark, G., 2008, Magma migration, folding, and disaggregation of migmatites in the Karakoram shear zone, Ladakh, NW India, Geological Society of America Bulletin, v. 120, p. 994–1009, doi: 10.1130/B26227.1.

Weinberg, R.F, Mark, G., and Reichardt, H., 2009, Magma ponding in the Karakoram shear zone, Ladakh NW India, Geological Society of America Bulletin, v. 121, p. 278–285, doi: 10.1130/B26358.1.

Whitney, D.L., Teyssier, C., and Vanderhaeghe, O., 2004, Gneiss domes and crustal flow, *in* Whitney, D.L., Teyssier, C., and Siddoway, C.S., eds., Gneiss domes in orogeny: Geological Society of America Special Paper 380, p. 15–33.

Whitney, D.L., Teyssier, C., and Heizler, M.T., 2007, Gneiss domes, metamorphic core complexes, and wrench zones: Thermal and structural evolution of the Nigde Massif, central Anatolia: Tectonics, v. 26, doi: 10.1029/2006TC002040.

Williams, I.S., 1998, U-Th-Pb geochronology by ion microprobe, *in* McKibben, M.A., Shanks III, W.C., and Ridley, W.I., eds., Application of Microanalytical Techniques to Understanding Mineralizing Processes, Reviews in Economic Geology, Littleton, CO, Society of Economic Geologists, p. 1–35.

Figure Captions

Figure 4.1. Three-dimensional block diagrams of three end-member scenarios that show the relationship between the oblique divergence angle (α) and fabrics in partially molten crust during the development of a dilation zone: pure wrench (α = 0º), wrench-dominated transtension (α = 15–25º), and extension-dominated transtension (α = 45º). Diagrams also show the instantaneous and finite strain ellipses.

Figure 4.2**.** Geologic map of the Fosdick Mountains showing regions of migmatite and granite, bounding structures, and lineations. Outlines represent cliff exposures. Cross-section (A-A') shows the foliations and orientations of the bounding faults. Stereographic projections display data points and kamb contours, with a 2 sigma contour interval, of fold axes, poles to foliation, and stretching lineations. Equal area stereographic projections were made with Stereonet v.6.3.3, by Richard Allmendinger. Inset shows the stretching axis and long axis of the Fosdick dome.

Figure 4.3**.** a) Photo and b) sketch of the leucogranite sheeted complex from Bird Bluff, where sample C6-BB112 was collected. Granite is light gray, migmatitic orthogneiss is gray, and migmatitic paragneiss is dark gray. Mafic dikes (black) within the leucogranite layers are boudinaged and buckled (see also Smith, 1997). Geologist within circle at base of exposure is used for scale.

Figure 4.4**.** Tera-Wasserburg concordia diagrams of U-Pb SHRIMP isotopic data. Insets are probability density plots with stacked histograms. Weighted mean $^{206}Pb/^{238}U$ age and uncertainty is given at 95% confidence and includes the uncertainty in the U/Pb ratio calibration of the reference zircon. a, b) Steep granite sill, sample M6-L188, from Mt. Lockhart, and c, d) subhorizontal leucogranite sheet, sample C6-BB112, from Bird Bluff. e, f) CL images of representative zircons analyzed from samples M6-L188 and C6-BB112.

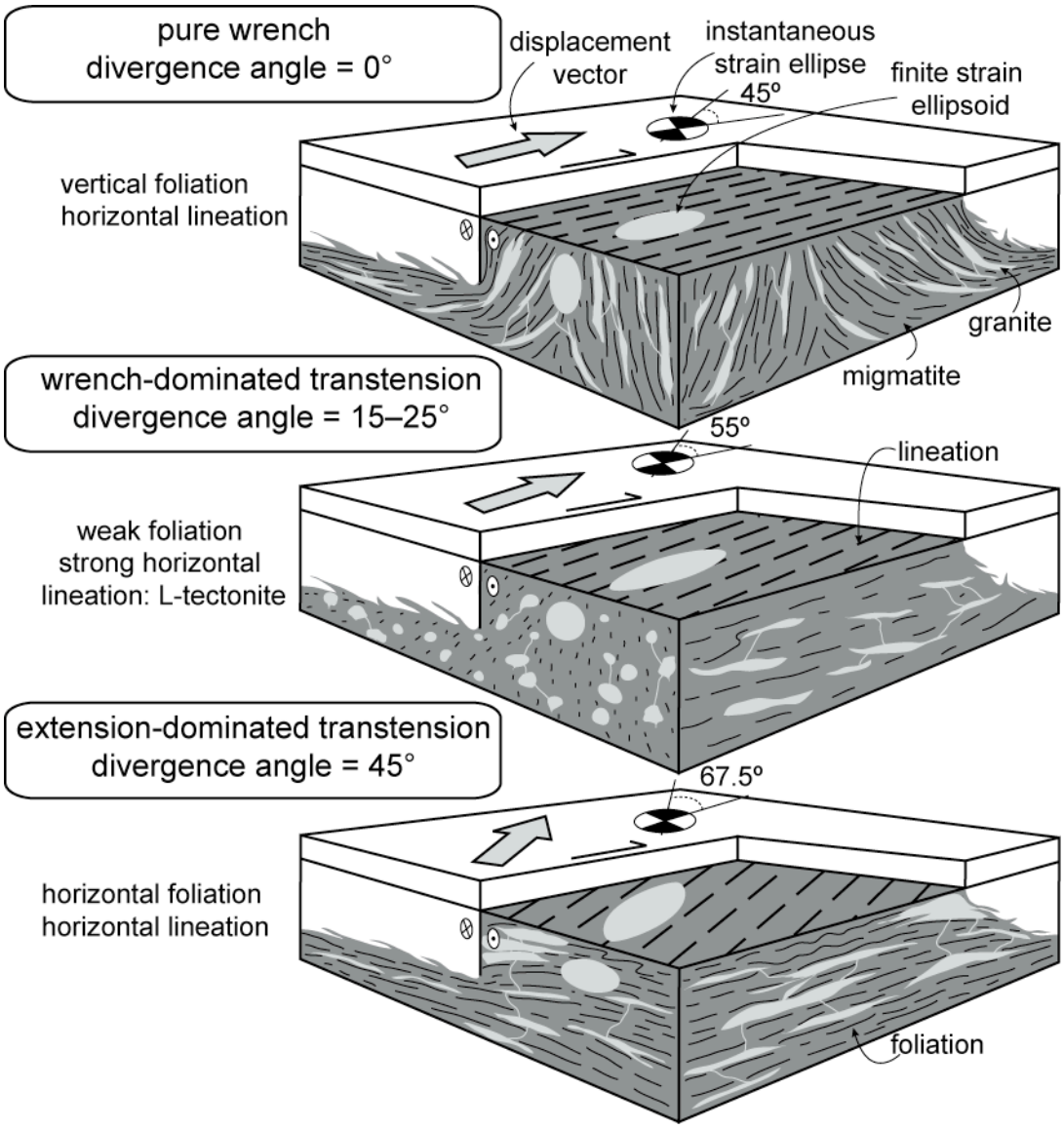

Figure 4.1 Three-dimensional diagrams of strain vs. fabrics in partially molten crust

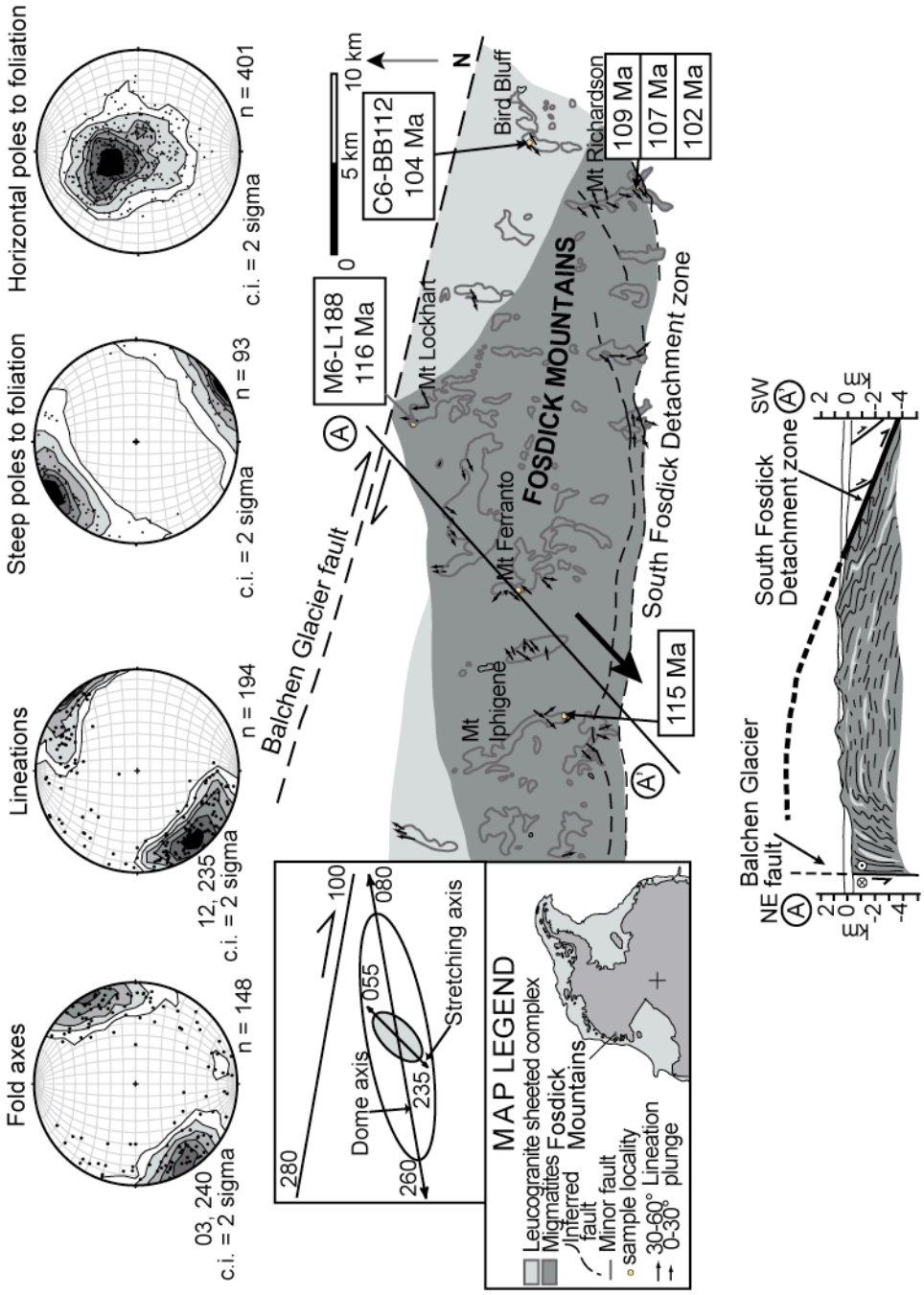

Figure 4.2 Geologic map of the Fosdick Mountains.

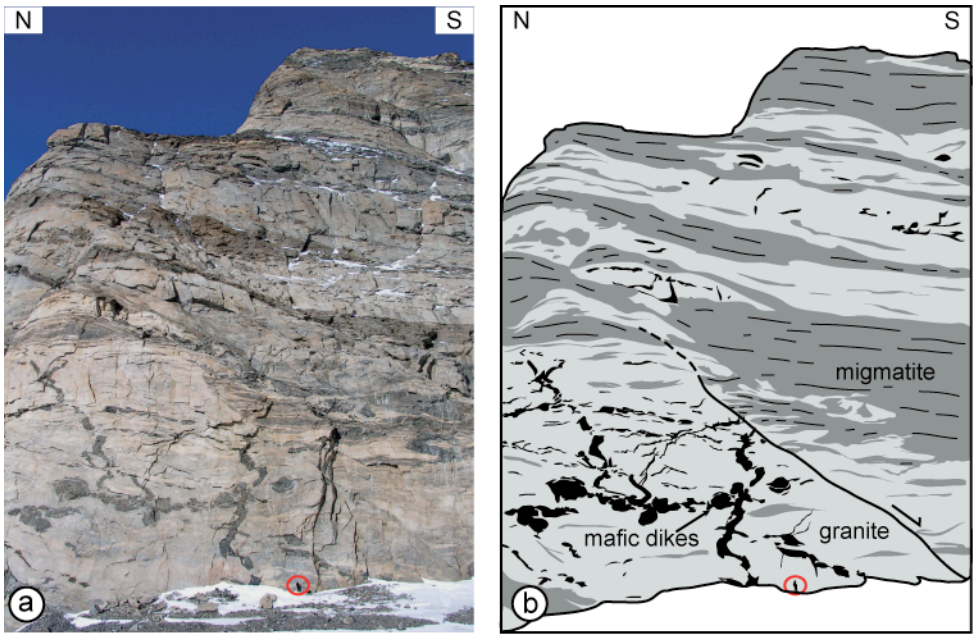

Figure 4.3 Photo and sketch of leucogranite sheeted complex.

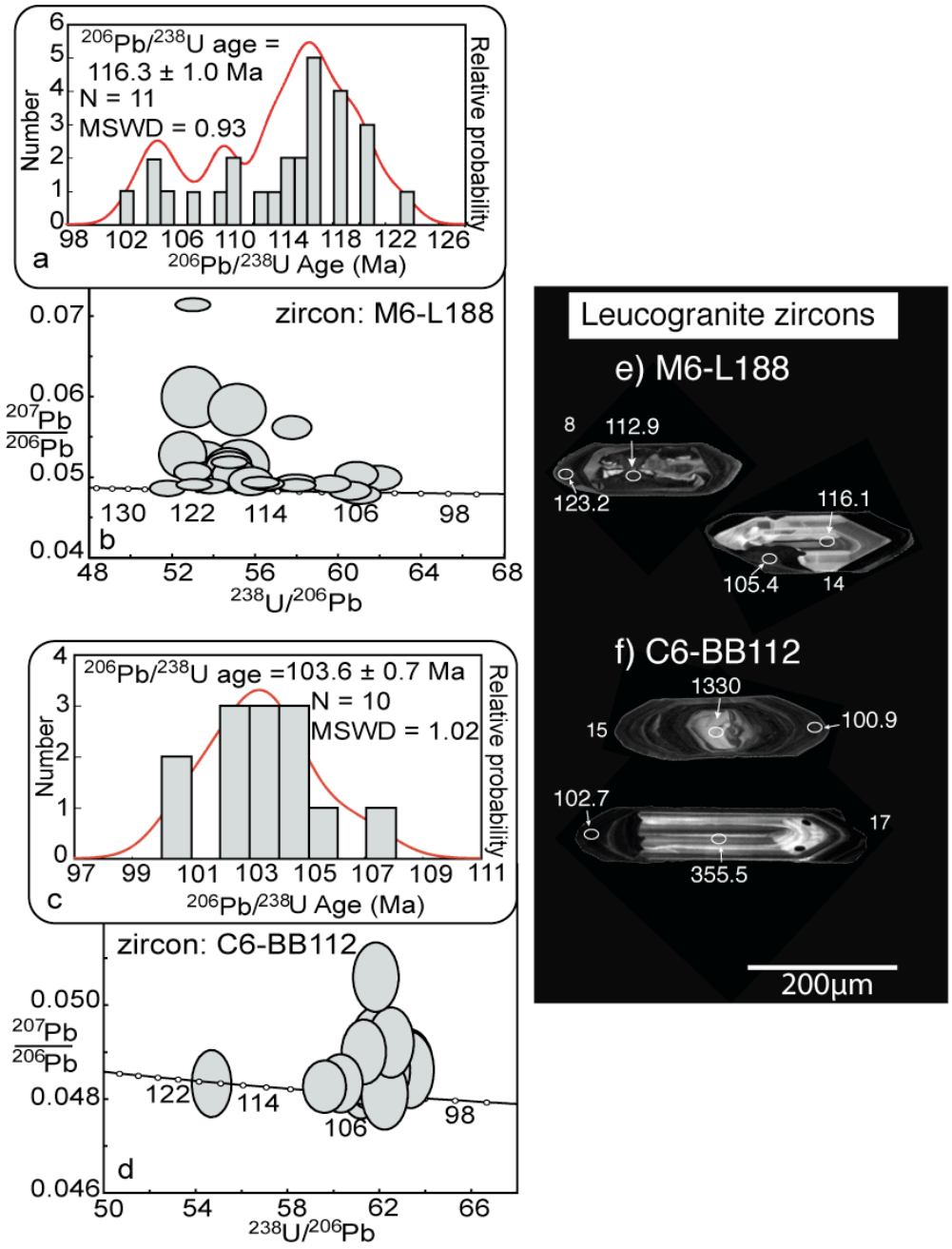

Figure 4.4 U-Pb data plots from granite in specific structural sites.

TABLE 4.1 Summary of SHRIMP U-Pb zircon results for leucogranite sheets in the Fosdick Mountains

							Total				Radiogenic ratios		Age (Ma)	
Grain spot	U (ppm)	Th (ppm)	Th/U	$^{206}Pb^*$ (ppm)	$^{204}Pb/^{206}Pb$	f_{206} %	$^{238}U/^{206}Pb$	±	$^{207}Pb/^{206}Pb$	±	$^{206}Pb/^{238}U$	±	$^{206}Pb/^{238}U$	±
***Sample M6-L188** - granite sill from Mt. Lockhart (Location:S 76° 26.435 , W 145° 11.623)														
Rims														
1.1	763	42	0.055	10.6	0.000302	0.25	61.98	0.74	0.0500	0.0010	0.0161	0.0002	102.9	1.2
3.1	1517	142	0.094	24.2	-	0.08	53.89	0.58	0.0490	0.0006	0.0185	0.0002	118.4	1.3
4.2	2613	10	0.004	39.9	0.000034	0.15	56.28	0.59	0.0495	0.0005	0.0177	0.0002	113.4	1.2
6.1	1210	6	0.005	17.4	0.000046	0.15	59.65	0.66	0.0493	0.0007	0.0167	0.0002	107.0	1.2
8.1	2545	7	0.003	38.7	0.000046	0.13	56.53	0.60	0.0493	0.0005	0.0177	0.0002	112.9	1.2
12.1	1002	29	0.029	14.1	-	<0.01	61.08	0.69	0.0480	0.0008	0.0164	0.0002	104.7	1.2
13.1	1043	33	0.032	14.7	0.000400	0.29	60.94	0.68	0.0505	0.0010	0.0164	0.0002	104.6	1.2
14.1	1009	5	0.005	14.3	0.000164	0.04	60.61	0.68	0.0485	0.0007	0.0165	0.0002	105.4	1.2
15.1	479	165	0.344	24.7	0.000112	0.13	16.67	0.19	0.0552	0.0006	0.0599	0.0007	375.0	4.2
17.1	2496	149	0.060	40.4	0.000149	0.10	53.11	0.56	0.0492	0.0005	0.0188	0.0002	120.1	1.3
18.1	1683	66	0.039	25.0	0.000815	1.02	57.81	0.62	0.0563	0.0010	0.0171	0.0002	109.4	1.2
20.1	1915	31	0.016	28.4	0.000236	0.18	57.98	0.62	0.0497	0.0005	0.0172	0.0002	110.0	1.2
21.1	2623	53	0.020	42.5	0.001755	2.91	53.04	0.55	0.0715	0.0005	0.0183	0.0002	116.9	1.2
22.1	1713	8	0.005	25.4	0.000023	0.11	58.03	0.61	0.0491	0.0005	0.0172	0.0002	110.0	1.2
Cores														
2.1	172	216	1.261	2.7	0.000693	1.28	55.18	0.91	0.0585	0.0021	0.0179	0.0003	114.3	1.9
4.1	100	106	1.058	1.6	0.002504	1.47	53.00	0.96	0.0601	0.0025	0.0186	0.0003	118.7	2.2
5.1	419	166	0.396	6.6	0.000482	0.41	54.81	0.72	0.0516	0.0011	0.0182	0.0002	116.1	1.5
6.2	306	450	1.470	4.8	0.000946	0.43	54.78	0.73	0.0518	0.0013	0.0182	0.0002	116.1	1.5
7.1	851	151	0.178	13.8	0.000068	0.29	53.03	0.60	0.0508	0.0008	0.0188	0.0002	120.1	1.4
8.2	1172	314	0.268	19.4	-	0.03	51.82	0.57	0.0488	0.0006	0.0193	0.0002	123.2	1.3

							Total				Radiogenic ratios		Age (Ma)	
Grain spot	U (ppm)	Th (ppm)	Th/U	$^{206}Pb^*$ (ppm)	$^{204}Pb/^{206}Pb$	f_{206} %	$^{238}U/^{206}Pb$	±	$^{207}Pb/^{206}Pb$	±	$^{206}Pb/^{238}U$	±	$^{206}Pb/^{238}U$	±
9.1	2099	14	0.006	32.9	0.000270	0.46	54.81	0.58	0.0520	0.0005	0.0182	0.0002	116.0	1.2
10.1	225	138	0.611	3.7	0.000779	0.56	52.57	0.75	0.0529	0.0019	0.0189	0.0003	120.8	1.7
11.1	131	107	0.814	2.0	0.000790	0.42	55.31	0.93	0.0516	0.0021	0.0180	0.0003	115.0	1.9
12.2	140	123	0.881	2.2	0.000305	0.39	53.61	0.88	0.0515	0.0020	0.0186	0.0003	118.7	2.0
13.2	419	468	1.117	6.4	0.000375	0.17	55.82	0.71	0.0497	0.0011	0.0179	0.0002	114.3	1.4
14.2	365	350	0.958	5.7	0.000257	0.27	54.86	0.71	0.0505	0.0012	0.0182	0.0002	116.1	1.5
15.2	1189	880	0.740	60.4	0.000013	<0.01	16.92	0.18	0.0539	0.0004	0.0591	0.0006	370.2	3.9
16.1	401	101	0.252	6.3	-	0.28	55.04	0.70	0.0505	0.0012	0.0181	0.0002	115.8	1.5
18.2	779	138	0.177	77.5	0.000035	0.04	8.633	0.101	0.0633	0.0006	0.1158	0.0014	706.2	8.1
19.1	312	373	1.195	5.0	-	0.21	53.87	0.72	0.0501	0.0013	0.0185	0.0002	118.3	1.6

							Total				Radiogenic ratios		Age (Ma)	
Grain spot	U (ppm)	Th (ppm)	Th/U	$^{206}Pb^*$ (ppm)	$^{204}Pb/^{206}Pb$	f_{206} %	$^{238}U/^{206}Pb$	±	$^{207}Pb/^{206}Pb$	±	$^{206}Pb/^{238}U$	±	$^{206}Pb/^{238}U$	±
***Sample C6-BB112** - leucogranite sheet from Bird Bluff (Location: S 76° 30.197 , W 144° 35.618)														
Rims														
1.1	1365	41	0.03	19.0	0.000027	0.12	61.75	0.67	0.0490	0.0006	0.0162	0.0002	103.4	1.1
2.1	3400	244	0.07	49.0	0.000133	0.02	59.66	0.62	0.0483	0.0004	0.0168	0.0002	107.1	1.1
3.1	2833	181	0.06	40.3	-	0.03	60.35	0.63	0.0484	0.0004	0.0166	0.0002	105.9	1.1
4.1	1873	87	0.05	26.2	0.000180	0.08	61.33	0.65	0.0487	0.0005	0.0163	0.0002	104.2	1.1
5.1	2823	144	0.05	39.6	0.000089	0.05	61.21	0.64	0.0485	0.0006	0.0163	0.0002	104.4	1.1
6.1	3417	242	0.07	47.8	0.000060	0.12	61.36	0.64	0.0490	0.0005	0.0163	0.0002	104.1	1.1
7.1	2535	223	0.09	39.8	0.000046	0.00	54.75	0.57	0.0484	0.0005	0.0183	0.0002	116.7	1.2
8.1	2416	121	0.05	33.2	0.000059	0.15	62.54	0.66	0.0492	0.0005	0.0160	0.0002	102.1	1.1
9.1	2011	61	0.03	27.3	0.000128	0.08	63.37	0.67	0.0486	0.0005	0.0158	0.0002	100.9	1.1
12.1	1829	80	0.04	25.5	-	0.07	61.53	0.66	0.0487	0.0006	0.0162	0.0002	103.9	1.1
13.1	2282	108	0.05	31.5	0.000086	0.07	62.29	0.71	0.0486	0.0005	0.0160	0.0002	102.6	1.2
14.1	1696	34	0.02	35.6	-	0.18	40.87	0.43	0.0506	0.0005	0.0244	0.0003	155.5	1.6

							Total				Radiogenic ratios		Age (Ma)	
Grain spot	U (ppm)	Th (ppm)	Th/U	$^{206}Pb^{*}$ (ppm)	$^{204}Pb/^{206}Pb$	f_{206} %	$^{238}U/^{206}Pb$	±	$^{207}Pb/^{206}Pb$	±	$^{206}Pb/^{238}U$	±	$^{206}Pb/^{238}U$	±
15.1	1960	83	0.04	26.6	0.000054	0.08	63.35	0.68	0.0487	0.0005	0.0158	0.0002	100.9	1.1
16.1	2521	164	0.07	35.0	0.000177	0.32	61.89	0.65	0.0506	0.0005	0.0161	0.0002	103.0	1.1
17.1	2304	117	0.05	31.8	0.000112	0.01	62.26	0.67	0.0481	0.0005	0.0161	0.0002	102.7	1.1
Cores														
3.2	747	1430	1.91	36.9	-	0.13	17.40	0.19	0.0548	0.0005	0.0574	0.0006	359.8	3.8
10.1	680	50	0.07	33.7	0.000049	<0.01	17.35	0.19	0.0533	0.0005	0.0577	0.0006	361.4	3.9
11.1	693	407	0.59	32.4	0.000087	0.10	18.35	0.20	0.0541	0.0005	0.0544	0.0006	341.7	3.6
12.2	2009	1091	0.54	318.8	0.000010	0.02	5.415	0.055	0.0757	0.0002	0.1846	0.0019	1092	10
15.2	323	147	0.46	63.7	0.000049	0.08	4.360	0.048	0.1093	0.0006	0.2292	0.0025	1330	13
17.2	250	327	1.31	12.2	-	0.04	17.63	0.25	0.0540	0.0008	0.0567	0.0008	355.5	5.0

Uncertainties given at the 1σ level.

f_{206} % denotes the percentage of ^{206}Pb that is common Pb.

Correction for common Pb made using the measured $^{238}U/^{206}Pb$ and $^{207}Pb/^{206}Pb$ ratios following Tera and Wasserburg (1972) as outlined in Williams (1998).

*Error in Temora reference zircon calibration was 0.34% for the analytical session. (not included in above errors but required when comparing data from different mounts).

**Error in Temora reference zircon calibration was 0.29% for the analytical session. (not included in above errors but required when comparing data from different mounts).

***Error in Temora reference zircon calibration was 0.39% for the analytical session. (not included in above errors but required when comparing data from different mounts).

Chapter 5: Melt transport and magma accumulation during oblique tectonics in the Fosdick Mountains migmatite-cored gneiss dome, Marie Byrd Land, Antarctica

Synthesis

The transfer of melt through the crust and the accumulation of magma are integral components of continental differentiation. The remnant permeability network preserved in crystallized formerly partially molten crust, represented by leucosome and leucogranite dikes and veins, records the pathways of melt and magma transport. The Fosdick Mountains migmatite-cored gneiss dome in Marie Byrd Land, Antarctica hosts migmatites and granites that were emplaced during oblique plate convergence along the East Gondwana margin and intracontinental crustal extension associated with the West Antarctic Rift System in the mid-Cretaceous. Intermediate map-scale (km^2 to several 10s of km^2) distribution of units is used to relate structures developed in the Fosdick dome with large tectonic processes. Steep foliations with scarce lineations are overprinted, folded, and transposed by subhorizontal foliations, which we attribute to a transition from wrench deformation to oblique divergence. Steep structures in the dome host concordant leucosome and leucogranite that record melt transfer through the mid-crustal level of the Fosdick dome to the upper crust. A steep anisotropy is also preserved due to the segregation of melt and the development of migmatitic layering. In the Fosdick dome, subhorizontal domains predominate and host large volumes of subhorizontal diatexite and leucogranite sheets. The diatexite

preserves agmatitic and schollen structures and syntectonic, folded mafic dikes have dismembered fold noses, indicating that an influx of magma related to the subhorizontal sheets may have caused the steep anisotropy to breakdown. The timescale for the transition from wrench to oblique divergence is bracketed by the ages of leucosome and granites emplaced in steep and subhorizontal domains. Granites emplaced in steep foliation domains have U-Pb ages between ca. 117–115 Ma, whereas granites emplaced in subhorizontal domains have U-Pb ages between ca. 109–102 Ma. These ages indicate the timescale for the transition from wrench to oblique divergence was 6 myr. Granites with crystallization ages between ca. 109–102 Ma are also emplaced in the South Fosdick Detachment zone, indicating that the detachment was active during oblique divergence. $^{40}Ar/^{39}Ar$ analyses of amphibole and biotite record cooling of the dome rocks between ca. 101–99 Ma suggesting that the oblique divergence angle of the dome and the accumulation of subhorizontal magma sheets initiated a detachment zone that led to rapid cooling and exhumation of the dome.

1. Introduction

Investigations of migmatite terrains document the flow of partially molten crust, a process that fundamentally affects crustal differentiation and the transport of heat and mass in orogenic crust (Sawyer, 1996, 2001; Brown and Solar, 1998; Vanderhaeghe, 2001; Teyssier and Whitney, 2002; Teyssier et al., 2005; Brown, 2008). Exhumed migmatite-cored gneiss domes represent domains of crystallized formerly partially molten crust that offer direct access to the km-scale structural architecture of melt dominated middle and lower crust where the relationship between melt migration and deformation processes can be studied (e.g. Sawyer, 2001; Solar and Brown, 2001; Weinberg and Mark, 2008). These relationships are of contemporary interest because the transfer of melt affects the thermal structure of the crust and the kms-scale distribution of migmatite and granite units may influence the rheological layering of the crust.

In this paper we explore the development of a remnant permeability network and the flow, emplacement, and exhumation of partially molten crust. Our study discusses the influence of strain, lithologic heterogeneity, and crustal-scale structures on the transfer of melt through the crust and the accumulation of magma in the crust. To address these topics we document the leucosome and leucogranite networks, the intermediate map-scale (km^2 to several 10s of km^2) distribution of migmatite and granite units, and the structural fabrics from the Fosdick Mountains migmatite-cored gneiss dome, Marie Byrd Land, Antarctica.

2. Melt Generation, Transfer, and Emplacement

Crustal differentiation occurs by melt generation, melt segregation and extraction, magma ascent, and magma emplacement (Brown, 1994; Petford et al., 2000; Brown, 2007). Migmatite terrains are key to the study of continental evolution because they preserve evidence for the processes controlling the movement of melt from source to sink (e.g. Brown, 2008; Weinberg and Mark, 2008). Migmatites may denote a region of melt production (e.g. Brown et al., 1995; Milord et al., 2001; White et al., 2004; Clemens, 2006), a zone where segregated melt is extracted from the mafic residue (e.g. Sawyer, 2001; Solar and Brown, 2001; Guernina and Sawyer, 2003), a melt transfer zone where melt ascends through the crust, where melting occurred at a deeper level and was transported to higher crustal levels (e.g. Collins and Sawyer, 1996; Solar and Brown, 2001), and a magma accumulation zone (Sawyer, 1999; Marchildon and Brown, 2003; Weinberg et al., 2009). At a given structural level, the processes of melt extraction, transfer, and accumulation may have been active synchronously or diachronously, and the record of melt source, transfer, and sink must be resolved.

Migmatite terrains commonly have bulk rock compositions that are residual with respect to a granite melt composition, indicating melt extraction from the source (Solar and Brown, 2001; Guernia and Sawyer, 2003). Melt transport is recorded by the remnant permeability network, consisting of interconnected leucosomes and granite, and discrete structures that represent melt escape, including cuspate and sutured fold hinges (Sawyer, 2001; Marchildon and Brown, 2003; Weinberg and Mark, 2008).

Emplaced granite bodies of various shapes and sizes represent regions of magma accumulation (e.g. Brown, 2008). The development of an interconnected permeability network controls the transfer of melt through the crust (Weinberg, 1999). The geometries of the permeability network and the flow of melt along permeability pathways are controlled by pressure gradients created by local anisotropies, magma buoyancy, and tectonic deformation (e.g. Collins and Sawyer, 1996; Brown and Rushmer, 1997; Brown and Solar, 1998; Sawyer, 2001; Leitch and Weinberg, 2002). The interconnectivity of the permeability network in migmatites implies flow toward magma traps in low-pressure regions that arise due to anisotropy (e.g. Sawyer, 1996; Weinberg et al., 2009). As the melt fraction increases the solid framework breaks down leading to significant rheological weakening (Burg and Vanderhaeghe, 1993). Low melt fraction migmatites (0–20%), referred to as metatexite, preserve the solid framework, have a banded appearance, and deform plastically, whereas high melt fraction migmatites (>20%), referred to as diatexite, develop a disrupted framework, have a magmatic appearance, and experience viscous flow (Burg and Vanderhaeghe, 1993; Sawyer, 2008).

3. Intermediate Map-Scale and Oblique Tectonics

Migmatite terrains are commonly studied at the outcrop-scale, but intermediate map-scale observations reveal the relationship between the distribution of melt in a migmatite terrain and large tectonic structures, information essential to crustal flow and crustal differentiation (e.g. Brown and Solar, 1998; Solar and Brown, 2001). However, lack of sufficient exposure commonly makes documenting the map-scale

distributions difficult. In oblique tectonic settings, understanding this relationship is crucial because it pertains to three-dimensional strain theory (e.g. Tikoff and Teyssier, 1999). The fabric orientations and geometry of remnant transport networks may thus be used to determine the evolution of three-dimensional strain in the crust. In wrench and oblique tectonic zones, dilation zones may develop due to lithologic heterogeneities that exist along large strike-slip faults, creating space for ascent and emplacement of magma and partially molten crust (e.g. Hutton, 1990; D'Lemos et al., 1992; Tikoff and Teyssier, 1992; Talbot et al., 2005). Migmatite-cored gneiss domes and core complexes may be emplaced in these dilation zones (Oldow et al., 2003; Talbot et al., 2005; Foster et al., 2007; Whitney et al., 2007), and the possibility exists that oblique dilation zones play an essential role in the localization and exhumation of partially molten crust by creating pressure gradients that enhance melt transport, magma accumulation, and formation of detachments (e.g. Brown and Solar, 1998; Teyssier et al., 2005; Weinberg and Mark, 2008; Weinberg et al., 2009).

During oblique deformation, the divergence angle (α) controls the strain field and the fabrics that develop. In transtension (oblique divergence), the material lines and planes and the maximum finite strain axis are all attracted toward the direction of oblique divergence and rotate into parallelism with the divergence direction if the strain axes change in orientation (Teyssier and Tikoff, 1999). Thus, they record the divergence angle and obliquity. In addition, strain is commonly divided into a wrench component (strike-slip) and an extensional strain component (thinning). Wrench-dominated transtension occurs between $0° < \alpha < 20°$ and extension-dominated

transtension occurs between 20°< α <90° (Fossen and Tikoff, 1993; Tikoff and Teyssier, 1994). Vertical foliation and horizontal lineation prevail during wrench deformation (α = 0º), but with low divergence angle, the material deforms in constriction to produce an L-tectonite; with increased finite strain, foliation ultimately switches to horizontal. If the divergence angle is >20º, foliation forms and remains in a horizontal geometry whatever the amount of strain (Fossen and Tikoff, 1993; Teyssier and Tikoff, 1999).

The Fosdick Mountains migmatite-cored gneiss dome in Marie Byrd Land, Antarctica offers three-dimensional exposures over a 15 x 80 km area. Structural relief is ~8 km, consisting of migmatites with a broad variation in granite percentage (5–50% granite), nappe-scale folds, and subhorizontal leucogranite sheets. Leucosomes, representing a formerly melt-rich part of partially molten rocks, and leucogranites, representing a coalesced melt body (probably partially drained), comprise the remnant permeability network through which an unknown volume of melt passed. The km-scale exposures in the Fosdick Mountains allow us to relate granites emplaced in diverse structures to the transfer of melt through the migmatites to higher crustal levels and the accumulation of granite within the dome. In addition, we consider the implications of an evolving strain field on the geometry of the remnant permeability network, low-pressure magma accumulation zones, and cooling and exhumation of the dome. To document the evolution of the dome, from inception to exhumation, we present structural observations of migmatite and granite fabrics and the crystallization and cooling history of the dome rocks.

4. Regional Geology

The Ross Province of Marie Byrd Land (Pankhurst et al., 1998) consists of Paleozoic Swanson Formation metagraywacke (Bradshaw et al., 1983; Adams, 1986), Devono-Carboniferous Ford Granodiorite (Weaver et al., 1991; Pankhurst et al., 1998), and Cretaceous Byrd Coast Granite (Weaver et al., 1992), with minor Pleistocene basaltic volcanics (Gaffney and Siddoway, 2007). In the Fosdick Mountains, the intrusion of the Ford Granodiorite coincided with metamorphism and partial melting of the host Swanson Formation metagraywackes (Siddoway et al., 2004b; Siddoway and Fanning, 2009). Migmatites associated with Paleozoic melting record metamorphic conditions of 820–870 ºC and 7.2–11.8 kbar (Korhonen et al., *in revision*). A second, major melting event in the Fosdick Mountains occurred in the mid-Cretaceous (Siddoway et al., 2004b; Siddoway, 2008; McFadden et al., *in review*). Mineral equilibrium modeling of the Cretaceous Fosdick migmatites record temperatures of 830–865 ºC and 6.2–7.4 kbar indicating metamorphic conditions sufficient to induce melting were attained (Korhonen et al., *in revision*). Sr-Nd isotopic and whole-rock major and trace element compositions indicate two types of Cretaceous granites, either from melts derived from plutonic host sources (Ford Granodiorite) or from metasedimentary host sources (Swanson Formation), possibly originating from greater depth than the Fosdick dome (Korhonen et al., *in review*).

The Mesozoic active continental margin of East Gondwana experienced a transition from oblique convergence to oblique divergence, leading to rifting and continental break-up (Sutherland and Hollis, 2001; Vaughan and Livermore, 2005;

Siddoway, 2008) (Fig. 5.1). West Antarctica and Zealandia (New Zealand + submarine plateaus) comprised a significant portion of the once contiguous margin (Luyendyk et al., 1995; Bradshaw et al., 1997; Mortimer et al., 2006). The Median Batholith in New Zealand with magmatism between 145–120 Ma (Bradshaw et al., 1997; Mortimer et al., 1999) and the Amundsen province of Marie Byrd Land (Pankhurst et al., 1998) with magmatism between ca. 124–96 Ma (Pankhurst et al., 1998; Mukasa and Dalziel, 2000) represent the Mesozoic magmatic arc. Inboard of the magmatic arc, backarc extension, backarc plutonism (Weaver et al., 1992, 1994), high temperature metamorphism, and crustal melting occurred (Smith, 1997; Spell et al., 2000; Siddoway et al., 2004b; Scott and Cooper, 2006). U-Pb ages on accessory minerals (e.g. zircon, titanite, monazite) from mid-crustal migmatites, gneisses, and granites record high temperature metamorphism and crustal melting between ca. 126–100 Ma in New Zealand (e.g. Kimbrough and Tulloch, 1989; Ireland and Gibson, 1998; Scott and Cooper, 2006) and Marie Byrd Land (Siddoway, 2008; McFadden et al., *in review*). The mid-crustal rocks are syn-kinematic with extensional structures, including core complexes and deep level shear zones in New Zealand (Gibson et al., 1988; Tulloch and Kimbrough, 1989; Forster and Lister, 2003; Spell et al., 2000; Scott and Cooper, 2006; Kula et al., 2007) and detachment structures in the Fosdick Mountains, Marie Byrd Land (McFadden et al., 2007) and in the Ross Sea (Fitzgerald and Baldwin, 1997; Siddoway et al., 2004a) (Fig. 5.1). In Marie Byrd Land, alkalic plutonism and mafic magmatism manifest as the Byrd Coast Granite and mafic dike arrays accompanied regional deformation and heating in mid-Cretaceous time

(Weaver et al., 1992; Adams, 1987; Storey et al., 1999; Siddoway et al., 2005). These relationships indicate that a significant region experienced crustal heating and crustal thinning, creating conditions conducive to flow of partially molten crust.

Kinematics of brittle and ductile structures in the Ross province of Marie Byrd Land indicate that transcurrent deformation occurred during intracontinental rifting that brought about the opening of the West Antarctic Rift System (Siddoway et al., 2005; Siddoway, 2008). Kinematic data from mafic dikes and brittle faults (Siddoway et al., 2005) and from ductile structures in the Fosdick gneiss dome (Siddoway et al., 2004b; McFadden et al., 2007) record ENE-WSW stretching due to dextral transtension over a >1000 km^2 region. Aerogeophysical data and brittle fault studies identify a conjugate geometry of ~E-W oriented dextral and NE-SW sinistral strike-slip faults formed during the regional strain (Ferracioli et al., 2002; Luyendyk et al., 2003; Siddoway et al., 2005). Exposures of Byrd Coast Granite commonly occur near inferred crustal-scale strike-slip faults suggesting that magma transport to upper crustal levels localized along these faults (Siddoway, 2008).

5. Fosdick Architecture

The Fosdick Mountains migmatite-cored gneiss dome is an elongate dome consisting of mid-crustal migmatites and multiple phases of granite (Siddoway et al., 2004b; McFadden et al., *in review*) (Figs. 5.2, 5.3). A layered plutonic association and folded paragneisses form an ~5 km thick layered sequence. Regions of the paragneiss and layered plutonic association experienced partial melting in the Paleozoic (Siddoway et al., 2004b; Siddoway, 2008; Siddoway and Fanning, 2009; Korhonen et

al., *in revision*) and other regions experienced partial melting in the mid-Cretaceous (Siddoway et al., 2004b; Siddoway, 2008; Korhonen et al., *in review*, McFadden et al., *in review*). Multiple generations of leucosome and granitic dikes and veins and tabular granite bodies are hosted within these units (Figs. 5.2, 5.3, and 5.4). Interstitial, optically continuous quartz forming grain boundary films and cuspate and lobate interstices on subhedral plagioclase grains represent microstructures indicative of former melt presence (McFadden et al., *in review*; e.g. Holness, 2008). Leucosomes show petrologic continuity with crosscutting leucogranite dikes. Interlocking feldspar grains display mechanical kinking at grain-to-grain contacts in coarse-grained phases, indicating the phases acted as a solid framework with interstitial permeability that allowed migration of a melt portion (McFadden et al., *in review*; e.g. Holness, 2008) and subhedral plagioclase and k-feldspar grains preserve mechanical kinking along grain boundaries that form a solid framework. An ~2 km thick section of voluminous, subhorizontal leucogranite sheets occur above the folded migmatites (Figs. 5.2, 5.3, and 5.5). The leucogranite sheets are bounded above by a km-thick section of low melt fraction metatexite migmatites that exhibit solid-state fabrics imparted by the dextral normal oblique South Fosdick Detachment zone (SFD) (McFadden et al., 2007). The Balchen Glacier strike-slip fault and the paragneiss and orthogneiss units form the lower boundary of the leucogranite sheets. The SFD forms the southern boundary of the dome (McFadden et al., 2007). The northern boundary of the dome is the inferred, dextral strike-slip Balchen Glacier fault (Siddoway et al., 2004, 2005). Mafic dikes that intruded throughout the dome evolution are boudinaged and buckled. Late-

tectonic mafic dikes and other tensile structures are oriented WNW-ESE (Richard, 1992; Siddoway et al., 2004b, 2005).

5.1 Rock Units

5.1.1 Metatexitic Paragneiss

Domains of residual metatexitic paragneisses that represent the metamorphosed and partially melted Swanson Formation metagraywackes (Siddoway and Fanning, 2009; Korhonen et al., *in revision*; McFadden et al., *in review*) are exposed in the north-central (Mt. Avers–type locality) and western portions of the Fosdick Range (Figs. 5.4, 5.6A, and B). The stromatic metatexite migmatites are characterized by discrete mm- to cm-thick in-source leucosome, the integrated product (residual crystals + crystallized melt) of segregated melt, and melanosome, part of solid framework from which melt has been extracted (Marchildon and Brown, 2003; migmatite terminology following Sawyer, 2008) (Fig. 5.6A) and leucogranite sills and bodies derived from sources outside the host (Korhonen et al., *in revision, in review*). Melanosomes contain biotite + quartz + plagioclase + K-feldspar ± garnet ± cordierite ± sillimanite and the leucosomes contain quartz + plagioclase + K-feldspar ± garnet ± cordierite ± biotite. The metatexitic paragneisses exhibit steep foliation that is folded into upright dm-scale folds. Foliation is defined by stromatic compositional layering. The paragneiss hosts m-thick layers of concordant leucogranite that lacks internal foliation (Fig. 5.6B). At Mt. Avers, the metatexitic paragneiss forms a N-vergent, cylindrical km-scale fold nappe.

5.1.2 Metatexitic Orthogneiss

Layers of metatexitic orthogneiss 65–100 m thick, interlayered with m- to 10 m thick metatexitic paragneiss occur in the north-central and western portion of the dome (Marujupu Peak, Mt. Lockhart, Mt. Avers, and Mt. Iphigene) (Figs. 5.4, 5.5, 5.6C, and D). The metatexitic orthogneisses are well foliated and contain discrete to diffuse leucosomes and paleosome (part of migmatite unaffected by partial melting—following Sawyer, 2008). Paleosomes are homogeneous textured with an even distribution of phases, consisting of medium-grained quartz + plagioclase + K-feldspar + biotite ± garnet ± hornblende. Aligned biotite and feldspar-quartz shape fabric define foliation. Millimeter to cm-scale leucosomes are predominantly concordant, but oblique, crosscutting leucocratic veins and segregations transect the orthogneiss (Fig. 5.6C). In folded layers, paleosomes are rimmed by leucogranite (Fig. 5.6D). Garnet-bearing, patchy neosomes occur and are commonly connected by a mm- to cm-scale leucosome network.

5.1.3 Diatexite Migmatite

Exposed along the Ochs Glacier in the central portion of the Fosdick dome (Mt. Ferranto, Marujupu Peak, and Mt. Iphigene) is a formerly melt-rich horizon of diatexite migmatite (Figs. 5.4A, B, 5.6E, and F). The diatexite unit is up to 1 km thick and is subhorizontal. The diatexite has a diffuse contact with orthogneiss and paragneiss layers and semi-concordant dm-scale paragneiss and orthogneiss layers are preserved in the diatexite (Fig. 5.4A, B). Near the contact with the diatexite, leucosome and leucogranite veins and dikes intrude and disrupt the paragneiss and

orthogneiss. Agmatitic and schollen structures with rafts of paragneiss paleosome and disrupted mafic dikes are observed in the diatexite (Fig. 5.6E, F). The diatexite neosome (part of migmatite affected by partial melting, commonly quartzofeldspathic) has indistinct boundaries between leucosome and residuum (part of neosome that is the solid fraction left after partial melting and melt extraction, commonly preserves microstructures indicative of former melt presence) (Fig. 5.7E, F).

5.1.4 Leucogranite Sheeted Complex

In the eastern Fosdick Mountains, from Mt. Bitgood to Bird Bluff, 50 to 100 m thick subhorizontal leucogranite sills were emplaced. Meters-thick subhorizontal layers of ortho- and paragneiss separate these sills. The leucogranite sheets form a composite ~2 km-thick leucogranite sheeted complex (McFadden et al., *in review*) (Figs. 5.5, 5.7A, and B). The thickness and proportion of leucogranite sheets increases towards the east (towards Bird Bluff) (Fig. 5.5). The leucogranite sheets at Mt. Bitgood are involved in a nappe-scale fold. The magmatic foliation preserved in the leucogranite sheets is parallel to the metamorphic layering of gneissic sheets. Mafic dikes that intrude the leucogranite sheets are boudinaged parallel to the magmatic fabric and buckled perpendicular to the sheet margins (Fig. 5.7E, F). Leucogranite-filled, outcrop-scale shear bands crosscut the leucogranite sheets (Fig. 5.7A). The paragneiss and orthogneiss layers are predominantly metatexitic, but some orthogneiss layers are diatexitic, with ghostly biotite foliation and indistinct contacts between residuum and leucosome (Fig. 5.5C, D). Orthogneisses associated with the leucogranite sheeted complex contain 1–3 cm thick, in-source leucosome with m-scale

spacing. Paragneiss layers within the leucogranite complex have cm- to m-scale folds and rootless, intrafolial folds. Concordant leucosomes are most common, but discordant subvertical leucosomes occur. Leucogranite-filled shear bands and melanosome within shear bands commonly offset the leucosomes.

5.1.5 Metatexite Migmatite

A km thick zone of interlayered and interfolded metatexitic paragneiss and orthogneiss with solid-state ductile fabrics is associated with the South Fosdick Detachment zone (Fig. 5.7C, D). The metatexites commonly display mm- to cm-scale concordant in-source leucosome and poorly developed discordant leucosome and granite networks (Fig. 5.7C). However, in the southeast (Mt. Richardson), leucogranite sheets associated with the leucogranite sheeted complex intrude the migmatites parallel to foliation. Proximal to the leucogranite sheets, concordant leucosomes several centimeters thick, granite-filled shear bands, and sigmoidal boudins are within the steep foliation of the Mt. Richardson shear zone (Fig. 5.7D).

5.1.6 Mafic and Felsic Dikes

Deformed and undeformed mafic dikes are found throughout the Fosdick dome (Fig. 5.7E, F). The dikes are mostly doleritic, consisting of fine-grained hornblende ± pyroxene + acicular plagioclase ± biotite, with some hornblende or pyroxene porphyry. The deformed dikes are commonly 2–4 m thick, discordant to the migmatitic foliation, buckled perpendicular to the subhorizontal foliation, and boudinaged (Fig. 5.7F). Numerous folded mafic dikes have disrupted and

dismembered hinge zones, and the rafts of disrupted dike material are entrained within the neosome or in the migmatitic foliation (Fig. 5.7E). The rafts commonly preserve an internal foliation or folding (Fig. 5.6F).

Late discordant felsic dikes and stocks crosscut the metamorphic foliations in the Fosdick dome. These dikes commonly have magmatic foliation and subvertical margins.

5.2 Structural Observations

Migmatites in the Fosdick dome display predominantly subhorizontal foliations, associated with shallowly plunging stretching lineations oriented 055–235 that are defined by biotite, sillimanite, and quartz (Fig. 5.9C). The lineation trend is interpreted as the maximum finite stretching axis during transtension. Fold axes are also shallowly plunging and NE-SW trending, with an average orientation of 060–240 (Fig. 5.9D). The stretching axis is oblique to the Balchen Glacier fault, oriented 100–280, and the long axis of the dome, oriented 080–260. These data from the Fosdick dome and from brittle upper crust in neighboring ranges record dextral to dextral oblique motion along the South Fosdick Detachment zone and the Balchen Glacier fault (Siddoway et al., 2005; McFadden et al., 2007). There are regions that preserve subvertical to steeply dipping foliations (Figs. 5.8, 5.9A, and B). To document melt transport and sites of magma accumulation in the Fosdick Mountains we distinguish regions with subvertical structures from subhorizontal structures.

5.2.1 Domains of Steep Foliation

Steeply dipping to subvertical NE-SW striking foliations occur along the northern side of the Fosdick dome from Mt. Iphigene to Mt. Lockhart (Figs. 5.8 and 5.9). The steep foliation domains are primarily exposed in the paragneiss and orthogneiss units, but at Mt. Lockhart subvertical leucogranite sheets exhibit steep foliation (Fig. 5.8A). Subvertical mafic dikes intrude the leucogranites, and these leucogranites and dikes are folded. In the metatexitic paragneiss at Mt. Ferranto, subvertical layers of leucosome and residuum display pronounced m-scale asymmetric folds with subhorizontal fold axes (Fig. 5.8B). Northern Mt. Ferranto also preserves a steep lithological contact between metatexitic paragneiss and diatexite migmatite. The contact is steep and diffuse (10 m-wide). A subhorizontal leucogranite sheet (Fig. 5.8C) and subhorizontal, finely layered metatexitic paragneiss domain (Fig. 5.8D) crosscut finely layered (mm- to cm-thick) metatexitic paragneiss with concordant leucosome. In addition, isoclinal folds and transposed layering of likely steep foliations have been documented at Mt. Avers (Siddoway et al., 2004b).

In the steep domains, paragneiss and orthogneiss host multiple generations of leucosome, leucogranite dikes, and leucogranite sills. U-Pb geochronology of leucogranites that intrude parallel to the steep foliation provide an age constraint of the development of the steep foliation. In the north-central portion of the dome (Mt. Lockhart) a 2 m-thick leucogranite sill that is concordant to the steep metamorphic layering and folded with the layering has a U-Pb zircon crystallization age of 117 Ma (McFadden et al., *submitted*) (Fig. 5.2). A recumbently folded leucogranite sill from

south-central portion of the dome (Mt. Iphigene) has a U-Pb zircon age of 115 Ma (McFadden et al., *in review*).

5.2.2 Domains of Subhorizontal Foliation

In the Fosdick dome, migmatite and granite foliations are primarily subhorizontal and strike NE-SW (Fig. 5.9B). The subhorizontal fabrics overprint or transpose the steep fabrics (Siddoway et al., 2004) (Fig. 5.8). The metatexitic layers in the subhorizontally dipping rocks have well-preserved lineations and shallowly plunging microfolds (Fig. 5.9). The diatexite migmatite, exposed in the Ochs Glacier region (Mt. Iphigene, Marujupu Peak, and Mt. Ferranto), has a diffuse contact with the metatexitic paragneiss and orthogneiss (Figs. 5.4A, B, and 5.6E). However, the boundaries of the diatexite unit define a generally subhorizontal, composite km-thick sheet (Fig. 5.4A, B). In the leucogranite sheeted complex, leucogranite sheets, and their internal foliation, are parallel to the metamorphic layering. Trends of intrafolial fold axes within the subhorizontal leucogranite sheeted complex are oriented 060–240 and are parallel with recumbent fold axes trends in the migmatite core (Siddoway et al., 2004) (Fig. 5.9). Within the subhorizontal domains, mafic dikes are buckled about subhorizontal axes and boudinaged (Smith, 1997; McFadden et al., *submitted*) (Figs. 5.7A, E, and F).

A subhorizontal, concordant 20 cm-thick leucosome in the metatexitic paragneiss at Mt. Ferranto has a U-Pb zircon age of 104 Ma (McFadden et al., *in review*) (Fig. 5.2). At Bird Bluff, a subhorizontal leucogranite sheet, from the

leucogranite sheeted complex records a U-Pb zircon age of 104 Ma (McFadden et al., *in review*).

5.2.3 Solid-State Deformation Domains (South Fosdick Detachment Zone)

Solid-state deformation in the Fosdick dome is associated with the SFD. The SFD forms the interface between ductile, suprasolidus deformation in the Fosdick dome and brittle deformation in the neighboring ranges, and it forms the southern boundary of the Fosdick dome (Figs. 5.2 and 5.3). Solid-state fabrics affect a 1 km thick region of metatexitic paragneiss and orthogneiss and record top-to-the-SW oblique transport (Fig. 5.7C, D). The detachment zone generally dips 20–30º, but at Mt. Richardson the zone dips up to 70º. The detachment zone is intruded by syntectonic, subhorizontal leucogranite sheets and leucogranite and leucosome accumulated in extensional structures, including shear bands and inter-boudin partitions. These former melt-present structures are preserved in rocks that display a strong solid-state fabric (McFadden et al., 2007, *in review*). The metatexitic migmatites in the SFD have a penetrative foliation and lineation defined by stretched quartz and biotite, as well as asymmetric feldspar porphyroclasts and C-S fabrics that record top-to-the-SW oblique motion (McFadden et al., 2007). At Mt. Richardson, sigmoidal boudins that also record top-to-the-SW oblique transport are bordered by leucogranite (Fig. 5.7D). Synkinematic leucogranite and leucosome emplaced in the SFD have U-Pb zircon ages between 109–102 Ma (McFadden et al., *in review*) (Fig. 5.2).

5.2.4 Late Structures

Granite-filled shear bands, mafic and felsic dikes, muscovite-coated brittle fractures, and brittle shears crosscut the detachment zone and foliations in the core of the Fosdick dome. The granite-filled shear bands strike ESE-WNW, record a 015–195 stretching direction, and record top-down-to-the-north or south kinematic sense (Siddoway et al., 2004b; McFadden et al., *in review*) (Fig. 5.10). Subvertical felsic and mafic dikes, brittle fractures, and brittle normal-sense shears strike ~E-W and record ~N-S stretching (Richard, 1992; Siddoway et al., 2005; McFadden et al., 2007) (Fig. 5.10).

6. Geochronology and Thermochronology

We have used U-Pb SHRIMP zircon and titanite geochronology to determine the timing of migmatite and granite crystallization for controls on the age of suprasolidus deformation and movement on the detachment zone. For insight on exhumation and cooling, we employed $^{40}Ar/^{39}Ar$ thermochronology to document the cooling histories of migmatites of the high-grade core and in the detachment. We summarize the key results from the U-Pb study of Cretaceous tectonism (McFadden et al., *in review*) and previous $^{40}Ar/^{39}Ar$ thermochronology (Richard et al., 1994), and present new $^{40}Ar/^{39}Ar$ data from the Fosdick Mountains that are relevant to the timing and rate of deformation and cooling and Cretaceous exhumation of the dome.

6.1 Previous Geochronology and Thermochronology

Migmatites and granites in the Fosdick dome yield U-Pb zircon ages that indicate suprasolidus deformation between ca. 117–102 Ma (Fig. 5.2). Taken together, the crystallization ages indicate a 15 myr duration of melt-present deformation (McFadden et al., *in review*). The granite ages fall within two groups that do not overlap in age. Granites that occur in steep structures or are in folded layers range in age from ca. 117 to 115 Ma. Younger granite emplaced in the SFD or concordant to subhorizontal foliation domains range in age from ca. 109–102 Ma.

Late and post-tectonic discordant dikes were emplaced between ca. 101–97 Ma. A discordant granitic dike crosscuts the SFD solid-state fabric and lacks foliation, thus providing a lower age limit on deformation at ca. 97–96 Ma (McFadden et al., 2007; *in review*). A similar U-Pb age was obtained on monazite from a post-tectonic granite stock (Richard et al., 1994). U-Pb titanite ages for diorite dikes that crosscut the migmatitic foliation range from ca. 101–97 Ma. An older dike is discordant but deformed and a younger dike is strongly discordant and undeformed, suggesting the dikes intruded during the culminating stages of movement of the SFD (McFadden et al., *in review*). Dike emplacement coincided with, or narrowly preceded, the crystallization and cooling of the entire gneiss dome, documented by $^{40}Ar/^{39}Ar$ cooling ages between ca. 101 to 94 Ma for hornblende, muscovite, biotite, and K-feldspar across the range (Richard et al., 1994). $^{40}Ar/^{39}Ar$ muscovite cooling ages on muscovite-bearing brittle shears are ca. 96 Ma (Richard et al., 1994). These results

suggest that high temperatures were sustained in the Fosdick Mountains until the verge of the exhumation event that led to rapid cooling.

6.2 $^{40}Ar/^{39}Ar$ Thermochronology

To clarify the cooling history in the Fosdick dome, we measured $^{40}Ar/^{39}Ar$ cooling ages for biotite and amphibole from a syn-tectonic diorite dike and for biotite from metatexite migmatite that experienced solid-state deformation in the South Fosdick Detachment zone. Throughout the Fosdick dome, diorite sills and diorite dikes intrude the migmatites and granites. Conventional step heating was conducted at the USGS Denver. Samples and standards were irradiated for 20 MWH in the central thimble position of the Triga reactor in Denver, Colorado (Dalrymple et al., 1981). Samples were cadmium-lined to minimize the ^{40}Ar produced from ^{40}K. All analyses were made using a 25W CO_2 laser, and were progressively heated by increasing the laser power. Analyzed samples ranged from one to several individual grains. Errors are reported at the 1 σ confidence level. The $^{40}Ar/^{39}Ar$ results are presented as age spectra. The integrated ages shown represent integrated weighted mean ages calculated for selected portions of each age spectrum (Fig. 5.11). A preferred age is defined as the part of an age spectrum composed of contiguous increments that fall within 1 σ uncertainty in age of neighboring steps within the subset. The initial low-temperature increasing steps were not used in calculating the preferred ages. For the samples we assigned a plateau age by choosing higher temperature heating steps that yield the oldest apparent ages. For these samples most of the spectrum is used for plateau age calculation, and the ages are distributed about their weighted mean square

weighted deviation (MSWD) values. K/Ca ratio plots are determined from the Ca-derived ^{37}Ar and K-derived ^{39}Ar. K/Cl ratios are also plotted.

$^{40}Ar/^{39}Ar$ analyses of amphibole and biotite from a syn-tectonic diorite sill at Mt. Iphigene (M5-I7) yield flat spectra. We interpret the flat spectra to indicate rapid cooling, indicative of rapid cooling. Amphibole analyses yielded an $^{40}Ar/^{39}Ar$ age of 100.5 ± 0.2 Ma. Biotite analyses yielded an $^{40}Ar/^{39}Ar$ age of 100.4 ± 0.2 Ma (Fig. 5.11).

A sample of metatexite migmatite from the SFD at Mt. Richardson (M5-R136A) that yielded a U-Pb age of ca. 105 Ma (McFadden et al., *in review*) was analyzed for $^{40}Ar/^{39}Ar$ biotite. Age spectra are flat and the age is 99.8 ± 0.2 Ma (Fig. 5.11).

7. Transition from Wrench to Oblique Divergence

Structural observations from western Marie Byrd Land and the Fosdick Mountains indicate that the region experienced transcurrent deformation that affected the brittle upper crust and ductile middle to lower crust (Siddoway et al., 2004, 2005; McFadden et al., 2007). The foliations, lineations, and fold axes preserved in the dome and the long axis of the dome provide a record of the rotation of strain axes during wrench to oblique motion.

Steep foliations with scarce lineations are overprinted by subhorizontal foliation, making it clear that the steep foliations developed earlier in the Fosdick dome history (Fig. 5.8). The steep structures are folded and transposed by subhorizontal folds that generally align with the regional finite strain axes (Siddoway

et al., 2005). Wrench to transtension strain theory (e.g. Tikoff and Teyssier, 1994) provides insight into the explanation for the transition from vertical to horizontal strain fabrics over a time period of just 9 myr or less (Fig. 5.12A).

Subvertical foliations are predominantly preserved in outcrops bordering the Balchen Glacier fault, suggesting that the fabric development was more intense or more prevalent near the transcurrent fault. Such an increase in fabric stability is observed toward crustal-scale faults by several studies (e.g. McCaffrey et al., 1999; Tirel et al., 2004; Katrinová et al., 2007; Denèle et al., 2008). Alternatively, the subvertical fabrics may have arisen near strain heterogeneities arising from crustal anisotropy with competency difference between metatexitic paragneiss and diatexite migmatite causing deformation partitioning (McFadden et al., *in review*). However, subvertical foliation domains developed in most of the rock types, including metatexitic paragneiss, metatexitic orthogneiss, and diatexite migmatite.

Foliations in the Fosdick dome are predominantly subhorizontal and they crosscut and transpose earlier steep foliations (Fig. 5.8). Stretching lineations in the subhorizontal domains trend 055–235 (Fig. 5.9). In addition, nappe-scale recumbent folds and dm- to m-scale folds have similar subhorizontal fold axes trends of 060–240, suggesting contemporaneity of mesoscopic and megascopic folds (Fig. 5.9). We interpret the stretching axis of strain to be parallel to the 235 ± 5 trend of the dominant lineations and fold axes. The orientation of the stretching axis determined from folds and lineations, relative to the 100–280 orientation of the Balchen Glacier fault indicates a divergence angle of 45º. Therefore, the subhorizontal fabrics and oblique

stretching direction likely developed during oblique divergence (extension-dominated transtension) (Fig. 5.12B).

The domains of steep foliations and the domains of prevalent overprinting subhorizontal foliations indicate a transition from wrench to extension-dominated transtension. Mafic dikes emplaced throughout the dome development mark the progressive deformation. They are boudinaged generally parallel to the subhorizontal foliation and buckled perpendicular to the subhorizontal foliation (Fig. 5.7E, F). The sharp transitions from steep foliations to subhorizontal foliations suggest the variation in divergence angle, from 0º to 45º may have been abrupt. However, L-tectonites developed within the SFD at Mt. Richardson may preserve fabric development during the strain field rotation.

8. Evolution of the Remnant Permeability Network

The km-scale exposures in the Fosdick Mountains migmatite-cored gneiss dome that preserve fabrics related to the flow of partially molten crust and multiple generations of leucosome and leucogranite dikes and veins allow us to consider the relationships between melt transport through the crust, magma accumulation, and strain (Fig. 5.12). The strain field and the anisotropy of the crust control the geometries of the permeability network and the movement of melt along melt pathways is controlled by pressure gradients created by buoyancy and deformation.

The former partially molten crust of the Fosdick Mountains is exposed near an inferred crustal-scale strike-slip fault (Balchen Glacier fault), and throughout the Ford Ranges, upper crustal Byrd Coast Granite plutons are exposed near inferred crustal-

scale strike-slip faults (Siddoway, 2008). The localization of crystallized melt and magma near crustal-scale strike-slip faults suggests that the differential stress along these faults focused melt and created regions for melt transport through the crust during melting and flow of partially molten crust (e.g. LeLoup et al., 2001; Depine et al., 2008). The subvertical leucosome and leucogranite, inferred to be former melt pathways preserved in the Fosdick Mountains suggest melt transport may have been subvertical. The older suite of granites has whole rock and trace element compositions that suggest they may be the less evolved equivalents of the regionally exposed Byrd Coast Granite (Korhonen et al., *in review*). Both were likely sourced from Ford Granodiorite (Korhonen et al., *in review*). However, under the conditions of Cretaceous metamorphism, the Ford Granodiorite at the level of the Fosdick Mountains is not a fertile source, suggesting the migration of melt into the Fosdick Mountains from a deeper level (Korhonen et al., *in revision*). Byrd Coast Granite from the nearby hanging wall, at Neptune Nunatak has a LA-ICP-MS zircon age of ca. 119 Ma (Korhonen et al., *in review*) (Fig. 5.2). If borne out by further geochronology work, this age that corresponds to the "older" granites of the Fosdick dome may be from a site of accumulation. The subvertical melt pathways may have been conduits for melt migrating to upper crustal plutons, making the Fosdick dome a melt transfer zone during the wrench phase (Fig. 5.12A).

During deformation and flow of partially molten crust, a strong crustal anisotropy is likely to develop due to segregation of melt concentrating in specific domains (Sawyer, 2008). The steep foliations preserved in the Fosdick dome reflect

the steeply dipping anisotropy that developed during wrenching. In migmatites, as the melt fraction increases the anisotropy diminishes due to the breakdown of the solid framework and the advection of heat with the melts (Burg and Vanderhaeghe, 1993; Weinberg and Mark, 2008).

In the Fosdick dome, the leucosome and leucoganite networks preserved in the pristine three-dimensional cliff-faces records the breakdown of the wrench-related anisotropy. In the northeastern portion of the dome, the exposed cliff-face of Mt. Bitgood displays low melt fraction metatexite orthogneiss with leucosome generally parallel to the metamorphic foliation, reflecting the mechanical anisotropy of the rock (Fig. 5.6D). As melt fraction increases, the migmatite becomes more isotropic and interconnected melt-filled fractures and deformation bands develop (Fig. 5.5A, B). Melt migrated along foliation planes and accumulated within shear bands and inter-boudin partitions, suggesting melt movement was coeval with deformation (e.g. Collins and Sawyer, 1996; Sawyer, 2001; Solar and Brown, 2001; Leitch and Weinberg, 2002).

In the central Fosdick dome (Mt. Iphigene, Marujupu Peak, and Mt. Ferranto), the cliff-faces expose diatexite migmatite schollen structures that record loss of cohesion of the solid framework (Figs. 5.4A, B, 5.6E, and F). The disruption of the framework may have been caused by a volume increase, possibly due to melt accumulation in the middle crust. Agmatite and schollen structures may arise when the influx of melt increases the pore fluid pressure to greater than the competent layer tensile strength, which causes hydraulic fracturing (Clemens and Mawer, 1992; Burg

and Vanderhaeghe, 1993). Once the framework is disrupted, a diatexite forms by viscous flow (Sawyer, 2001; Brown and Rushmer, 1997; Milord and Sawyer, 2003). Folded mafic dikes have fold noses dismembered by subhorizontal folds with leucogranite-filled axial planes. The structures may indicate high fluid pressure and axial planar melt flow. The melt flows along the axial plane and breaks through the hinge causing disruption and dismemberment of the dike, leading to rafts of mafic dike material in the diatexite (e.g. Weinberg and Mark, 2008).

The subhorizontal diatexite migmatite and leucogranite sheeted complex equate to a rock volume of >150 km^3 that may have accumulated as magma. The increase in thickness of leucogranite sheets to the east may have been related lateral eastward crustal flow possibly caused by the presence of a low-pressure region related to a dilation zone and unroofing of the upper crust (Siddoway et al., 2008; McFadden et al., *in review; submitted*). The boudinage of mafic dikes within the volume, parallel to the subhorizontal layering, is consistent with vertical shortening and horizontal extension (Fig. 5.7E, F).

9. Timescale for the Evolution of Oblique Motion

The crystallization ages of leucosome and leucogranite layers that are emplaced in steep versus subhorizontal domains may be used to examine the timing of fabric development and constrain the transition from wrench to oblique divergence. The steep domains host leucosome and leucogranite layers that are concordant to the steep foliation, and later folded with the dominant subhorizontal metamorphic layering. The leucosome and leucogranite layers of the older group of Cretaceous

granites in the Fosdick dome have ages between ca. 117–115 Ma (McFadden et al., *in review, submitted*). Leucosome and leucogranite emplaced in subhorizontal layers are part of the younger group of Cretaceous granites of ca. 109–102 Ma. A concordant, subhorizontal leucosome has a U-Pb zircon age of 105 Ma and a subhorizontal leucogranite sheet from Bird Bluff has a U-Pb zircon age of 104 Ma. Leucogranites and leucosome emplaced into the SFD at Mt. Richardson also record ages between ca. 109–102 Ma (see discussion in following section) (McFadden et al., *in review*, *submitted*). The timing of granite emplacement in the subhorizontal domains versus the steep domains is in accord with the crosscutting field relations. In addition, the youngest U-Pb ages from subvertical granites (ca. 115 Ma) and the oldest U-Pb ages from subhorizontal granites (ca. 109 Ma) indicate that the transition from wrench to extension-dominated transtension occurred in as little as 6 myr.

10. Exhumation and Cooling During Detachment Development

In the South Fosdick Detachment zone, solid-state fabrics record top-to-the-SW transport of the upper crust (McFadden et al., 2007). Syntectonic, tabular leucogranites intrude the detachment zone and leucogranite and leucosome accumulated in shear and dilational structures, indicating melt movement during Cretaceous deformation (Fig. 5.7D). A tabular leucogranite and the accumulated leucosome and leucogranite have U-Pb zircon ages between ca. 109–102 Ma (McFadden et al., *in review*). Top-to-the-SW oblique solid-state fabrics that trend 055–235, the presence of leucogranitic material of Cretaceous age in the SFD, as well as the timing of leucogranite crystallization indicate the SFD was active during the

transtensional phase of deformation. These fabrics, structures, and temporal constraints suggest that melt transport and magma accumulation are linked with the development of detachments (e.g. Armstrong and Ward, 1991; Lister and Baldwin, 1993). During transtension, the influx of melt and the orientation of the divergence angle initiated the SFD and exhumation of the dome.

Biotite and amphibole from a diorite dike (M5-I7) within the SFD have, within error, the same $^{40}Ar/^{39}Ar$ cooling age of ca. 100.5 Ma (Fig. 5.11). The closure temperature of biotite during rapid cooling is ~325ºC (Harrison et al., 1985), whereas the amphibole closure temperature is ~500ºC (Harrison, 1981). The overlap in age suggests very rapid cooling. Biotite from a metatexitic orthogneiss (M5-R136A) within the SFD at Mt. Richardson has a cooling age of ca. 99.8 Ma (Fig. 5.11). All three analyses display flat spectra. The flat spectra and overlapping cooling ages from biotite and amphibole indicate rapid cooling of the dome, consistent with previous argon thermochronology (Richard et al., 1994). Along the SFD, U-Pb titanite ages of late tectonic discordant diorite dikes are between ca. 101–97 Ma and a discordant granitic dike that crosscuts the solid-state fabric has a U-Pb zircon age of ca. 97 Ma (McFadden et al., *in review*). These relationships show that rapid cooling below ~325ºC occurred by ca. 100–99 Ma and ductile deformation ceased along the SFD by 97 Ma. Based on these cooling ages and the youngest U-Pb zircon ages from SFD at ca. 102 Ma, the cooling rate in the Fosdick Mountains from >700ºC to <325ºC was likely >100 ºC/m.y. The dramatic cooling rate may be due to emplacement in a transtensional dilation zone with decompression and exhumation along the detachment

zone or may be due to shallow emplacement of granites in a region of compressed isotherms due to high heat flow.

The SFD preserves microstructures that represent the former presence of melt in rocks that experienced solid-state deformation, and were subsequently overprinted by brittle deformation (McFadden et al., 2007; *in review*). In the high temperature and solid-state fabrics lineations are oriented 055–235, which is consistent with the footwall rocks, and C-S fabrics and asymmetric porphyroclasts record top-to-the-SW oblique motion. Brittle faults, and late leucocratic veins and dikes that transect the solid-state fabrics record stretching oriented 010–190 (Richard, 1992). The orientation of brittle structures is similar in the hanging wall, exposed in the Chester Mountains and Neptune Nunataks. The hanging wall brittle faults that crosscut massive Ford Granodiorite and Byrd Coast Granite record stretching oriented 005–185 (McFadden et al., 2007). The overprinting relationships of these ductile and brittle structures and the change in extension direction with increasingly later structures suggest counterclockwise rotation of the strain field during cooling and exhumation of the Fosdick dome. The temporal change in extension direction is confirmed by U-Pb analyses on leucosome and leucogranite emplaced in ductile structures and cooling ages on muscovite shears present along brittle structures (Richard et al., 1994; McFadden et al., *in review*). The presence of these fabrics and structures indicates a temporal and spatial transition from high temperature deformation to solid-state ductile deformation to brittle deformation. The preservation of former melt textures in the SFD overprinted by solid-state to brittle fabrics suggest rapid cooling that would

cause a change from plastic to brittle deformation styles (McFadden et al., 2007; e.g. Marchildon and Brown, 2001).

The detachment zone was initiated when the divergence angle reached a critical angle (α >20º) and the subhorizontal leucogranite sheets began to accumulate. The rapid cooling suggests the progression from subhorizontal sheet emplacement to exhumation along the detachment occurred quickly.

11. Summary

In the Fosdick Mountains, the oblique deformation and the heterogeneity of the crust prior to Cretaceous migmatization controlled the geometries of leucosome and leucogranite networks and the distribution of high melt fraction migmatites (diatexite) and leucogranite sheets. The construction, stabilization, and exhumation of the Fosdick dome occurred during a transition in the divergence angle from wrench (α = 0º) to oblique divergence (α = 45º). During wrench, the Fosdick dome acted as a melt transfer zone for melt and magma transport to higher crustal levels. Then, as the divergence angle rotated towards extension-dominated transtension, a dilation zone formed and voluminous magmatic sheets accumulated in the Fosdick dome. The rotation of the divergence angle and the accumulation of magma led to detachment initiation and rapid cooling and exhumation of the dome.

Acknowledgments

Work supported by National Science Foundation-Office of Polar Programs grants NSF-OPP 0337488 to Teyssier and NSF-OPP 0338279 to Siddoway, and partially supported by GSA Bruce L. "Biff" Reed Student Scholarship awarded to McFadden.

References Cited

Adams, C.J., 1986, Geochronological studies of the Swanson Formation of Marie Byrd Land, West Antarctica, and correlation with northern Victoria Land, East Antarctica and the South Island, New Zealand, New Zealand Journal of Geology and Geophysics, v. 29, p. 345–358.

Adams, C.J., 1987, Geochronology of granite terranes in the Ford Ranges, Marie Byrd Land, West Antarctica, New Zealand Journal of Geology and Geophysics, v. 30, p. 51–72.

Armstrong, R.L., and Ward, P., 1991, Evolving geographical patterns of Cenozoic magmatism in the North American Cordillera: The temporal and spatial association of magmatism and metamorphic core complexes, Journal of Geophysical Research, v. 96 (B8), p. 13,201–13,224.

Bradshaw, J.D., Andrew, B., and Field, B.D., 1983, Swanson Formation and related rocks of Marie Byrd Land and a comparison with the Robertson Bay Group of northern Victoria Land, *in* Oliver, R.L., James, P.R., and Jago, J.B., eds., Antarctic Earth Science, Australian Academy of Science, p. 274–279.

Bradshaw, J.D., Pankhurst, R.J., Weaver, S.D., Storey, B.C., Muir, R.J., and Ireland, T.R., 1997, New Zealand superterranes recognized in Marie Byrd Land and Thurston Island, in *The Antarctic Region, Geological Evolution and Processes*, edited by C.A. Ricci, pp. 429–436, Terra Antartica Publication, Siena, Italy.

Brown, M., 1994, The generation, segregation, ascent and emplacement of granite magma: the migmatite-to-crustally-derived granite connection in thickened orogens, Earth-Science Reviews, v. 36, p. 83–130

Brown, M., 2007, Crustal melting and melt extraction, ascent and emplacement in orogens: mechanisms and consequences, Journal of the Geological Society of London, v. 164, p. 709–730.

Brown, M., 2008, Granites, migmatites and residual granulites: relationships and processes, Mineralogical Association of Canada Short Course 38, Quebec City, Quebec, p. 97–144.

Brown, M., Averkin, Y.A., McLellan, E.L., and Sawyer, E.W., 1995, Melt segregation in migmatites, Journal of Geophysical Research, v. 100, p. 15,655–15,679.

Brown, M, and Rushmer, T., 1997, The role of deformation in the movement of granite melt: views from the laboratory and the field, *Deformation-enhanced Fluid Transport in the Earth's Crust and Mantle,* edited by M. Holness, Mineral. Soc. Series: 8, London: Chapman and Hall, p. 111–144.

Brown, M., and Solar, G.S., 1998, Granite ascent and emplacement during contractional deformation in convergent orogens, Journal of Structural Geology, v. 20, p. 1365–1393.

Brun, J.P., Sokoutis, D., and Van Den Driessche, J., 1994, Analogue modeling of detachment fault systems and core complexes; Geology, v. 22, p. 319–322.

Burg, J.P., and Vanderhaeghe, O., 1993, Structures and way-up criteria in migmatites, with application to the Velay dome (French Massif Central), Journal of Structural Geology, v. 15, p. 1293–1301.

Clemens, J.D., 2006, Melting of the continental crust: fluid regimes, melting reactions, and source-rock fertility, *in* Evolution and Differentiation of the Continental Crust, Brown, M., and Rushmer, T., eds., Cambridge University Press, p. 297–331.

Clemens, J.D., and Mawer, C.K., 1992, Granitic magma transport by fracture propagation, Tectonophysics, v. 204, p. 339–360.

Collins and Sawyer, 1996, Pervasive granitoid magma transfer through the lower-middle crust during non-coaxial compressional deformation, Journal of Metamorphic Geology, v. 14, p. 565–579.

D'Lemos, R.S., Brown, M., and Strachan, R.A., 1992, Granite magma generation, ascent and emplacement within a transpressional orogen: Journal Geological Society of London, v. 149, p. 487–490.

Dalrymple, G.B., Alexander, E.C., Lanphere, M.A., and Kraker, G.P., 1981, Irradiation of samples for $^{40}Ar/^{39}Ar$ dating using the Geological Survey TRIGA reactor, U.S. Geological Survey Professional Paper, v. 1176, p. 55.

Denèle, Y., Olivier, P., and Gleizes, G., 2008, Progressive deformation of a zone of magma transfer in a transpressional regime: Variscan Merens shear zone (Pyrenees, France), Journal of Structural Geology, v. 30, p. 1138–1149.

Depine, G.V., Andronicos, C.L., and Phipps-Morgan, J., 2008, Near isothermal conditions in the middle and lower crust induced by melt migration, Nature, v. 452, p. 80–83.

Ferraccioli, F., Bozzo E., and Damaske, D., 2002, Aeromagnetic signatures over western Marie Byrd Land provide insight into magmatic arc basement, mafic magmatism and structure of the eastern Ross Sea rift flank: Tectonophysics, v. 347, p. 139–65.

Fitzgerald, P.G., and Baldwin, S.L., 1997, Detachment fault model for the Evolution of the Ross Embayment, in *The Antarctic Region: Geological Evolution and Processes*, edited by C.A. Ricci, p. 555–564, *Terra Antarctica* Publication, Siena, Italy.

Forster, M.A., and Lister, G.S., 2003, Cretaceous metamorphic core complexes in the Otago Schist, New Zealand, Austrialian Journal of Earth Sciences, v. 50, p. 181–198.

Fossen, H., and Tikoff, B., 1993, The deformation matrix for simultaneous simple shearing, pure shearing and volume change, and its application to transpression-transtension tectonics, Journal of Structural Geology, v. 15, p. 413–422.

Foster, D.A., Dought, P.T., Kalakay, T.J., Fanning, C.M., Coyner, S., Grice, W.C., and Vogl, J., 2007, Kinematics and timing of exhumation of metamorphic core

complexes along the Lewis and Clark fault zone, northern Rocky Mountains, USA, *in* Till, A.B., Roeske, S.M., Sample, J.C., and Foster, D.A., eds., Exhumation Associated with Continental Strike-slip Fault Systems: Geological Society of America Special paper 434, p. 207–232, doi: 10.1130/2007.2434(10).

Gaffney, A.M., and Siddoway, C.S., 2007, Heterogeneous sources for Pleistocene lavas of Marie Byrd Land, Antarctica: New data from the SW Pacific Diffuse Alkaline Magmatic Province. *In* Antarctica: A Keystone in a Changing World—Online Proceedings for the Tenth International Symposium on Antarctic Earth Sciences, eds. Cooper, A.K., Raymond, C.R., et al., USGS Open-File Report 2007-1047, Extended Abstract 063, http://pubs.usgs.gov/of/2007/1047/.

Gibson, G.M., McDougall, I., and Ireland, T.R., 1988, Age constraints on metamorphism and the development of a metamorphic core complex in Fiordland, southern New Zealand, Geology, v. 16, p. 405–408.

Guernia, S, and Sawyer, E.W., 2003, Large-scale melt-depletion in granulite terrains: An example from the Archean Ashuanipi Subprovince of Quebec, Journal of Metamorphic Geology, v. 21, p. 181–201.

Harrison, T.M., 1981, Diffusion of 40Ar in hornblende, Contributions to Mineralogy and Petrology, v. 78, p. 324–331.

Harrison, T.M., Duncan, I.J., McDougall, I., 1985, Diffusion of 40Ar in biotite: temperature, pressure and compositional effects, Geochimica Cosmochimica Acta, v. 49, p. 2461–2468.

Hutton, D.H.W., 1990, A new mechanism of granite emplacement: Intrusion in active extensional shear zones: Nature, v. 343, p. 452–455.

Ireland, T.R., and Gibson, G.M., 1998, SHRIMP monazite and zircon geochronology of high-grade metamorphism in New Zealand, Journal of Metamorphic Geology, v. 16, p. 149–167.

Katrinová, Z., Schulmann, K., Edel, J.B., Jezek, J., and Schaltegger, U., 2007, Model of successive granite sheet emplacement in transtensional setting: Integrated microstructural and anisotropy of magnetic susceptibility study, Tectonics, v. 26, TC6003, doi: 10.1029/2006TC002035.

Kimbrough, D.L., and Tulloch, A.J., 1989, Early Cretaceous age of orthogneiss from the Charleston Metamorphic Group, New Zealand, Earth and Planetary Science Letters, v. 95, p. 130–140.

Korhonen, F.J., Saito, S., Brown, M., and Siddoway, C.S., *in revision*, Modeling multiple melt loss events in the evolution of an active continental margin, Lithos.

Korhonen, F., Saito, S., Brown, M., Siddoway, C.S., and Day, J., *in review*, Multiple generations of granite in the Fosdick Mountains, Marie Byrd Land, West Antarctica: Implications for polyphase intracrustal differentiation in a continental margin setting, Journal of Petrology.

Kula, J., Tulloch, A.J., Spell, T.L., and Wells, M.L., 2007, Two-stage rifting of Zealandia-Australia-Antarctica: Evidence from $^{40}Ar/^{39}Ar$ thermochronometry of the Sisters shear zone, Stewart Island, New Zealand, Geology, v. 35, p. 411-414, doi: 10.1130/G23432A.1.

Leitch, A.M., and Weinberg, R.F., 2002, Modeling granite migration be mesoscale pervasive flow, Earth and Planetary Science Letters, v. 200, p. 131–146.

LeLoup, P.H., Arnaud, N., Lacassin, R., Kienast, J.R., Harrison, T.M., Phan Trong, T.T., Replumaz, A., and Tapponnier, P., 2001, New constraints on the structure, thermochronology, and timing of the Ailao Shan-Red River shear zone, SE Asia, Journal of Geophysical Research, v. 106, p. 6683–6732.

Lister, G.S., and Baldwin, S.L., 1993, Plutonism and the origin of metamorphic core complexes, Geology, v. 21, p. 607–610.

Luyendyk, B.P., 1995, Hypothesis for Cretaceous Rifting of East Gondwana Caused by Subducted Slab Capture, Geology, v. 23, p. 373-376.

Luyendyk, B. P., Wilson, D.S., and Siddoway C.S., 2003, The eastern margin of the Ross Sea Rift in western Marie Byrd Land: Crustal structure and tectonic development: Geochemistry, Geophysics, Geosystems, doi: 10.1029/2002GC000462.

Marchildon, N., and Brown, M., 2003, Spatial distribution of melt-bearing structures in anatectic rocks from southern Brittany: implications for melt-transfer at grain-to orogen-scale, Tectonophysics, v. 364, p. 215–235.

McCaffrey, K.J.W., Miller, C.F., Karlstrom, K.E., and Simpson, C., 1999, Synmagmatic deformation patterns in the Old Woman Mountains, SE California, Journal of Structural Geology, v. 21, p. 335–349.

McFadden, R., Siddoway, C.S., Teyssier, C., Fanning, C.M., and Kruckenberg, S.C., 2007, Cretaceous oblique detachment tectonics in the Fosdick Mountains, Marie Byrd Land, Antarctica, *in* Cooper, A.K., Raymond, C.R., and ISAES Editorial Team, eds., Antarctica: A Keystone in a Changing World - Online Proceedings of the 10th ISAES, USGS Open-File Report 2007-1047, Short Research Paper 047, 5 p.; doi: 10.3133/of2007-1047.srp047.

McFadden, R., Siddoway, C.S., Teyssier, C., and Fanning, C.M., *in review*, Cretaceous intracontinental extension in the Fosdick Mountains migmatite-granite complex, West Antarctica: Tectonics.

Milord, I., Sawyer, E.W., and Brown, M., 2001, Formation of diatexite migmatite and granite magma during anatexis of semi-pelitic metasedimentary rocks: an example from St. Malo, France, Journal of Petrology v. 42, p. 487–505.

Milord, I., and Sawyer, E.W., 2003, Schlieren formation in diatexite migmatite: examples from the St. Malo migmatite terrain, France, Journal of Metamorphic Geology, v. 21, p. 347–362.

Mortimer, N., Tulloch, A.J., Spark, R.N., Walker, N.W., Ladley, E., Allibone, A., and Kimbrough, D.L., 1999, Overview of the Median Batholith, New Zealand: a new interpretation of the geology of the Median Tectonic Zone and adjacent rocks, Journal of African Earth Sciences v. 29, p. 257–268.

Mortimer, N., Hoernle, K., Hauff, F., Palin, J.M., Dunlap, W.J., Werner, R., and Faure, K., 2006, New constraints on the age and evolution of the Wishbone Ridge, southwest Pacific Cretaceous microplates, and Zealandia-West Antarctica breakup, Geology, v. 3, p. 185–188.

Mukasa, S.B., and Dalziel, I.W.D., 2000, Marie Byrd Land, West Antarctica: Evolution of Gondwana's Pacific margin constrained by zircon U-Pb geochronology and feldspar common-Pb isotopic compositions. Geological Society of America Bulletin, v. 112, p. 611–627.

Oldow, J.S., 2003, Active transtensional boundary zone between the western Great Basin and Sierra Nevada block, western U.S. Cordillera: Geology, v. 31, p. 1033–1036, doi: 10.1038/333349a0.

Pankhurst, R.J., Weaver, S.D., Bradshaw, J.D., Storey, B.C., and Ireland, T.R., 1998, Geochronology and geochemistry of pre-Jurassic superterranes in Marie Byrd Land, Antarctica: Journal of Geophysical Research, v. 103, p. 2529–2547.

Petford, N., Cruden, A.R., McCaffrey, K.J.W., and Vigneresse, J.L., 2000, Granite magma formation, transport and emplacement in the Earth's crust, Nature, v. 408, p. 669–673.

Richard, S.M., Smith, C.H., Kimbrough, D.K., Fitzgerald, G., Luyendyk, B.P., and McWilliams, M.O., 1994, Cooling history of the northern Ford Ranges, Marie Byrd Land, West Antarctica, Tectonics, v. 13, p. 837–857.

Sawyer, E.W., 1996, Melt segregation and magma flow in migmatites: Implications for the generation of granite magmas: Transactions of the Royal Society Edinburgh: Earth Sciences, v. 87, p. 85–94.

Sawyer, E.W., 1999, Criteria for the recognition of partial melting, Physics and Chemistry of the Earth (A), v. 24, p. 269–279.

Sawyer, E.W., 2001, Melt segregation in the continental crust: distribution and movement of melt in anatectic rocks, Journal of Metamorphic Geology, v. 19, p. 291–309.

Sawyer, E.W., 2008, Working with migmatites: nomenclature for the constituent parts, Mineralogical Association of Canada Short Course 38, Quebec City, Quebec, 1–28.

Scott, J.M., and Cooper, A.F., 2006, Early Cretaceous extensional exhumation of the lower crust of a magmatic arc: Evidence from the Mount Irene Shear Zone, Fiordland, New Zealand, Tectonics, v. 25, doi.10.1029/2005TC001890.

Siddoway, C.S., Baldwin, S.L., Fitzgerald, P.G., Fanning, C.M., and Luyendyk, B.P., 2004a, Ross Sea mylonites and the timing of intracontinental extension within the West Antarctic rift system, Geology, v. 32, p. 57–60.

Siddoway, C.S., Richard, S.M., Fanning, C.M., and Luyendyk, B.P., 2004b, Origin and emplacement of a middle Cretaceous gneiss dome, Fosdick Mountains, West Antarctica, *in* Whitney, D.L., Teyssier, C., and Siddoway, C.S., eds., Gneiss domes in Orogeny, Geological Society America Special Paper 380, p. 267–294.

Siddoway, C.S., Sass III, L.C., and Esser, R., 2005, Kinematic history of Marie Byrd Land terrane, West Antarctica: Direct evidence from Cretaceous mafic dykes, *in* Vaughan et al., eds., Terrane Processes at the Margin of Gondwana, Geological Society, London, Special Publications, 246, p. 417-438.

Siddoway, C.S., 2008, Tectonics of the West Antarctic rift system: New light on the history and dynamics of distributed intracontinental extension, *in* Cooper, A.K., et al., eds. Antarctica: A Keystone in a Changing World, National Academy of Sciences.

Siddoway, C.S., and Fanning, C.M., 2009, SHRIMP U-Pb zircon geochronology of a migmatite-granite complex in West Antarctica, with bearing on the character and extent of Paleozoic tectonism on the East Gondwana margin: Tectonophysics, doi: 10.1016/j.tecto.2009.04.021.

Smith, C.H., 1997, Mid-crustal processes during Cretaceous rifting, Fosdick Mountains, Marie Byrd Land, *in* Ricci, C.A., ed., The Antarctic Region: Processes and Evolution, Terra Antarctica Publications, p. 313–320.

Solar, G.S., and Brown, M., 2001, Deformation partitioning during transpression in response to Early Devonian oblique convergence, northern Appalachian orogen, USA, Journal of Structural Geology, v. 23, p. 1043–1065.

Spell, T.L., McDougall, I., and Tulloch, A.J., 2000, Thermochronological constraints on the breakup of the Pacific Gondwana margin: The Paparoa metamorphic core complex, South Island, New Zealand, Tectonics, v. 19, p. 433–451.

Storey, B., Leat, T., Weaver, S.D., Pankhurst, R.J., Bradshaw, J.D., and Kelley, S., 1999, Mantle plumes and Antarctica-New Zealand rifting: Evidence from mid-Cretaceous mafic dykes, Journal of the Geological Society of London, v. 156, p. 659–671.

Talbot, J-Y, Faure, M., Chen, Y., and Martelet, G., 2005, Pull-apart emplacement of the Margeride granitic complex (French Massif Central). Implications for the late evolution of the Variscan orogen, Journal of Structural Geology, v. 27, p. 1610–1629.

Teyssier, C., and Tikoff, B., 1999, Fabric stability in oblique convergence and divergence, Journal of Structural Geology, v. 21, p. 969–974.

Teyssier, C., and Whitney, D.L., 2002, Gneiss domes and orogeny, Geology, v. 30, p. 1139–1142.

Teyssier, C., Ferre, E.C., Whitney, D.L., Norlander, B., Vanderhaeghe, O., and Parkinson, D., 2005, Flow of partially molten crust and origin of detachments during collapse of the Cordilleran orogen, *in* Bruhn, D., and Burlini, L., eds, High-strain zones: Structure and Physical Properties: Geological Society, London, Special Publications, 245, p. 39–64.

Tikoff, B., and Teyssier, C., 1992, Crustal-scale, en echelon "P-shear" tensional bridges: A possible solution to the batholithic room problem, Geology, v. 20, p. 927–930.

Tikoff, B., and Teyssier, C., 1994, Strain modeling of displacement-field partitioning in transpressional orogens, Journal of Structural Geology, v. 16, p. 1575–1588.

Tirel, C., Brun, J.P., and Burov, E., 2004, Thermomechanical modeling of extensional gneiss domes, *in* Whitney, D.L., Teyssier, C., and Siddoway, C.S., Gneiss Domes in Orogeny, Boulder, Colorado, Geological Society of America Special Paper 380, p. 67–78.

Vanderhaeghe, O., 2001, Melt segregation, pervasive melt migration and magma mobility in the continental crust: the structural record from pores to orogens: Physics and Chemistry of Earth, (A), v. 26, p. 213–223.

Vaughan, A.M., and Livermore, R.A., 2005, Episodicity of Mesozoic terrane accretion along the Pacific margin of Gondwana: Implications for superplume interactions, *in* Terrane Processes at the Margin of Gondwana*,* eds., A. Vaughan, Leat, P., and Pankhurst, R.J., Geological Society of London Special Publication 246, p. 143–178.

Weaver, S.D., Bradshaw, J.D., and Adams, C.J., 1991, Granitoids of the Ford Ranges, Marie Byrd Land, Antarctica, in Geological evolution of Antarctica, edited by M. R. A. Thomson, J. A. Crame, and J. W. Thomson, Cambridge, Cambridge University Press, p. 345–351.

Weaver, S.D., Adams, C.J., Pankhurst, R.J., and Gibson, I.L., 1992, Granites of Edward VII Peninsula, Marie Byrd Land, Antarctica, *in* Brown, E., and Chappell, B.W., eds., Proceedings of the Second Hutton Symposium on the Origin of Granites and Related Rocks, Transactions of the Royal Society of Edinburgh, Earth Sciences, v. 83, p. 281–290.

Weaver, S.D., Storey, B.C., Pankhurst, R.J., Mukasa, S.B., Divenere, V., and Bradshaw, J.D., 1994, Antarctic-New Zealand rifting and Marie Byrd Land lithospheric magmatism linked to ridge subduction and mantle plume activity, Geology, v. 22, p. 811–814

Weinberg, R.F., 1999, Mesoscale pervasive felsic magma migration: alternatives to diking, Lithos, v. 46, p. 393–410.

Weinberg, R.F., and Mark, G., 2008, Magma migration, folding, and disaggregation of migmatites in the Karakoram shear zone, Ladakh, NW India, Geological Society of America Bulletin, v. 120, p. 994–1009, doi: 10.1130/B26227.1.

Weinberg, R.F, Mark, G., and Reichardt, H., 2009, Magma ponding in the Karakoram shear zone, Ladakh NW India, Geological Society of America Bulletin, v. 121, p. 278–285, doi: 10.1130/B26358.1.

White, R.W., Powell, R., and Haplin, J.A., 2004, Spatially-focussed melt formation in aluminous metapelites from Broken Hill, Australia, Journal of Metamorphic Geology, v. 22, p. 825–845.

Whitney, D.L., Teyssier, C., and Vanderhaeghe, O., 2004, Gneiss domes and crustal flow, *in* Whitney, D.L., Teyssier, C., and Siddoway, C.S., eds., Gneiss domes in orogeny: Geological Society of America Special Paper 380, p. 15–33.

Whitney, D.L., Teyssier, C., and Heizler, M.T., 2007, Gneiss domes, metamorphic core complexes, and wrench zones: Thermal and structural evolution of the Nigde Massif, central Anatolia: Tectonics, v. 26, doi: 10.1029/2006TC002040.

Figure Captions

Figure 5.1. A) Geographic map of West Antarctica (after Pankhurst et al., 1998). B) Tectonic plate reconstruction of the East Gondwana margin at 95 Ma, modified from Tulloch et al. (2006). The locations of detachment structures are shown as dark gray ovals. The long axes of the ovals represent the local stretching direction.

Figure 5.2. Geologic map of the Fosdick Mountains migmatite-cored gneiss dome and the Chester Mountains (after Siddoway et al., 2004). The location of the Fosdick Mountains in Marie Byrd Land, Antarctica is shown in the map legend. Large arrows represent the lineation trend for migmatites. Dashed red lines represent mapped foliation trajectories. U-Pb SHRIMP ages from previous studies and $^{40}Ar/^{39}Ar$ biotite and amphibole cooling ages described in this study are shown on the map. A-A', B-B', and C-C' are the locations of the cross-sections in Figure 3.

Figure 5.3. Geologic cross-sections of the Fosdick Mountains migmatite-cored gneiss dome. The cross-sections show the layering and contact relationships between units in the Fosdick dome. Localities of cliff-face photos and sketches in Figures 4 and 5 are shown on the cross-sections.

Figure 5.4. A) Cliff-face sketch of the east face of Mt. Iphigene showing the folded, subhorizontal layers of metatexitic orthogneiss and paragneiss and diatexite migmatite. A granite network intrudes the para- and orthogneiss, disrupts the structural layering and forms a diatexite migmatite with agmatitic and schollen structures. The rafts of schollen are disrupted mafic dikes and para- and orthogneiss. B) Cliff-face photographic stitch of the east face of Mt. Iphigene.

Photos by S. Kruckenberg. C) Cliff-face sketch of the east face of Mt. Avers buttress D (western most buttress). The wall shows a 50 meter thick layer of metatexitic orthogneiss and 10s of meter thick layers of metatexitic paragneiss that are intruded by a integrated granite network. A subhorizontal leucogranite sheet intrudes metatexitic orthogneiss and paragneiss layers. The para- and orthogneiss layers are transected by leucogranite dikes and veins and leucosome in numerous orientations including concordant, in source leucosomes, folded leucosomes that are thicker in the fold nose, and discordant leucosomes. D) Cliff-face photographic stitch of the east face of Mt. Avers buttress D.

Figure 5.5. A) Cliff-face sketch of the west face of Mt. Bitgood. A 100 m thick subhorizontal leucogranite sheet intruded metatexitic orthogneiss and paragneiss. The orthogneiss layers display patchy leucosome and the paragneiss show concordant leucosome. The contact between the leucogranite sheet and gneisses is a gradational contact with increasing percentage of leucosome towards the leucogranite sheet. Subvertical leucogranite dikes with zigzag contacts and subvertical leucogranite veins and leucosome transect the entire outcrop. B) Cliff-face photographic stitch of the west face of Mt. Bitgood. C) The cliff-face sketch of the west face of Bird Bluff shows the leucogranitic sheeted complex. Subhorizontal leucogranite sheets (50–100 m thick) form a composite leucogranite complex. The sheets intrude paragneiss and orthogneiss layers that are metatexitic and diatexitic. D) Cliff-face photographic stitch of the west face of Bird Bluff.

Figure 5.6. A) Photo of metatexitic paragneiss from Mt. Avers. Photos shows the folded paragneiss layers with cm- to m-thick leucosome interlayered with leucogranite. Transecting the steeply dipping paragneisses are subhorizontal leucosomes and granite-filled shear bands. Geologist at the cliff base are circled for scale. B) Photo of the mm- to cm-scale folded layering in the stromatic metatexitic paragneiss from Mt. Avers. Photo shows mm- to cm-scale layering of leucosome and melanosome. A fine-grained 20 cm leucogranitic dike cuts the folded layering. C) Folded layering in the metatexitic orthogneiss from northern Mt. Iphigene. Leucogranite (white) collects mostly below and some above the paleosome portions of dioritic gneiss (dark gray). Metatexitic orthogneiss (gray) has mm- to cm-scale concordant in source leucosomes and patchy in situ leucosomes that are connected by thin mm-scale discordant leucosomes. The leucosome network and the leucogranite are connected. Photo by C. Teyssier. D) Metatexitic orthogneiss from Mt. Avers. Concordant, mm- to cm-thick in source leucosomes and 10 cm thick leucosomes connected by cm-thick, melt-filled shear (oblique to fabric) and dilation (normal to fabric) bands. Photo by C.S. Siddoway. E) Cliff-face exposure of agmatitic and schollen-rich diatexite (white), schollen-rich orthogneiss (gray), and metatexitic paragneiss (brown). The orthogneiss at the bottom of the cliff contains concordant leucosome and leucosome material in contact with paleosome rafts and schollen of paragneiss and dismembered mafic dikes. The paragneiss forms layers that are disaggregated near the contacts with diatexite neosome. Neosome in the diatexite is unfoliated and contains paleosome

rafts and schollen that are deformed and folded dismembered mafic dikes and paragneiss. Geologists are circled at cliff base for scale. Photo by S.C. Kruckenberg. F) Diatexite migmatite with an agmatitic structure from Marujupu Peak. The neosome is predominantly leucosome (white) with minor wispy regions of residuum. The paleosome consists of rafts of dismembered portions of mafic dikes and diorite gneiss. The rafts preserve mm- to cm-scale concordant leucosome, foliation, and are folded.

Figure 5.7. A) Photo of the leucogranite sheeted complex at Bird Bluff. Subhorizontal sheets of leucogranite (light yellow) intrude strongly deformed meters to 10s of meters thick metatexitic paragneiss (brown) and orthogneiss (gray). Within the leucogranite sheets mafic dikes are boudinaged and buckled. Shallowly dipping extensional shear bands transect the leucogranite complex. Photo by C.S. Siddoway. B) Photo of two leucogranite sheets that intrude a dismembered metatexitic paragneiss layer. Leucogranite has very indistinct portions of metatexitic orthogneiss residuum. Photo by C.S. Siddoway. C) Photo of metatexite migmatite from the South Fosdick Detachment zone on the cliff-face at Mt. Getz. Metatexitic orthogneiss (gray) and metatexitic paragneiss (brown) are interfolded and interlayered. Concordant and steep, discordant in source cm- to dm-scale leucosomes transect the migmatites. D) Solid-state deformed metatexite migmatite from the South Fosdick Detachment zone at Mt. Richardson. Leucosome occur as cm- to dm-thick layers concordant to the metamorphic foliation and leucosome fill transverse shear bands. The residuum consists of orthogneiss layers and

asymmetric sigmoidal boudins. E) Photo of a folded mafic dike within the diatexite migmatite at Marujupu Peak. The nose of the fold is disrupted and the dismembered portions of the dike form rafts in the diatexite. The dismembered fold nose is in contact with a high proportion of neosome material from the diatexite. F) Photo of folded mafic dikes within the diatexite migmatite at Mt. Ferranto. Two m-wide dikes are broadly folded and transect the diatexite fabric. Thinner, cm-wide dikes are buckled with subhorizontal fold axes. Leucosome (white) and layers and rafts of residuum (gray) comprise the diatexite neosome. Some of the residuum rafts are folded.

Figure 5.8. A) Photo of steeply dipping leucogranite sheets and metatexitic orthogneiss from Mt. Lockhart. Subvertical mafic dikes crosscut the leucogranite. Rafts of dismembered mafic dikes are distributed throughout the leucogranite. B) Subvertical layers of metatexitic paragneiss from Mt. Ferranto. The western edge of the photo shows the contact between metatexitic paragneiss and diatexite. The metatexite layering is folded into weakly asymmetric folds with shallow fold axes. C) Photo of metatexitic paragneiss and leucogranite from Mt. Avers. The metatexite fabric, defined by cm-thick layers of residuum and leucosome, is subvertical. The steep fabric is crosscut by horizontal leucogranite that shows an intrusive contact with the metatexite. D) Photo of metatexite paragneiss from Mt. Ferranto. Garnet-rich melanosome and mm- to cm-thick leucosome display a subvertical fabric that is crosscut by a transposed horizontal fabric defined by mm-

to cm-thick leucosome and melanosome. Folded leucosomes with subhorizontal axes are rarely preserved.

Figure 5.9. Map showing the location of steep foliation domains in the Fosdick dome with stereographic projections that display data points and kamb contours (2 sigma contour interval) for field data from the Fosdick Mountains. The stereographic projections are of A) poles to foliation from steep domains, B) poles to foliation from subhorizontal domains, C) stretching lineations, defined by biotite, sillimanite, ± quartz, and D) fold axes. Equal area stereographic projections were made with Stereonet v.6.3.3 by Richard Allmendinger.

Figure 5.10. Equal area stereographic projects that display data points and kamb contours (2 sigma contour interval) and kinematic solutions from the Fosdick Mountains. A) Mineral stretching lineations. B) Normal-sense extensional shear bands. Numbers represent strain axes C) Poles to N-S dipping felsic veins and dikes. D) Poles to N-S dipping muscovite shears from the SFD. E) Brittle shears of the Chester Mountains. Numbers represent strain axes. Red squares represent maximum compression direction and blue squares represent maximum extension direction. Stereograhic projections were made with Stereonet v. 6.3.3 by R.W. Allmendinger. Kinematic solutions were calculated with the FaultKin 4.3.5 application, by R.W. Allmendinger.

Figure 5.11. A) Amphibole $^{40}Ar/^{39}Ar$ age spectra for sample M5-I7. B) Biotite $^{40}Ar/^{39}Ar$ age spectra for sample M5-I7. C) Biotite $^{40}Ar/^{39}Ar$ age spectra for sample M5-R136A. K/Ca ratios are shown above each respective spectra and K/Cl

ratios are shown above the K/Ca ratios. Errors on plotted release step ages and calculated mean ages are one sigma.

Figure 5.12. Three-dimensional block diagrams of the Fosdick dome that show the relationship between the oblique divergence angle (α) and fabrics in partially molten crust. A) Depicts the wrench ($\alpha = 0^{o}$) phase of deformation, displaying the role of the Fosdick dome as a region of melt transfer. B) Depicts the oblique divergence ($\alpha = 45^{o}$) phase of deformation and shows the Fosdick dome as a magma accumulation zone.

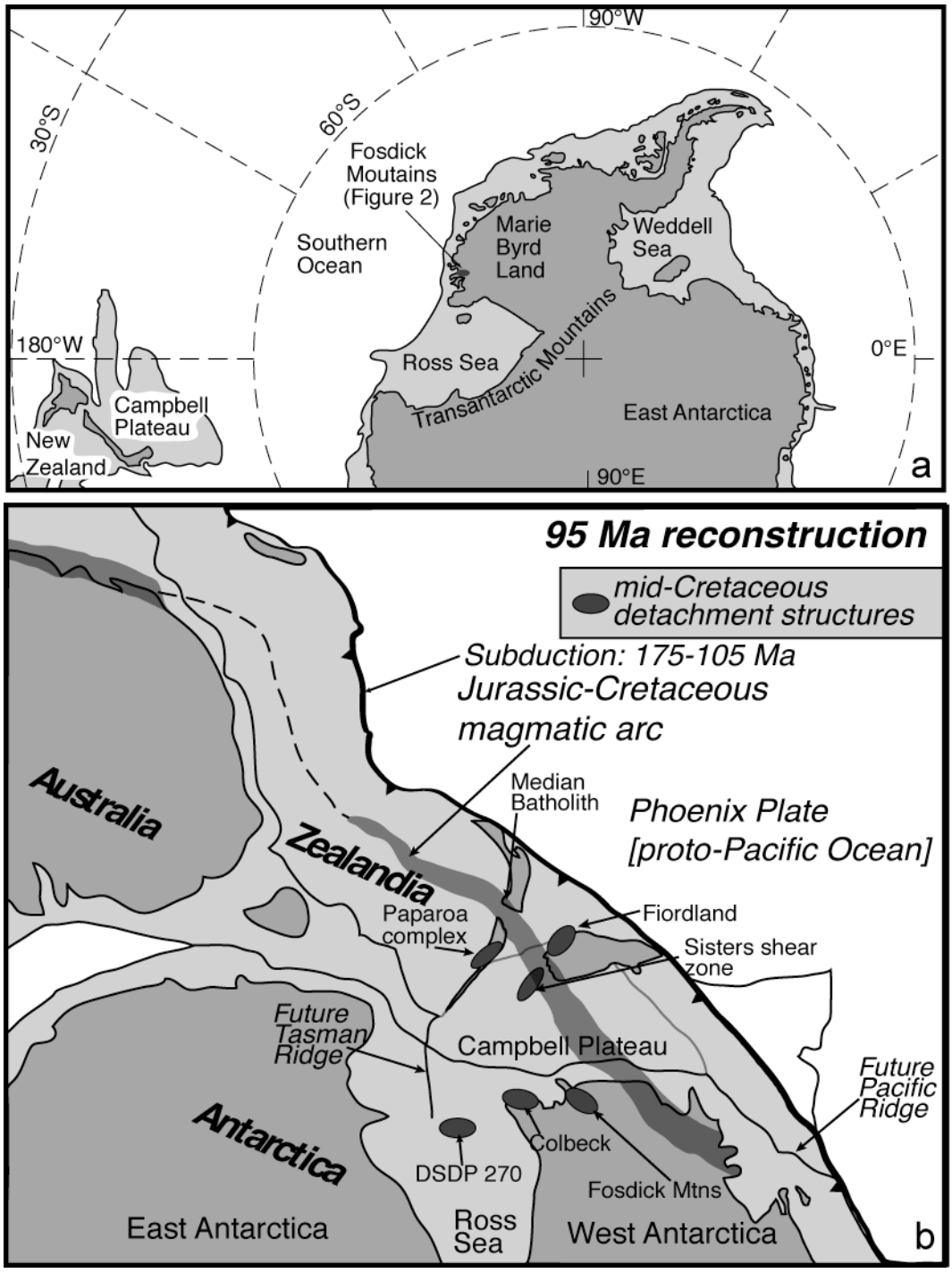

Figure 5.1 Geographic map of West Antarctica and tectonic reconstruction of East Gondwana margin.

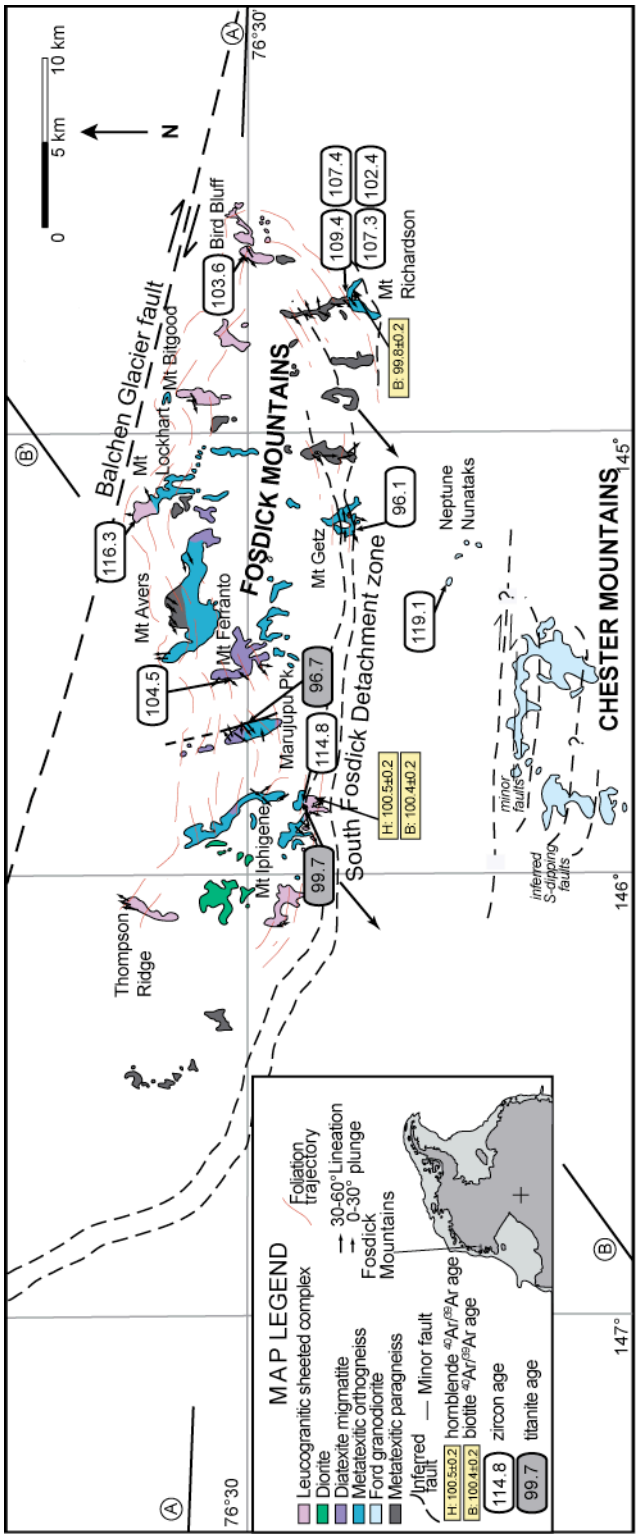

Figure 5.2 Geologic map of the Fosdick Mountains migmatite-cored gneiss dome.

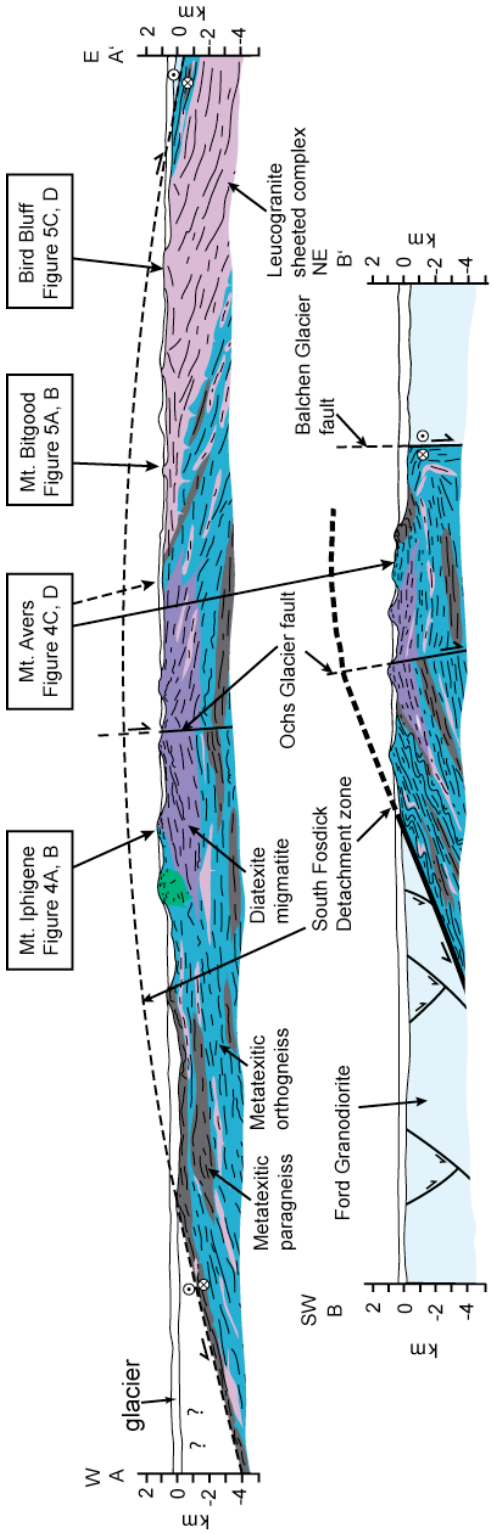

Figure 5.3 Geologic cross-sections of the Fosdick migmatite-cored gneiss dome.

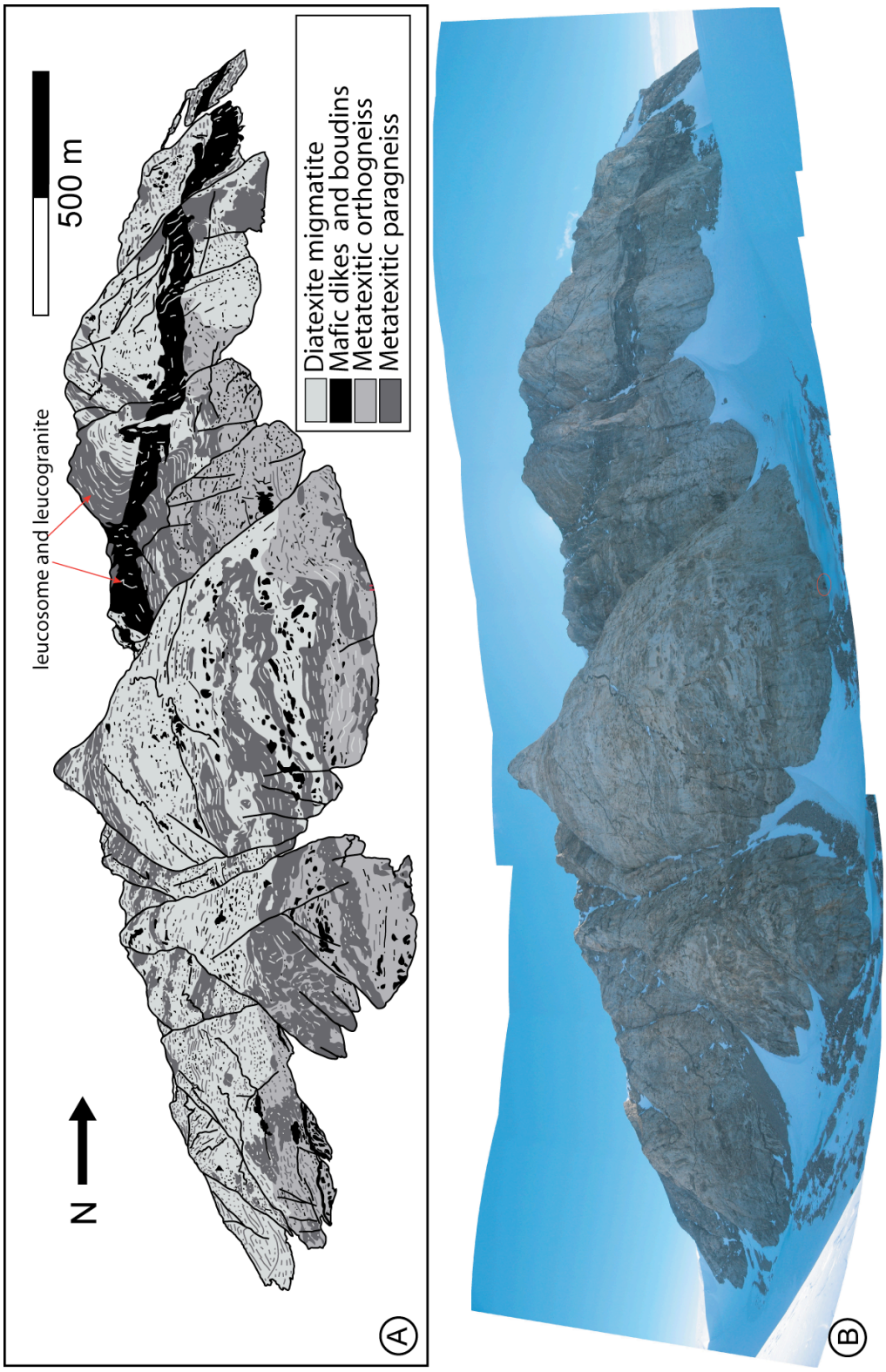

Figure 5.4 Photos and sketches of Mt. Iphigene and Mt. Avers buttress D.

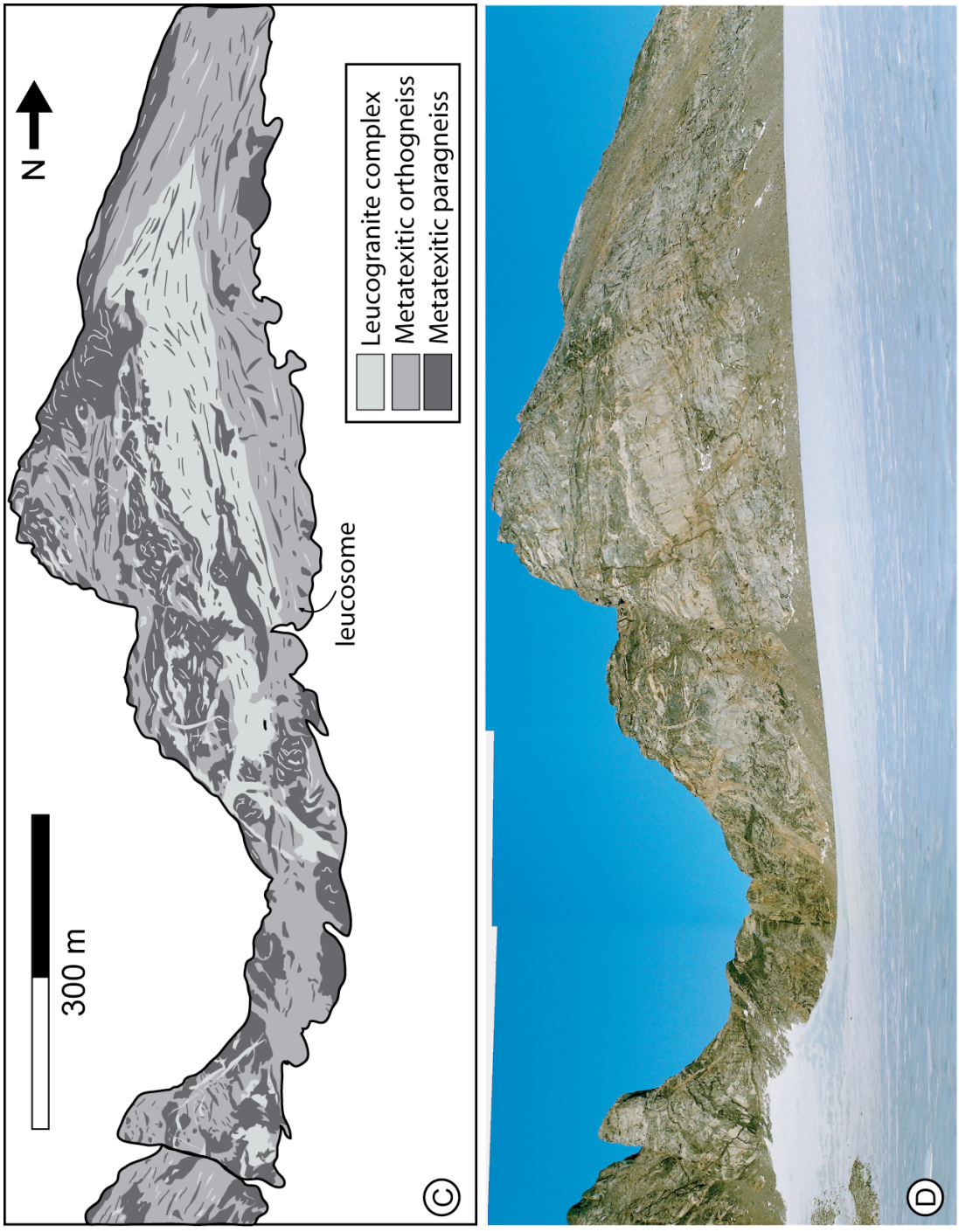

Figure 5.4 Photos and sketches of Mt. Iphigene and Mt. Avers buttress D.

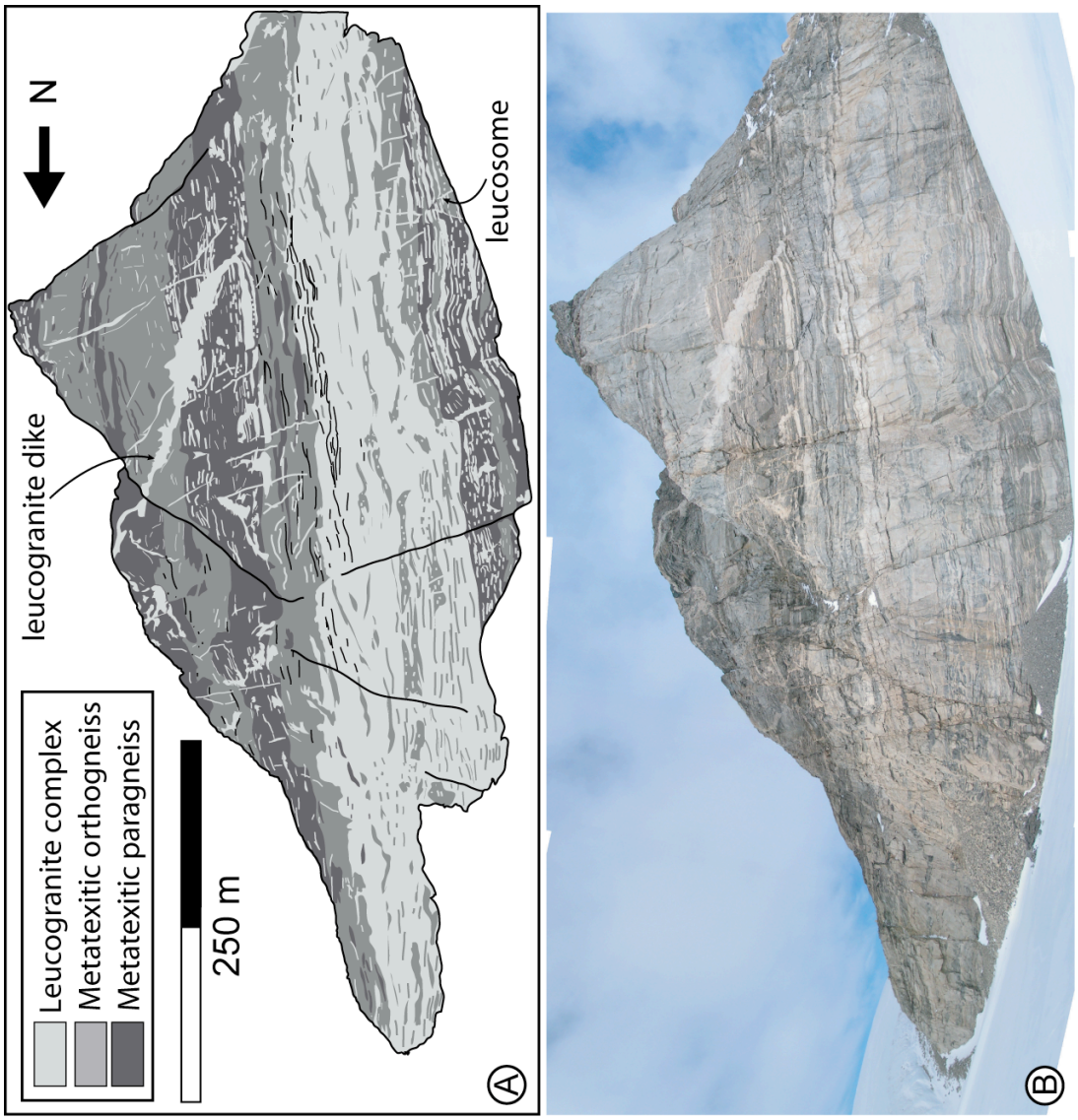

Figure 5.5 Photos and sketches of Mt. Bitgood and Bird Bluff.

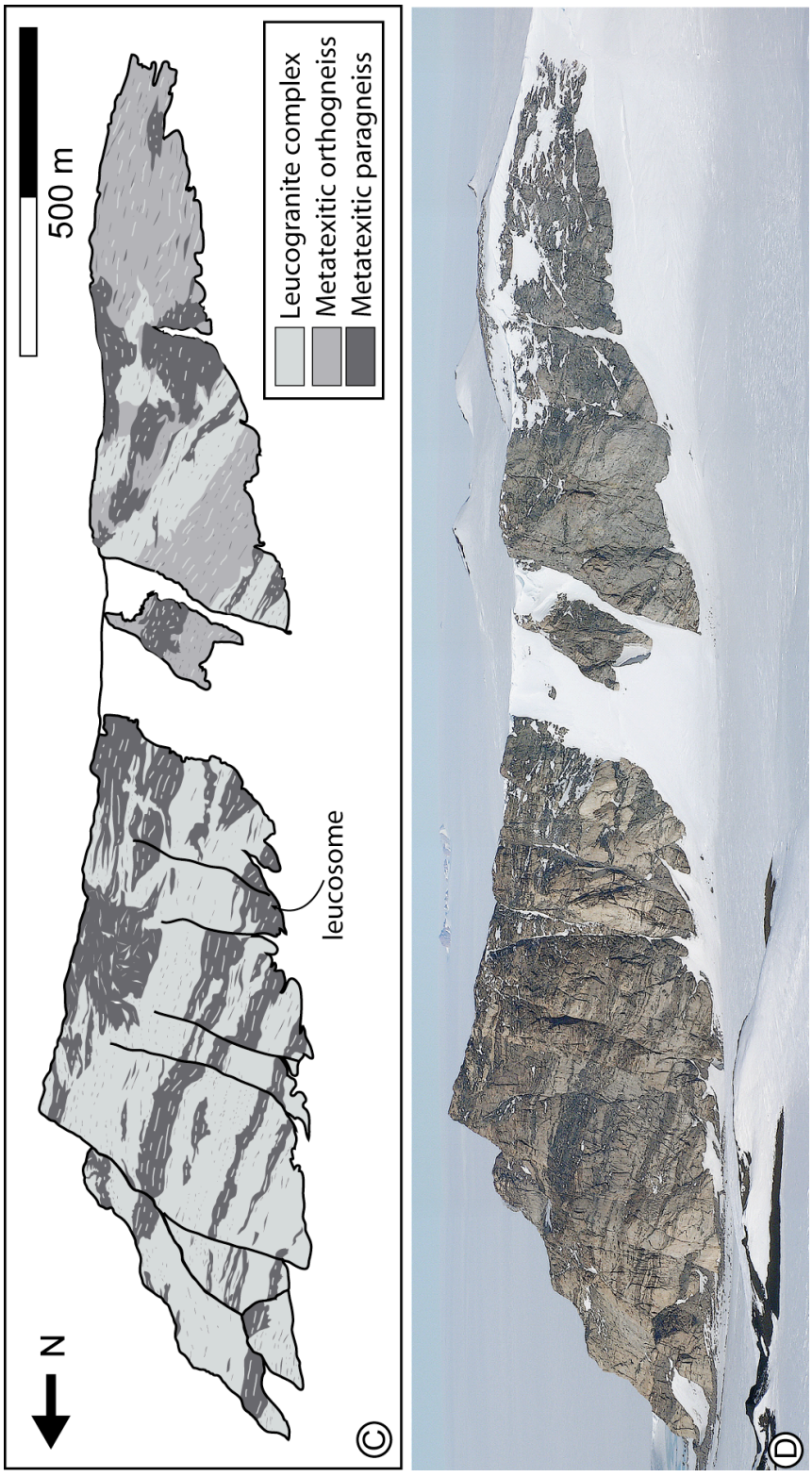

Figure 5.5 Photos and sketches of Mt. Bitgood and Bird Bluff.

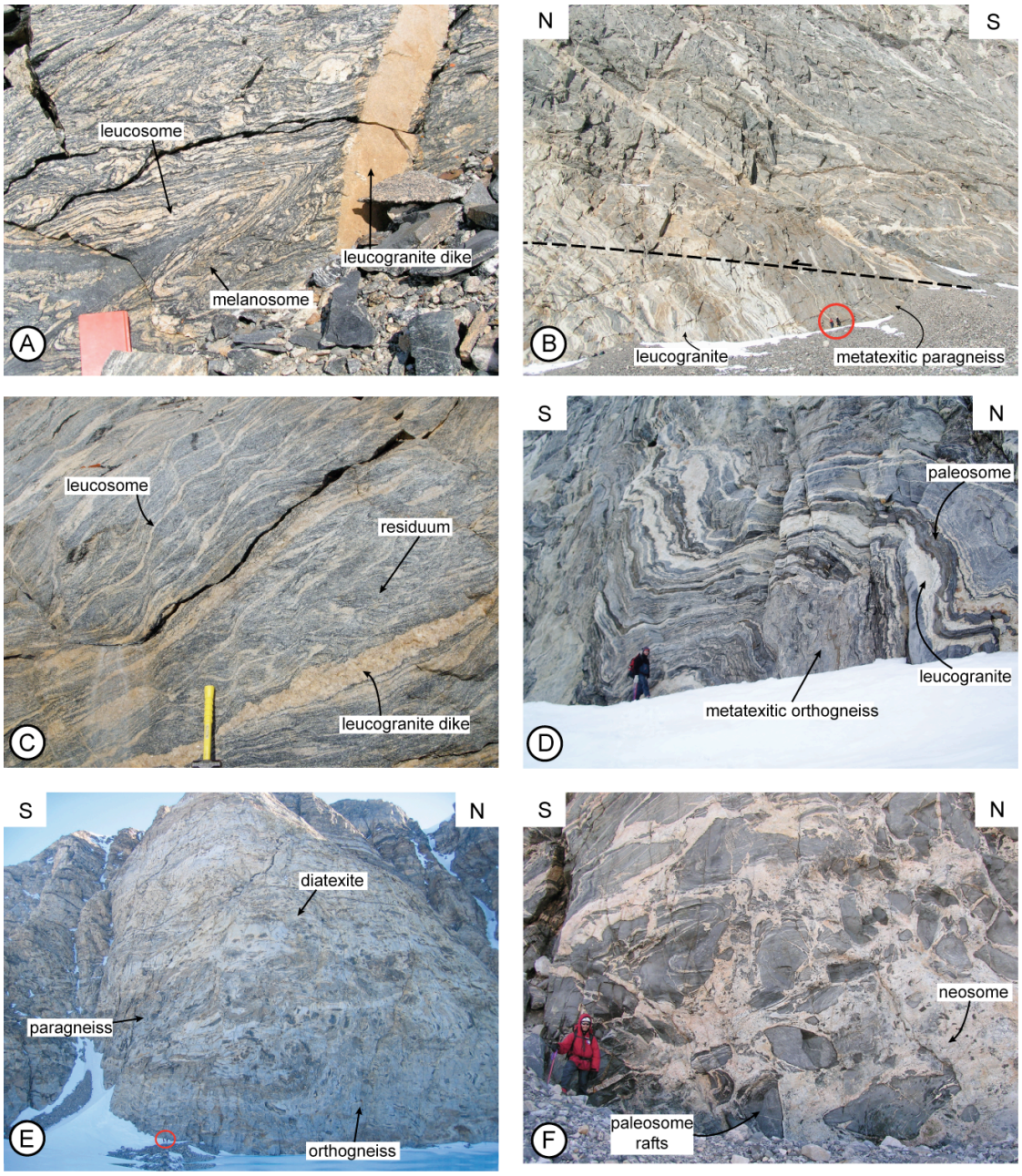

Figure 5.6 Representative photos of rock units in the Fosdick dome.

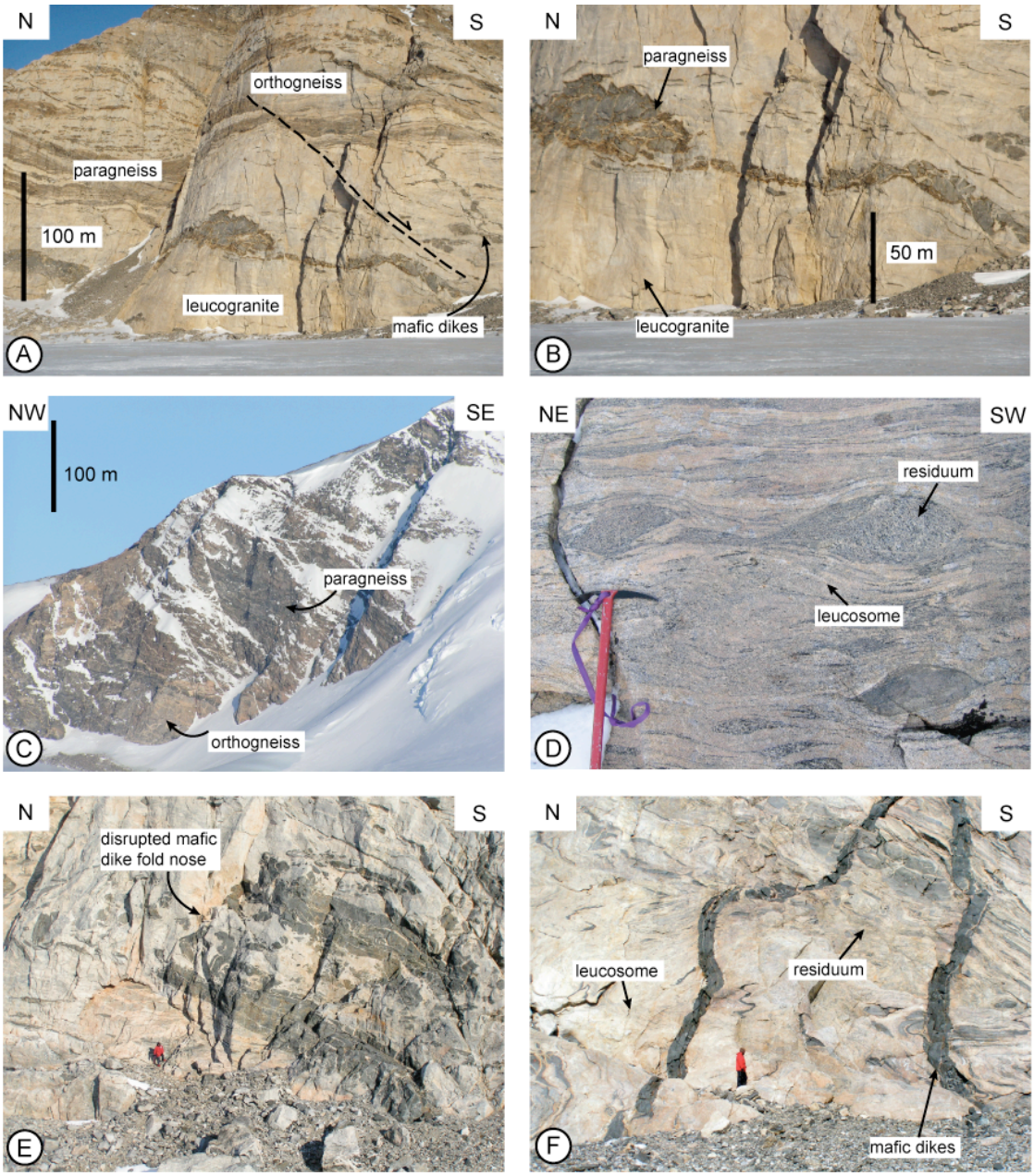

Figure 5.7 Representative photos of rock units in the Fosdick dome.

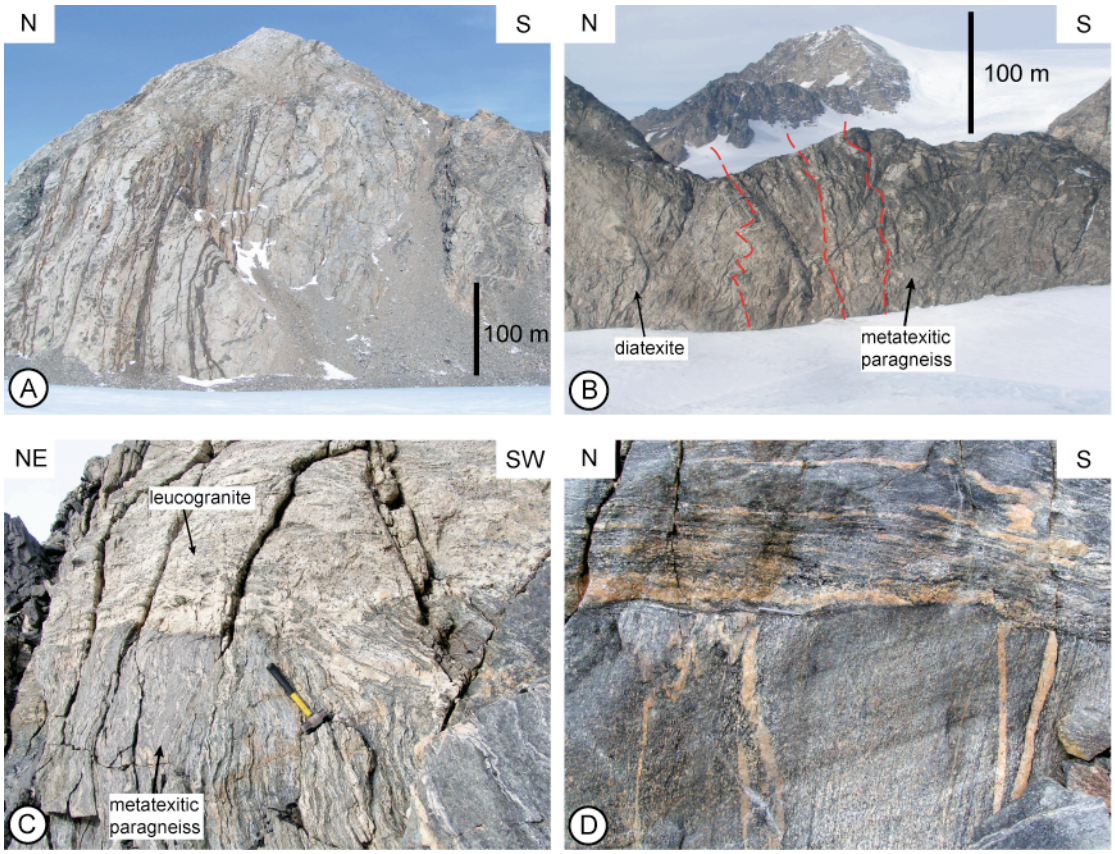

Figure 5.8 Photos of steep structures in the Fosdick dome.

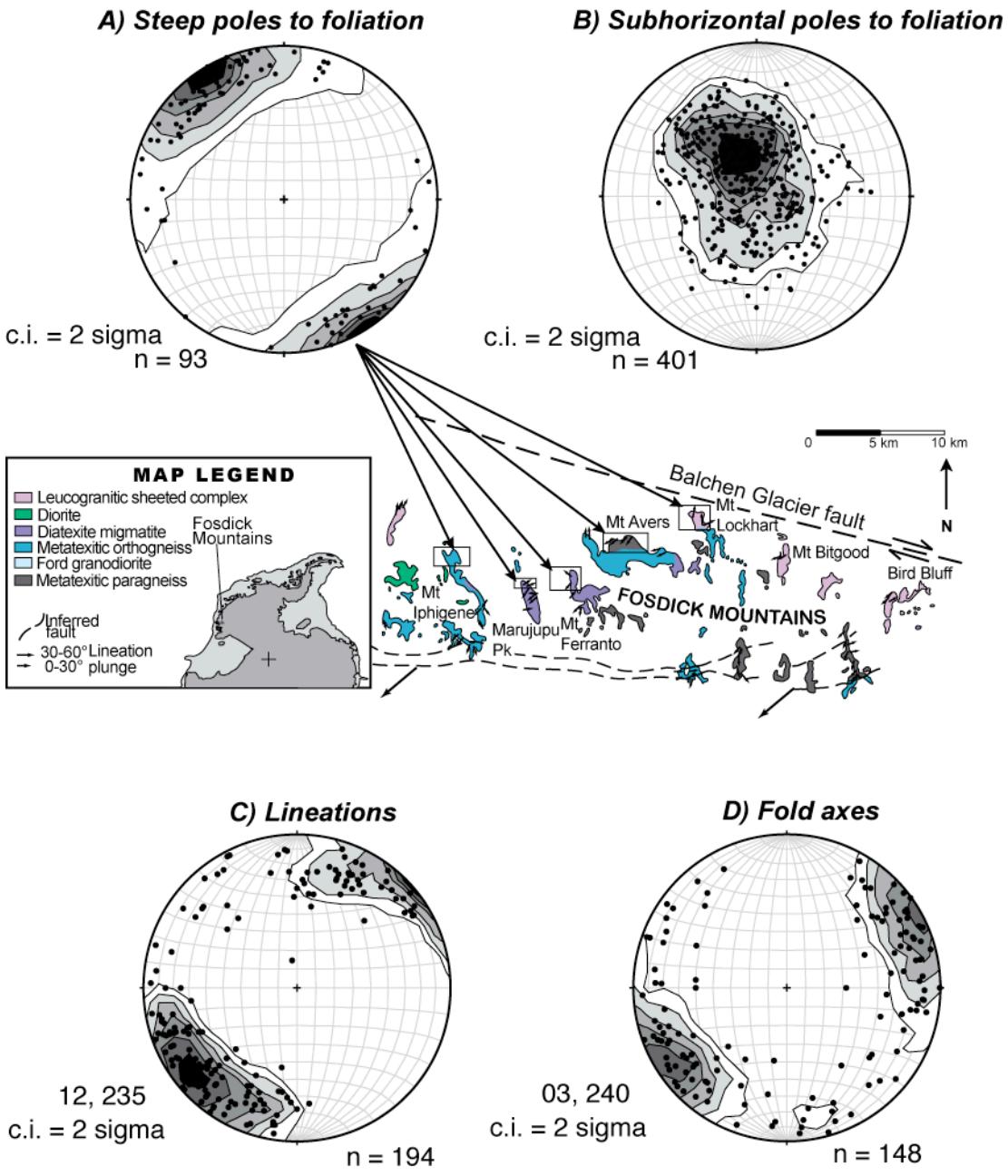

Figure 5.9 Locations of steep foliation domains in the Fosdick dome.

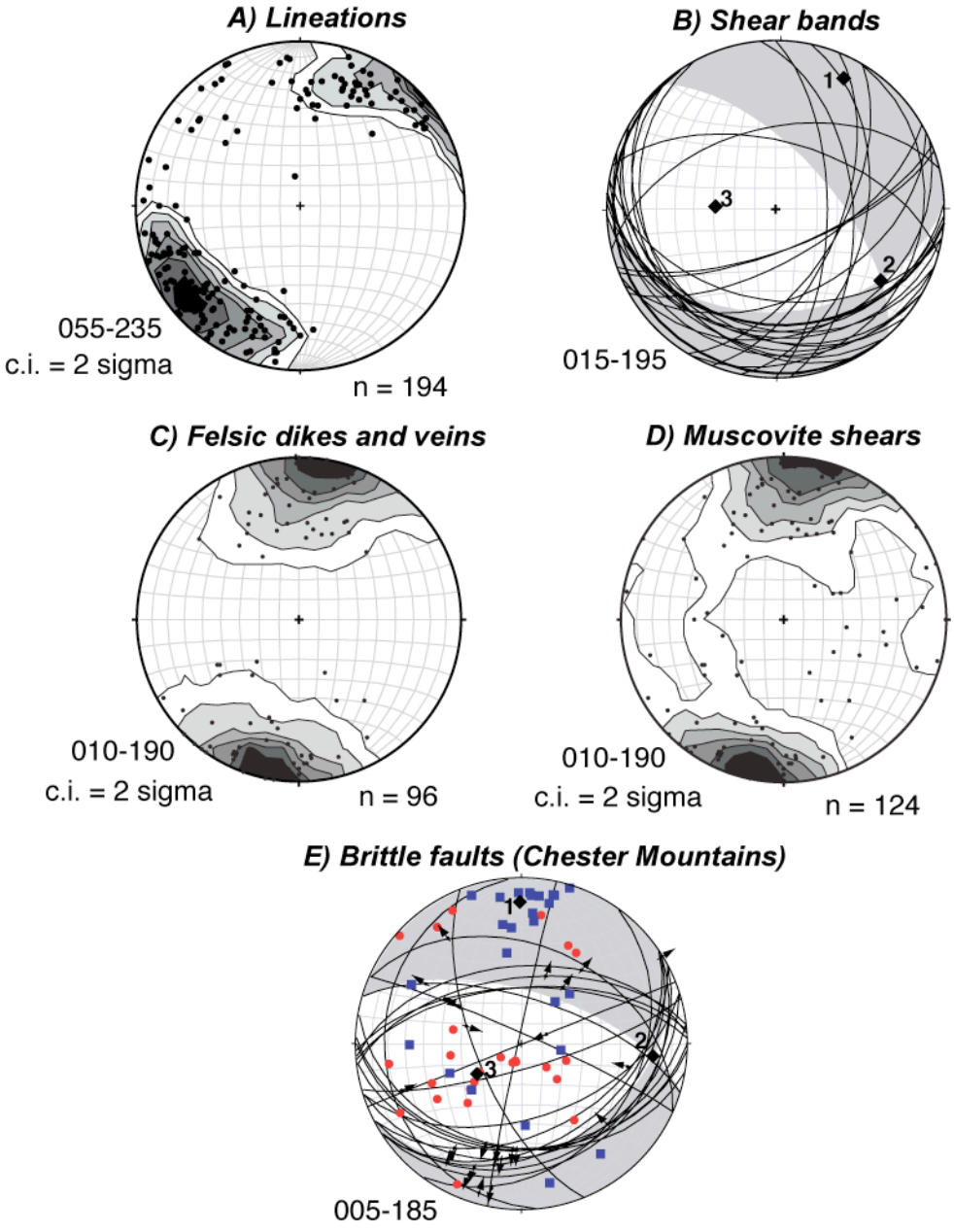

Figure 5.10 Stereonets of ductile and brittle structures in the Fosdick Mountains

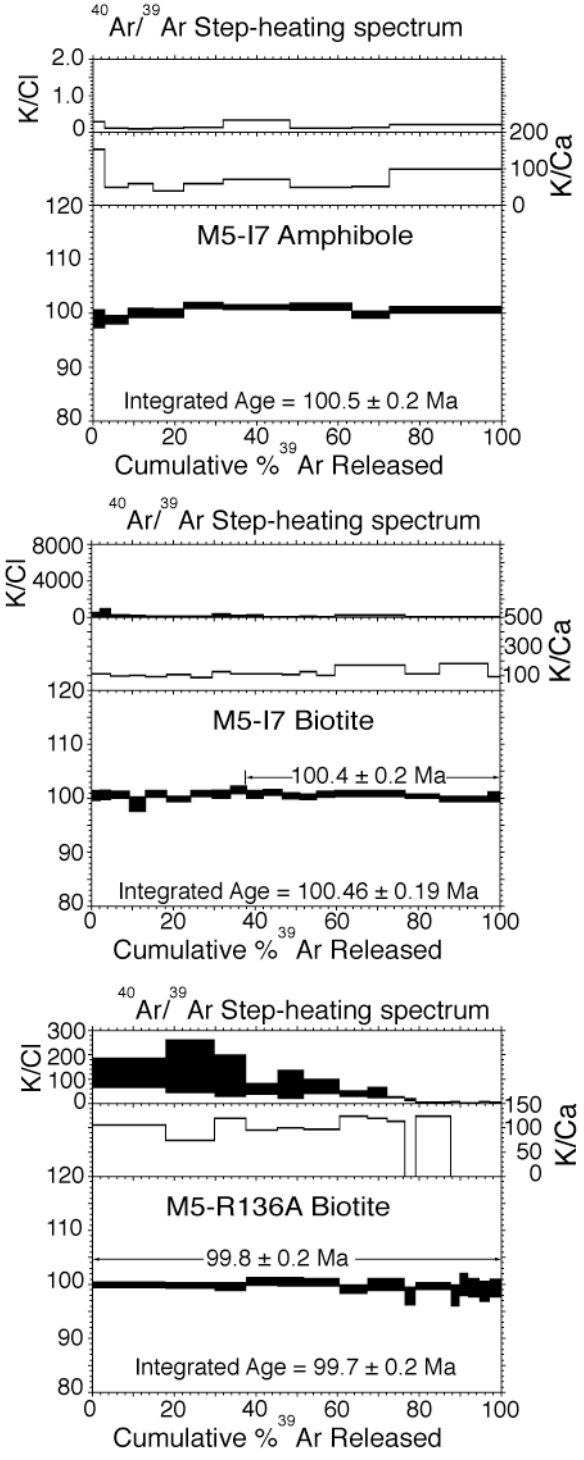

Figure 5.11 $^{40}Ar/^{39}Ar$ thermochronology age spectra.

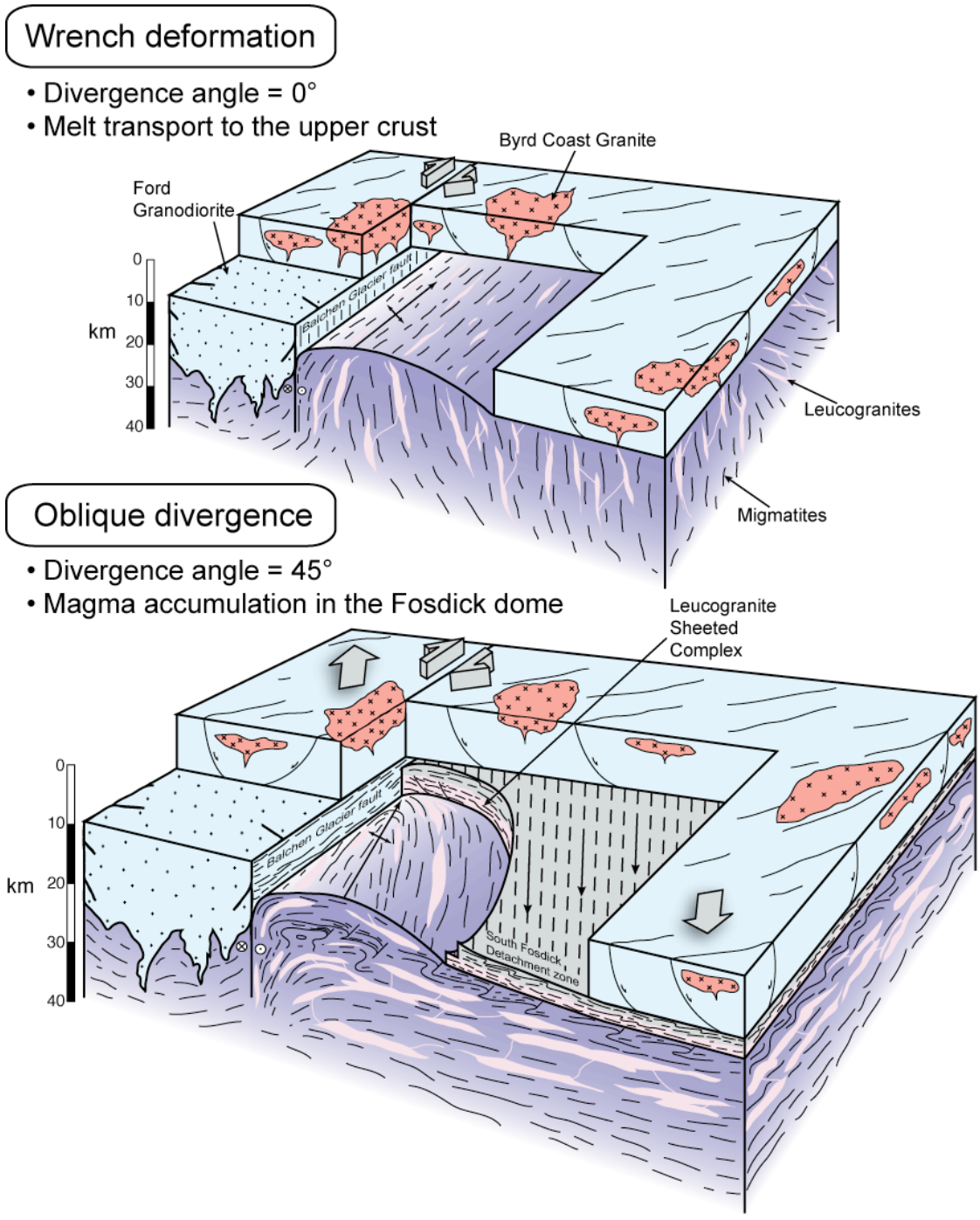

Figure 5.12 Three-dimensional diagrams that represent two stages in the evolution of the Fosdick dome.

Chapter 6: Summary and Conclusions

The three-dimensional, expansive cliff-face exposures in the Fosdick Mountains migmatite-cored gneiss dome enabled the documentation of middle to lower crustal rocks that experienced suprasolidus deformation and melt migration at a scale significant for continental differentiation and crustal flow. Using field relations and U-Pb geothermochronology, work in the Fosdick dome has addressed the role of oblique deformation in the flow of partially molten crust, the internal segregation and emplacement of granite, and the relation between oblique detachment systems and exhumation of migmatite terrains.

The Fosdick dome developed in the mid-Cretaceous during oblique plate convergence along the East Gondwana margin and intracontinental crustal extension associated with the development of the West Antarctic Rift System. The Fosdick dome records the middle to lower crustal response to transtension during intracontinental extension and the flow of partially molten crust.

The distribution of melt-rich and melt-poor units in the Fosdick dome display the differentiation of crust due to the influence of deformation, crustal anisotropy, and strain heterogeneities related to heterogeneous crust. The Fosdick Mountains are bounded to the north by the inferred Balchen Glacier strike-slip fault and bounded to the south by the dextral normal oblique South Fosdick Detachment zone. The dome rocks consist of mid-crustal migmatites and multiple phases of granite. The migmatite units form a folded and interlayered section of low melt fraction metatexitic

paragneiss and metatexitic orthogneiss, and high melt fraction diatexite. The transition from metatexite to diatexite shows the affect of melt fraction on the destruction of the structural framework. Leucosomes and leucocratic dikes and veins preserve the polyphase remnant permeability network, which records the polyphase transfer of melt within the migmatites. Tabular granite sheets and dilatant sites including granite-filled interboudin partitions and shear bands represent magma accumulation sites. Subhorizontal leucogranite sheets form an ~2 km thick composite section above the migmatites. The leucogranite sheets are bounded by a km thick section of metatexite migmatites that record solid-state fabrics associated with the South Fosdick Detachment zone.

Structures in the Fosdick dome record the evolution of oblique motion that occurred during melt transport and dome emplacement. Foliations, lineations, crosscutting relationships, and granite and leucosome in specific structural sites track the rotation of divergence angle and the influence of three-dimensional deformation on flowing partially molten crust.

The transport of melt through the level of the Fosdick dome occurred during wrench deformation. Steep foliation domains strike NE-SW near the Balchen Glacier fault. These foliations are crosscut, transposed, and folded by subhorizontal foliations. Steeply dipping mafic dikes are folded perpendicular to the subhorizontal foliation and boudinaged paralell to the subhorizontal foliation. The steep domains host concordant leucosomes that are interconnected with leucocratic veins and dikes and folded leucogranite layers.

As the divergence angle rotated into a regime of extension-dominated transtension subhorizontal foliations developed. In the Fosdick dome, foliations are predominantly subhorizontal with an ENE-WSW strike. Lineations and fold axes record a stretching axis oriented 235 ± 5. In the subhorizontal domains, prevalent concordant leucosomes are connected with oblique and dilational leucosomes. The subhorizontal leucogranite sheeted complex and the subhorizontal diatexite unit are also concordant with the subhorizontal foliation. The leucosomes and subhorizontal granite sheets suggest that during extension-dominated transtension magma accumulated in the Fosdick dome. The subhorizontal leucogranite sheets were emplaced near the boundaries of the Fosdick dome, indicating that the opening of an oblique dilation zone created space for magma accumulation.

Leucogranite sheets syntectonically intrude the South Fosdick Detachment zone and are deformed by solid-state deformation, indicating the initiation of movement on the detachment zone was related to the emplacement of subhorizontal leucogranite sheets and the rotation of the divergence angle. Structures in the detachment zone also display the relationship between the middle to lower crust and the upper crust during oblique deformation. The detachment zone preserves high temperature fabrics, solid-state fabrics, and brittle fabrics. In the high temperature and solid-state fabrics lineations are oriented 055–235, which is consistent with the footwall rocks, and C-S fabrics and asymmetric porphyroclasts record top-to-the-SW oblique motion. Brittle faults, and late felsic veins and dikes that transect the solid-state fabrics record stretching oriented 010–190. The orientation of brittle structures is

similar in the hanging wall, exposed in the Chester Mountains and Neptune Nunataks. The hanging wall brittle faults that crosscut massive Ford Granodiorite and Byrd Coast Granite record stretching oriented 005–185. The overprinting relationships of these ductile and brittle structures and the change in extension direction with increasingly later structures suggest counterclockwise rotation of the strain field during cooling and exhumation of the Fosdick dome. The temporal change in extension direction is confirmed by U-Pb analyses on leucosome and leucogranite emplaced in ductile structures and cooling ages on muscovite shears present along brittle structures.

In the Fosdick Mountains, U-Pb SHRIMP zircon analyses on leucosome and (leuco-) granites in specific structural sites indicate a 15 myr period of suprasolidus deformation between ca. 117–102 Ma. The crystallization ages in the Fosdick dome can be divided into two groups. An older group with ages between ca. 117–115 Ma and a younger group with ages between ca. 109–102 Ma. The older leucosome and leucogranites are hosted by steep structures and some are folded with the host migmatites. The younger leucosome and leucogranites are concordant with subhorizontal foliation domains or are emplaced in the South Fosdick Detachment zone. A sample from the subhorizontal leucogranite sheeted complex has an age of ca. 104 Ma. A suite of samples from the South Fosdick Detachment zone record a 7myr period between ca. 109–102 Ma of melt-present deformation. These data make it possible to estimate the timescale for the transition from wrench deformation to extension-dominated transtension. The youngest emplaced granite in the older group

has an age of ca. 115 Ma and the oldest emplaced granite in the younger group has an age of ca. 109 Ma. These ages indicate that the switch from wrench to extension-dominated transtension occurred in as little as 6 myr. This is also the time period when movement on the detachment commenced.

U-Pb SHRIMP zircon and titanite analyses on mafic and felsic dikes and $^{40}Ar/^{39}Ar$ thermochronology on biotite and amphibole indicate the Fosdick dome cooled and was exhumed rapidly. U-Pb zircon ages from a felsic dike and titanite ages from discordant, syntectonic mafic dikes are between ca. 101–97 Ma. $^{40}Ar/^{39}Ar$ cooling ages of biotite and amphibole are between ca. 100–99 Ma. When combined with U-Pb zircon ages, these data indicate up to 100 ºC/m.y. cooling rates.

Structures and geothermochronology show that the Fosdick dome was constructed, stabilized, and exhumed during a major counterclockwise rotation of the regional strain field. The rotation of oblique divergence, along with crustal heterogeneity, crustal-scale structures, and melt fraction, greatly affected deformation and melt pathways. The structures related to deformation and the remnant permeability network exposed in several km^2 cliff-faces display the transition from a zone of melt transport to a zone of melt production and magma accumulation, and ultimately a cooled and exhumed portion of the once partially molten crust.

Complete Bibliography

Adams, C.J., 1986, Geochronological studies of the Swanson Formation of Marie Byrd Land, West Antarctica, and correlation with northern Victoria Land, East Antarctica and the South Island, New Zealand, New Zealand Journal of Geology and Geophysics, v. 29, p. 345–358.

Adams, C.J., 1987, Geochronology of granite terranes in the Ford Ranges, Marie Byrd Land, West Antarctica, New Zealand Journal of Geology and Geophysics, v. 30, p. 51–72.

Aleinikoff, J.N., Wintsch, R.P., Tollo, R.P., Unruh, D.M., Fanning, C.M., and Schmitz, M.D., 2007, Ages and origins of rocks of the Killingworth dome, south-central Connecticut: Implications for the tectonic evolution of southern New England, American Journal of Science, p. 63–118.

Andronicos, C.L., Chardon, D.H., Hollister, L.S., Gehrels, G.E., and Woodsworth, G.L., 2003, Strain partitioning in an obliquely convergent orogen, plutonism, and synorogenic collapse: Coast Mountains Batholith, Canada, Tectonics, v. 22, doi: 10.1029/2001TC001312.

Armstrong, R.L., and Ward, P., 1991, Evolving geographical patterns of Cenozoic magmatism in the North American Cordillera: The temporal and spatial association of magmatism and metamorphic core complexes, Journal of Geophysical Research, v. 96 (B8), p. 13,201–13,224.

Babeyko, A.Y., Sobolev, S.V., Trumbull, R.B., Oncken, P., and Lavier, L.L., 2002, Numerical models of crustal scale convection and partial melting beneath the Altiplano-Puna plateau, Earth and Planetary Science Letters v. 199, p. 373–388.

Bachmann, O., and Bergantz, G.W., 2004, On the origin of crystal-poor rhyolites: Extracted from batholithic crystal mushes, Journal of Petrology, v. 45, p. 1565–1582.

Beaumont, C., Jamieson, R.A., Nguyen, M.H., and Lee, B., 2001, Himalayan tectonics explained by extrusion of a low-viscosity crustal channel coupled to focus surface denudation, Nature, v. 414, p. 738–742.

Bellot, J.P., 2007, Pre- to syn-extensional melt-assisted nucleation and growth of extensional gneiss domes: The western French Massif Central (Variscan belt), Journal of Structural Geology, v. 29, p. 863–880.

Black, L. P., Kamo, S.L., Allen, C.M., Aleinikoff, J.N., Davis, D.W., Korsch, R.J., and Foudulis, C., 2003, TEMORA 1: a new zircon standard for Phanerozoic U-Pb geochronology, Chemical Geology, v. 200, p. 155–170.

Blumenfeld, P., and Bouchez, J.-L., 1988, Shear criteria in granite and migmatite deformed in the magmatic and solid states, Journal of Structural Geology, v. 10, p. 361–372.

Bradshaw, J.D., Andrew, B., and Field, B.D., 1983, Swanson Formation and related rocks of Marie Byrd Land and a comparison with the Robertson Bay Group of northern Victoria Land, *in* Oliver, R.L., James, P.R., and Jago, J.B., eds., Antarctic Earth Science, Australian Academy of Science, p. 274–279.

Bradshaw, J.D., 1989, Cretaceous geotectonic patterns in the New Zealand region, Tectonics, v. 8, p. 803–820.

Bradshaw, J.D., Pankhurst, R.J., Weaver, S.D., Storey, B.C., Muir, R.J., and Ireland, T.R., 1997, New Zealand superterranes recognized in Marie Byrd Land and Thurston Island, in *The Antarctic Region, Geological Evolution and Processes*, edited by C.A. Ricci, pp. 429–436, Terra Antartica Publication, Siena, Italy.

Brown, M., 1994, The generation, segregation, ascent and emplacement of granite magma: the migmatite-to-crustally-derived granite connection in thickened orogens, Earth-Science Reviews, v. 36, p. 83–130

Brown, M., 2007, Crustal melting and melt extraction, ascent and emplacement in orogens: mechanisms and consequences, Journal of the Geological Society of London, v. 164, p. 709–730.

Brown, M., 2008, Granites, migmatites and residual granulites: relationships and processes, Mineralogical Association of Canada Short Course 38, Quebec City, Quebec, p. 97–144.

Brown, M., Averkin, Y.A., McLellan, E.L., and Sawyer, E.W., 1995, Melt segregation in migmatites, Journal of Geophysical Research, v. 100, p. 15,655–15,679.

Brown, M, and Rushmer, T., 1997, The role of deformation in the movement of granite melt: views from the laboratory and the field, *Deformation-enhanced Fluid Transport in the Earth's Crust and Mantle,* edited by M. Holness, Mineral. Soc. Series: 8, London: Chapman and Hall, p. 111–144.

Brown, M., and Solar, G.S., 1998a, Shear zone systems and melts: feedback relations

and self-organisation in orogenic belts. Journal of Structural Geology, v. 20, p. 211–227.

Brown, M., and Solar, G.S., 1998b, Granite ascent and emplacement during contractional deformation in convergent orogens, Journal of Structural Geology, v. 20, p. 1365–1393.

Brun, J.P., Sokoutis, D., and Van Den Driessche, J., 1994, Analogue modeling of detachment fault systems and core complexes; Geology, v. 22, p. 319–322.

Burg, J.P., and Vanderhaeghe, O., 1993, Structures and way-up criteria in migmatites, with application to the Velay dome (French Massif Central), Journal of Structural Geology, v. 15, p. 1293–1301.

Clemens, J.D., 2006, Melting of the continental crust: fluid regimes, melting reactions, and source-rock fertility, *in* Evolution and Differentiation of the Continental Crust, Brown, M., and Rushmer, T., eds., Cambridge University Press, p. 297–331.

Clemens, J.D., and Mawer, C.K., 1992, Granitic magma transport by fracture propagation, Tectonophysics, v. 204, p. 339–360.

Collins, W.J., and Sawyer, E.W., 1996, Pervasive granitoid magma transfer through the lower-middle crust during non-coaxial compressional deformation, Journal of Metamorphic Geology, v. 14, p. 565–579.

Cooper, A.K., Davey, F.J., and Hinz, K., 1991, Crustal extension and origin of sedimentary basins beneath the Ross Sea and Ross Ice Shelf, Antarctica, *Geologic Evolution of Antarctica*, edited by M. R. A. Thomson et al., Cambridge: Cambridge University Press, p. 285–291.

Cooper, R.A., and Tulloch, A., 1992, Early Paleozoic terranes in New Zealand and their relationship to the Lachlan Fold Belt, Tectonophysics, v. 214, p. 129–144.

D'Lemos, R.S., Brown, M., and Strachan, R.A., 1992, Granite magma generation, ascent and emplacement within a transpressional orogen: Journal Geological Society of London, v. 149, p. 487–490.

Davey F.J., and Brancolini, G., 1995, The Late Mesozoic and Cenozoic structural setting of the Ross Sea region, in *Geology and Seismic Stratigraphy of the Antarctic Margin*, edited by A. K. Cooper, P. F. Barker, and G. Brancolini, Antarct. Res. Ser. AGU v. 68, p. 167–182.

Dalrymple, G.B., Alexander, E.C., Lanphere, M.A., and Kraker, G.P., 1981, Irradiation of samples for $^{40}Ar/^{39}Ar$ dating using the Geological Survey TRIGA reactor, U.S. Geological Survey Professional Paper, v. 1176, p. 55.

Davey, F.J., and Brancolini, G., 1995, The Late Mesozoic and Cenozoic structural setting of the Ross Sea region, in *Geology and Seismic Stratigraphy of the Antarctic Margin*, edited by A.K. Cooper, P.F. Barker, and G. Brancolini, Antarctic Research Series AGU 68, p. 167–182.

Denèle, Y., Olivier, P., and Gleizes, G., 2008, Progressive deformation of a zone of magma transfer in a transpressional regime: Variscan Merens shear zone (Pyrenees, France), Journal of Structural Geology, v. 30, p. 1138–1149.

Depine, G.V., Andronicos, C.L., and Phipps-Morgan, J., 2008, Near isothermal conditions in the middle and lower crust induced by melt migration, Nature, v. 452, p. 80–83.

Dewey, J.F., and Strachan, R.A., 2003, Changing Silurian-Devonian relative plate motion in the Caledonides: Sinistral transpression to sinistral transtension, Journal of the Geological Society, London, v. 160, p. 219–229.

Ferraccioli, F., Bozzo E., and Damaske, D., 2002, Aeromagnetic signatures over western Marie Byrd Land provide insight into magmatic arc basement, mafic magmatism and structure of the eastern Ross Sea rift flank: Tectonophysics, v. 347, p. 139–65.

Fitzgerald, P.G., and Baldwin, S.L., 1997, Detachment fault model for the Evolution of the Ross Embayment, in *The Antarctic Region: Geological Evolution and Processes*, edited by C.A. Ricci, p. 555–564, *Terra Antarctica* Publication, Siena, Italy.

Forster, M.A., and Lister, G.S., 2003, Cretaceous metamorphic core complexes in the Otago Schist, New Zealand, Austrialian Journal of Earth Sciences, v. 50, p. 181–198.

Fossen, H., and Tikoff, B., 1993, The deformation matrix for simultaneous simple shearing, pure shearing and volume change, and its application to transpression-transtension tectonics, Journal of Structural Geology, v. 15, p. 413–422.

Foster, D.A., Gray, D.R., and Spaggiari, C. 2005, Timing of subduction and exhumation along the Cambrian East Gondwana margin and the formation of Paleozoic back-arc basins, GSA Bulletin, v. 117, p. 105–116.

Foster, D.A., Dought, P.T., Kalakay, T.J., Fanning, C.M., Coyner, S., Grice, W.C., and Vogl, J., 2007, Kinematics and timing of exhumation of metamorphic core

complexes along the Lewis and Clark fault zone, northern Rocky Mountains, USA, *in* Till, A.B., Roeske, S.M., Sample, J.C., and Foster, D.A., eds., Exhumation Associated with Continental Strike-slip Fault Systems: Geological Society of America Special paper 434, p. 207–232, doi: 10.1130/2007.2434(10).

Gaffney, A.M., and Siddoway, C.S., 2007, Heterogeneous sources for Pleistocene lavas of Marie Byrd Land, Antarctica: New data from the SW Pacific Diffuse Alkaline Magmatic Province. *In* Antarctica: A Keystone in a Changing World—Online Proceedings for the Tenth International Symposium on Antarctic Earth Sciences, eds. Cooper, A.K., Raymond, C.R., et al., USGS Open-File Report 2007-1047, Extended Abstract 063, http://pubs.usgs.gov/of/2007/1047/.

Gibson, G.M., McDougall, I., and Ireland, T.R., 1988, Age constraints on metamorphism and the development of a metamorphic core complex in Fiordland, southern New Zealand, Geology, v. 16, p. 405–408.

Gibson, G.M., and Ireland, T.R., 1996, Extension of Delamerian (Ross) Orogen into western New Zealand; evidence from zircon ages and implications for crustal growth along the Pacific margin of Gondwana, Geology, v. 24, p. 1087–1090.

Glazner, A.F., 1991, Plutonism, oblique subduction and continental growth: An example from the Mesozoic of California, Geology, v. 19, p. 784–786.

Glen, R.A., 2005, The Tasmanides of eastern Australia, *Terrane Processes at the Margin of Gondwana*, edited by A. Vaughan et al., Geol. Soc. London Spec. Pub. 246, pp. 23–96, Geol. Soc., London.

Grocott, J., Brown, M., Dallmeyer, R.D., Taylor, G.K., and Trelor, P.J., 1994, Mechanisms of continental growth: An example from the Andean plate-boundary zone, Geology, v. 22, p. 391–394.

Guernia, S, and Sawyer, E.W., 2003, Large-scale melt-depletion in granulite terrains: An example from the Archean Ashuanipi Subprovince of Quebec, Journal of Metamorphic Geology, v. 21, p. 181–201.

Guo, J., O'Reilly, S.Y., and Griffin, W.L., 1996, Zircon inclusions in corundum megacrysts: I. Trace element geochemistry and clues to the origin of corundum megacrysts in alkali basalts, Geochim. Cosmochim. Acta, v. 60, p. 2347–2363.

Harrison, T.M., 1981, Diffusion of 40Ar in hornblende, Contributions to Mineralogy and Petrology, v. 78, p. 324–331.

Harrison, T.M., Duncan, I.J., McDougall, I., 1985, Diffusion of 40Ar in biotite: temperature, pressure and compositional effects, Geochimica Cosmochimica Acta, v. 49, p. 2461–2468.

Hasalová, P., Schulmann, K., Lexa, O., Stipska, P., Hrouda, F., Ulrich, S., Haloda, J., and Tycova, 2008, Origin of migmatites by deformation-enhanced melt infiltration of orthogneiss: a new model based on quantitative microstructural analysis, Journal of Metamorphic Geology, v. 26, p. 29–53.

Hollis, J.A., Clarke, G.L., Klepeis, K.A., Daczko, N.R., and Ireland, T.R., 2004, The regional significance of Cretaceous magmatism and metamorphism in Fiordland, New Zealand, from U-Pb zircon geochronology, Journal of Metamorphic Geology, v. 22, p. 607–627.

Holness, M.B., 2008, Decoding migmatite microstructures, Mineralogical Association of Canada Short Course 38, Quebec City, Quebec, p. 57–76.

Hoskin, P.W.O. 1998, Minor and trace element analysis of natural zircon (ZrSiO4) by SIMS and laser ablation ICPMS: a consideration and comparison of two broadly competitive techniques, J. Trace Microprobe Tech., v. 16, p. 301–326.

Hutton, D.H.W., 1990, A new mechanism of granite emplacement: Intrusion in active extensional shear zones: Nature, v. 343, p. 452–455.

Ireland, T.R., Flottmann, T., Fanning, C.M., Gibson, G.M., and Preiss, W.V., 1998, Development of the early Paleozoic Pacific margin of Gondwana from detrital-zircon ages across the Delamerian orogen, Geology, v. 26, p. 243–246.

Ireland, T.R., and Gibson, G.M., 1998, SHRIMP monazite and zircon geochronology of high-grade metamorphism in New Zealand, Journal of Metamorphic Geology, v. 16, p. 149–167.

Ireland, T.R., and Wlotzka, F., 1992, The oldest zircons in the solar system, Earth and Planetary Science Letters, v. 109, p. 1–10.

Katrinová, Z., Schulmann, K., Edel, J.B., Jezek, J., and Schaltegger, U., 2007, Model of successive granite sheet emplacement in transtensional setting: Integrated microstructural and anisotropy of magnetic susceptibility study, Tectonics, v. 26, TC6003, doi: 10.1029/2006TC002035.

Kimbrough, D.L., and Tulloch, A.J., 1989, Early Cretaceous age of orthogneiss from the Charleston Metamorphic Group, New Zealand, Earth and Planetary Science Letters, v. 95, p. 130–140.

Korhonen, F.J., Brown, M., Saito, S., and Siddoway, C.S., *in revision*, Modeling multiple melt loss events in the evolution of an active continental margin, Lithos.

Korhonen, F., Satoshi, S., Brown, M., Siddoway, C.S., and Day, J., *in review*, Multiple generations of granite in the Fosdick Mountains, Marie Byrd Land, West Antarctica: Implications for polyphase intracrustal differentiation in a continental margin setting, Journal of Petrology.

Kula, J., Tulloch, A.J., Spell, T.L., and Wells, M.L., 2007, Two-stage rifting of Zealandia-Australia-Antarctica: Evidence from $^{40}Ar/^{39}Ar$ thermochronometry of the Sisters shear zone, Stewart Island, New Zealand, Geology, v. 35, p. 411-414, doi: 10.1130/G23432A.1.

Leitch, A.M., and Weinberg, R.F., 2002, Modeling granite migration be mesoscale pervasive flow, Earth and Planetary Science Letters, v. 200, p. 131–146.

LeLoup, P.H., Arnaud, N., Lacassin, R., Kienast, J.R., Harrison, T.M., Phan Trong, T.T., Replumaz, A., and Tapponnier, P., 2001, New constraints on the structure, thermochronology, and timing of the Ailao Shan-Red River shear zone, SE Asia, Journal of Geophysical Research, v. 106, p. 6683–6732.

Lister, G.S., and Baldwin, S.L., 1993, Plutonism and the origin of metamorphic core complexes, Geology, v. 21, p. 607–610.

Ludwig, K.R., 2001, SQUID 1.02, A User's Manual; Berkeley Geochronology Center Special Publication, vol. 2, Berkeley Geochronology Center Special Publication, 2455 Ridge Road, Berkeley, CA 94709, USA.

Ludwig, K.R., 2003, User's Manual for Isoplot/Ex, Version 3.0, A geochronological toolkit for Microsoft Excel Berkeley Geochronology Center Special Publication, v. 4, Berkeley Geochronology Center, 2455 Ridge Road, Berkeley, CA 94709, USA.

Luyendyk, B.P., 1995, Hypothesis for Cretaceous Rifting of East Gondwana Caused by Subducted Slab Capture, Geology, v. 23, p. 373-376.

Luyendyk, B. P., Wilson, D.S., and Siddoway C.S., 2003, The eastern margin of the Ross Sea Rift in western Marie Byrd Land: Crustal structure and tectonic development: Geochemistry, Geophysics, Geosystems, doi: 10.1029/2002GC000462.

Maas, R., Kinny, P.D., Williams, I.S., Froude, D.O., and Compston, W., 1992, The Earth's oldest known crust: a geochronological and geochemical study of 3900–4200 Ma old detrital zircons from Narryer and Jack Hills, Western Australia, Geochem. Cosmochim. Acta v. 56, p. 1281–1300.

Marchildon, N., and Brown, M., 2001, Melt segregation in late syn-tectonic anatectic migmatites: an example from the Onawa Contact aureole, Maine, USA, Physics and Chemistry of Earth (A), v. 26, p. 225–229.

Marchildon, N., and Brown, M., 2002, Grain-scale melt distribution in two contact aureole rocks: implication for controls on melt localization and deformation, Journal of Metamorphic Geology, v. 20, p. 381–396.

Marchildon, N., and Brown, M., 2003, Spatial distribution of melt-bearing structures in anatectic rocks from southern Brittany: implications for melt-transfer at grain-to orogen-scale, Tectonophysics, v. 364, p. 215–235.

McCaffrey, K.J.W., Miller, C.F., Karlstrom, K.E., and Simpson, C., 1999, Synmagmatic deformation patterns in the Old Woman Mountains, SE California, Journal of Structural Geology, v. 21, p. 335–349.

McFadden, R., Siddoway, C.S., Teyssier, C., Fanning, C.M., and Kruckenberg, S.C., 2007, Cretaceous oblique detachment tectonics in the Fosdick Mountains, Marie Byrd Land, Antarctica, *in* Cooper, A.K., Raymond, C.R., and ISAES Editorial Team, eds., Antarctica: A Keystone in a Changing World - Online Proceedings of the 10th ISAES, USGS Open-File Report 2007-1047, Short Research Paper 047, 5 p.; doi: 10.3133/of2007-1047.srp047.

McFadden, R., Siddoway, C.S., Teyssier, C., and Fanning, C.M., *in review*, Cretaceous intracontinental extension in the Fosdick Mountains migmatite-cored gneiss dome, West Antarctica: Tectonics.

McKenzie, D., Nimmo, F., Jackson, J., Gans, P.B., and Miller, E.L., 2000, Characteristics and consequences of flow in the crust, Journal of Geophysical Research, v. 105, p. 11029–11046.

Milord, I., Sawyer, E.W., and Brown, M., 2001, Formation of diatexite migmatite and granite magma during anatexis of semi-pelitic metasedimentary rocks: an example from St. Malo, France, Journal of Petrology v. 42, p. 487–505.

Milord, I., and Sawyer, E.W., 2003, Schlieren formation in diatexite migmatite: examples from the St. Malo migmatite terrain, France, Journal of Metamorphic Geology, v. 21, p. 347–362.

Mortimer, N., Tulloch, A.J., Spark, R.N., Walker, N.W., Ladley, E., Allibone, A., and Kimbrough, D.L., 1999, Overview of the Median Batholith, New Zealand: a new interpretation of the geology of the Median Tectonic Zone and adjacent rocks, Journal of African Earth Sciences v. 29, p. 257–268.

Mortimer, N., Hoernle, K., Hauff, F., Palin, J.M., Dunlap, W.J., Werner, R., and Faure, K., 2006, New constraints on the age and evolution of the Wishbone Ridge, southwest Pacific Cretaceous microplates, and Zealandia-West Antarctica breakup, Geology, v. 3, p. 185–188.

Muir, R., Ireland, T.R., Weaver, S.D., and Bradshaw, J.D., 1994, Ion microprobe U-Pb zircon geochronology of granitic magmatism in the Western Province of the South Island, New Zealand: Chemical Geology, v. 113, p. 171–189.

Muir, R.J., Ireland, T.R., Weaver, S.D., and Bradshaw, J.D., 1996, Ion microprobe dating of Paleozoic granitoids: Devonian magmatism in New Zealand and correlations with Australia and Antarctica: Chemical Geology, v. 127, p. 191–210.

Muir, R.J., Ireland, T.R., Weaver, S.D., Bradshaw, J.D., Waight, T.E., Jongens, R., and Eby, G.N., 1997, SHRIMP U-Pb geochronology of Cretaceous magmatism in northwest Nelson-Westland, South Island, New Zealand, New Zealand Journal of Geology and Geophysics, v. 40, p. 453–463.

Mukasa, S.B., and Dalziel, I.W.D., 2000, Marie Byrd Land, West Antarctica: Evolution of Gondwana's Pacific margin constrained by zircon U-Pb geochronology and feldspar common-Pb isotopic compositions. Geological Society of America Bulletin, v. 112, p. 611–627.

Mulchrone, K.F., Grogan, S., and De, P., 2005, The relationship between magmatic tiling, fluid flow and crystal fraction, Journal of Structural Geology, v. 27, p. 179–197.

Nelson, K.D., Zhao, W., Brown, L.D., Kuo, J., Che, J., Liu, X., Klemperer, S.L., Makovsky, Y., Meissner, R., Mechie, J., Kind, R., Wenzel, F., Ni, J., Nabelek, J., Leshou, C., Tan, H., Wei, W., Jones, A.G., Booker, J., Unsworth, M., Kidd, W.S.F., Hauck, M., Alsdorf, D., Ross, A., Cogan, M., Wu, C., Sandoval, E., and Edwards, M., 1996, Partially molten middle crust beneath southern Tibet: Synthesis of Project INDEPTH results, Science, v. 274, p. 1684–1688.

O'Halloran, G.J., and Rey, P.F., 1999, Isostatic constraints on the Central Victorian lower crust: Implications for the tectonic evolution of the Lachlan Fold Belt, Australian Journal of Earth Sciences, v. 46, p. 633–639.

Oldow, J.S., 2003, Active transtensional boundary zone between the western Great Basin and Sierra Nevada block, western U.S. Cordillera: Geology, v. 31, p. 1033–1036, doi: 10.1038/333349a0.

Olsen, S.N., Marsh, B.D., and Baumgartner, L.P., 2004, Modelling mid-crustal migmatite terrains as feeder zones for granite plutons: the competing dynamics of melt transfer by bulk versus porous flow, Transactions of the Royal Society Edinburgh: Earth Sciences, v. 95, p.49–58.

Pankhurst, R.J., Weaver, S.D., Bradshaw, J.D., Storey, B.C., and Ireland, T.R., 1998, Geochronology and geochemistry of pre-Jurassic superterranes in Marie Byrd Land, Antarctica: Journal of Geophysical Research, v. 103, p. 2529–2547.

Pavlis, T.L., 1996, Fabric development in syn-tectonic intrusive sheets as a consequence of melt-dominated flow and thermal softening of the crust, Tectonophysic, v. 253, p. 1–31.

Philpotts, A.R., Shi, J., and Brustman, C., 1998, Role of plagioclase crystal chains in the differentiation of partly crystallized basaltic magma, Nature, v. 395, p. 343–346.

Petford, N., Cruden, A.R., McCaffrey, K.J.W., and Vigneresse, J.L., 2000, Granite magma formation, transport and emplacement in the Earth's crust, Nature, v. 408, p. 669–673.

Rey, P.F., Teyssier, C., and Whitney, D.L., 2009, Extension rates, crustal melting, and core complex dynamics: Geology, v. 37, p. 391–394, doi: 10.1130G25460A.1.

Richard, S.M., 1992, Structure and Cooling History of the Fosdick Metamorphic Complex, Marie Byrd Land, West Antarctica, in Recent Progress in Antarctic Earth Science, edited by Y. Yoshida et al., Terra Scientific Publishing, Tokyo, p. 289-294.

Richard, S.M., Smith, C.H., Kimbrough, D.K., Fitzgerald, G., Luyendyk, B.P., and McWilliams, M.O., 1994, Cooling history of the northern Ford Ranges, Marie Byrd Land, West Antarctica, Tectonics, v. 13, p. 837–857.

Rosenberg, C.L., and Handy, M.R., 2005, Experimental deformation of partially melted granite revisited: implication for the continental crust, Journal of Metamorphic Geology, v. 23, p. 19–28.

Sambridge, M.S. Compston, W., 1994, Mixture modeling of multi-component data

sets with application to ion-probe zircon ages, Earth and Planetary Science Letters 128, v. 3–4, p.373–390.

Sawyer, E.W., 1994, Melt segregation in the continental crust, Geology, v. 22, p. 1019–1022.

Sawyer, E.W., 1996, Melt segregation and magma flow in migmatites: Implications for the generation of granite magmas: Transactions of the Royal Society Edinburgh: Earth Sciences, v. 87, p. 85–94.

Sawyer, E.W., 1998, Formation and evolution of granite magma during crustal reworking: The significance of diatexites, Journal of Petrology, v. 39, p. 1147–1167.

Sawyer, E.W., 1999, Criteria for the recognition of partial melting, Physics and Chemistry of the Earth (A), v. 24, p. 269–279.

Sawyer, E.W., 2001, Melt segregation in the continental crust: distribution and movement of melt in anatectic rocks, Journal of Metamorphic Geology, v. 19, p. 291–309.

Sawyer, E.W., 2008, Working with migmatites: nomenclature for the constituent parts, Mineralogical Association of Canada Short Course 38, Quebec City, Quebec, 1–28.

Schilling, F.R., and Partzsch, G.M., 2001, Quantifying partial melt fraction in the crust beneath the central Andes and the Tibetan Plateau, Physics and Chemistry Earth, v. 26, p. 239–246.

Scott, J.M., and Cooper, A.F., 2006, Early Cretaceous extensional exhumation of the lower crust of a magmatic arc: Evidence from the Mount Irene Shear Zone, Fiordland, New Zealand, Tectonics, v. 25, doi.10.1029/2005TC001890.

Siddoway, C.S., Baldwin, S.L., Fitzgerald, P.G., Fanning, C.M., and Luyendyk, B.P., 2004a, Ross Sea mylonites and the timing of intracontinental extension within the West Antarctic rift system, Geology, v. 32, p. 57–60.

Siddoway, C.S., Richard, S.M., Fanning, C.M., and Luyendyk, B.P., 2004b, Origin and emplacement of a middle Cretaceous gneiss dome, Fosdick Mountains, West Antarctica, *in* Whitney, D.L., Teyssier, C., and Siddoway, C.S., eds., Gneiss domes in Orogeny, Geological Society America Special Paper 380, p. 267–294.

Siddoway, C.S., Sass III, L.C., and Esser, R., 2005, Kinematic history of Marie Byrd Land terrane, West Antarctica: Direct evidence from Cretaceous mafic dykes, *in* Vaughan et al., eds., Terrane Processes at the Margin of Gondwana, Geological Society, London, Special Publications, 246, p. 417-438.

Siddoway, C.S., Fanning, C.M., Kruckenberg, S.C., and Fadrhonc, S.C., 2006, U-Pb SHRIMP investigation of the timing and duration of melt production and migration in a Pacific margin gneiss dome, Fosdick Mountains, Antarctica, Eos Trans. AGU, 87 (52), Fall Meet. Suppl., abstract V23D-0661.

Siddoway, C.S., 2008, Tectonics of the West Antarctic rift system: New light on the history and dynamics of distributed intracontinental extension, *in* Cooper, A.K., et al., eds. Antarctica: A Keystone in a Changing World, National Academy of Sciences.

Siddoway, C.S., and Fanning, C.M., 2009, SHRIMP U-Pb zircon geochronology of a migmatite-granite complex in West Antarctica, with bearing on the character and extent of Paleozoic tectonism on the East Gondwana margin: Tectonophysics, doi: 10.1016/j.tecto.2009.04.021.

Smith, C.H., 1997, Mid-crustal processes during Cretaceous rifting, Fosdick Mountains, Marie Byrd Land, *in* Ricci, C.A., ed., The Antarctic Region: Processes and Evolution, Terra Antarctica Publications, p. 313–320.

Solar, G.S., and Brown, M., 2001, Deformation partitioning during transpression in response to Early Devonian oblique convergence, northern Appalachian orogen, USA, Journal of Structural Geology, v. 23, p. 1043–1065.

Soula, J.P., Debat, P., Brusset, S., Bessiere, G., Christophoul, F., and Deramond, J., 2001, Thrust-related, diapiric, and extensional doming in a frontal orogenic wedge: Example of the Montagne Noire, Southern French Hercynian Belt, Journal of Structural Geology, v. 23, p. 1677–1699. doi: 10.1016/S0191-8141(01)00021-9.

Spell, T.L., McDougall, I., and Tulloch, A.J., 2000, Thermochronological constraints on the breakup of the Pacific Gondwana margin: The Paparoa metamorphic core complex, South Island, New Zealand, Tectonics, v. 19, p. 433–451.

Squire, R.J., and Wilson, C.J., 2005, Interaction between collisional orogenesis and convergent-margin processes: evolution of the Cambrian proto-pacific margin of East Gondwana, J. Geol. Soc. London, v. 162, p. 749–761.

Storey, B., Leat, T., Weaver, S.D., Pankhurst, R.J., Bradshaw, J.D., and Kelley, S., 1999, Mantle plumes and Antarctica-New Zealand rifting: Evidence from mid-

Cretaceous mafic dykes, Journal of the Geological Society of London, v. 156, p. 659–671.

Sutherland, R., 1999, Basement geology and tectonic development of the greater New Zealand region: an interpretation from regional magnetic data, Tectonophysics, v. 308, p. 341–362.

Sutherland, R., and Hollis, C., 2001, Cretaceous demise of the Moa plate and strike-slip motion at the Gondwana margin, Geology, v. 29, p. 279–282.

Talbot, J-Y, Faure, M., Chen, Y., and Martelet, G., 2005, Pull-apart emplacement of the Margeride granitic complex (French Massif Central). Implications for the late evolution of the Variscan orogen, Journal of Structural Geology, v. 27, p. 1610–1629.

Tera, F., and Wasserberg G., 1972, U-Th-Pb systematics in three Apollo 14 basalts and the problem of initial Pb in lunar rocks, Earth and Planetary Science Letters, v. 14, p. 281–304.

Teyssier, C., Ferre, E.C., Whitney, D.L., Norlander, B., Vanderhaeghe, O., and Parkinson, D., 2005, Flow of partially molten crust and origin of detachments during collapse of the Cordilleran orogen, *in* Bruhn, D., and Burlini, L., eds, High-strain zones: Structure and Physical Properties: Geological Society, London, Special Publications, 245, p. 39–64.

Teyssier, C., and Tikoff, B., 1999, Fabric stability in oblique convergence and divergence, Journal of Structural Geology, v. 21, p. 969–974.

Teyssier, C., and Whitney, D.L., 2002, Gneiss domes and orogeny, Geology, v. 30, p. 1139–1142.

Tikoff, B., and Teyssier, C., 1992, Crustal-scale, en echelon "P-shear" tensional bridges: A possible solution to the batholithic room problem, Geology, v. 20, p. 927–930.

Tikoff, B., and Teyssier, C., 1994, Strain modeling of displacement-field partitioning in transpressional orogens, Journal of Structural Geology, v. 16, p. 1575–1588.

Tirel, C., Brun, J.P., and Burov, E., 2004, Thermomechanical modeling of extensional gneiss domes, *in* Whitney, D.L., Teyssier, C., and Siddoway, C.S., Gneiss Domes in Orogeny, Boulder, Colorado, Geological Society of America Special Paper 380, p. 67–78.

Tulloch, A.J., and Kimbrough, D.L., 1989, The Paparoa metamorphic core complex, New Zealand: Cretaceous extension associated with fragmentation of the Pacific margin of Gondwana, Tectonics, v. 8, p. 1217–1234.

Tulloch, A.J., Kimbrough, D.L., and Wood, R.A., 1991, Carboniferous granite basement dredged from a site on the southwest margin of the Challenger Plateau, Tasman Sea, New Zealand Journal of Geology and Geophysics v. 34, p. 121–126.

Tulloch, A.J., and Kimbrough, D.L., 2003, Paired plutonic belts in convergent margins and the development of high Na, Al, Sr, low Y magmatism: the Peninsular Ranges Batholith of California and the Median Batholith of New Zealand, in Tectonic evolution of the northwestern Mexico and the southwestern USA, edited by S. E.

Johnson, S. R. Paterson, J. Fletcher, G. H. Girty, D. L. Kimbrough, A. Martin-Barajas, Boulder, Colorado, GSA Special Paper 374, p. 275–295.

Tulloch, A.J., Beggs, M., Kula, J., Spell, T. and Mortimer, N. 2006, Cordillera Zealandia, the Sisters Shear Zone and their influence on the early development of the Great South Basin, Field Developments and Production/Keynote paper.

Vanderhaeghe, O., 1999, Pervasive melt migration from migmatites to leucogranite in the Shuswap metamorphic core complex, Canada: control of regional deformation, Tectonophysics, v. 312, p. 35–55.

Vanderhaeghe, O., 2001, Melt segregation, pervasive melt migration and magma mobility in the continental crust: the structural record from pores to orogens: Physics and Chemistry of Earth, (A), v. 26, p. 213–223.

Vanderhaeghe, O., and Teyssier, C., 2001, Partial melting and flow of orogens, Tectonophysics, v. 342, p. 451–472.

Vaughan, A.M., and Livermore, R.A., 2005, Episodicity of Mesozoic terrane accretion along the Pacific margin of Gondwana: Implications for superplume interactions, *in* Terrane Processes at the Margin of Gondwana*,* eds., A. Vaughan, Leat, P., and Pankhurst, R.J., Geological Society of London Special Publication 246, p. 143–178.

Vernon, R.H., Clarke, G.L., and Collins, W.J., 1990, Local, mid-crustal granulite facies metamorphism and melting: and example in the Mount Stafford area, central Australia, *High Temperature Metamorphism and Crustal Anatexis*, edited by J. R. Ashworth, and M. Brown, Unwin-Hyman, London, p. 272–319.

Vincenzo, G.D., Carosi, R., Palmer, R., and Tiepolo, M., 2007, A comparative U-Th-Pb (zircon-monazite) and ^{40}Ar-^{39}Ar (muscovite-biotite) study of shear zones in northern Victoria Land (Antarctica): implications for geochronology and localized reworking of the Ross Orogen, Journal of Metamorphic Geology v. 25, p. 605–630, doi: 10.1111/j.1525-1314.2007.00717.x.

Wade, F.A., Cathey, C.A., and Oldham, J.B., 1978, Reconnaissance geologic map of the Gutenko Nunataks quadrangle, Marie Byrd Land, Antarctica: USARP Antarctic Geological Map A-11: Reston, Virginia, U. S. Geological Survey, scale 1:250,000.

Wandres, A.M., and Bradshaw, J.D., 2005, New Zealand tectonostratigraphy and implications from conglomeratic rocks for the configuration of the SW Pacific margin of Gondwana, in *Terrane Processes at the Margin of Gondwana*, edited by A. Vaughan et al., Geol. Soc. London, Spec. Publ. v. 246, p. 179–216.

Weaver, S.D., Bradshaw, J.D., and Adams, C.J., 1991, Granitoids of the Ford Ranges, Marie Byrd Land, Antarctica, in Geological evolution of Antarctica, edited by M. R. A. Thomson, J. A. Crame, and J. W. Thomson, Cambridge, Cambridge University Press, p. 345–351.

Weaver, S.D., Adams, C.J., Pankhurst, R.J., and Gibson, I.L., 1992, Granites of Edward VII Peninsula, Marie Byrd Land, Antarctica, *in* Brown, E., and Chappell, B.W., eds., Proceedings of the Second Hutton Symposium on the Origin of Granites and Related Rocks, Transactions of the Royal Society of Edinburgh, Earth Sciences, v. 83, p. 281–290.

Weaver, S.D., Storey, B.C., Pankhurst, R.J., Mukasa, S.B., Divenere, V., and Bradshaw, J.D., 1994, Antarctic-New Zealand rifting and Marie Byrd Land lithospheric magmatism linked to ridge subduction and mantle plume activity, Geology, v. 22, p. 811–814.

Weinberg, R.F., 1999, Mesoscale pervasive felsic magma migration: alternatives to diking, Lithos, v. 46, p. 393–410.

Weinberg, R.F., 2006, Melt segregation structures in granitic plutons, Geology, v. 34, p. 305–308.

Weinberg, R.F., and Mark, G., 2008, Magma migration, folding, and disaggregation of migmatites in the Karakoram shear zone, Ladakh, NW India, Geological Society of America Bulletin, v. 120, p. 994–1009, doi: 10.1130/B26227.1.

Weinberg, R.F, Mark, G., and Reichardt, H., 2009, Magma ponding in the Karakoram shear zone, Ladakh NW India, Geological Society of America Bulletin, v. 121, p. 278–285, doi: 10.1130/B26358.1.

Weinberg, R.F., and Searle, M.P., 1998, The Pangong Injection Complex Indian Karakoram: a case of pervasive granite flow through hot viscous crust, J. Geol. Soc. London, 155, p. 883–891.

White, P.J., 1995, Thermobarometry of the Charleston Metamorphic Group and implications for the evolution of the Paparoa Metamorphic Core Complex, New Zealand, New Zealand Journal of Geology and Geophysics, v. 37, p. 201–209.

White, R.W., Powell, R., and Haplin, J.A., 2004, Spatially-focussed melt formation in aluminous metapelites from Broken Hill, Australia, Journal of Metamorphic Geology, v. 22, p. 825–845.

Whitney, D.L., Teyssier, C., and Vanderhaeghe, O., 2004, Gneiss domes and crustal flow, *in* Whitney, D.L., Teyssier, C., and Siddoway, C.S., eds., Gneiss domes in orogeny: Geological Society of America Special Paper 380, p. 15–33.

Whitney, D.L., Teyssier, C., and Heizler, M.T., 2007, Gneiss domes, metamorphic core complexes, and wrench zones: Thermal and structural evolution of the Nigde Massif, central Anatolia: Tectonics, v. 26, doi: 10.1029/2006TC002040.

Whittington, A.G., and Treloar, P.J., 2002, Crustal anatexis and its relation to the exhumation of collisional orogenic belts, with particular reference to the Himalaya, Mineralogical Magazine, v. 66, p. 53–91.

Wilbanks, J.R., 1972, Geology of the Fosdick Mountains, Marie Byrd Land, in Antarctic Geology and Geophysics, edited by R. J. Adie, Oslo, Universitetsforlaget, p. 277–284.

Williams, I.S., 1998, U-Th-Pb geochronology by ion microprobe, *in* McKibben, M.A., Shanks III, W.C., and Ridley, W.I., eds., Application of Microanalytical Techniques to Understanding Mineralizing Processes, Reviews in Economic Geology, Littleton, CO, Society of Economic Geologists, p. 1–35.

Williams, P.F., and Jiang, D, 2005, An investigation of lower crustal deformation: evidence for channel flow and its implications for tectonic and structural studies, Journal of Structural Geology, v. 27, p. 1486–1505.